Microwave Laboratory
W. W. Hansen Laboratories of Physics
Stanford University
Stanford, California

FREQUENCY CONVERSION AND AMPLIFICATION USING DOPPLER-SHIFT METHODS IN SOLIDS

by

C. S. Tsai

M. L. Report No. 1395

December 1965

Technical Report
for
Contract AF 49(638)-1429
Project - Task 9768-02

prepared for

Air Force Office of Scientific Research
Washington, D. C. 20333

ERRATA

for

FREQUENCY CONVERSION AND AMPLIFICATION USING DOPPLER-SHIFT METHODS IN SOLIDS

by

C. S. Tsai

M. L. Report No. 1395

Page	
iv	Second line from bottom, last word, should be "integral" rather than "integer."
6	Figure 2.1, symbols in right hand figure should have a prime superscript, not "1."
11	Figure 2.3, reverse the direction of the arrowhead on the ω_1 line.
17	First line, change reference 5 to 13.
19	Equation (2.38) last term of last equation, change Z_i to "
27	Figure 3.1, near top of figure, change the $\vec{m}$ to "$\vec{n}$" .
28	Second line from the bottom, insert a square root sign over $\sqrt{\mu_0 t_0}$.
46	Second line of text below Eq. (3.51) change (3.57) to (3.51).
51	Second line, insert a period at end of line.
54	Line 5, change the word "odd" to "even" .
80	Equation (3.111), change the last subscript in the last term to "t" instead of "i" .
85	First and second lines of text below Eq. (3.122), change all "v's" to capital "V" .
87	First line of text below Eq. (3.128), change v to "V" .
88	Equation (3.130) and first line following, change v to "V" (3 times).
97	Figure 4.1, insert a comma in the terms below "Medium 2" to read "μ_2, ϵ, H_{02}" .
112	Figure 4.7, the two uppermost curves, above the horizontal point ω_t , should be made heavier and darker.

Page

133 Equation (5.38), in the third matrix frame, the upper right hand term, add a minus sign to read "W^{+-}" .

140 Second line, change (5.63) to "(5.62)" .

141 Line below Eq. (5.66), change (5.54) to "(5.65)" .

144 Line 15, insert "increase of" after "rate of" to read "...waves, the rate of increase of momentum...."

161 Equation (6.10), expression following "and" , far right hand side, insert a parenthesis.

165 Section 6.4, line 9, change "(3.13) and (3.14)" to "(3.19) and (3.20)" .

167 First line below Eq. (6.23), insert a two after the first word to read "$2\Delta\eta \equiv$ " .

175 Equation (6.46), inside large parenthesis, far right term, change "s" to "S" .

190 Figure 7.1 caption – change the word "experiment" to "experimental" .

192 Second line from bottom, Figs. 7.5 and 7.6 should read "7.5a and 7.5b" .

193 Third line from bottom, reference numbers should be "72,86" .

195 Figure 7.5 caption should read (a. along the wide dimension) (b. along the narrow dimension).

200 Second last line in second paragraph, delete the "m" after P_r .

203 Seventh line from top of page, correct the spelling of "ultrasonic" field.

204 Sixth line from top of page, change to read [Eq. (6.41)] .

226 Second line in second paragraph should read "to shift the laser frequency by integral multiples...."

228 Under Section 8.2.1, line 6, change "C/2L" to read "c/2L" .

244 First line of second paragraph should read "into Eq. (8.32)" .

245 Second line after Eq. (8.43) should read "[from Eqs. (8.38) and (8.41)] .

ABSTRACT

In this study the interaction of electromagnetic and acoustic waves with moving reflectors in solids was investigated. The first part of the study contains theoretical predictions of the frequency shifts and amplitude changes of an electromagnetic or acoustic wave after interacting with a moving interface between regions of different characteristic impedances or a series of such moving interfaces, termed the "Moving Reflector Theory." The seccnd part contains experimental results concerning the diffraction of laser light using kilomegacycle acoustic waves in solids. The latter is considered as a specific case of the general theory developed in the first part.

The theory predicts that a high frequency amplification or deamplification of an electromagnetic wave can probably be obtained more easily by reflecting from a moving interface or a series of moving interfaces which are induced by sending an electromagnetic pumping signal into a nonlinear material (e.g., ferroelectric or ferromagnetic crystals). The theory also predicts that a frequency shift which occurs in a wave (transmitted through a moving nonabrupt interface) is independent of the width of the interface and the conversion of a longitudinal acoustic wave to a transverse acoustic wave or vice versa in a ferromagnetic material. Several kinds of Doppler shift experiments are proposed. Various similarities with and distinctions between the moving reflector theory and the conventional parametric amplification theory are discussed.

Various ways of enhancing the amount of diffraction were employed to achieve a large diffraction. Using a suitable single crystal (TiO_2) and a high-efficiency transducer (ZnO wafer) giving a ribbon-shaped acoustic beam, it was possible to diffract in the first-order 10% of the incident light using 15 watts of cw rf power, and 60% diffraction was achieved with a pulse 60 watts peak power source. The possibility

of diffracting such a large percentage of the light obviously has a number of possible device applications. In the high power experiments additional diffracted spots of light (second- and third-order) appeared; these are also compared with calculated value. The measured enhancement of the diffraction intensity due to acoustic resonance was shown to be in good agreement with the theoretical prediction. Measured and calculated diffraction patterns from multiple acoustic beams in one crystal of $SrTiO_3$ are given. They both show the characteristic shape of a multiple-slit diffraction pattern in optics. The measured frequency shift in the diffracted beam is shown to agree with both the moving reflector theory and the parametric principle. Finally, two schemes of using multiple diffraction to shift the laser frequency by integer multiples of the acoustic wave frequency are analyzed.

ACKNOWLEDGEMENTS

I am deeply grateful to Dr. B. A. Auld, my research advisor, for his expert guidance, for his many contributions, and for his encouragement throughout the course of this study. I also would like to express my appreciation to Dr. H. J. Shaw for his suggestion of the experimental part of this study and many helpful discussions. Other members of the laboratory who helped with discussions and encouragement include Drs. D. K. Winslow, R. H. Pantell, T. Wessel-Berg, K. B. Mallory, B. J. Elliott, C. F. Quate, A. Karp, and K. J. Harker.

Special thanks go to Chris Wilkinson and Don Caddes for many helpful and critical discussions and for their reading and comments on the manuscript. Technical assistance from Bill Haydl is appreciated.

Much indispensible aid in making the apparatus came from Al Moody and other members of the machine shop. The samples used were polished by Bob Griffin and transducers bonded by Jack Seaton; their excellent work was vital to the success of the experimental part of this project. Les Yingst and Willy Heintzen helped with the instrumentation.

Finally, I wish to express my appreciation to Professors R. L. White and A. T. Waterman for their reading and comments on the manuscript, to Mr. A. S. Braun for his excellent supervision in the preparation of this dissertation, to Mesdames I. L. Williams, D. M. Lacey, B. H. Dutton, P. R. Brady, and P. H. Cummings for typing the manuscript and to Messrs. A. Vacek and N. B. Bettini for drawing the figures.

TABLE OF CONTENTS

	Page
Abstract	iii
Acknowledgments	v
List of figures	x
I. Introduction	1
PART I	
II. Lorentz transformation of electromagnetic wave quantities	5
2.1. Doppler effect existing between two inertial frames which have relative velocity V in vacuum	5
2.2. Mirror effect in vacuum	10
2.3. Doppler and mirror effects in material media	14
2.4. Lorentz transformation of the electric and magnetic field intensities	16
2.5. Transformation of TEM wave field components; permittivity; permeability; impedance; Poynting vector under Lorentz transformation	18
2.6. Electrodynamics of moving media	21
III. Wave interactions with moving boundaries	25
3.1. Reflection and refraction of electromagnetic waves at a moving boundary or interface -- general case	26
3.1.1. Frequency shifts in the reflected and transmitted waves	26
3.1.2. Amplitude changes in the reflected and transmitted waves	33
3.2. Reflection and refraction of electromagnetic waves at a moving interface -- normal incidence, moving medium (nonrelativistic)	35
3.2.1. Frequency shifts in the reflected and transmitted waves	35

Page

3.2.2. Amplitude changes in the reflected and transmitted waves 39
3.3. Reflection and refraction of electromagnetic waves at a moving interface – Normal incidence, stationary media 40
3.3.1. Frequency shifts in the reflected and transmitted waves 42
3.3.2. Amplitude changes in the reflected and transmitted waves 44
3.4. Wave interactions with moving slabs 51
3.4.1. Frequency shifts for a single moving slab . . . 51
3.4.2. Wave matrix for a single moving interface . . . 54
3.4.3. Reflection and transmission coefficients for a single moving slab 60
3.4.4. Frequency shifts and amplitude changes for a series of moving slabs 67
3.4.5. The effects of a nonabrupt interface 70
3.5. A transmission line model for frequency conversion and amplification at a moving interface in a stationary medium 72
3.5.1. Frequency shifts in the reflected and transmitted waves 73
3.5.2. Calculation of Doppler amplification from the principle of conservation of energy 75
3.6. The effects of dispersion 80
3.7. Compression of electromagnetic waves 81
IV. The realization of Doppler interactions in real materials . . 96
4.1. Reflection and transmission of an electromagnetic wave at a large magnetic field step-function or pulse 96
4.2. A survey of potential ferroelectric materials for the Doppler shift experiments. 102

Page

4.3. Conversion of a longitudinal acoustic wave to a transverse acoustic wave in a ferromagnetic material 105
4.4. Possible configurations for Doppler shift experiments . 114
4.5. Examples of frequency conversion and amplification using Doppler shift methods 117
V. Wave interactions with a moving periodic structure 121
5.1. Derivations of the power relations for the cases of a single, perfect moving reflector and a single moving "nonreflecting interface" using the laws of conservation of energy and momentum 121
5.1.1. A perfect moving reflector 122
5.1.2. A perfect moving "nonreflecting interface" . . 125
5.2. The power transfer between the pumping wave and small signal wave in a nonlinear material 128
5.3. Wave interaction with a semi-infinite moving periodic structure 132
5.4. Application of the general theory to the frequency converters 135
5.5. Doppler shift frequency converter and electrically or mechanically tunable filter 146

PART II

VI. A nonrelativistic case: Laser light interactions with high frequency acoustic waves 149
6.1. Introduction 149
6.2. The Raman-Nath and the related theory 151
6.3. Moving reflector theory 158
6.4. The calculation of diffraction intensity using the ray-tracing method 165
6.5. Parametric theory 180
6.6. Large diffraction of light 183
6.6.1. Choice of a proper crystal for diffraction . . 183
6.6.2. The requirement of a high efficiency transducer. 184
6.6.3. Generation of a Ribbon-shaped acoustic beam . . 184
6.6.4. Acoustic resonance 184

Page

6.7. Enhancement of diffraction due to acoustic resonance . 185

VII. Light diffraction using kilomegacycles acoustic waves in solids 189

7.1. Experimental technique and preliminary experimental results of Bragg-diffraction 189

7.2. Large diffraction of laser light using rutile crystal 192

7.3. Measured enhancement of the diffraction intensity due to acoustic resonance 205

7.4. Diffraction pattern 209

7.5. Light diffraction using multiple acoustic beams in $SrTiO_3$ crystal 212

7.6. The measurement of frequency shift in the diffracted beam using Fabry-Perot etalon 225

VIII. Multiple diffraction techniques 226

8.1. Simultaneous generation of the upper and lower side-bands using a pair of Porro prisms 226

8.2. Simultaneous generation of the upper and lower side-bands using a pair of optical cavities 228

8.2.1. Introduction 228

8.2.2. Derivation of the "harmonic-oscillator-like" linear differential equation for the expansion coefficients of the optical fiels 230

8.2.3. Recursion formula for the pertinent mode amplitudes and their solutions 243

Appendix A 251

References 257

LIST OF FIGURES

		Page
2.1.	Two inertial frames with constant velocity V parallel to the x and x' axes	6
2.2.	The doppler effect between two inertial frames	8
2.3.	The configuration showing the mirror effect	11
2.4.	The field components of a uniform TEM wave measured in two inertial frames	18
3.1.	Configuration of a uniform TEM wave interacting with a moving boundary – general case	27
3.2.	The configuration of a monochromatic acoustic wave interacting with a moving boundary	32
3.3.	Configuration showing a uniform TEM wave interacting with a moving medium of nonrelativistic velocity	36
3.4.	The configuration showing a uniform TEM wave normally incident upon a moving interface separating two media at rest	41
3.5.	The configuration showing a uniform TEM wave normally incident on two moving interfaces which make up a moving slab	52
3.6.	The configuration showing a stationary interface separating two media	55
3.7.	The configuration showing a moving interface separating two media at rest	55
3.8.	Configuration showing the scattered waves resulting from a uniform TEM wave incident upon a moving slab.	61
3.9.	The configuration showing a series of moving interfaces . .	69
3.10.	The configuration of a moving ramp-type interface	71
3.11.	The configuration of a moving "Kinked Ramp" interface . . .	71
3.12.	The configuration of a moving trapezoidal slab	71

Page

3.13. A lossless transmission line with a moving discontinuity. (The coordinate origin is chosen such that at $t = 0$ the moving junction is at $x = 0$ as shown.) 73

3.14. The configuration showing the conversion of power between the pumping source and the transmitted wave using the parametric principle 77

3.15. The configuration showing the energy balance for an infinitesimal section of the transmission line 77

3.16. The configuration showing the compression of a uniform TEM wave between two conducting plates (one fixed, one moving) . 83

3.17. The frequency variation of a uniform TEM wave during the course of compression by two moving conducting plates . . . 89

3.18. Energy density variation of a uniform TEM wave during the course of compression between two conducting plates (one fixed, one moving) 94

4.1. The configuration of a uniform TEM wave interacting with a moving boundary in a ferromagnetic medium 97

4.2. The complete dispersion diagram for an infinite ferromagnetic medium. The dashed lines are for the ordinary waves and the solid curves for the extraordinary waves . . . 98

4.3. The configuration showing a spin-wave interacting with a moving interface 109

4.4. The spin-wave manifold 109

4.5. The configuration showing the conversion of a transverse acoustic wave to a longitudinal acoustic wave using a non-abrupt magnetic step function 111

4.6. The $\omega - K$ diagram of the longitudinal and transverse acoustic waves 111

4.7. The combined $\omega - K$ diagram showing the spin-phonon coupling region (indicated by the dashed lines) and the shift in operating point 112

4.8. Possible arrangement for the Doppler shift experiment utilizing single reflection 116

Page

4.9. Typical arrangement for the Doppler shift experiment utilizing multiple reflection - the compression of electromagnetic waves 118

4.10. Configuration showing a moving boundary interacting with a video pulse 119

5.1. A perfect moving reflector in a material medium. The region bounded by the reflector and the reference plane is considered as a system 123

5.2. A moving "nonreflecting interface" in a material medium. The region bounded by the two reference planes is considered as a system 123

5.3. The nonlinear spring used to illustrate the power transfer between the pumping wave and the small signal wave in a nonlinear material 129

5.4. (a) A semi-infinite moving periodic structure. (b) The rectangular pumping wave used to induce the moving periodic structure (a) in a nonlinear material 133

5.5. An infinite moving periodic structure induced in a nonlinear material using a square-wave pump 136

5.6. A semi-infinite moving periodic structure induced in a nonlinear material using a square-wave pump 136

5.7. Frequency and wave number relations for frequency converters. (a) up-conversion; (b) down-conversion 142

5.8. (a) A semi-infinite "moving paddles" structure. (b) A semi-infinite train of short pulses used to induce the structure of (a) in nonlinear materials 145

5.9. (a) An rf pulse. (b) A moving periodic structure induced by the rf pulse in a nonlinear material 147

6.1. The configuration for the diffraction of light by ultrasonics (oblique incidence) 152

6.2. Configuration for the diffraction of light by ultrasonics (normal incidence) 155

6.3. The frequency shifts in the diffracted light using traveling acoustic waves 156

Page

6.4. The frequency shifts in the diffracted light using standing acoustic waves 156
6.5. The moving periodic structure induced by a traveling acoustic wave 160
6.6. The configuration showing the reflection and transmission from a series of moving interfaces 162
6.7. The wave-vector relation for Bragg diffraction 165
6.8. The reflection and refraction of a light wave from a single nonrelativistic moving interface 166
6.9. (a) Configuration showing the multiple reflection of light between the interfaces of two layers (light incident from left) (b) Configuration showing the multiple reflection of light between the interfaces of two layers (light incident from right) 168
6.10. Configuration showing the cascade network for a series of moving interfaces 170
6.11. Saturation of the diffraction intensity 173
6.12. Configuration showing the diffraction of light from an acoustic column 174
6.13. Plots of strain vs acoustic power density for various crystals 179
6.14. Configuration showing the system of acoustic resonance . . . 186
7.1. The experimental arrangement for the measurement of Bragg diffraction 190
7.2. Configuration showing the dimensions of cavity center post, rutile crystal, ZnO transducer and air gap 193
7.3. Acoustic echoes at 1.1 Gc/s with no mercury termination . . 194
7.4. Acoustic echoes at 1.1 Gc/s with mercury termination 194
7.5. Acoustic beam mapping (along the wide dimension) (along the narrow dimension) 195
7.6. (a) First-order diffraction pattern. (b) Second-order diffraction pattern. (c) Third-order diffraction pattern . 196
7.7. Photographs of the diffraction spots for various angles of incidence 197
7.8. The rf power dependence of the first- and second-order diffraction intensities 199

Page

7.9. Configuration for estimating the difference in the diffraction intensity between a perfect traveling wave and a non-perfect traveling wave 201
7.10. The rf power dependence of the right- and left-hand side first-order diffraction intensities at normal incidence . 206
7.11. The acoustic echoes at 810 Mc/s with no mercury termination 207
7.12. The Q-curve of the cavity with the acoustic delay line (no frequency marker) 207
7.13. The Q-curve of the cavity with the acoustic delay line. (The frequency between two consecutive frequency markers is 1 Mc/s.). 207
7.14. The diffraction spectrum with mercury termination 208
7.15. The diffraction spectrum with no mercury termination . . . 208
7.16. Configuration showing the directions of propagation of the laser light and the acoustic wave 210
7.17. (a) The dimensions and the orientation of the wedge-shaped transducer, (b) The variation of the air gap spacing between the transducer and the center post 213
7.18. Acoustic beam mapping (along the wide dimension) 214
7.19. Acoustic beam mapping (along the narrow dimension) 215
7.20. Acoustic beam mapping (along the wide dimension). (a) f = 1100.5 Mc/sec. (b) f = 1106.5 Mc/sec. (c) f = 1115.0 Mc/sec 217
7.21. Dimensions of the wedge-shaped transducer 218
7.22. (a) First-order diffraction pattern (measured) 220
(b) First-order diffraction pattern (calculated) 221
7.23. Second-order diffraction pattern (measured). 222
7.24. Photographs of the diffraction spots for various angles of incidence 223
7.25. Fabry-Perot patterns of (a) the undiffracted beam; (b) the diffracted beam with up-shifted frequency; and (c) the diffracted beam with down-shifted frequency 224

Page

8.1. Configuration for simultaneous generation of the upper and lower sidebands using a pair of Porro prisms 227

8.2. Configuration for the simultaneous generation of the upper and lower sidebands using a pair of optical cavities 229

CHAPTER I

INTRODUCTION

This study reports the results of a theoretical and experimental investigation of the interaction of waves with moving reflectors in solids. It is divided into two parts: The first part contains theoretical predictions of the frequency shifts and amplitude changes of an electromagnetic or acoustic wave after interacting with a moving interface between regions of different characteristic impedance or a series of such moving interfaces, and the second part contains experimental results concerning the diffraction of light using high frequency acoustic waves in solids. The latter can be considered as a specific case of the general theory developed in the first part.

The frequency shift in any kind of oscillation resulting from the relative motion between a transmitter and a receiver is generally termed the "Doppler Effect." The Doppler effect itself has long played an interesting and beautiful role in theoretical physics. However, the application of this effect has not been explored in detail. The importance of the Doppler effect in applications is well illustrated by the fact that any kind of wave, when reflected from a moving reflector (e.g., a moving mirror), is shifted in frequency and changed in amplitude. This phenomena is termed the "Double Doppler Effect."[1] In general, the closer the velocity of the reflector to that of the wave, the larger the shift in frequency and the change in amplitude.

Landecker[2] first examined the possibility of frequency multiplication and wave amplification by reflection from a fast electron cloud. He specifically considered the possibility of generating a millimeter wave by reflecting an X-band microwave signal from the relativistic electron beam of an electron accelerator such as a betatron.

Fainberg and Tkalich[3] first discussed the reflection of monochromatic waves from an electron plasma (nonrelativistic beam) moving in a dielectric

medium. It was shown that by using a slow-wave structure[3,4] significant changes in frequency and amplitude may be attained even with nonrelativistic beams. The possibility of further enhancement of the changes of frequency and amplitude through the use of multiple reflection was pointed out by Fainberg[5] and Ginzton.[6] An experimental demonstration on the effect of multiple reflection using a plasma "piston" was reported a few years later.[7]

Due to the complexity and high cost inherent in Landecker's approach, and the uncertainty and difficulty in controlling the plasma involved in Fainberg and Tkalich's approach, the usefulness and practicality of these two methods seem limited. A third approach is given in this study. It is shown that a high frequency amplification or deamplification of an electromagnetic wave can probably be obtained more easily by interaction with a moving interface or a series of moving interfaces which are created by sending an electromagnetic pumping signal into a nonlinear material (e.g., ferroelectric or ferromagnetic crystals). This is because both the pumping signal and the small signal are electromagnetic in nature. With the sophisticated microwave techniques presently existing, the experimental technique required for this approach seems simpler than the employment of an accelerator or plasma. Furthermore, an interesting and simple physical picture is provided by the third approach.

In Chapter II, various aspects of relativistic and nonrelativistic Doppler effects for electromagnetic waves are discussed. In addition, a few applications of the Lorentz transformation, and the consequences of the transformations, are illustrated. They serve both as the background and the stimulus for the development of later chapters.

The approach for the derivation of the changes in frequency and amplitude of an electromagnetic wave interacting with a moving abrupt interface is outlined in Chapter III for the most general case. The detailed calculations are given in the appendix. The rest of Chapter III contains a detailed derivation of the changes in frequency and amplitude for the case in which normal incidence and the motion of only the interface is considered. A physical picture for explaining the frequency shifts and amplitude changes using the transmission line analogy and the parametric principle is also given in Chapter III. Chapter III extends the application of the basic results, which are derived for an abrupt

interface, to the cases of gradual impedance tapers and series of interfaces induced by dc and rf pulses or a series of dc and rf pulses. The effects of frequency dispersion of a medium upon the frequency shifts are also discussed. Chapter III concludes with the analysis for the compression of EM waves between two moving conducting plates.

The application of the general theory of Chapter III to the compression of EM waves in ferroelectric and ferromagnetic crystals is illustrated in Chapter IV. Proposals for experimental configurations and surveys of promising ferroelectric materials for this purpose are also contained in this chapter. The conversion of longitudinal acoustic waves to transverse acoustic waves or vice versa, in a ferromagnetic material, which is an excellent application of the general theory developed in Chapter III for the transmitted wave, is also given. This approach results in a device termed "Transmission-type Doppler Frequency Converter." The feasibility of the various kinds of Doppler shift experiments described is illustrated by giving two examples of the Doppler shift experiments appearing in the literature.

Chapter V extends the application of the general theory developed in Chapter III to the case of a semi-infinite periodic structure. The distinctions between the moving reflector theory and the conventional parametric theory are discussed. A model for the energy balance between the pumping signal and the small signal in a nonlinear dielectric is also given in Chapter V.

The second part of this study starts with a brief survey of the general theory of light diffraction using high frequency acoustic waves. The agreement between the frequency shift in the diffracted beams, as determined by the general theory of this report (i.e., moving reflector theory), and that given by the generalized Raman-Nath theory is shown in the beginning of Chapter VI. It is followed by the calculation of the diffraction intensity using the method of "Ray-Tracing and Cascade Networks." After comparing the diffracting power of various kinds of crystals which one might use, various ways of enhancing the amount of diffraction are discussed. A theoretical analysis which determines the enhancement of the diffraction due to acoustic resonance (with some numerical values) is also given.

Chapter VII gives the results of various kinds of Bragg diffraction experiments. Using a suitable single crystal (TiO_2) and a high-efficiency transducer (ZnO) giving a ribbon-shaped acoustic beam, it was possible to diffract in the first-order 10% of the incident light using 10 watts of cw rf power, and 50% diffraction was achieved with a pulsed 60 watts peak power source. The possibility of diffracting such a large percentage of the light obviously has a number of possible device applications. In the high power experiments additional diffracted spots of light (second- and third-order) appeared; these are also discussed. The measured enhancement of the diffraction intensity due to acoustic resonance was shown to be in good agreement with the theoretical prediction. Measured and computed diffraction patterns from multiple acoustic beams in one crystal of $SrTiO_3$ are given. They both show the characteristic shape of a multiple-slit diffraction pattern in optics. Finally, the measured frequency shift in the diffracted beam is shown to agree with both the Doppler shift principle and the parametric principle. Finally, two schemes of using multiple diffraction to shift the laser frequency by integral multiples of the acoustic wave frequency are analyzed (in Chapter VIII).

PART I

CHAPTER II

LORENTZ TRANSFORMATION OF ELECTROMAGNETIC WAVE QUANTITIES

Doppler effects occur due to the relative motion between the transmitter (source) and the receiver (observer). If the frames S and S' are attached to the source and the observer, respectively, the results of Doppler effects can be easily obtained by the space-time transformation, i.e., Lorentz transformation, between these two inertial frames, for the case of a constant relative motion. The transformation of the various electromagnetic wave quantities between two inertial frames can be most easily obtained by using the four-dimensional vector and the four-dimensional tensor formulations.[8] In the following sections, some well-known results are illustrated and some less widely known results which are not available in the literature are derived. They serve both as the background and the stimulus for the development of later chapters.

2.1 DOPPLER EFFECT EXISTING BETWEEN TWO INERTIAL FRAMES WHICH HAVE RELATIVE VELOCITY V IN VACUUM

The Lorentz transformation for the coordinates of space and time between two inertial frames which have a constant relative velocity V , as shown in Fig. 2.1 is

$$x = \frac{x' + Vt'}{\sqrt{1 - \frac{V^2}{c^2}}} \quad , \quad y = y' \quad , \quad z = z' \quad , \quad t = \frac{t' + V\frac{x'}{c^2}}{\sqrt{1 - \frac{V^2}{c^2}}} \quad , \quad \ldots \qquad (2.1)$$

where $c = 1\sqrt{\mu_0 \epsilon_0}$, is the velocity of light in vacuum (μ_0 is the permeability of vacuum, ϵ_0 is the permittivity of vacuum).

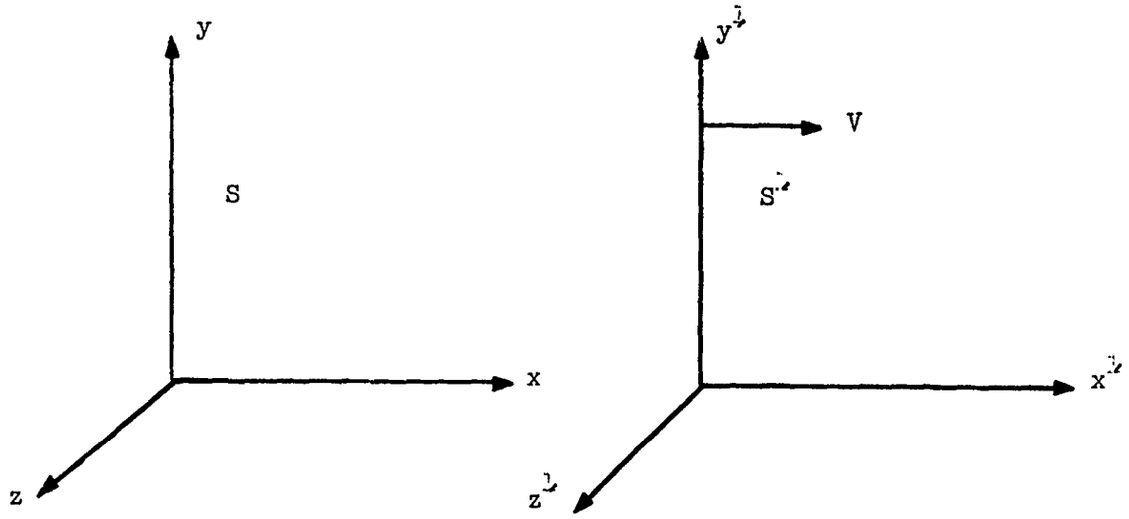

FIG. 2.1--Two inertial frames with constant velocity V parallel to the x and x' axes.

We now define τ to be ict. The vector, with components x, y, z, τ is called the four-dimensional radius vector.[8] Denoting its components by x_i, where $i = 1, 2, 3, 4$, so that $x_1 = x$, $x = y$, $x_3 = z$, $x_4 = \tau = ict$, the systems of Eqs. (2.1) becomes

$$x_1 = \frac{x_1' - i\frac{V}{c}x_4'}{\sqrt{1 - \frac{V^2}{c^2}}}, \quad x_2 = x_2', \quad x_3 = x_3', \quad x_4 = \frac{x_4' + i\frac{V}{c}x_1'}{\sqrt{1 - \frac{V^2}{c^2}}}. \tag{2.2}$$

To express the primed components in terms of the unprimed components we simply transform V to -V and change the primed to the unprimed, the unprimed to the primed.

In general a set of four quantities A_1 , A_2 , A_3, A_4 , which under transformations of the four-dimensional coordinate system transform like the components x_i in the system of Eqs. (2.2), is called a four-dimensional vector A_i .[8] Thus, under a Lorentz transformation, the A_i transform as follows:

$$A_1 = \frac{A_1' - i\frac{V}{c}A_4'}{\sqrt{1-\frac{V^2}{c^2}}} \quad , \quad A_2 = A_2' \quad , \quad A_3 = A_3' \quad , \quad A_4 = \frac{A_4' + i\frac{V}{c}A_1'}{\sqrt{1-\frac{V^2}{c^2}}} \quad \cdots \tag{2.3}$$

For a monochromatic electromagnetic wave propagating in free space the wave quantities vary as $e^{j(\omega t - \vec{K}\cdot\vec{r})}$, where $\vec{r}$ is the space-radius vector. Since the phase $\phi = \omega t - \vec{K}\cdot\vec{r}$ of any wave is invariant to a Lorentz transformation,[9] wave vector $\vec{K}$ and the frequency ω form a four-dimensional wave vector K_i with components[8]

$$K_1 = K_x \quad , \quad K_2 = K_y \quad , \quad K_3 = K_z \quad , \quad K_4 = i\frac{\omega}{c} \quad \ldots\ldots \tag{2.4}$$

Thus, the K_i in system (2.4) transform from one inertial frame to another like A_i in system (2.3)

Now we derive the Doppler effect for the simple and important configuration shown in Fig. 2 2. A monochromatic electromagnetic wave of frequency ω , with the wave vector $\vec{K}$ at an angle α with respect to the x axis and in the x-y plane in the inertial frame S , will have frequency ω' , with the wave vector $\vec{K}'$ at an angle α' respect to the x' axis in the inertial frame S' . By substituting (2.4) into (2.3), and using the relation $K_x = K\cos\alpha = \omega/c\cos\alpha$, we have the following exact formulas for the Doppler effect and the aberration. The

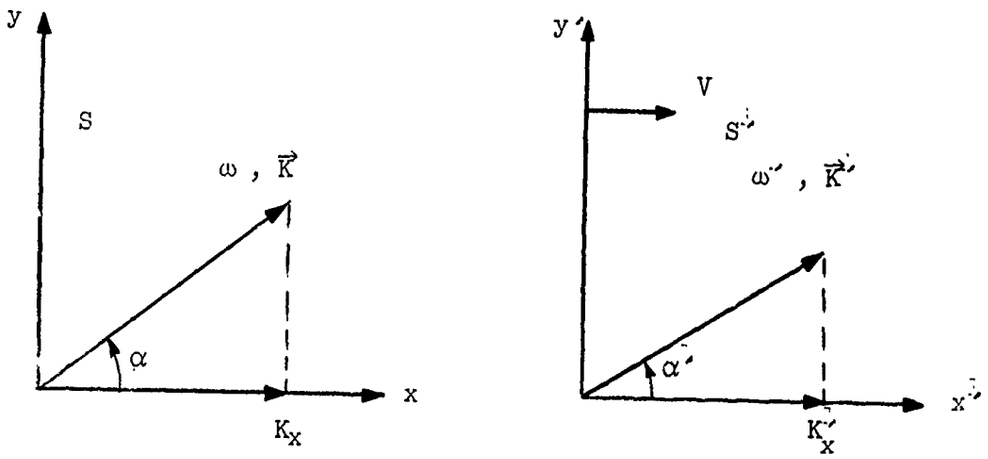

FIG. 2.2--The Doppler effect between two inertial frames.

direction of a light ray depends on the velocity of the light source relative to the observer. The phenomena is called aberration:

$$\omega = \omega' \frac{1 + \frac{V}{c} \cos \alpha'}{\sqrt{1 - \frac{V^2}{c^2}}} \tag{2.5}$$

$$\cos \alpha = \frac{\cos \alpha' + V/c}{1 + V/c \cos \alpha'} \tag{2.6}$$

$$\frac{\omega}{c} \sin \alpha = \frac{\omega'}{c} \sin \alpha' \quad . \tag{2.7}$$

By using the inverse transformation, Eqs. (2.5) and (2.6) can be replaced by

$$\omega = \omega' \frac{\sqrt{1 - V^2/c^2}}{1 - V/c \cos \alpha} \tag{2.8}$$

$$\cos \alpha' = \frac{\cos \alpha - V/c}{1 - V/c \cos \alpha} \quad . \tag{2.9}$$

The advantage of Eq. (2.8) is that the frequency ω' measured by an observer in the inertial frame S' is given in terms of the parameters measured in the inertial frame S .

When $V/c \ll 1$ and orders higher than the first in V/c are neglected, Eq. (2.5) becomes

$$\omega \cong \omega'(1 + V/c \cos \alpha') \quad . \tag{2.10}$$

Expression (2.10) is called the nonrelativistic Doppler effect or classical Doppler effect. But when V/c is not much smaller than unity, we have

$$\omega = \omega' \left[1 + V/c \cos \alpha' + \frac{1}{2} \left(\frac{V}{c}\right)^2 + \frac{1}{2} \left(\frac{V}{c}\right)^3 \cos \alpha' + \frac{3}{8} \left(\frac{V}{c}\right)^4 + \ldots \right]. \quad (2.11)$$

The terms result from $(V/c)^2$ or higher in Eq. (2.11) are called the relativistic Doppler effect.

We further notice that, when $\alpha' = 90^\circ$, we have

$$\omega = \omega' \frac{1}{\sqrt{1 - \frac{V^2}{c^2}}} , \quad (2.12)$$

and when $\alpha' = 0^\circ$

$$\omega = \omega' \frac{1 + V/c}{\sqrt{1 - \frac{V^2}{c^2}}} . \quad (2.13)$$

Equations (2.12) and (2.13) show the so called "Transverse Doppler Effect"[10] and "Longitudinal Doppler Effect,"[10] respectively, and that the second order relativistic Doppler effect is independent of α'.

It is important to emphasize that the velocity of macroscopic objects is much smaller than the velocity of light, so that the relativistic Doppler effect is hard to observe.

2 2 MIRROR EFFECT IN VACUUM

As an illustration for the Doppler principle given in the first section, the well-known mirror effect will be derived here by a double application of the four-dimensional wave vector transformation between two inertial frames.

Consider a perfect mirror moving with a velocity V in vacuum as shown in Fig. 2.3. A plane light-wave of frequency ω_i whose propagation

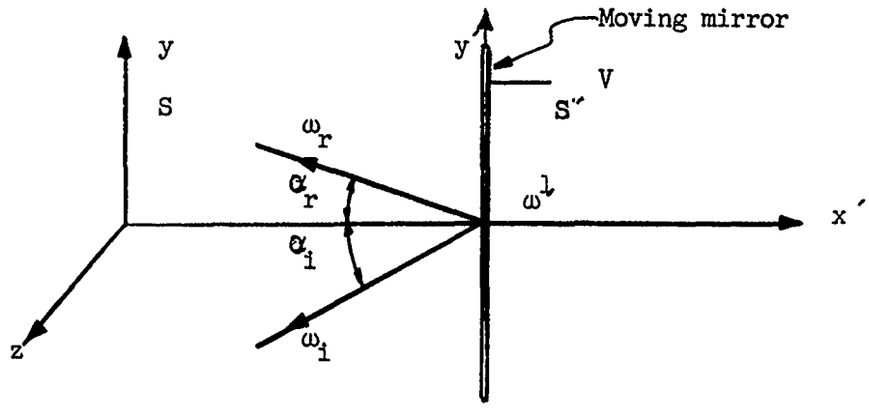

FIG. 2.3--The configuration showing the mirror effect.

direction makes angle α_i with the x-axis and on the x-z plane is incident upon this mirror. We imagine an inertial frame attached to the moving mirror S' . By transforming ω_i and α_i to the frame S' [from Eqs. (2.7) and (2.8)], we have

$$\omega_i = \omega_i' \frac{\sqrt{1 - V^2/c^2}}{1 - V/c \cos \alpha_i} \tag{2.14}$$

and

$$\frac{\omega_i}{c} \sin \alpha_i = \frac{\omega_i'}{c} \sin \alpha_i' \quad . \tag{2.15}$$

Secondly, by transforming ω_i' and α_i' to the frame S for the reflected wave, we have

$$\omega_r = \omega_i' \frac{\sqrt{1 - V^2/c^2}}{1 - V/c \cos(\pi - \alpha_r)} = \omega_i' \frac{\sqrt{1 - V^2/c^2}}{1 + V/c \cos \alpha_r} \tag{2.16}$$

and

$$\frac{\omega_r}{c} \sin \alpha_r = \frac{\omega_i'}{c} \sin \alpha_i' \quad , \tag{2.17}$$

using Snell's law. By combining (2.14) – (2.17) we have

$$\frac{\omega_r}{\omega_i} = \frac{1 - V/c \cos \alpha_i}{1 + V/c \cos \alpha_r} \tag{2.18}$$

and

$$\omega_r \sin \alpha_r = \omega_i \sin \alpha_i \quad . \tag{2.19}$$

Equations (2.18) and (2.19) can be combined to find ω_r/ω_i in terms of α_i only. After some algebraic manipulation, the well-known results are obtained as follows:

$$\frac{\omega_r}{\omega_i} = \frac{1 - 2V/c \cos \alpha_i + V^2/c^2}{1 - V^2/c^2} \tag{2.20}$$

$$\cos \alpha_r = - \frac{\cos \alpha_i - 2V/c + (V/c)^2 \cos \alpha_i}{1 - 2V/c \cos \alpha_i + (V/c)^2} \tag{2.21}$$

and

$$\sin \alpha_r = \frac{[1 - (V/c)^2] \sin \alpha_i}{1 - 2V/c \cos \alpha_i + (V/c)^2} \quad . \tag{2.22}$$

For the case $V/c \ll 1$, Eqs. (2.20) – (2.22) have the following approximate forms:

$$\frac{\omega_r}{\omega_i} \simeq (1 - 2V/c \cos \alpha_i) \tag{2.23}$$

$$\cos \alpha_r \simeq - \cos \alpha_i + 2V/c \sin^2 \alpha_i \tag{2.24}$$

and

$$\sin \alpha_r \simeq (1 + 2V/c \cos \alpha_i) \sin \alpha_i \quad . \tag{2.25}$$

Finally, for the case of normal incidence $(\alpha_i = 0)$, Eqs. (2.20) – (2.22) reduce to the following simple relations:

$$\frac{\omega_r}{\omega_i} = \frac{1 - V/c}{1 + V/c} \tag{2.26}$$

and

$$\alpha_r = \pi \quad , \tag{2.27}$$

and $\omega_r \simeq \omega_i(1 - 2V/c)$ when $V/c \ll 1$.

It is important to notice that the results given in this section are for the case when the mirror recedes from the incident wave. The frequency of the reflected wave is down-shifted. When the mirror approaches the incident wave the appropriate results are obtained simply by changing V to -V in all of the expressions given in this section. The frequency of the reflected wave will be up-shifted in this case. We further notice

the velocity of a real material mirror will in practice be much smaller than the velocity of light so that the frequency shift of the reflected wave will be extremely small. In contrast to this, in a material medium such as we shall analyze herein the moving reflector is considered to be induced through nonlinearity by a pumping electromagnetic wave or elastic wave. We shall see that the velocity of the moving reflector can be either smaller, or approximately equal to, or larger than the phase velocity of the small-signal electromagnetic or elastic wave concerned. Thus the "Double Doppler Effect" (or the Mirror Effect) in a material medium can in principle be large in a nonlinear material medium.

To conclude this section we mention that the mirror effect can be more easily and directly derived by the principle of "equality of phases," as will be shown in the next chapter.

2.3 DOPPLER AND MIRROR EFFECTS IN MATERIAL MEDIA

We have discussed the Doppler and mirror effects in vacuum in the previous two sections. We shall describe briefly in this section these same effects in a material medium. For a monochromatic electromagnetic wave propagating in a continuous material medium with permittivity ϵ and permeability μ, the wave quantities vary as $e^{j(\omega t - \vec{K}\cdot\vec{r})}$, where $\vec{r}$ is the space-radius vector. The wave vector $\vec{K}$ and the frequency ω again form a four-dimensional wave vector[2,8] K_i with components

$$K_1 = K_x \quad , \quad K_2 = K_y \quad , \quad K_3 = K_z \quad , \quad K_4 = i\frac{\omega}{c} \quad . \tag{2.28}$$

Thus the K_i in system (2.28) also tranform like A_i in system (2.3) under Lorentz transformation. To derive the Doppler effect existing between two coordinate frames such as Fig. 2.2, we simply substitute (2.28) into (2.3) and use the relation $K_x = K\cos\alpha = \omega\sqrt{\mu\epsilon}\cos\alpha$. We give only the frequency transformation here:

$$\omega = \omega' \frac{(1 + V\cdot\sqrt{\mu\epsilon}\cos\alpha')}{\sqrt{1 - (V^2/c^2)}} \quad . \tag{2.29}$$

Using the above formula for frequency transformation twice, the mirror effect in a material medium can be found in the same way as in the vacuum case. For a monochromatic electromagnetic wave normally incident on a perfect moving reflector with velocity V in a material medium, the frequency in the reflected wave is

$$\frac{\omega_r}{\omega_i} = \frac{1 + V\sqrt{\mu\epsilon}}{1 - V\sqrt{\mu\epsilon}} = \frac{1 + V/v_p}{1 - V/v_p} \tag{2.30}$$

where $v_p = \frac{1}{\sqrt{\mu\epsilon}}$ is the phase velocity of the electromagnetic wave in the material media. Equation (2.30) is for the case when the reflector moves against the incident wave. Since the phase velocity of an electromagnetic wave is reduced by a factor (the index of refraction) in a material medium, we immediately see from Eq. (2.30) that a larger frequency shift can be obtained in a material medium than in vacuum for the same reflector velocity.

In Chapter III we will give a detailed derivation, using the principle of "equality of phases," for the frequency shifts in the reflected and transmitted waves due to a partial reflector in a material medium.

Another kind of Doppler and mirror effect which is of interest for this investigation is that for the case of elastic waves. The four-dimensional wave vector approach is applicable in the case of elastic waves as well as in the case of electromagnetic waves.[11] Thus the frequency of a harmonic elastic wave transforms according to Eq. (2.31) under Lorentz transformations (i.e., Doppler effect):

$$\omega = \omega' \frac{\left(1 + \frac{V}{v} \cos \alpha'\right)}{\sqrt{1 - \frac{V^2}{c^2}}} \quad . \tag{2.31}$$

The notation used in the case of electromagnetic waves is carried over to the case of elastic waves. We note particularly that v denotes the velocity of the elastic wave in the medium. The corresponding mirror effect for elastic waves can be easily obtained using the principle of "equality of phases" as will be demonstrated in Chapter III.

2.4 LORENTZ TRANSFORMATION OF THE ELECTRIC AND MAGNETIC FIELD INTENSITIES

According to the "Principle of Relativity," Maxwell's equations must have the same form in all inertial frames. Therefore, the electric field intensity $\vec{E}$ and magnetic field intensity $\vec{H}$ must transform in such a way that Maxwell's equations remain invariant under the Lorentz transformation.

It is known that the component of the electric and magnetic field intensities are the components of four-dimensional tensors of the second rank[8,12] F_{ik} and G_{ik} and that Maxwell's equations can be written in the four-dimensional form

$$\frac{\partial F_{ik}}{\partial x_\ell} + \frac{\partial F_{k\ell}}{\partial x_i} + \frac{\partial F_{\ell i}}{\partial x_k} = 0 \qquad (2.32)$$

and

$$\frac{\partial G_{ik}}{\partial x_k} = 0 \quad . \qquad (2.33)$$

Thus, the components of the electric and magnetic field intensities transform, under the Lorentz transformation, like the products of the corresponding coordinates of the system (2.2) in Section I2.1. The

transformations are[5] (in M.K.S. system):

$$
\begin{aligned}
B'_{\parallel} &= B_{\parallel} \quad , \quad B'_{\perp} = \frac{1}{\sqrt{1 - \frac{V^2}{c^2}}} \left(\vec{B} - \frac{1}{c^2} \vec{V} \times \vec{E} \right)_{\perp} \quad , \\
E'_{\parallel} &= B_{\parallel} \quad , \quad E'_{\perp} = \frac{1}{\sqrt{1 - \frac{V^2}{c^2}}} \left(\vec{E} + \vec{V} \times \vec{B} \right)_{\perp}
\end{aligned}
\tag{2.34}
$$

$$
\begin{aligned}
H'_{\parallel} &= H_{\parallel} \quad , \quad H'_{\perp} = \frac{1}{\sqrt{1 - \frac{V^2}{c^2}}} \left(\vec{H} - \vec{V} \times \vec{D} \right)_{\perp} \\
D'_{\parallel} &= D_{\parallel} \quad , \quad D'_{\perp} = \frac{1}{\sqrt{1 - \frac{V^2}{c^2}}} \left(\vec{D} + \frac{1}{c^2} \vec{V} \times \vec{H} \right)_{\perp} \quad ,
\end{aligned}
\tag{2.35}
$$

where $\parallel$ denotes components parallel, and $\perp$ components perpendicular to the axis of translation.

For the case $V/c \ll 1$, (2.34) and (2.35) reduce to the approximate formulas:

$$
\begin{aligned}
\vec{B}'_{\parallel} &= \vec{B}_{\parallel} \quad , \quad \vec{B}'_{\perp} = \vec{B}_{\perp} \\
\vec{E}'_{\parallel} &= \vec{E}_{\parallel} \quad , \quad \vec{E}'_{\perp} = \vec{E}_{\perp} + (\vec{V} \times \vec{B})_{\perp} \\
\vec{H}'_{\parallel} &= \vec{H}_{\parallel} \quad , \quad \vec{H}'_{\perp} = \vec{H}_{\perp} - (\vec{V} \times \vec{D})_{\perp}
\end{aligned}
\tag{2.36}
$$

and

$$
\vec{D}'_{\parallel} = \vec{D}_{\parallel} \quad , \quad \vec{D}'_{\perp} = \vec{D}_{\perp} \quad .
\tag{2.37}
$$

2.5 TRANSFORMATION OF TEM WAVE FIELD COMPONENTS; PERMITTIVITY; PERMEABILITY; IMPEDANCE; POYNTING VECTOR UNDER LORENTZ TRANSFORMATION

Consider a uniform TEM wave propagating in an infinite medium with permittivity ϵ_1 and permeability μ_1. Since $\vec{E} \cdot \vec{H} = 0$ in the inertial frame S, we have[8] $E' \cdot H' = 0$ in the inertial frame S'. From Eqs. (2.36) and (2.37), we see that the field components are not rotated in the inertial frame S'. Thus the orientation of the field components is as shown in Fig. 2.4.

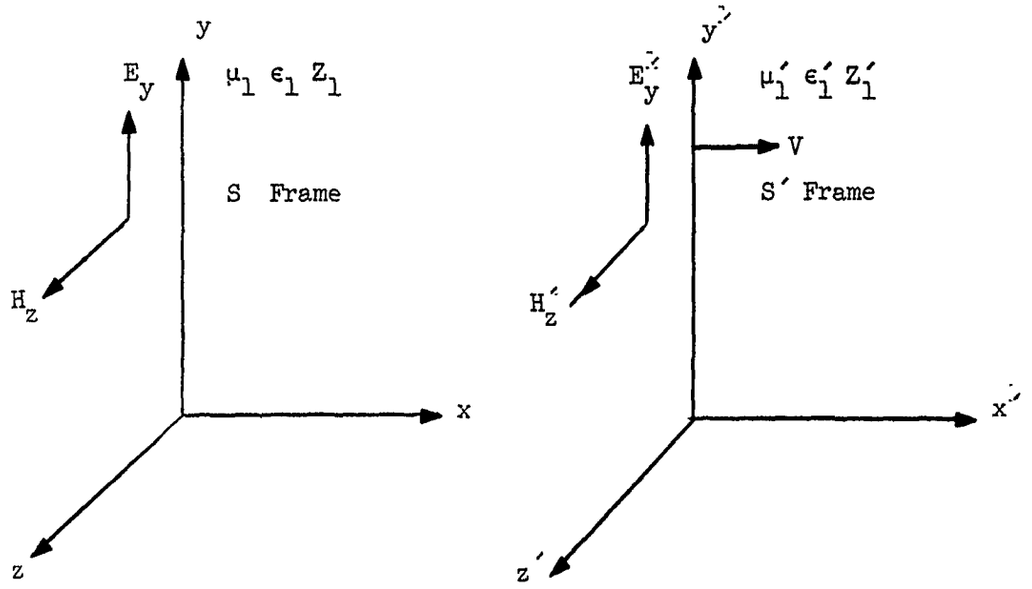

FIG. 2.4--The field components of a uniform TEM wave measured in two inertial frames.

Now, we have the following relations in the S frame:

$$D_y = \epsilon_1 E_y \quad , \quad B_z = \mu_1 H_z \tag{2.38}$$

$$Z_1 \equiv \frac{E_y}{H_z} = \sqrt{\frac{\mu_1}{\epsilon_1}} = \text{Impedance}$$

$$W \equiv \text{Energy Density} = \frac{1}{2}\epsilon_1 E_y^2 \ ;$$

$$\vec{P}_1 \equiv \text{Poynting Vector} = \vec{E} \times \vec{H} = \hat{x} E_y H_z = \hat{x} \frac{E_y^2}{Z_i} \ .$$

Substituting the material equations (2.38) into Eqs. (2.34) and (2.35), we have the transformed field components

$$\begin{cases} B_z' = \dfrac{1}{\sqrt{1 - \dfrac{V^2}{c^2}}} \left(\mu_1 + \dfrac{V}{c^2} \sqrt{\dfrac{\mu_1}{\epsilon_1}} \right) H_z \\ E_y' = \dfrac{1}{\sqrt{1 - \dfrac{V^2}{c^2}}} \left(\sqrt{\dfrac{\mu_1}{\epsilon_1}} + V\mu_1 \right) H_z \\ H_z' = \dfrac{1}{\sqrt{1 - \dfrac{V^2}{c^2}}} \left(1 + V\sqrt{\mu_1 \epsilon_1'} \right) H_z \\ D_y' = \dfrac{1}{\sqrt{1 - \dfrac{V^2}{c^2}}} \left(\sqrt{\mu_1 \epsilon_1'} + \dfrac{V}{c^2} \right) H_z \ . \end{cases} \tag{2.39}$$

Combining Eqs. (2.37) and (2.39), the following transformations in permittivity, permeability, impedance, energy density and Poynting vector are obtained

$$(\epsilon_1')_{yy} \equiv \frac{D_y'}{E_y'} = \frac{\sqrt{\mu_1\epsilon_1'} + V/c^2}{\sqrt{\mu_1/\epsilon_1'} + V\mu_1} \tag{2.40}$$

$$(\mu_1')_{zz} \equiv \frac{B_z'}{H_z'} = \frac{\mu_1 + \frac{V}{c^2}\sqrt{\frac{\mu_1'}{\epsilon_1}}}{1 + V\sqrt{\mu_1\epsilon_1'}} \tag{2.41}$$

$$Z_1' \equiv \frac{E_y'}{H_z'} = \frac{\sqrt{\frac{\mu_1'}{\epsilon_1}} + V\mu_1}{1 + V\sqrt{\mu_1\epsilon_1'}} = \sqrt{\frac{\mu_1'}{\epsilon_1'}} = \sqrt{\frac{\mu_1}{\epsilon_1}} = Z_1 \tag{2.42}$$

$$\vec{P}_1' \equiv \vec{E}' \times \vec{H}' = \hat{x}' E_y' H_z' = \hat{x}' \left(\frac{1 + V\sqrt{\mu_1\epsilon_1'}}{\sqrt{1 - \frac{V^2}{c^2}}} \right)^2 E_y H_z$$

$$= \left(\frac{1 + V\sqrt{\mu_1\epsilon_1'}}{\sqrt{1 - \frac{V^2}{c^2}}} \right)^2 \vec{P}_1 \quad , \tag{2.43}$$

and

$$W' = \frac{1}{2}\epsilon_1' E_y'^2 = \left(\frac{\sqrt{\mu_1\epsilon_1'} + V/c^2}{\sqrt{\frac{\mu_1}{\epsilon_1}} + V\mu_1} \right) \left(\frac{1 + V\sqrt{\mu_1\epsilon_1'}}{\sqrt{1 - \frac{V^2}{c^2}}} \right)^2 E_y^2$$

$$= \frac{(\sqrt{\mu_1\epsilon_1'} + V/c^2)(1 + V\sqrt{\mu_1\epsilon_1'})}{\sqrt{\mu_1\epsilon_1'}\left(1 - \frac{V^2}{c^2}\right)} W \quad . \tag{2.44}$$

From Eqs. (2.40) – (2.44), we conclude that only the impedance of the TEM wave is invariant under the Lorentz transformation, while the permittivity, permeability, energy density and the Poynting vector are not. The invariant nature of the impedance should imply a special importance of the impedance concept in the field of moving electrodynamics. It is obvious that when $V \to 0$, Eqs. (2.40) – (2.44) all reduce to well known results.

2.6 ELECTRODYNAMICS OF MOVING MEDIA

As indicated in Section 2.4, the form of Maxwell's equations is invariant under the Lorentz transformation, according to the principle of relativity. Thus, the form of Maxwell's equations in a moving medium remains the same as in the medium at rest. But, as illustrated by the simple example in the preceding section, the macroscopic parameters ϵ and μ are subject to transformation under the Lorentz transformation. This may be ascribed to an actual change in the structure of matter in motion.[13]

The components of $\vec{E}$ and $\vec{B}$, and that of $\vec{D}$ and $\vec{H}$ separately constitute four-dimensional tensors F_{ik} and G_{ik} . We define the velocity four-vector[8] of the medium U_i as

$$U_1 = \frac{V_x}{\sqrt{1 - \frac{V^2}{c^2}}} \quad , \quad U_2 = \frac{V_y}{\sqrt{1 - \frac{V^2}{c^2}}} \quad , \quad U_3 = \frac{V_z}{\sqrt{1 - \frac{V^2}{c^2}}} \quad , \quad U_4 = \frac{i}{\sqrt{1 - \frac{V^2}{c^2}}} \tag{2.45}$$

The combinations $F_{ik}U_k$ and $G_{ik}U_k$ can be made to obtain the desired relations between $\vec{D}$ and $\vec{E}$, $\vec{B}$ and $\vec{H}$ in a moving medium which generalize the relations $\vec{D} = \epsilon\vec{E}$ and $\vec{B} = \mu\vec{H}$ valid in a medium at rest.

The results are as follows:

$$\vec{D} + \frac{1}{c^2}\vec{V} \times \vec{H} = \epsilon(\vec{E} + \vec{V} \times \vec{B}) \tag{2.46}$$

and

$$\vec{B} - \frac{1}{c^2}\vec{V} \times \vec{E} = \mu(\vec{H} - \vec{V} \times \vec{D}) \quad . \tag{2.47}$$

These formulae were first derived by Minkowski. Notice that these formulae can also be obtained directly from Eqs. (2.34) and (2.35). They show the most distinctive nature of the relativistic electrodynamics of a moving media and should be coupled to the Maxwell's equations in solving the problem. We note that $\vec{V}$ denotes either the constant velocity of the moving medium or the relative velocity of the inertial frame for the Lorentz transformation. Thus we cannot distinguish between motion of the inertial frame and motion of the medium.

From Eqs. (2.46) and (2.47) we note that a medium which is isotropic in its electromagnetic properties acquires anisotropic properties when it moves. This is why the permittivity and permeability in Eq. (2.40) and (2.41) were written as components of a tensor. The degree of anisotropy depends on the direction of the velocity of the medium with respect to that of the field components. Also, the higher the velocity the larger the degree of anisotropy.

Notice that Eqs. (2.46) and (2.47) can be combined and written in a simpler form:

$$\vec{D}_{\|} = \epsilon\vec{E}_{\|} \quad , \quad \vec{B}_{\|} = \mu\vec{H}_{\|}$$

$$(1 - \epsilon\mu V^2)\,\vec{D}_{\perp} = \epsilon\left(1 - \frac{V^2}{c^2}\right)\vec{E}_{\perp} + \left(\epsilon\mu - \frac{1}{c^2}\right)\vec{V} \times \vec{H} \tag{2.48}$$

$$(1 - \epsilon\mu V^2)\,\vec{B}_{\perp} = \mu\left(1 - \frac{V^2}{c^2}\right)\vec{H}_{\perp} + \left(\frac{1}{c^2} - \epsilon\mu\right)\vec{V} \times \vec{E} \quad .$$

When $V/c \ll 1$, $\epsilon\mu V^2 \ll 1$, and $\epsilon\mu$ does not much differ from $\epsilon_0\mu_0$ these become, retaining only the first order in V/c ,

$$\vec{D}_{\parallel} = \epsilon\vec{E}_{\parallel}$$

$$\vec{B}_{\parallel} = \mu\vec{H}_{\parallel}$$

$$\vec{D}_{\perp} \simeq \epsilon\vec{E}_{\perp} + \epsilon\mu\left(1 - \frac{1}{\epsilon\mu c^2}\right)\vec{V} \times \vec{H} \qquad (2.49)$$

$$\vec{B}_{\perp} \simeq \mu\vec{H}_{\perp} - \epsilon\mu\left(1 - \frac{1}{\epsilon\mu c^2}\right)\vec{V} \times \vec{E} \quad .$$

For a medium with high $\epsilon\mu$, the term $1/\epsilon\mu c^2$ can be ignored.

Another distinctive feature of the moving electrodynamics is the change in boundary conditions on Maxwell's equations. From the equations $\text{div}\,\vec{D} = 0$ and $\text{div}\,\vec{B} = 0$, the continuity of the normal components of $\vec{B}$ and $\vec{D}$ is seen to be the same as for the case of a boundary at rest, i.e.,

$$D_{n1} = D_{n2} \ , \ B_{n1} = B_{n2} \quad . \qquad (2.50)$$

By contrast the tangential boundary conditions are different at a moving boundary. In this case the tangential components of $\vec{E} + \vec{V} \times \vec{B}$ and $\vec{H} - \vec{V} \times \vec{D}$ are continuous. This can be easily demonstrated by transforming $\vec{E}$, $\vec{H}$, $\vec{D}$, $\vec{B}$ into an inertial frame which is att- hed to the moving boundary. The tangential electric and magnetic field intensity measured in this inertial frame are

$$\frac{1}{\sqrt{1 - \frac{V^2}{c^2}}}\left(\vec{E} + \vec{V} \times \vec{B}\right)_{\perp}$$

and

$$\frac{1}{\sqrt{1 - \frac{V^2}{c^2}}} \left(\vec{H} - \vec{V} \times \vec{D}\right)_{\perp} \quad ,$$

respectively, and they are continuous in this inertial frame. Thus, we have

$$\begin{aligned} \left(\vec{E} + \vec{V} \times \vec{B}\right)_{1 \text{ tangential}} &= \left(\vec{E} + \vec{V} \times \vec{B}\right)_{2 \text{ tangential}} \\ \left(\vec{H} - \vec{V} \times \vec{D}\right)_{1 \text{ tangential}} &= \left(\vec{H} - \vec{V} \times \vec{D}\right)_{2 \text{ tangential}} \quad . \end{aligned} \tag{2.51}$$

CHAPTER III

WAVE INTERACTIONS WITH MOVING BOUNDARIES

When a wave, either electromagnetic or elastic, impinges upon a moving boundary or interface separating two different media, an interaction will occur. Both the frequency and amplitude of the reflected and transmitted waves are changed. This is just the double Doppler effect described in Chapter II. The double Doppler effect will be analyzed, using electromagnetic waves and the effect extended to include elastic waves, in the following chapters.

There are several physical configurations in which a moving boundary or interface separates two different media. The most general case is the one in which the medium behind the interface is also in motion and its velocity differs from that of the interface. The shock wave formation in a gas or fluid is a typical example of this general case. A moving plasma or beam of charged particles in free space is an example in which the medium behind the interface moves with the same velocity as the interface. The simplest case is the one in which the medium behind the interface is at rest. This is the case, as will be shown, of most interest in this study.

After solving the general case in Section 3.1, the investigation is concentrated on the simplest case. A moving interface separating two media at rest might be induced by applying a step function electric or magnetic field to a nonlinear dielectric or magnetic medium. The case in which the medium behind the interface is moving with a nonrelativistic velocity equal to that of the interface is also treated briefly. There may be a number of applications of this model (e.g., the plasma piston, referred to in Chapter I).

3.1. REFLECTION AND REFRACTION OF ELECTROMAGNETIC WAVES AT A MOVING BOUNDARY OR INTERFACE -- - GENERAL CASE

First, consider Fig. 3.1. The abrupt interface, which is in the y-z plane, divides the unbounded space into two regions. Medium 1 is stationary, homogeneous, dispersionless and has permeability μ_1 and permittivity ϵ_1 , while medium 2 moves with velocity V_2 and has permeability μ_2 and permittivity ϵ_2 in its own frame of reference. It is also assumed that medium 2 is homogeneous and dispersionless in its own frame of reference. The abrupt interface is assumed to move with velocity V .

Consider a uniform TEM wave of frequency ω_i and wave vector $\vec{K}_i$ incident upon the moving interface. The frequency and wave vector of the reflected and transmitted wave are ω_r , $\vec{K}_r$ and ω_t , $\vec{K}_t$, respectively. Let α_i , α_r , α_t be the angles between $\vec{K}_i$, $\vec{K}_r$, $\vec{K}_t$ and the normal to the interface $\vec{n}$, respectively; $\vec{K}_i$, $\vec{K}_r$ and $\vec{K}_t$ are all in the x-z plane. All of these wave parameters are measured in the laboratory frame. We now set forth to determine the frequency shifts and amplitude changes in the reflected and transmitted waves.

3.1.1. Frequency Shifts in the Reflected and Transmitted Waves

Let us write the incident, reflected and transmitted waves as

$$A_i \, e^{j(\omega_i t - \vec{K}_i \cdot \vec{r})} \quad ,$$

$$A_r \, e^{j(\omega_r t - \vec{K}_r \cdot \vec{r})} \quad ,$$

and

$$A_t \, e^{j(\omega_t t - \vec{K}_t \cdot \vec{r})} \quad ,$$

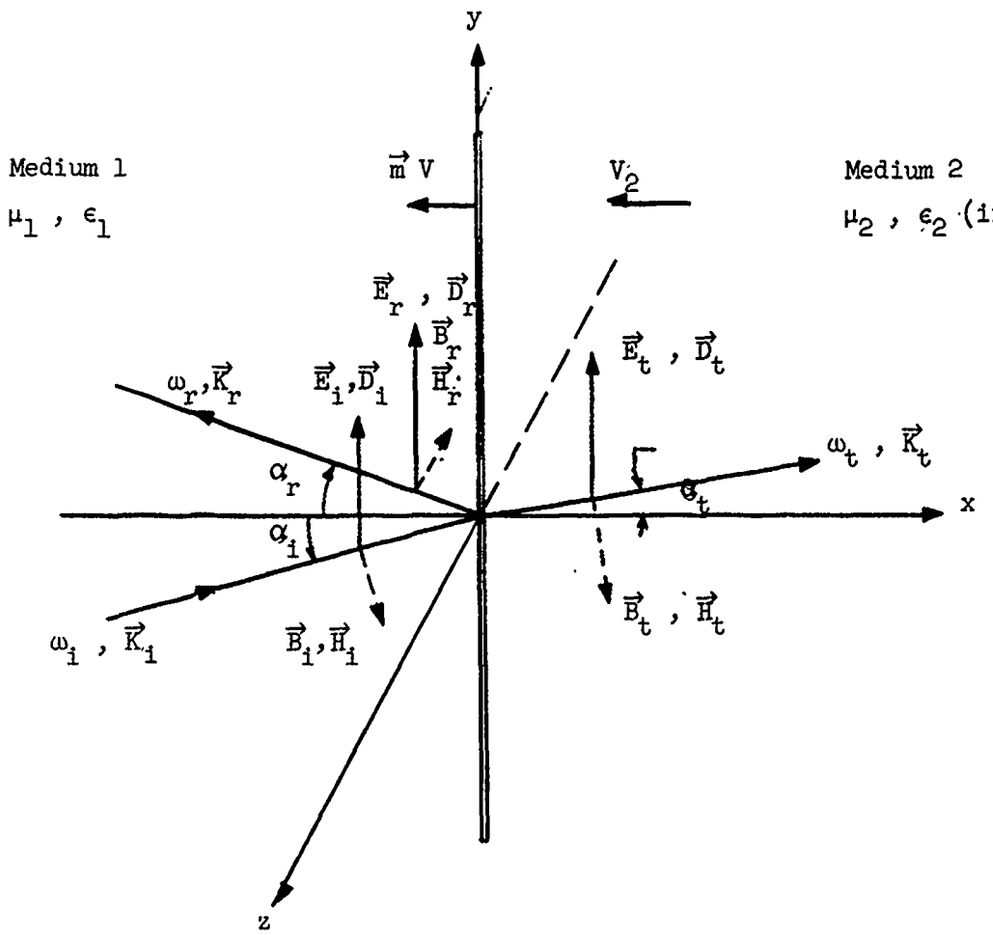

FIG. 3.1--Configuration of a uniform TEM wave interacting with a moving boundary – general case.

respectively, where A_i , A_r and A_t designate the corresponding field amplitudes. To satisfy the boundary condition on the interface at all times, the phases of the three waves are required to be equal at all points on the interface and at all times. (This is the principle of "equality of phases" which has been referred to in the previous chapter.) This condition leads to Eqs. (3.1) and (3.2),

$$\vec{n} \times \vec{K}_i = \vec{n} \times \vec{K}_r = \vec{n} \times \vec{K}_t \quad ,$$

i.e.,

$$K_i \sin \alpha_i = K_r \sin \alpha_r = K_t \sin \alpha_t \equiv I_1 \quad ; \tag{3.1}$$

$$\omega_i - \vec{K}_i \cdot \vec{V} = \omega_r - \vec{K}_r \cdot \vec{V} = \omega_t - \vec{K}_t \cdot \vec{V}$$

i.e.,

$$\omega_i + K_i V \cos \alpha_i = \omega_r - K_r V \cos \alpha_r = \omega_t + K_t V \cos \alpha_t \equiv - I_2 \quad . \tag{3.2}$$

In terms of the mks system, the ω and K for each wave are furthermore related by[14]

$$\frac{\omega_i^2}{c^2} - K_i^2 + \chi_i \cdot \frac{(\omega_i - \vec{K}_i \cdot \vec{V}_i)^2}{1 - (V_i/c)^2} = 0 \quad , \tag{3.3}$$

where

$$\chi_i \equiv \epsilon_i \mu_i - \frac{1}{c^2} \quad , \quad i = 1,2$$

c = velocity of light in vacuum $= \frac{1}{\mu_0 \epsilon_0}$

V_i = velocity of the medium i .

Since medium 1 is stationary, and medium 2 is in motion, Eq. (3.3) gives

for $i = 1$,

$$K_i = \sqrt{\mu_1 \epsilon_1}\ \omega_i \tag{3.4}$$

$$K_r = \sqrt{\mu_1 \epsilon_1}\ \omega_r \tag{3.5}$$

for $i = 2$,

$$\frac{\omega_t^2}{c^2} - K_t^2 + \chi_2 \cdot \frac{(\omega_t + cK_t\ \beta_2 \cos \alpha_t)^2}{1 - \beta_2^2} = 0 \quad , \tag{3.6}$$

where

$$\beta_2 \equiv \frac{V_2}{c} \quad .$$

We notice that the relation given by Eq. (3.6) agrees with that given by Eqs. (2.46) and (2.47). Both show that a medium which is isotropic in its electromagnetic properties acquires anisotropic properties when it moves. From Eqs. (3.1), (3.2) and (3.4), we have

$$I_1 = \omega_i \sqrt{\mu_1 \epsilon_1}\ \sin \alpha_i \tag{3.7}$$

$$I_2 = -\omega_i (1 + \beta c \sqrt{\mu_1 \epsilon_1}\ \cos \alpha_i) \tag{3.8}$$

where

$$\beta \equiv \frac{V}{c} \quad .$$

After some algebraic manipulations [combining the first set of equations of (3.1) and (3.2), see Appendix A.], ω_r and K_{rx} (normal component of K_r with respect to the interface) are obtained:

$$\omega_r = \omega_i \frac{(1 + \mu_1\epsilon_1 c^2\beta^2) + 2\beta c \sqrt{\mu_1\epsilon_1} \cos \alpha_i}{1 - \mu_1\epsilon_1 c^2\beta^2} \tag{3.9}$$

$$K_{rx} = -\omega_i \frac{\sqrt{\mu_1\epsilon_1}(1 + \mu_1\epsilon_1 c^2\beta^2) \cos \alpha_i + 2\mu_1\epsilon_1 c\beta}{1 - \mu_1\epsilon_1 c^2\beta^2} \tag{3.10}$$

Similarly, by combining the second set of equations of (3.1) and (3.2), ω_t and K_{tx} (normal component of K_t with respect to the interface) are obtained:

$$\omega_t = -(I_2) \frac{1 + \chi_2 c^2 \beta_2 \cdot \frac{\beta - \beta_2}{1 - \beta_2^2} - \beta \sqrt{1 + \chi_2 c^2 + \left(\frac{I_1}{I_2}\right)^2 \left[\frac{\chi_2 c^2 (\beta - \beta_2)^2}{1 - \beta_2^2} - (1 - \beta^2)\right]}}{(1 - \beta^2) - \chi_2 c^2 \cdot \frac{(\beta - \beta_2)^2}{1 - \beta_2^2}} \tag{3.11}$$

$$K_{tx} = -(I_2) \cdot \frac{-\left[\beta + \chi_2 c^2 \cdot \frac{\beta - \beta_2}{1 - \beta_2^2}\right] + \sqrt{1 + \chi_2 c^2 + \left(\frac{I_1}{I_2}\right)^2 \left[\frac{\chi_2 c^2 (\beta - \beta_2)^2}{1 - \beta_2^2} - (1 - \beta^2)\right]}}{(1 - \beta^2) - \chi_2 c^2 \cdot \frac{(\beta - \beta_2)^2}{(1 - \beta_2^2)}} \tag{3.12}$$

It is obvious that the expressions for ω_r , K_{rx} , and ω_t , K_{tx} become very complicated when the medium behind the interface is in motion.

Finally, it is important to note that the principle of equality of phases for all waves on the interface, as used in this section for determining the frequency shifts, also applies for the elastic case.[15]

Consider the configuration shown in Fig. 3.2. A monochromatic acoustic wave is obliquely incident upon a moving discontinuity or abrupt-interface such as the one induced by shock waves in an infinite acoustic medium. We consider the simple case in which both medium 1 and 2 are stationary. As a consequence of the interaction between the acoustic waves and the moving interface, the reflected and transmitted waves are shifted in frequency and changed in amplitude. We assume that all of the wave vectors lie in the same plane (x-z plane) and $\vec{n}$ is the unit normal of the interface. The notations for the frequencies, wave vectors, angles of incidence, reflection and refraction are as shown. They are all measured in the laboratory frame. Furthermore, V , v_1 and v_2 are the velocity of the interface, acoustic wave velocity in medium 1 and 2, respectively.

From the principle of "equality of phases", we have the relations

$$\omega_i - \vec{K}_i \cdot \vec{V} = \omega_r - \vec{K}_r \cdot \vec{V} = \omega_t - \vec{K}_t \cdot \vec{V} \qquad (3.13)$$

and

$$\vec{n} \times \vec{K}_i = \vec{n} \times \vec{K}_r = \vec{n} \times \vec{K}_t \quad , \qquad (3.14)$$

at all points on the interface and at all times. Solving the first set of equations in Eqs. (3.13) and (3.14), we have

$$\frac{\omega_r}{\omega_i} = \left(\frac{1 + (V/v_1) \cos \theta_i}{1 + (V/v_1) \cos \theta_r} \right) \qquad (3.15)$$

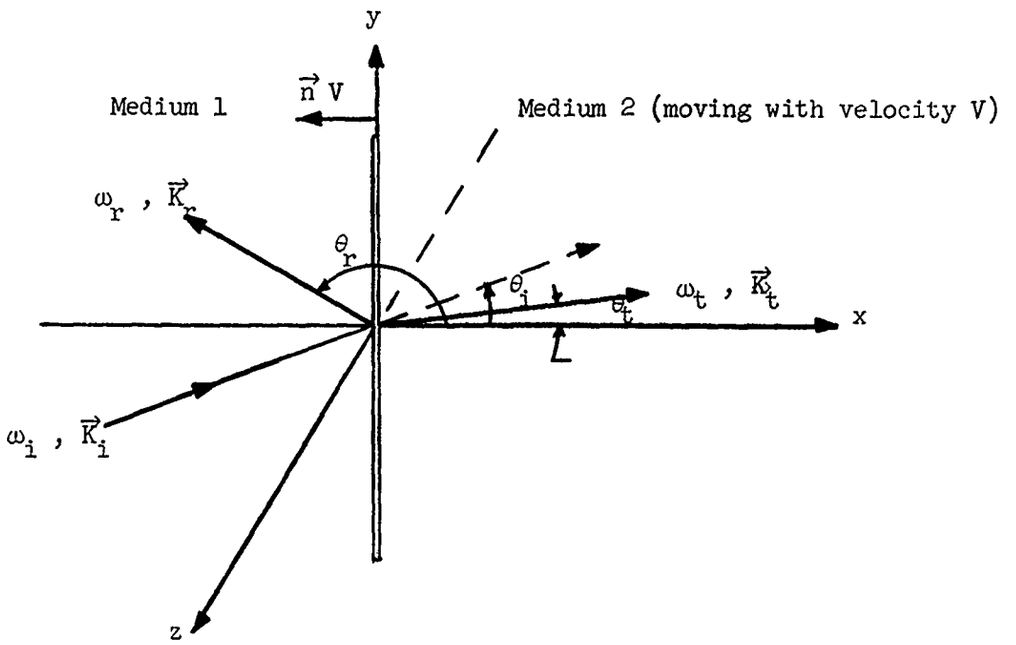

FIG. 3.2--The configuration of a monochromatic acoustic wave interacting with a moving boundary.

and

$$\left(\frac{1 + (V/v_1) \cos \theta_i}{\sin \theta_i}\right) = \left(\frac{1 + (V/v_1) \cos \theta_r}{\sin \theta_r}\right) \quad . \quad (3.16)$$

Similarly, solving the second set of equations in Eqs. (3.13) and (3.14), we have

$$\frac{\omega_t}{\omega_i} = \left(\frac{1 + (V/v_1) \cos \theta_i}{1 + (V/v_2) \cos \theta_t}\right) \quad (3.17)$$

and

$$\left(\frac{1 + (V/v_1) \cos \theta_i}{\sin \theta_i}\right) = \left(\frac{1 + (V/v_2) \cos \theta_t}{\sin \theta_t}\right) \quad . \quad (3.18)$$

Equations (3.15) and (3.17) determine the frequency shifts in the reflected and transmitted waves, respectively, wheareas Eqs. (3.16) and (3.18) determine the angles of reflection and refraction, respectively.

3.1.2. Amplitude Changes in the Reflected and Transmitted Waves

Let $\vec{E}_i$, $\vec{E}_r$ and $\vec{E}_t$ be the electric field intensities for the incident, reflected and transmitted waves, respectively. The corresponding $\vec{D}$, $\vec{B}$, $\vec{H}$ are designated in the same way. The procedures for calculating $\vec{E}_r$ and $\vec{E}_t$, and hence the reflection and transmission coefficients, are summarized here, while the detailed manipulations are shown in Appendix A.

(1) write down all of the field components in medium 1. Since medium 1 is at rest, the well known relations of $D = \epsilon_1 E$, $B = \mu_1 H$ hold.

(2) Write down all of the field components in medium 2. Since medium 2 is in motion, the relations $D = \epsilon E$ and $B = \mu H$ do not hold. They are replaced by the Minkowski relations:

$$\vec{D}_t + \vec{V}_2 \times \vec{H}_t/c^2 = \epsilon_2(\vec{E}_t + \vec{V}_2 \times \vec{B}_t)$$

$$\vec{B}_t + \vec{E}_t \times \vec{V}_2/c^2 = \mu_2(\vec{H}_t + \vec{D}_t \times \vec{V}_2) \quad .$$

(3) Transform all of the field components to the frame which is attached to the moving interface, and apply the boundary condition as shown in Chapter II on the interface, i.e., the tangential components of $\vec{E} + \vec{V} \times \vec{B}$ and $\vec{H} - \vec{V} \times \vec{D}$ are continuous on the interface.

(4) Two equations relating $\vec{E}_i$, $\vec{E}_r$ and $\vec{E}_t$ will result from section (3), and $\vec{E}_r$, $\vec{E}_t$ can be solved in terms of E_i .

The two simultaneous equations relating $\vec{E}_i$, $\vec{E}_r$ and $\vec{E}_t$ are as follows

$$[\omega_i\omega_r - c\beta\omega_r(K_{ix} - K_{tx})] E_i + [\omega_i\omega_r - c\beta\omega_i(K_{tx} - K_{rx})] E_r - \omega_i\omega_r E_t = 0 \qquad (3.19)$$

$$\begin{aligned} &\omega_i[\mu_2(K_{ix} + c\mu_1\epsilon_1\beta\omega_i)(1 - \beta_2^2 \cos\alpha_t) \\ &\quad - \mu_1 K_{ix}(1 - \mu_2\epsilon_2\beta_2^2 c^2 \cos\alpha_t + \beta\beta_2\mu_2\epsilon_2 c^2 - \beta\beta_2)] E_i \\ &+ \omega_i[\mu_2(K_{rx} + c\mu_1\epsilon_1\beta\omega_i)(1 - \beta_2^2 \cos\alpha_t) \\ &\quad - \mu_1 K_{ix}(1 - \mu_2\epsilon_2\beta_2^2 c^2 \cos\alpha_t + \beta\beta_2\mu_2\epsilon_2 c^2 - \beta\beta_2)] E_r \\ &+ [\omega_i\omega_r(\mu_1\mu_2\epsilon_2\beta c^2 + \mu_1\beta_2(\beta\beta_2 + \mu_2\epsilon_2 c^2 - 1)\cos\alpha_t] E_t = 0 \quad . \end{aligned} \qquad (3.20)$$

3.2. REFLECTION AND REFRACTION OF ELECTROMAGNETIC WAVES AT A MOVING INTERFACE — NORMAL INCIDENCE, MOVING MEDIUM (NONRELATIVISTIC)

The interaction of a uniform TEM wave at the boundary of a non-relativistic moving medium will be discussed in this section. As shown in Fig. 3.3, the velocity of the boundary is equal to that of the medium. The case of normal incidence is considered.

3.2.1. Frequency Shifts in the Reflected and Transmitted Waves

Imposing the equality of the phases for the incident, reflected and transmitted waves on the boundary at all time, we have

$$\omega_i - \vec{K}_i \cdot \vec{V} = \omega_r - \vec{K}_r \cdot \vec{V} = \omega_t - \vec{K}_t \cdot \vec{V} \quad . \tag{3.21}$$

The relations between the frequency and the wave vector for the three waves are

$$\omega_i = \frac{1}{\sqrt{\mu_1 \epsilon_1}} K_i = V_{p_i} K_i \tag{3.22}$$

$$\omega_r = \frac{1}{\sqrt{\mu_1 \epsilon_1}} K_r = V_{p_r} K_r \tag{3.23}$$

$$\frac{\omega_t^2}{c^2} - K_t^2 + \left(\mu_2 \epsilon_2 - \frac{1}{c^2}\right) \frac{(\omega_t - K_t V)^2}{\left(1 - \frac{V^2}{c^2}\right)} = 0 \quad . \tag{3.24}$$

For the case of interest, $V/c \ll 1$ and Eq. (3.24) reduces to

$$\omega_t^2 - \frac{2V[\mu_2 \epsilon_2 - (1/c^2)]}{\mu_2 \epsilon_2} K_t \omega_t - \frac{K_t^2}{\mu_2 \epsilon_2} = 0 \quad , \tag{3.25}$$

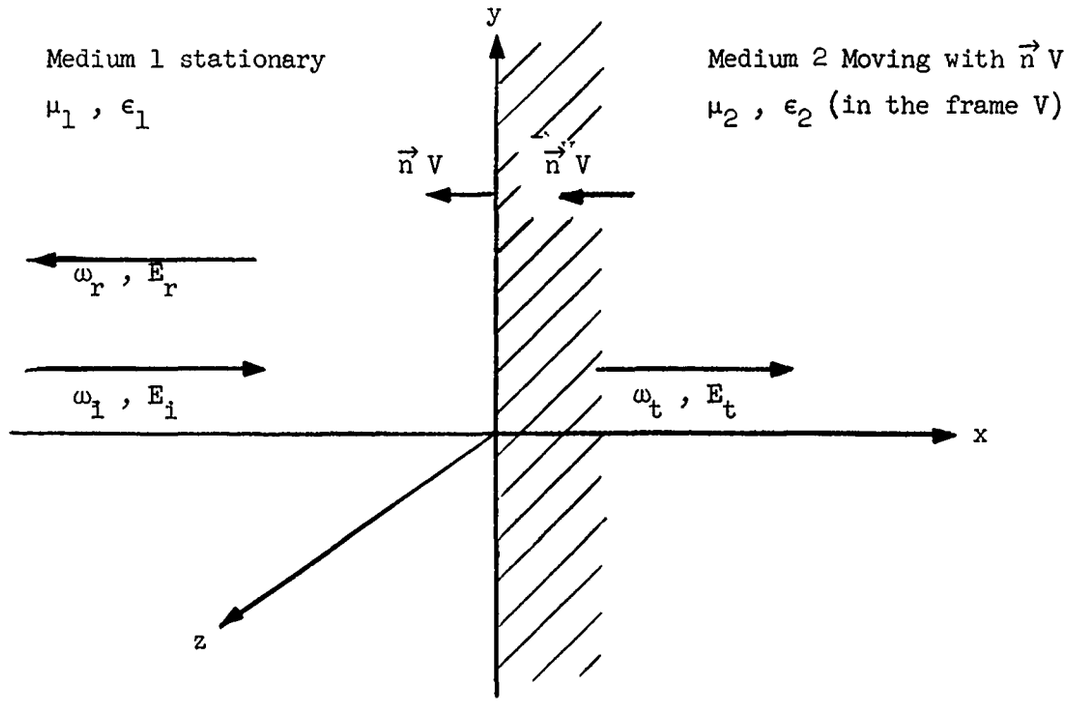

FIG. 3.3--Configuration showing a uniform TEM wave interacting with a moving medium of nonrelativistic velocity.

or

$$\omega_t \simeq \left(\frac{1}{\sqrt{\mu_2\epsilon_2}} + \frac{[\mu_2\epsilon_2 - (1/c^2)]}{\mu_2\epsilon_2} V \right) K_t \quad , \qquad (3.26)$$

for propagation in the positive x-direction, and

$$\omega_t \simeq \left(- \frac{1}{\sqrt{\mu_2\epsilon_2}} + \frac{[\mu_2\epsilon_2 - (1/c^2)]}{\mu_2\epsilon_2} V \right) K_t \quad , \qquad (3.26')$$

for propagation in the reverse direction. Notice that $\{1/\sqrt{\mu_2\epsilon_2}$ $+ [\mu_2\epsilon_2 - (1/c^2)]/\mu_2\epsilon_2 V\}$ is just the effective phase velocity in the moving medium.[16]

By combining Eqs. (3.21) - (3.23) and (3.26), the frequencies of the reflected and transmitted waves are obtained:

$$\frac{\omega_r}{\omega_i} = \frac{1 + V/V_{p_i}}{1 - V/V_{p_i}} \qquad (3.27)$$

$$\frac{\omega_t}{\omega_i} \simeq \frac{\left(1 + \frac{[\mu_2\epsilon_2 - (1/c^2)]}{\sqrt{\mu_2\epsilon_2}} \cdot V \right)(1 + V/V_{p_i})}{\left(1 + \frac{[2\mu_2\epsilon_2 - (1/c^2)]}{\sqrt{\mu_2\epsilon_2}} \cdot V \right)} \quad . \qquad (3.28)$$

For the case $\mu_2\epsilon_2 \gg 1/c^2$ but $2\sqrt{\mu_2\epsilon_2}\,V \ll 1$, Eq. (3.28) reduces to

$$\frac{\omega_t}{\omega_i} \simeq \frac{1 + V/V_{p_i}}{1 + V/V_{p_t}} \quad , \tag{3.29}$$

where

$$V_{p_t} = \frac{1}{\sqrt{\mu_2\epsilon_2}} \quad .$$

For the case of practical interest such as a plasma piston or beam of charged particles, medium 1 will be free space, so that $V_{p_i} = c$ and Eqs. (3.27) - (3.29) reduce to

$$\frac{\omega_r}{\omega_i} = \frac{1 + V/c}{1 - V/c} \quad , \tag{3.30}$$

and

$$\frac{\omega_t}{\omega_i} \simeq \frac{\left(1 + \dfrac{[\mu_2\epsilon_2 - (1/c^2)]}{\sqrt{\mu_2\epsilon_2}} \cdot V\right)(1 + V/c)}{\left(1 + \dfrac{[2\mu_2\epsilon_2 - (1/c^2)]}{\sqrt{\mu_2\epsilon_2}} \cdot V\right)} \tag{3.31}$$

$$\frac{\omega_t}{\omega_i} \simeq \frac{1 + V/c}{1 + V/V_{p_t}} \quad . \tag{3.32}$$

Notice that Eq. (3.30) is just the well known mirror effect, and Eqs. (3.30)-(3.32) give the mirror effect of a partial reflector.

3.2.2. Amplitude Changes in The Reflected and Transmitted Waves

Refer again to Fig. 3.3. The field components for the incident, reflected and transmitted waves are given in Eqs. (3.33), (3.34) and (3.35), respectively:

$$\begin{cases} D_i = \epsilon_1 E_i \\ B_i = \mu_1 H_i \\ H_i = \sqrt{\dfrac{\epsilon_1}{\mu_1}}\, E_i \\ B_i = \sqrt{\mu_1 \epsilon_1}\, E_i \end{cases} \tag{3.33}$$

$$\begin{cases} D_r = \epsilon_1 E_r \\ B_r = \mu_1 H_r \\ H_r = \sqrt{\dfrac{\epsilon_1}{\mu_1}}\, E_r \\ B_r = \sqrt{\mu_1 \epsilon_1}\, E_r \end{cases} \tag{3.34}$$

$$\begin{cases} D_t = \epsilon_2 E_t + (\epsilon_2 \mu_2 - 1/c^2)\, \vec{V} \times \vec{H}_t \\ B_t = \mu_2 H_t + (\epsilon_2 \mu_2 - 1/c^2)\, \vec{E}_t \times \vec{V} \end{cases} \tag{3.35}$$

By substituting Eqs. (3.33) - (3.35) into the boundary conditions (3.36) and (3.37), the amplitudes of the reflected and transmitted waves can be obtained.

$$E_{\text{medium 1}_\perp} - E_{\text{medium 2}_\perp} = \left\{ \vec{V} \times (\vec{B}_{\text{medium 2}} - \vec{B}_{\text{medium 1}}) \right\}_\perp \tag{3.36}$$

$$H_{\text{medium 1}_\perp} - H_{\text{medium 2}_\perp} = \left\{ \vec{V} \times (\vec{D}_{\text{medium 1}} - \vec{D}_{\text{medium 2}}) \right\}_\perp , \tag{3.37}$$

where $\perp$ denotes components tangential to the interface. We omit the detailed calculations of the amplitudes.

3.3. REFLECTION AND REFRACTION OF ELECTROMAGNETIC WAVES AT A MOVING INTERFACE - NORMAL INCIDENCE, STATIONARY MEDIA

In this section we treat the case of great interest in which both the media in front of and behind the interface are stationary, homogeneous and dispersionless (see Fig. 3.4). This will be the case when a step function electric or magnetic field is applied to a nonlinear ferroelectric or ferromagnetic material.

To obtain the frequency shifts and amplitude changes in the reflected and transmitted waves for a uniform TEM wave, we could simply set $\beta_2 = C$ and $\alpha_i = 0$ in the expressions in the first section; but in order to illustrate again the procedures involved in solving this type of boundary value problem, we give the derivation in detail.

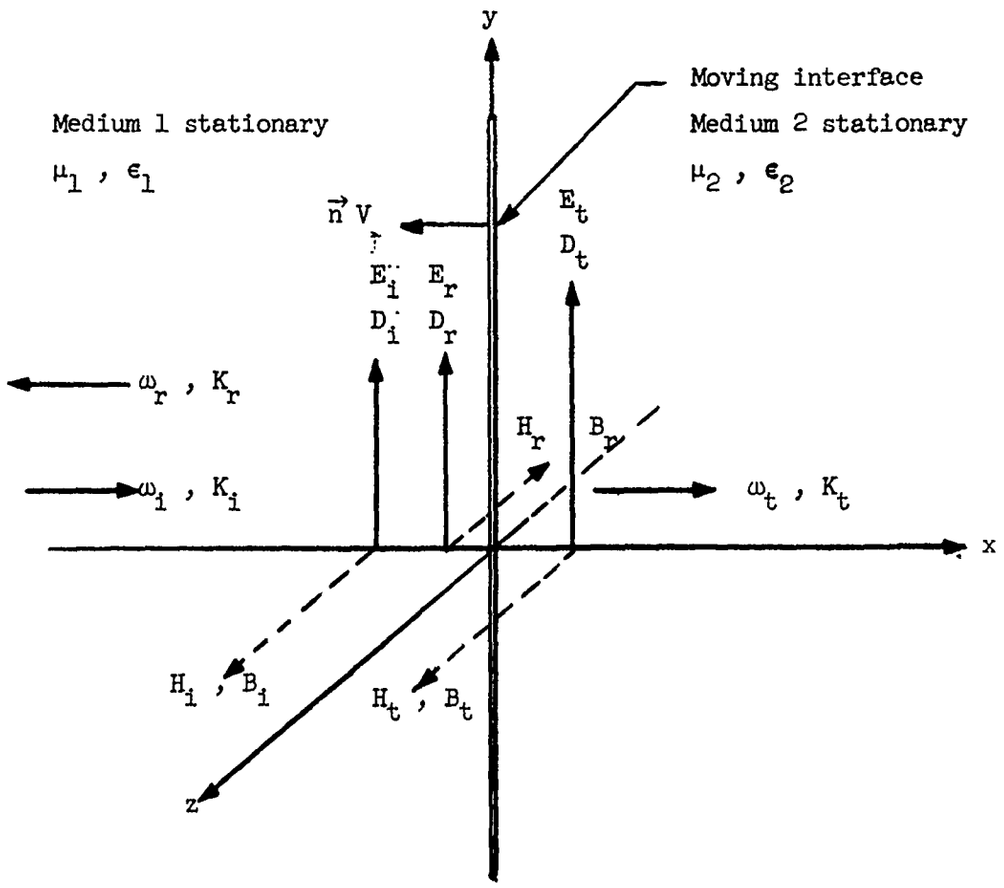

FIG. 3.4--The configuration showing a uniform TEM wave normally incident upon a moving interface separating two media at rest.

3.3.1 Frequency Shifts in The Reflected and Transmitted Waves

From the equality of phases for all waves on the interface at all times, we have

$$\omega_i - \vec{K}_i \cdot \vec{V} = \omega_r - \vec{K}_r \cdot \vec{V} = \omega_t - \vec{K}_t \cdot \vec{V} \quad , \tag{3.38}$$

but

$$\begin{cases} K_i = \omega_i(\mu_1\epsilon_1)^{1/2} = \dfrac{\omega_i}{V_{p_i}} \\ K_r = \omega_r(\mu_1\epsilon_1)^{1/2} = \dfrac{\omega_r}{V_{p_r}} \\ K_t = \omega_t(\mu_2\epsilon_2)^{1/2} = \dfrac{\omega_t}{V_{p_t}} \end{cases} , \tag{3.39}$$

where V_{p_i} , V_{p_r} and V_{p_t} are the phase velocities of the incident, reflected and transmitted waves, respectively.

Combining Eqs. (3.38) and (3.39), the frequencies of the reflected and transmitted waves are obtained:

$$\frac{\omega_r}{\omega_i} = \frac{1 + V/V_{p_i}}{1 - V/V_{p_i}} \tag{3.40}$$

$$\frac{\omega_t}{\omega_i} = \frac{1 + V/V_{p_i}}{1 + V/V_{p_t}} \quad . \tag{3.41}$$

From Eqs. (3.40), (3.41) and (3.27) – (3.29) we see that for the reflected wave the same amount of frequency shift will occur in the case of a moving medium as in the case of a moving interface, while for the transmitted wave, different amounts of frequency shift will occur in

general. For the special case, $\mu_2\epsilon_2 \gg 1/c^2$ but $2\sqrt{\mu_2\epsilon_2}\,V \ll 1$, the amount of frequency shift in the transmitted wave will be the same whether the medium behind the interface moves or not.

Notice that when the interface moves with a velocity comparable to the phase velocity of the wave in medium 1, the frequency up-shift in the reflected wave will be large, and that unless the phase velocities of medium 1 and medium 2 differ greatly, the frequency shift in the transmitted wave will be small. When the interface moves in the same direction as the propagation of the incident wave, the frequency shifts in the reflected and transmitted waves are obtained by changing V into $-V$ in Eqs. (3.40) and (3.41),

$$\frac{\omega_r}{\omega_i} = \frac{1 - V/V_{p_i}}{1 + V/V_{p_i}} \tag{3.42}$$

$$\frac{\omega_t}{\omega_i} = \frac{1 - V/V_{p_i}}{1 - V/V_{p_t}} \quad . \tag{3.43}$$

We further notice that Eqs. (3.40) and (3.42) are analogous to the mirror effect of Chapter II, and we may say that Eqs. (3.40), (3.42), (3.41) and (3.43) describe the mirror effect for a partial reflector.

Finally, we point out the conditions for the existence of the reflected or transmitted wave, or both, for the nondispersive media considered. For the reflected wave to exist the group velocity (in this case the same as the phase velocity) of the reflected wave must be greater than the velocity of the interface when the interface moves

against the incident wave; otherwise the waves cannot "break away" from the interface and therefore are not reflected.[17] This criterion also applies for the case of incident wave and interface moving in the same direction as long as the velocity of the incident wave is greater than that of the interface. When the interface moves against the incident wave, a transmitted wave always exists regardless of interface velocity. On the other hand, when the interface and incident wave move in the same direction for instance, from left to right, the existence of a transmitted wave requires that the velocity of the interface be less than the group velocity (or phase velocity, in this example) in the medium to the right of the interface.

3.3.2 Amplitude Changes in The Reflected and Transmitted Waves

Using the designations for the various field components as shown in Fig. 3.4 and the fact that both medium 1 and medium 2 are stationary, we have the following relations:

$$\begin{cases} D_i = \epsilon_1 E_1 \\ B_i = \mu_1 H_i \\ H_i = \sqrt{(\epsilon_1/\mu_1)}\, E_i \\ B_i = \sqrt{\mu_1 \epsilon_1}\, E_i \end{cases} \tag{3.44}$$

and

$$\begin{cases} D_r = \epsilon_1 E_r \\ B_r = \mu_1 H_r \\ H_r = \sqrt{(\epsilon_1/\mu_1)}\, E_r \\ B_r = \sqrt{\mu_1 \epsilon_1}\, E_r \end{cases} \tag{3.45}$$

$$\begin{cases} D_t = \epsilon_2 E_t \\ B_t = \mu_2 H_t \\ H_t = \sqrt{(\epsilon_2/\mu_2)}\, E_t \\ B_t = \sqrt{\mu_2 \epsilon_2}\, E_t \end{cases} \tag{3.46}$$

The boundary conditions on the interface as shown in Eq. (2.51) can be rewritten in the following form:

$$E_{\text{medium 1}\perp} - E_{\text{medium 2}\perp} = \left\{ \vec{V} \times (\vec{B}_{\text{medium 2}} - \vec{B}_{\text{medium 1}}) \right\}_\perp \tag{3.47}$$

$$H_{\text{medium 1}\perp} - H_{\text{medium 2}\perp} = \left\{ \vec{V} \times (\vec{D}_{\text{medium 1}} - \vec{D}_{\text{medium 2}}) \right\}_\perp , \tag{3.48}$$

where $\perp$ denotes components tangential to the interface.

Now, in our case we have

$$
\begin{aligned}
E_{\text{medium 1}} &= E_i + E_r \\
E_{\text{medium 2}} &= E_t \\
H_{\text{medium 1}} &= H_i - H_r \\
H_{\text{medium 2}} &= H_t \quad .
\end{aligned}
\tag{3.49}
$$

Substituting Eqs. (3.44) - (3.46), and (3.49) into Eqs. (3.47) and (3.48), two equations relating E_i, E_r and E_t are obtained:

$$
(1 - \sqrt{\mu_1\epsilon_1}\,V)\,E_r - (1 + \sqrt{\mu_2\epsilon_2}\,V)\,E_t = -(1 + \sqrt{\mu_1\epsilon_1}\,V)\,E_i
\tag{3.50}
$$

$$
\sqrt{\mu_2\epsilon_1}\,(1 - \sqrt{\mu_1\epsilon_1}\,V)\,E_r + \sqrt{\mu_1\epsilon_2}\,(1 + \sqrt{\mu_2\epsilon_2}\,V)\,E_t
$$

$$
= \sqrt{\mu_2\epsilon_1}\,(1 + \sqrt{\mu_1\epsilon_1}\,V)\,E_i \quad .
\tag{3.51}
$$

The reflection coefficient ρ and transmission coefficient τ are obtained by solving Eqs. (3.50) and (3.57), yielding

$$
\frac{E_r}{E_i} \equiv \rho = \frac{(1 + \sqrt{\mu_1\epsilon_1}\,V)}{(1 - \sqrt{\mu_1\epsilon_1}\,V)} \cdot \frac{(-\sqrt{\mu_2\epsilon_1} - \sqrt{\mu_1\epsilon_2})}{(-\sqrt{\mu_1\epsilon_2} - \sqrt{\mu_2\epsilon_1})}
\tag{3.52}
$$

$$
= \left(\frac{1 + V/V_{p_i}}{1 - V/V_{p_i}}\right)\left(\frac{Z_2 - Z_1}{Z_1 + Z_2}\right)
$$

and

$$\frac{E_t}{E_i} \equiv \tau = \frac{(1 + \sqrt{\mu_1\epsilon_1}\,V)}{(1 + \sqrt{\mu_2\epsilon_2}\,V)} \quad \frac{2\sqrt{\mu_2\epsilon_1}}{(\sqrt{\mu_1\epsilon_2} + \sqrt{\mu_2\epsilon_2})}$$

$$= \left(\frac{1 + V/V_{p_i}}{1 + V/V_{p_t}}\right) \cdot \left(\frac{2Z_2}{Z_1 + Z_2}\right) \quad , \qquad (3.53)$$

where $Z_1 \equiv \sqrt{\mu_1/\epsilon_1}$, $Z_2 \equiv \sqrt{\mu_2/\epsilon_2}$, are the impedances of medium 1 and 2, respectively. As indicated in Chapter II, it is proper to use the stationary impedances as commonly defined, because the quantity $\sqrt{\mu/\epsilon}$ is an invariant under the Lorentz transformation for the case of normal incidence.

From Eqs. (3.52) and (3.53), we see that the reflection and transmission coefficients are those of a stationary interface multiplied by the relativistic factors:

$$\left(\frac{1 + V/V_{p_i}}{1 - V/V_{p_i}}\right)$$

and

$$\left(\frac{1 + V/V_{p_i}}{1 + V/V_{p_t}}\right) \quad ,$$

respectively. We also note that these same relativistic factors appeared in the expressions for the frequency shifts.

These are the most remarkable results of a wave interaction with a moving interface. The appearence of the factors

$$\left(\frac{1 + V/V_{p_i}}{1 - V/V_{p_i}} \right)$$

and

$$\left(\frac{1 + V/V_{p_i}}{1 + V/V_{p_t}} \right)$$

implies a transfer of power to the reflected and transmitted waves from a step-function field which generates a moving interface in a nonlinear medium. When the interface moves against the incident wave with a velocity comparable to V_{p_i} a large frequency shift and power amplification in the reflected wave will be expected. If V and the V_{p_i} of the medium are not comparable, an appropriate slow-wave structure might be employed in order to reduce the phase velocity of the incident wave and thereby increase the frequency shift and amplification. The transformation of power between the pumping step-function and the reflected and transmitted waves will be related to the parametric principle in the latter part of this chapter, and also in Chapter V.

Finally, the power densities (Poynting vector) are given as follows:

$$\begin{aligned} \vec{P}_i &\equiv \vec{E}_i \times \vec{H}_i = \vec{x} \frac{E_i^2}{Z_1} \\ \vec{P}_r &\equiv \vec{E}_r \times \vec{H}_r = -\vec{x} \frac{E_r^2}{Z_1} \\ \vec{P}_t &\equiv \vec{E}_t \times \vec{H}_t = \vec{x} \frac{E_t^2}{Z_2} \end{aligned} \qquad (3.54)$$

Combining Eqs. (3.52) - (3.54), we have

$$\frac{P_r}{P_i} = \left(\frac{E_r}{E_i}\right)^2 = \left(\frac{1 + V/V_{p_i}}{1 - V/V_{p_i}}\right)^2 \cdot \left(\frac{Z_2 - Z_1}{Z_1 + Z_2}\right)^2 \tag{3.55}$$

$$= \left(\frac{\omega_r}{\omega_i}\right)^2 \cdot \left(\frac{Z_2 - Z_1}{Z_1 + Z_2}\right)^2$$

$$\frac{P_t}{P_i} = \left(\frac{E_t}{E_i}\right)^2 \cdot \left(\frac{Z_1}{Z_2}\right) = \left(\frac{1 + V/V_{p_i}}{1 + V/V_{p_t}}\right) \cdot \left(\frac{2\sqrt{Z_1 Z_2}}{Z_1 + Z_2}\right)^2 \tag{3.56}$$

$$= \left(\frac{\omega_t}{\omega_i}\right)^2 \cdot \left(\frac{2\sqrt{Z_1 Z_2}}{Z_1 + Z_2}\right)^2 ,$$

or

$$P_i : P_r : P_t = (\omega_i)^2 : \left[\omega_r\left(\frac{Z_2 - Z_1}{Z_1 + Z_2}\right)\right]^2 : \left[\omega_t\left(\frac{2\sqrt{Z_1 Z_2}}{Z_1 + Z_2}\right)\right]^2 . \tag{3.57}$$

Using Eqs. (3.40), (3.41), (3.55), (3.56) we consider the following special cases:

(a) Perfect transmission: $Z_1 = Z_2$, and $V_{p_i} = V_{p_t}$, that is,

$$\sqrt{\frac{\mu_1}{\epsilon_1}} = \sqrt{\frac{\mu_2}{\epsilon_2}}$$

and

$$\frac{1}{\sqrt{\mu_1\epsilon_1}} = \frac{1}{\sqrt{\mu_2\epsilon_2}} \quad ,$$

then

$$\begin{cases} P_t = P_i \qquad \omega_t = \omega_i \\ P_r = 0 \quad , \quad P_t = P_i \quad , \end{cases} \tag{3.58}$$

and since there is no interface the incident wave is not affected.

(b) Perfect transmission: $Z_1 = Z_2$, but $V_{p_i} \neq V_{p_t}$,

i.e.,

$$\sqrt{\frac{\mu_1}{\epsilon_1}} = \sqrt{\frac{\mu_2}{\epsilon_2}}$$

but

$$\frac{1}{\sqrt{\mu_1\epsilon_1}} \neq \frac{1}{\sqrt{\mu_2\epsilon_2}}$$

then

$$\omega_t = \left(\frac{1 + V/V_{p_i}}{1 + V/V_{p_t}}\right)\omega_i \tag{3.59}$$

$$P_r = 0 \ , \ P_t = \left(\frac{1 + V/V_{p_i}}{1 + V/V_{p_t}}\right)^2 P_i \quad .$$

Thus the moving interface in this case causes the conversion of frequency and power only in the transmitted wave:

(c) A perfect reflection: $Z_2/Z_1 \to 0$ or $\to \infty$, then

$$\omega_r = \left(\frac{1 + V/V_{p_i}}{1 - V/V_{p_i}} \right) \omega_i$$

$$P_r \to \left(\frac{1 + V/V_{p_i}}{1 - V/V_{p_i}} \right)^2 P_i \quad , \quad P_t \to 0 \quad . \qquad (3.60)$$

Thus the moving interface in this case causes conversion of frequency and power only in the reflected wave.

3.4. WAVE INTERACTIONS WITH MOVING SLABS

For the following analysis, a moving slab or series of slabs is considered to be induced by sending a strong electric and magnetic pulse or series of pulses through a nonlinear ferroelectric or a nonlinear ferromagnetic crystal. Thus the slab will not be moving physically, but is defined by a pair of moving interfaces.

The frequency shifts and field amplitude changes due to the moving interfaces which make up the moving slab or series of slabs will be given for the case of normal incidence of a uniform TEM wave.

3.4.1. Frequency Shifts for a Single Moving Slab

For convenience, we assume that the two moving interfaces which make up the moving slab are abrupt. The effect of nonabruptness will be discussed later in the section. The designation of the material constants, the frequencies, and the amplitudes of the waves in the three regions are as shown in Fig. 3.5.

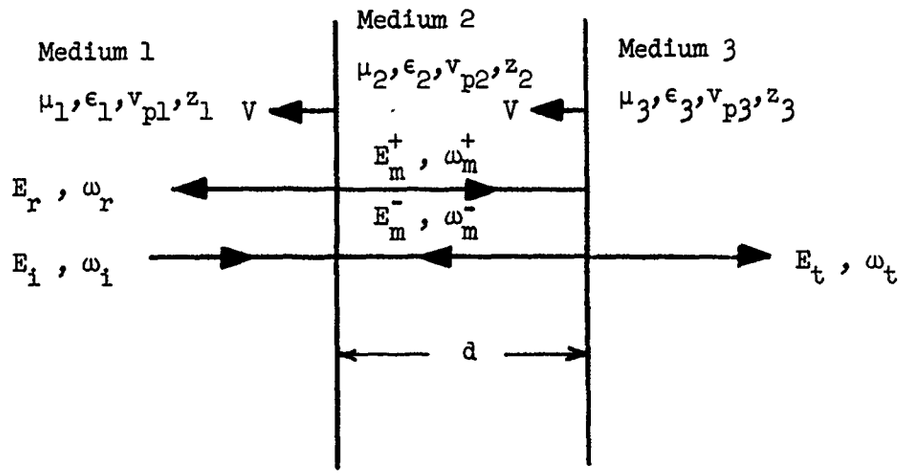

FIG. 3.5--The configuration showing a uniform TEM wave normally incident on two moving interfaces which make up a moving slab.

The equality of phases of the waves at the interfaces 1-2 and 2-3 lead separately to the relations

$$\omega_i - \vec{K}_i \cdot \vec{V} = \omega_r - \vec{K}_r \cdot \vec{V} = \omega_m^+ - \vec{K}_m^+ \cdot \vec{V} = \omega_m^- - \vec{K}_m^- \cdot \vec{V} \qquad (3.61)$$

$$\omega_m^+ - \vec{K}_m^+ \cdot \vec{V} = \omega_m^- - \vec{K}_m^- \cdot \vec{V} = \omega_t - \vec{K}_t \cdot \vec{V} \quad . \qquad (3.62)$$

Solving Eqs. (3.61) and (3.62), we have

$$\frac{\omega_r}{\omega_i} = \frac{1 + V/V_{p_1}}{1 - V/V_{p_1}} \qquad (3.63)$$

$$\frac{\omega_m^+}{\omega_i} = \frac{1 + V/V_{p_1}}{1 + V/V_{p_2}} \quad , \qquad (3.64)$$

and

$$\frac{\omega_m^-}{\omega_i} = \frac{1 + V/V_{p_1}}{1 - V/V_{p_2}} \qquad (3.65)$$

$$\frac{\omega_t}{\omega_i} = \frac{1 + V/V_{p_1}}{1 + V/V_{p_3}} \quad . \qquad (3.66)$$

Notice that when medium 3 is identical to medium 1, $\omega_t/\omega_i = 1$, and there is no frequency shift in the transmitted wave. In practice, the frequency shift in the transmitted wave might be more easily observed than that of reflected wave, as the transmission coefficient will be large except when the transition region is nearly an odd multiple of a quarter wavelength thick.

3.4.2. Wave Matrix for a Single Moving Interface

The method of wave matrices[19] is a powerful analytical tool for the study of multiple slabs. This powerful wave matrix method, which is analogous to the scattering matrix of quantum mechanics, leads to a straightforward calculation of reflection and transmission coefficients in the case of moving periodic structures (or a series of moving interfaces), involving merely matrix multiplication. As a preliminary it will be used in this subsection for calculating the reflection and transmission coefficients at a single interface. The wave matrix [W] is a matrix which relates the amplitudes of the forward- and backward-propagating waves on the output side to those on the input side. For example, consider the stationary system of single discontinuity shown in Fig. 3.6, with a TEM wave propagating from the left side, where A_1^+, A_1^- and A_2^-, A_2^+ designate the electric field amplitudes of the incident and reflected waves at the planes just left and right of the interface, respectively. The wave matrix for this case can be easily obtained by imposing the continuity of tangential components of electric and magnetic fields at the interface. Thus we have

$$\begin{cases} A_1^+ + A_1^- = A_2^+ + A_2^- & (3.67) \\ \dfrac{A_1^+}{Z_1} - \dfrac{A_1^-}{Z_1} = \dfrac{A_2^+}{Z_2} - \dfrac{A_2^-}{Z_2} \quad . & (3.68) \end{cases}$$

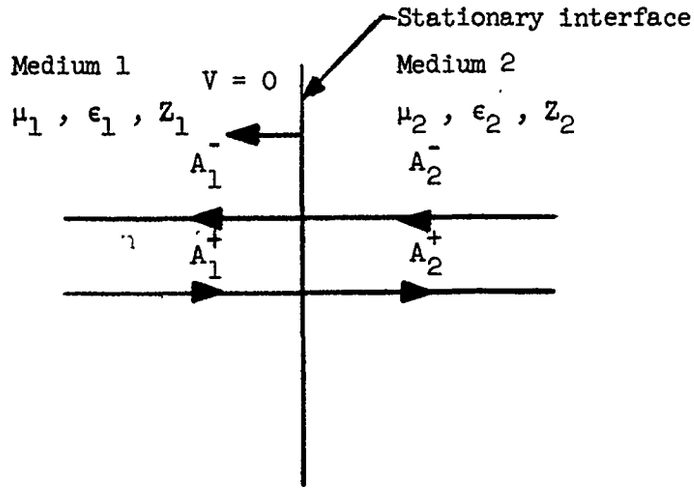

FIG. 3.6--The configuration showing a stationary interface separating two media.

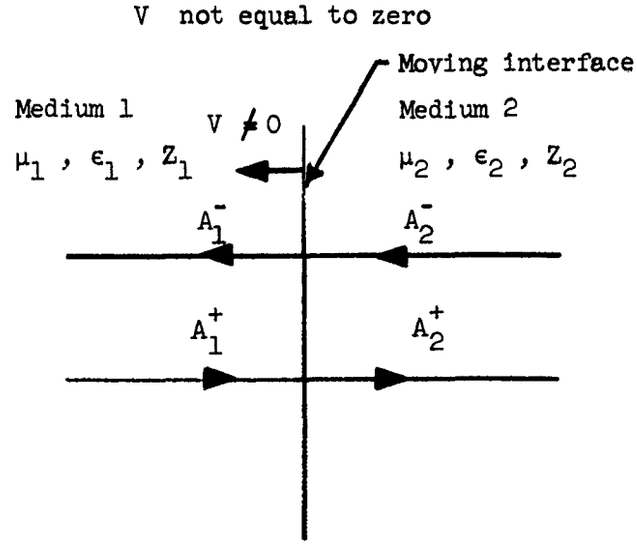

FIG. 3.7--The configuration showing a moving interface separating two media at rest.

Equations (3.67) and (3.68) can be written in a matrix form

$$\begin{bmatrix} A_1^+ \\ \\ A_1^- \end{bmatrix} = [W'] \begin{bmatrix} A_2^+ \\ \\ A_2^- \end{bmatrix} \quad , \qquad (3.69)$$

where the matrix $[W']$ is found to be

$$[W'] = \frac{1}{2} \begin{bmatrix} \left(1 + \frac{Z_1}{Z_2}\right) & \left(1 - \frac{Z_1}{Z_2}\right) \\ \\ \left(1 - \frac{Z_1}{Z_2}\right) & \left(1 + \frac{Z_1}{Z_2}\right) \end{bmatrix} . \qquad (3.70)$$

The elements of the wave matrix can also be written in terms of various reflection and transmission coefficients as

$$[W'] = \begin{bmatrix} W'^{++} & W'^{+-} \\ \\ W'^{-+} & W'^{--} \end{bmatrix} = \begin{bmatrix} \frac{1}{T'_{12}} & \frac{R'_2}{T'_{12}} \\ \\ \frac{R'_1}{T'_{12}} & T'_{21} \frac{R'_1 R'_2}{T'_{12}} \end{bmatrix} . \qquad (3.71)$$

where

T'_{12} , T'_{21} ≡ the transmission coefficients from medium 1 to 2 and medium 2 to 1, respectively,

R'_1 , R'_2 ≡ the reflection coefficients in medium 1 and 2, respectively.

This indicates that the reflection and transmission coefficients can be determined from the wave matrix directly:

$$T'_{12} = \frac{2Z_2}{Z_1 + Z_2} \quad , \quad T'_{21} = \frac{2Z_1}{Z_2 + Z_1}$$

$$R'_1 = \frac{Z_2 - Z_1}{Z_1 + Z_2} \quad , \quad R'_2 = \frac{Z_1 - Z_2}{Z_2 + Z_1} \quad . \tag{3.72}$$

Similarly, the wave matrix [W] for a TEM wave interacting with a moving interface can be obtained by imposing the continuity of tangential components of $\vec{E} + \vec{V} \times \vec{B}$ and $\vec{H} - \vec{V} \times \vec{D}$ on the interface (see Fig. 3.7):

$$\begin{cases} (A_1^+ + A_1^-) + V\mu_1 \left(\dfrac{A_1^+}{Z_1} - \dfrac{A_1^-}{Z_1} \right) \\ \qquad = (A_2^+ + A_2^-) + V\mu_2 \left(\dfrac{A_2^+}{Z_2} - \dfrac{A_2^-}{Z_2} \right) \end{cases} \tag{3.73}$$

$$\begin{cases} \left(\dfrac{A_1^+}{Z_1} - \dfrac{A_1^-}{Z_1} \right) + V\epsilon_1 (A_1^+ + A_1^-) \\ \qquad = \left(\dfrac{A_2^+}{Z_2} - \dfrac{A_2^-}{Z_2} \right) + V\epsilon_2 (A_2^+ + A_2^-) \quad . \end{cases} \tag{3.74}$$

After some manipulations, the wave matrix [W] for the moving interface,

$$\begin{bmatrix} A_1^+ \\ \\ A_1^- \end{bmatrix} = [W] \begin{bmatrix} A_2^+ \\ \\ A_2^- \end{bmatrix} , \qquad (3.75)$$

is found to be

$$[W] = \begin{bmatrix} \left(\frac{1 + V/V_{p_2}}{1 + V/V_{p_1}}\right)\left(\frac{Z_1 + Z_2}{2Z_2}\right) & \left(\frac{1 - V/V_{p_2}}{1 + V/V_{p_1}}\right)\left(\frac{Z_2 - Z_1}{2Z_2}\right) \\ \\ \left(\frac{1 + V/V_{p_2}}{1 - V/V_{p_1}}\right)\left(\frac{Z_2 - Z_1}{2Z_2}\right) & \left(\frac{1 - V/V_{p_2}}{1 - V/V_{p_1}}\right)\left(\frac{Z_2 + Z_1}{2Z_2}\right) \end{bmatrix} . \qquad (3.76)$$

As in Eq. (3.71), [W] can be written as

$$[W] = \begin{bmatrix} W^{++} & W^{+-} \\ \\ W^{-+} & W^{--} \end{bmatrix} = \begin{bmatrix} \frac{1}{T_{12}} & -\frac{R_2}{T_{12}} \\ \\ \frac{R_1}{T_{12}} & T_{21} - \frac{R_1 R_2}{T_{12}} \end{bmatrix} , \qquad (3.77)$$

where the unprimed parameters designate the case of a moving interface.

By comparing Eq. (3.76) with (3.75), we have the reflection and transmission coefficients for the moving interface:

$$\begin{cases} T_{12} = \dfrac{1}{W^{++}} = \left(\dfrac{1 + V/V_{p_1}}{1 + V/V_{p_2}}\right)\left(\dfrac{2Z_2}{Z_1 + Z_2}\right) = \left(\dfrac{1 + V/V_{p_1}}{1 + V/V_{p_2}}\right) T'_{12} \\ R_1 = T_{12}W^{-+} = \left(\dfrac{1 + V/V_{p_1}}{1 - V/V_{p_1}}\right)\left(\dfrac{Z_2 - Z_1}{Z_1 + Z_2}\right) = \left(\dfrac{1 + V/V_{p_1}}{1 - V/V_{p_1}}\right) R'_1 \\ R_2 = -T_{12}W^{+-} = \left(\dfrac{1 - V/V_{p_2}}{1 + V/V_{p_2}}\right)\left(\dfrac{Z_1 - Z_2}{Z_1 + Z_2}\right) = \left(\dfrac{1 - V/V_{p_2}}{1 + V/V_{p_2}}\right) R'_2 \\ T_{21} = W^{--} + \dfrac{R_1R_2}{T_{12}} = \left(\dfrac{1 - V/V_{p_2}}{1 - V/V_{p_1}}\right)\left(\dfrac{2Z_1}{Z_1 + Z_2}\right) = \left(\dfrac{1 - V/V_{p_2}}{1 - V/V_{p_1}}\right) T'_{21} \end{cases} \quad (3.78)$$

These check with Eqs. (3.52) and (3.53), as expected. Note that R_2 and T_{21} can be obtained by transforming 1 to 2 and V to $-V$ in R_1 and T_{12}, respectively.

3.4.3. Reflection and Transmission Coefficients for a Single Moving Slab

Referring to Fig. 3.8 and using the "wave matrix" method as illustrated in the last subsection, we have

$$\begin{bmatrix} A_1^+ \\ \\ A_1^- \end{bmatrix} = [W_1] \begin{bmatrix} A_2^+ \\ \\ A_2^- \end{bmatrix} \tag{3.79}$$

$$\begin{bmatrix} A_2^+ \\ \\ A_2^- \end{bmatrix} = [W_2] \begin{bmatrix} A_2^{+\prime} \\ \\ A_2^{-\prime} \end{bmatrix} \tag{3.80}$$

$$\begin{bmatrix} A_2^{+\prime} \\ \\ A_2^{-\prime} \end{bmatrix} = [W_3] \begin{bmatrix} A_3^+ \\ \\ 0 \end{bmatrix} , \tag{3.81}$$

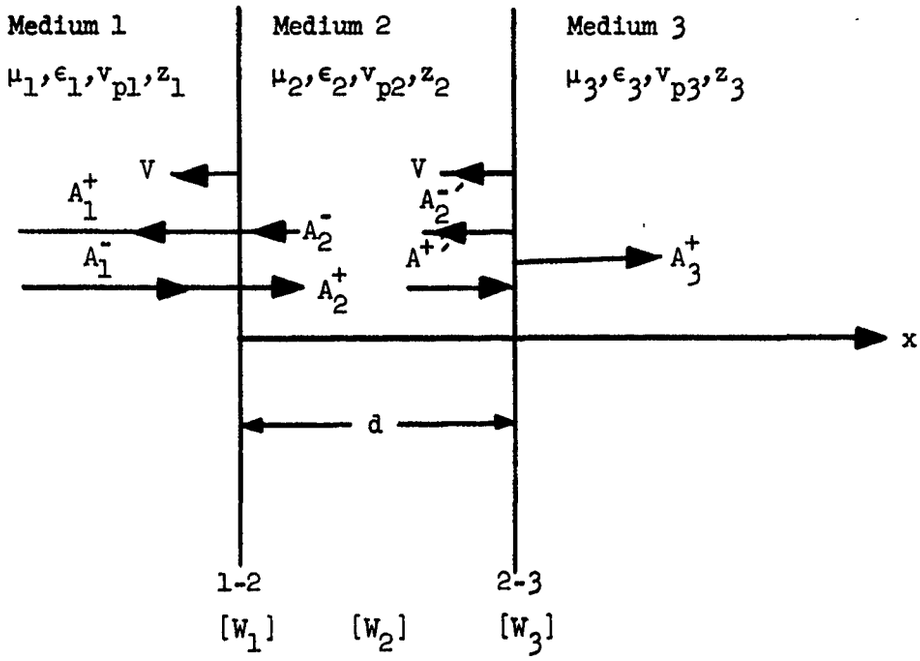

FIG. 3.8--Configuration showing the scattered waves resulting from a uniform TEM wave incident upon a moving slab.

and

$$\begin{bmatrix} A_1^+ \\ \\ A_1^- \end{bmatrix} = [W_1]\,[W_2]\,[W_3] \begin{bmatrix} A_3^+ \\ \\ 0 \end{bmatrix} = [W_T] \begin{bmatrix} A_3^+ \\ \\ 0 \end{bmatrix} , \quad (3.82)$$

where $[W_1]$, $[W_2]$, $[W_3]$ are:

$$[W_1] = \begin{bmatrix} \left(\frac{1 + V/V_{p_2}}{1 + V/V_{p_1}}\right)\left(\frac{Z_1 + Z_2}{2Z_2}\right) & \left(\frac{1 - V/V_{p_2}}{1 + V/V_{p_1}}\right)\left(\frac{Z_2 - Z_1}{2Z_2}\right) \\ \\ \left(\frac{1 + V/V_{p_2}}{1 - V/V_{p_1}}\right)\left(\frac{Z_2 - Z_1}{2Z_2}\right) & \left(\frac{1 - V/V_{p_2}}{1 - V/V_{p_1}}\right)\left(\frac{Z_2 + Z_1}{2Z_2}\right) \end{bmatrix} \quad (3.83)$$

$$[W_2] = \begin{bmatrix} e^{j\beta_{12}^+ d} & 0 \\ \\ 0 & e^{-j\beta_{12}^- d} \end{bmatrix} \quad (3.84)$$

$$[W_3] = \begin{bmatrix} \left(\frac{1 + V/V_{p_3}}{1 + V/V_{p_2}}\right)\left(\frac{Z_2 + Z_3}{2Z_3}\right) & \left(\frac{1 - V/V_{p_3}}{1 + V/V_{p_2}}\right)\left(\frac{Z_3 - Z_2}{2Z_3}\right) \\ \left(\frac{1 + V/V_{p_3}}{1 - V/V_{p_2}}\right)\left(\frac{Z_3 - Z_2}{2Z_3}\right) & \left(\frac{1 - V/V_{p_3}}{1 - V/V_{p_2}}\right)\left(\frac{Z_3 + Z_2}{2Z_3}\right) \end{bmatrix} \tag{3.85}$$

and

$$\beta_{12}^{+} = \left(\frac{1 + V/V_{p_1}}{1 + V/V_{p_2}}\right)\frac{\omega_i}{V_{p_2}} \quad , \quad \beta_{12}^{-} = \left(\frac{1 + V/V_{p_1}}{1 - V/V_{p_2}}\right)\frac{\omega_i}{V_{p_2}} \quad . \tag{3.86}$$

Combining Eqs. (3.82), (3.83), (3.84) and (3.85), we have

$$\begin{bmatrix} A_1^+ \\ \\ A_1^- \end{bmatrix} = \begin{bmatrix} \left(\frac{1 + V/V_{p_3}}{1 + V/V_{p_1}}\right)\left\{ \left(\frac{Z_1+Z_2}{2Z_2}\right)\left(\frac{Z_2+Z_3}{2Z_3}\right) e^{j\beta_{12}^+ d} + \left(\frac{Z_2-Z_1}{2Z_2}\right)\left(\frac{Z_3-Z_2}{2Z_3}\right) e^{-j\beta_{12}^- d} \right\} & \left(\frac{1 - V/V_{p_3}}{1 + V/V_{p_1}}\right)\left\{ \left(\frac{Z_1+Z_2}{2Z_2}\right)\left(\frac{Z_3-Z_2}{2Z_3}\right) e^{j\beta_{12}^+ d} + \left(\frac{Z_2-Z_1}{2Z_2}\right)\left(\frac{Z_3+Z_2}{2Z_3}\right) e^{-j\beta_{12}^- d} \right\} \\ \\ \left(\frac{1 + V/V_{p_3}}{1 - V/V_{p_1}}\right)\left\{ \left(\frac{Z_2-Z_1}{2Z_2}\right)\left(\frac{Z_2+Z_3}{2Z_3}\right) e^{j\beta_{12}^+ d} + \left(\frac{Z_2+Z_1}{2Z_2}\right)\left(\frac{Z_3-Z_2}{2Z_3}\right) e^{-j\beta_{12}^- d} \right\} & \left\{\left(\frac{1 - V/V_{p_3}}{1 + V/V_{p_1}}\right)\cdot\left(\frac{Z_2-Z_1}{2Z_3}\right)\left(\frac{Z_3-Z_2}{2Z_3}\right) e^{j\beta_{12}^+ d} + \left(\frac{1 - V/V_{p_3}}{1 - V/V_{p_1}}\right)\left(\frac{Z_2+Z_1}{2Z_2}\right)\left(\frac{Z_3+Z_2}{2Z_3}\right) e^{-j\beta_{12}^- d} \right\} \end{bmatrix} \begin{bmatrix} A_3^+ \\ \\ 0 \end{bmatrix} \quad (3.87)$$

From the wave matrix of Eq. (3.87), the reflection and transmission coefficients are:

Reflection coefficient

$$R \equiv \frac{A_1^-}{A_1^+} = \left(\frac{1 + V/V_{p_1}}{1 - V/V_{p_1}}\right) \frac{(Z_2 - Z_1)(Z_2 + Z_3)e^{j\beta_{12}^+ d} + (Z_2 + Z_1)(Z_3 - Z_2)e^{-j\beta_{12}^- d}}{(Z_1 + Z_2)(Z_2 + Z_3)e^{j\beta_{12}^+ d} + (Z_2 - Z_1)(Z_3 - Z_2)e^{-j\beta_{12}^- d}} \tag{3.88}$$

Transmission coefficient

$$T \equiv \frac{A_3^+}{A_1^+} = \left(\frac{1 + V/V_{p_1}}{1 + V/V_{p_3}}\right) \frac{4Z_2Z_3}{(Z_1 + Z_2)(Z_2 + Z_3)e^{j\beta_{12}^+ d} + (Z_2 - Z_1)(Z_3 - Z_2)e^{-j\beta_{12}^- d}} \tag{3.89}$$

Notice that the relativistic factors, $[(1 + V/V_{p_1})/(1 - V/V_{p_1})]$ and $[(1 + V/V_{p_1})/(1 + V/V_{p_3})]$, again appear only as multiplicative factors in the reflection and transmission coefficients, respectively. However, from Eq. (3.86) the internal phase shifts also depend upon the motion. It is interesting to see that as V approaches zero, $\beta_{12}^+ = \beta_{12}^- = \omega_i/V_{p_2}$, and the expressions (3.88), (3.89) reduce to those for the stationary slab.[13]

Finally, it is of interest to determine the width of the moving slab, d, for maximum reflection and minimum reflection with fixed values of Z_1, Z_2 and Z_3. Maximum reflection will occur when the waves E_m^+ and E_m^- add in phase on the first interface 1-2. Thus, the width d for

maximum reflection will be determined by the condition,

$$\beta_{12}^{+}d + \beta_{12}^{-}d = 2n\pi \quad , \quad n = 0, 1, 2, \ldots .$$

i.e.,

$$\left(\frac{1 + V/V_{p_1}}{1 + V/V_{p_2}}\right)\frac{\omega_i}{V_{p_2}}\, d + \left(\frac{1 + V/V_{p_1}}{1 - V/V_{p_2}}\right)\frac{\omega_i}{V_{p_2}}\, d = 2n\pi \quad , \quad n = 0, 1, 2, \ldots .$$

and

$$d = \frac{n\pi V_{p_2}(1 - V^2/V_{p_2}^2)}{\omega_i(1 + V/V_{p_1})} \quad , \quad n = 0, 1, 2, \ldots . \qquad (3.90)$$

$$R_{max} = \left(\frac{1 + V/V_{p_1}}{1 - V/V_{p_1}}\right)\left(\frac{Z_3 - Z_1}{Z_1 + Z_3}\right) \quad ; \qquad (3.91)$$

as

$$V \to 0 \quad ,$$

$$d \to \frac{n\pi V_{p_2}}{\omega_i} = \frac{n}{2} \cdot \frac{2\pi}{\omega_i/V_{p_2}} = \frac{n}{2}\lambda_2 \quad , \quad n = 0, 1, 2, \ldots .$$

$$R_{max} \to \left(\frac{Z_3 - Z_1}{Z_1 + Z_3}\right) \quad .$$

This checks with the result for a slab at rest, as it should.

Similarly, minimum reflection will occur when waves E_m^+ and E_m^- add out of phase on the first interface 1-2. Thus, the width d for minimum reflection will be determined by the condition

$$\beta_{12}^+ d + \beta_{12}^- d = n\pi \quad , \quad n = 1, 3, 5, \ldots .$$

and hence

$$d = \frac{n\pi V_{p_2}(1 - V^2/V_{p_2}^2)}{2\omega_i(1 + V/V_{p_1})} \quad , \quad n = 1, 3, 5, \ldots . \tag{3.92}$$

$$R_{min} = -\left(\frac{1 + V/V_{p_1}}{1 - V/V_{p_1}}\right)\left(\frac{Z_1Z_3 - Z_2^2}{Z_1Z_3 + Z_2^2}\right) \quad ; \tag{3.93}$$

as

$$V \to 0 \quad ,$$

$$d \to \frac{n}{4}\lambda_2 \quad , \quad n = 1, 3, 5, \ldots .$$

$$R_{min} \to -\left(\frac{Z_1Z_3 - Z_2^2}{Z_1Z_3 + Z_2^2}\right) \quad .$$

Again, this result checks with that for a slab at rest, as it should.

3.4.4. Frequency Shifts and Amplitude Changes for a Series of Moving Slabs

Consider a transition region consisting of N discontinuities moving with velocities V_1 , V_2 , ... V_{n-1} ; with μ_1 , ϵ_1 ; μ_2 , ϵ_2 , ... ; μ_{n-1} , ϵ_{n-1} ; μ_n , ϵ_n as the parameters of the media as shown

in Fig. 3.9. The results of Section 3.4.1 for two moving discontinuities can be extended by induction to this more complicated case,

$$\frac{\omega_r}{\omega_i} = \frac{1 + V/V_{p_1}}{1 - V/V_{p_1}} \tag{3.94}$$

and

$$\frac{\omega_t}{\omega_i} = \left(\frac{1 + V_1/V_{p_1}}{1 + V_1/V_{p_2}}\right)\left(\frac{1 + V_2/V_{p_2}}{1 + V_2/V_{p_3}}\right) \cdots \cdots \left(\frac{1 + V_{n-2}/V_{p_{n-2}}}{1 + V_{n-2}/V_{p_{n-1}}}\right)\left(\frac{1 + V_{n-1}/V_{p_{n-1}}}{1 + V_{n-1}/V_{p_n}}\right) \tag{3.95}$$

For the case in which all of the interfaces move with the same velocity V, ω_t/ω_i in Eq. (3.95) reduces to

$$\frac{\omega_t}{\omega_i} = \frac{1 + V/V_{p_1}}{1 + V/V_{p_n}} \quad , \tag{3.96}$$

and the frequency shift in the transmitted wave depends only on the parameters of the first and last media. From Eqs. (3.95) and (3.96) we notice that a significant frequency shift can occur in the transmitted wave if $V_1, V_2, \cdots V_{n-2}, V_{n-1}$; $V_{p_1}, V_{p_2} \cdots V_{p_{n-1}}, V_{p_n}$ can be adjusted properly.

Finally, with the wave matrix method described in Section 3.4.2, the problem of calculating the reflection and transmission coefficients for a series of moving slabs reduces to a straightforward matrix multiplication.

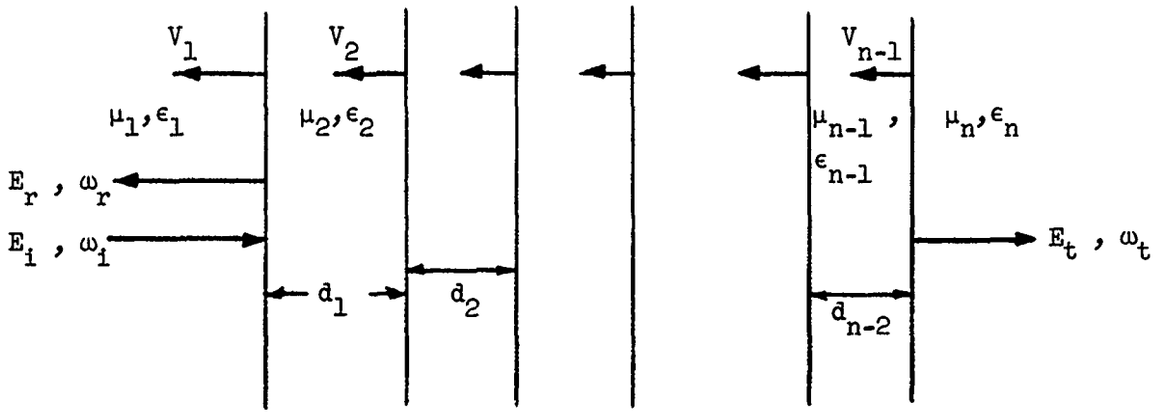

FIG. 3.9--The configuration showing a series of moving interfaces.

This method will be especially powerful when the number of moving slabs is small. In Chapter V, this method will be employed to calculate the reflection and transmission coefficients for a semi-infinite moving periodic structure. Here we only indicate the applicability of this techniques to a ramp-type moving interface or a trapezoid-type moving slab as shown in Figs. 3.10 - 3.12.

3.4.5. The Effects of a Nonabrupt Interface

In all of the previous treatment, an abrupt moving interface was assumed. The abruptness of an interface is, of course, a relative concept. An interface is said to be abrupt if the width of the interface is much smaller than the wavelengths of the waves concerned.

For the field-induced moving interface we considered, e.g., in a nonlinear ferroelectric, an abrupt moving interface requires that three conditions be met: a short rise-time, sufficiently large amplitude voltage step-function, and that the polarization of the mediur can follow the step-function. For example, a strontium titanite single crystal has a large dielectric nonlinearity in the vicinity of its Curie temperature, $37^{\circ}K$. At liquid nitrogen temperature a 12% change of dielectric constant can be produced at an electric field strength of 10 kV/cm. If we assume the velocity of the interface to be of the order of the phase velocity of the material, then for a voltage step-function with typical rise time of one nanosecond the width of the interface will be several wavelengths at S band, and we have a nonabrupt moving interface. A survey of the limitations of nonlinear materials in this respect will be given in Chapter IV.

The results of the frequency shifts in the reflected and transmitted waves obtained for an abrupt moving interface are also valid for a nonabrupt moving interface. This is because a nonabrupt interface can be considered as a series of abrupt interfaces between thin slabs and the principle of equality of phase can be applied to each one. The reflection and transmission coefficients should however, be modified, as a considerable reduction in the reflection is expected for a nonabrupt interface. These conclusions will be elaborated in more detail in the following analysis.

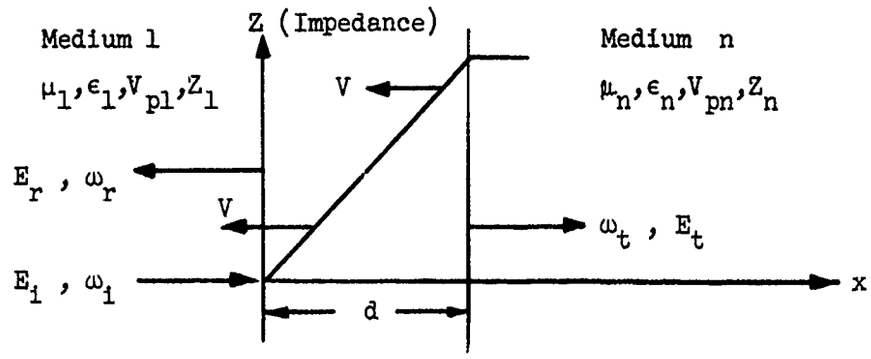

FIG. 3.10--The configuration of a moving ramp-type interface.

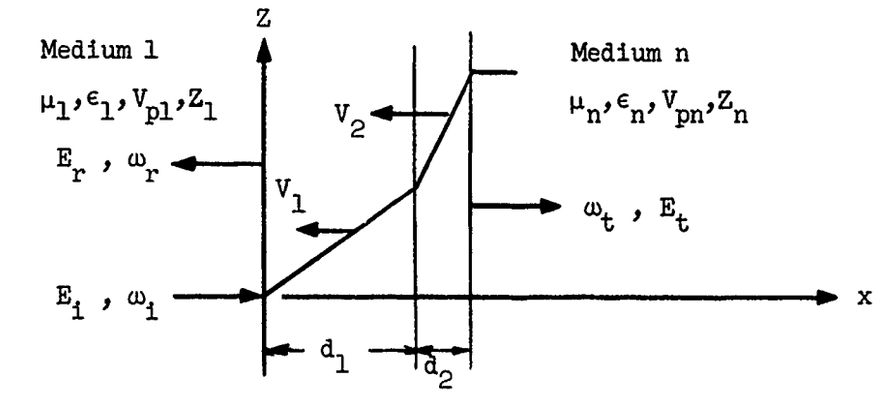

FIG. 3.11--The configuration of a moving "Kinked Ramp" interface.

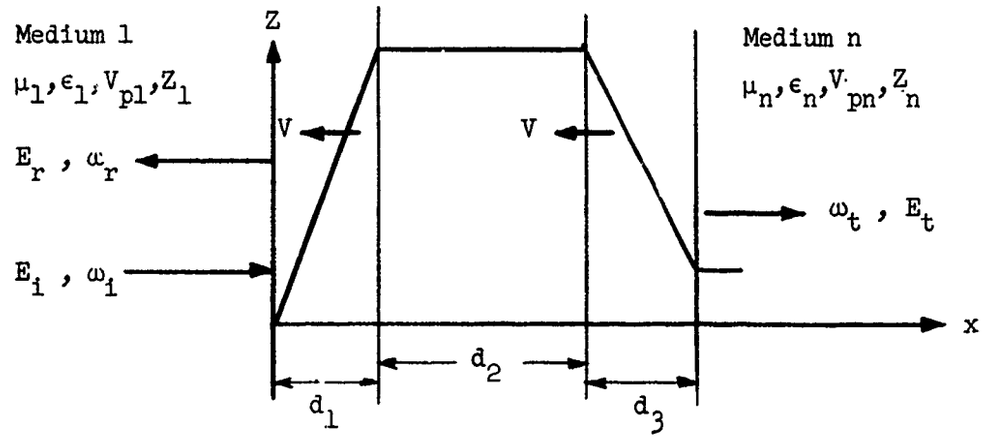

FIG. 3.12--The configuration of a moving trapezoidal slab.

Consider a ramp-type moving interface or moving slab, such as shown in Figs. 3.10 - 3.12. We divide the transition region d into a sufficiently large number of layers such that in each individual layer the material constants μ and ϵ are almost homogeneous. Then, for the configuration of Fig. 3.10 the results in Eqs. (3.94) and (3.96) are valid, because all interfaces move with the same velocity. For the configuration of Fig. 3.11, we again have $\omega_r/\omega_i = (1 + V_1/V_{p_1})/(1 - V_1/V_{p_1})$ and $\omega_t/\omega_i = (1 + V_1/V_{p_1})/(1 + V_2/V_{p_n})$. This shows that the frequency shift is independent of the ramp profile. Similarly, the frequency shifts in the configuration of Fig. 3.12 can be determined. By dividing the transition region d to a proper number of layers such that the width of each layer is considerably smaller than the wavelength of the waves we are interested in, the amplitudes of the reflected and transmitted waves can be easily calculated by multiplying all of the corresponding wave matrices for the interfaces and layers. It would be interesting to carry out a numerical example for a moving ramp-type interface using the wave matrix method and compare the results with that of a stationary ramp-type interface.[20] It appears physically obvious that the reflection must go to zero as the gradient of the ramp approaches zero.

3.5. A TRANSMISSION LINE MODEL FOR FREQUENCY CONVERSION AND AMPLIFICATION AT A MOVING INTERFACE IN A STATIONARY MEDIUM

The frequency shifts and amplitude changes for a uniform TEM wave interacting with a moving interface have been claculated in detail in Section 3.3. In this section, the same results will be derived for the nonrelativistic case using a more intuitive and less mathematical approach, by way of a transmission line analogy. This approach serves to illustrate in more detail how a wave interaction with a moving interface leads to changes in frequency and amplitude.

3.5.1. Frequency Shifts in the Reflected and Transmitted Waves

We consider (see Fig. 3.13) a lossless transmission line, originally uniform with parameters L_1 and C_1, where L_1 is the inductance per unit length and C_1 is the capacitance per unit length. Imagine that the inductors and capacitors are nonlinear and that a pumping step-function of voltage is applied to the line from the right terminal. This creates an interface between regions of different inductance and capacitance, the interface moving with velocity V, as shown. The parameters for the portion of the line behind the interface are L_2 and C_2. We specifically consider the nonrelativistic case, i.e., $V/V_{p_i} \ll 1$, $V/V_{p_t} \ll 1$, where $V_{p_i} = 1/\sqrt{L_1 C_1}$, $V_{p_t} = 1/\sqrt{L_2 C_2}$. When the impedances in the two parts of the line are not equal, both reflection and transmission will be expected.

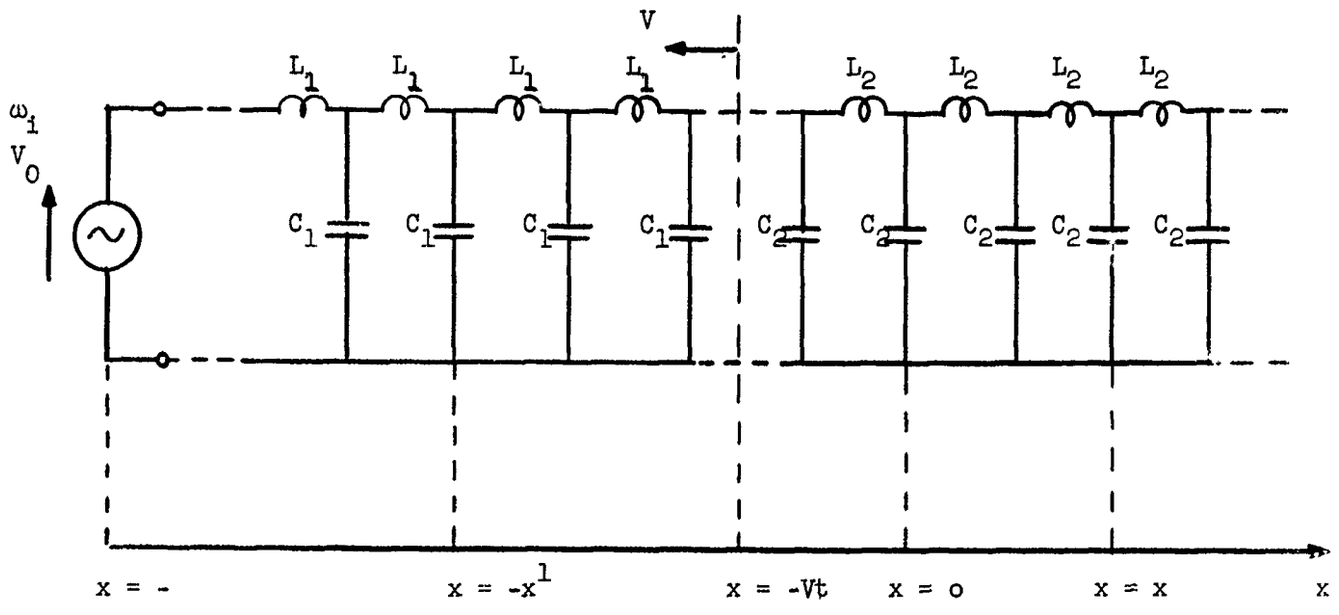

FIG. 3.13--A lossless transmission line with a moving discontinuity. (The coordinate origin is chosen such that at $t = 0$ the moving junction is at $x = 0$ as shown.)

A frequency shift in the reflected voltage is expected, as the phase difference between the reflected voltage and the incident voltage varies linearly with respect to time, because of the motion of the junction. Likewise there will be a frequency shift in the transmitted voltage.

Let the incident voltage from the left terminal be

$$V_i(x,t) = V_0 e^{j(\omega_i t - K_i x)} , \qquad (3.97)$$

where $K_i \equiv \omega_i \sqrt{L_1 C_1} = (\omega_i / V_{p_i})$ = the propagation constant in the left-hand part of the line. Then, for lossless case, the incident voltage at the moving junction will be

$$V_i(x,t)\Big|_{x=-Vt} = V_0 e^{j(\omega_i t - K_i x)}\Big|_{x=-Vt} = V_0 e^{j(\omega_i + K_i V)t} . \qquad (3.98)$$

The reflected and transmitted voltages at the moving junction are

$$V_r(x,t)\Big|_{x=-Vt} = RV_i(x,t)\Big|_{x=-Vt} = RV_0 e^{j(\omega_i + K_i V)t} \qquad (3.99)$$

$$V_t(x,t)\Big|_{x=-Vt} = TV_i(x,t)\Big|_{x=-Vt} = TV_0 e^{j(\omega_i + K_i V)t} , \qquad (3.100)$$

where

$K_t \equiv \omega_t \sqrt{L_2 C_2} = \dfrac{\omega_t}{V_{p_t}}$ = the propagation constant to the right of the interface

$R \equiv$ the reflection coefficient

$T \equiv$ the transmission coefficient .

Here, R and T are not necessarily the same as for the stationary junction.

Let the observation points for the reflected and transmitted voltages be at $x = -x'$ and $x = x''$, respectively, then

$$V_r(x',t) = RV_0 e^{j(\omega_i+K_iV)t} e^{jK_i(x'+Vt)}$$

$$= RV_0 e^{j[(\omega_i+2K_iV)t+K_ix']}$$

$$= RV_0 e^{j[\omega_i(1+2V/V_{p_i})t+K_ix']} , \qquad (3.101)$$

and

$$V_t(x'',t) = TV_0 e^{j(\omega_i+K_i)t} e^{-jK_t(x''+Vt)}$$

$$= TV_0 e^{j\{[\omega_i+(K_i-K_t)V]t-K_tx''\}}$$

$$= TV_0 e^{j\{\omega_i[1+V(1/V_{p_i}-1/V_{p_t})]t-K_tx''\}} \qquad (3.102)$$

From Eqs. (3.101) and (3.102), the frequencies of the reflected and transmitted voltages are identified as $\omega_i[1 + 2 (V/V_{p_i})]$ and $\omega_i[1+V(1/V_{p_i}-1/V_{p_t})]$, respectively. These agree with Eqs. (3.40) and (3.41) for the non-relativistic case.

3.5.2. Calculation of Doppler Amplification from the Principle of Conservation of Energy

In Subsection 3.3.2, it was shown that a moving interface can produce power amplification in the reflected or transmitted waves, or both. One naturally may ask where does this power come from. In this subsection, a

detailed calculation of the power transfer from the moving interface to the transmitted wave will be made for the nonrelativistic case, using the transmission line analogy.

Referring to Fig. 3.14, we imagine that an external mechanical force F is applied to change the spacing of the capacitor plates. For convenience, we consider a nonabrupt interface, e.g., ramp-type transition for which there is no reflected wave. Let the transition move along the line with velocity V . For the direction of motion shown in the figure, the plate spacing increases with time. From the law of conservation of energy the increase in energy of the transmitted wave must equal the mechanical work done on the capacitors.

To illustrate the energy balance, we consider an infinitesimal section of the line Δx as shown in Fig. 3.15, Then we have

$$\text{The power flow } P = \frac{1}{2} IV = \frac{1}{2} \frac{C}{\sqrt{LC}} V^2 = \frac{1}{2} CV^2 V_p \quad . \quad (3.103)$$

$$\text{The capacitive energy density } U \text{ per unit length} = \frac{1}{2} CV^2 = \frac{1}{2} \frac{SQ^2}{\epsilon_0 A} \quad . \quad (3.104)$$

The external force applied per unit length is

$$\frac{dF}{dx} = \frac{\partial U}{\partial S} = \frac{1}{2} \frac{Q^2}{\epsilon_0 A} = \frac{1}{2} \frac{CV^2}{S} \quad , \quad (3.105)$$

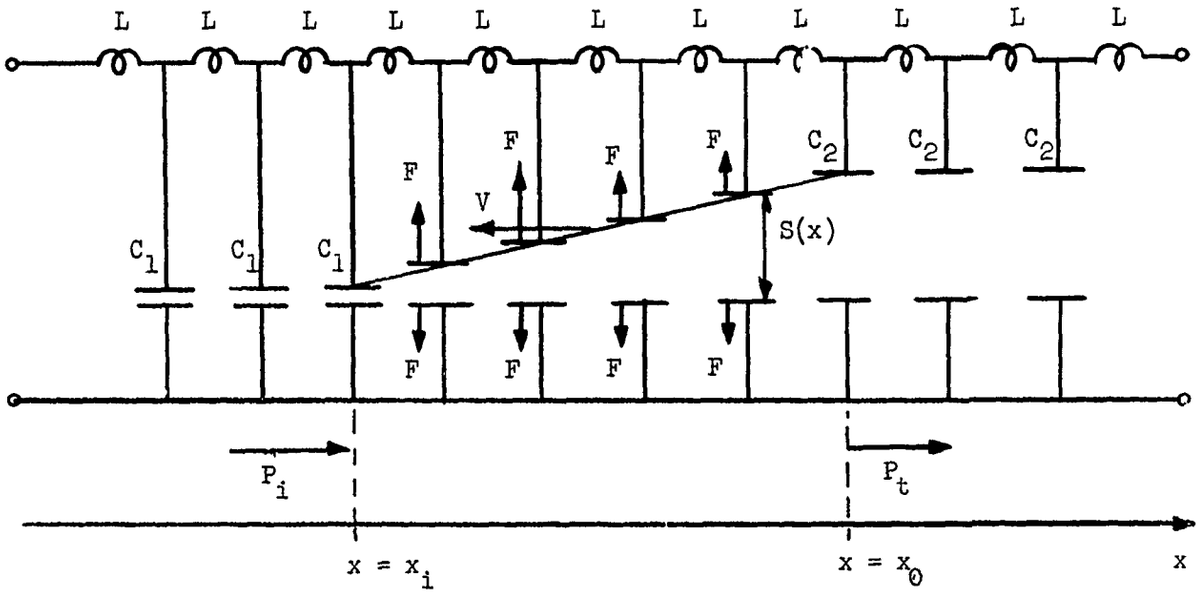

FIG. 3.14--The configuration showing the conversion of power between the pumping source and the transmitted wave using the parametric principle.

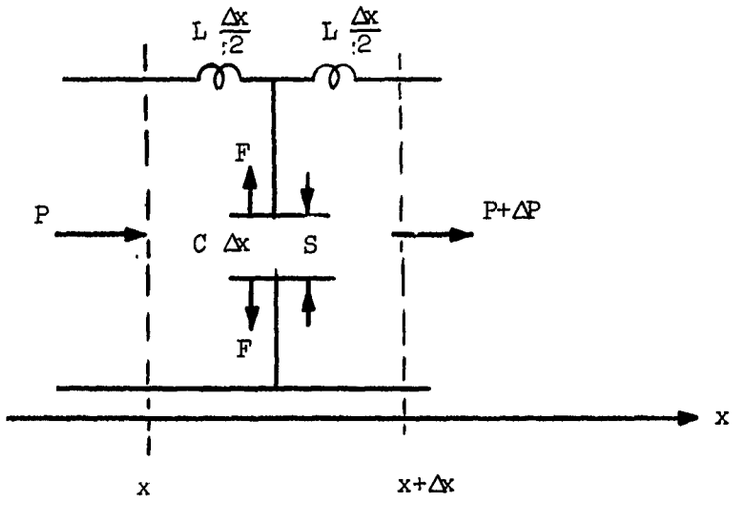

FIG. 3.15--The configuration showing the energy balance for an infinitesimal section of the transmission line.

where

V = line voltage

I = line current

C = capacitance per unit length

L = inductance per unit length

$V_p = 1/\sqrt{LC}$ = phase velocity of the wave

Q = charge per unit length

A = area of the capacitor plate per unit length

S = spacing at the capacitor plates .

From Eqs. (3.105), the external force applied for the infinitesimal section Δx is

$$dF = \frac{1}{2} \frac{CV^2}{S} dx \quad . \tag{3.106}$$

Thus, the mechanical power input to the infinitesimal section Δx is

$$dP = dF \cdot \dot{S} = \frac{1}{2} \frac{\dot{S}}{S} CV^2 dx \quad , \tag{3.107}$$

where $\dot{S}$ is the transverse velocity of the capacitor plate. Combining Eqs. (3.103) and (3.107), we have

$$dP = \frac{\dot{S}}{S} \sqrt{LC} \, P dx = \frac{\dot{S}}{S} \cdot \frac{P}{V_p} dx \quad , \tag{3.108}$$

but

$$\dot{S} = V \frac{dS}{dx} \quad ,$$

$$\frac{1}{V_p} = \sqrt{LC} = \sqrt{L\epsilon_0 A}\, S^{-1/2} \quad ,$$

where dS/dx is the slope of the ramp (Fig. 3.14); therefore

$$dP = \sqrt{L\epsilon_0 A}\, V_p \frac{dS}{S^{3/2}} \quad .$$

Integration yields

$$K + \ln P = -2\sqrt{L\epsilon_0 A}\, V S^{-1/2} = -2\frac{V}{V_p} \quad , \qquad (3.109)$$

where K is an integration constant. Now, at $x = x_i$, we have $V_p = V_{p_i}$ and $P = P_i$; therefore $K = -\ln P_i - 2(V/V_{p_i})$ and

$$\ln \frac{P}{P_i} = 2V\left(\frac{1}{V_{p_i}} - \frac{1}{V_p}\right) \quad ,$$

resulting in

$$P = P_i\, e^{2V(1/V_{p_i} - 1/V_p)} \quad . \qquad (3.110)$$

For $V/V_p \ll 1$, we have

$$P \simeq P_i \left[1 + 2V \left(\frac{1}{V_{p_i}} - \frac{1}{V_p} \right) \right] \quad .$$

At the output terminal $x = x_0$, $V_p = V_{p_t}$, $P = P_t$, and we have

$$P_t \simeq P_i \left[1 + 2V \left(\frac{1}{V_{p_i}} - \frac{1}{V_{p_i}} \right) \right] \quad . \qquad (3.111)$$

This power relation agrees with Eq. (3.59) for the nonrelativistic case.

3.6. THE EFFECTS OF DISPERSION

A medium is said to be spatially dispersive at a given frequency , if the properties of the medium depend on the magnitude of the wave-vector. On the other hand, it is said to be anisotropic if the properties depend upon the direction of the wave-vector. This may occur without spatial dispersion. Acoustic wave propagation in a quartz crystal is an example. Spin wave propagation in a ferromagnetic material is an example of both anisotropy and spatial dispersion. Notice that in above treatment, it has been assumed that the media are spatially dispersionless in their rest frames. But from the Minkowski's relations [Eqs. (2.46) and (2.47)] and Maxwell's equations, it is evident that a medium which is not spatially or frequency dispersive in its own rest frame will become anisotropic when it moves. On the other hand if a medium has frequency dispersion property in its own rest frame, then due to the Doppler effect it will also become spatially dispersive when it moves, i.e., the properties of the medium will depend on the direction of wave propagation at a given frequency. These facts are important for the general case considered in Section 3.1. It is a difficult matter to take these dispersion properties into account for the treatment of wave interactions

with moving medium.[21] For the cases we are specially interested in, only the interface moves and this kind of difficulty will not occur. Thus, within the frequency range for which the material is nondispersive, all of the results on frequency and amplitude obtained previously are valid. At frequencies above this range, the maximum frequency shift in the reflected wave will be limited.

We recall (see Section 3.3.1) that in a nondispersive stationary medium it is the relative velocity of the interface with respect to the group velocity (equal to the phase velocity in this case) which determines the existence of the reflected or transmitted waves. In a dispersive stationary medium the group velocity differs from the phase velocity and may become very small. In this case the reflected wave may vanish over a certain range of frequencies.

In Chapter IV the intrinsically dispersive nature of a ferromagnetic material will be taken into account in calculating the frequency shifts due to a moving interface. It will be found that the maximum frequency shift in the reflected wave is limited by the condition that the group velocity of the reflected wave should be larger than or equal to the velocity of the interface. Furthermore, due to dispersion, the transmitted wave might not exist under certain conditions, and hence total reflection would occur.

3.7. COMPRESSION OF ELECTROMAGNETIC WAVES

It is obvious from the results of Chapter II that the double-Doppler effect produced when an electromagnetic wave is reflected once from a moving reflector is significant only when the velocity of the reflector is close to the phase velocity of the wave in the medium. This is particularly so when the reflector moves with a nonrelativistic velocity.

Although a single reflection from a nonrelativistic moving reflector will in general give a small double-Doppler effect, a considerable enhancement can be obtained by multiple reflection. Thus, it is interesting to know how an electromagnetic wave which is contained by two infinite parallel reflectors changes its frequency and amplitude during the course of multiple

reflection resulting from the motion of the reflectors toward each other. This is essentially the compression of an electromagnetic field. As a consequence of the motion of the reflectors, the frequency of the waves will vary in time. The amplitude of the waves (assuming the lossless case) will also increase in the course of compression due to the reduction of the volume occupied by the waves and the external work done on the waves by the reflectors against the radiation pressure of the waves.

For simplicity, we consider the case of a uniform TEM wave with electric field in the y-direction and magnetic field in the z-direction; see Fig. 3.16. Consider the case where the separation of the two conducting plates (perfect reflectors) is L at $t = 0$, and the second plate starts to move with the velocity V in the direction shown at $t = 0+$. This is an initial and boundary value problem for the Maxwell's Eqs. (3.112) and (3.113) with a moving boundary. For the case of TEM wave considered, Eqs. (3.112) and (3.113) reduce to Eqs. (3.114) and (3.115), where ϵ and μ are the permittivity and the permeability of the medium, respectively:

$$\nabla \times \vec{E} = -\mu \frac{\partial \vec{H}}{\partial t} \tag{3.112}$$

$$\nabla \times \vec{H} = \epsilon \frac{\partial \vec{E}}{\partial t} \tag{3.113}$$

$$\frac{\partial E_y(x,t)}{\partial x} = -\mu \frac{\partial H_z(x,t)}{\partial t} \tag{3.114}$$

$$\frac{\partial H_z(x,t)}{\partial x} = \epsilon \frac{\partial E_y(x,t)}{\partial t} \quad . \tag{3.115}$$

Combining Eqs. (3.114) and (3.115), the wave equation for $E_y(x,t)$ is obtained:

$$\frac{\partial^2 E_y(x,t)}{\partial x^2} - \mu\epsilon \frac{\partial^2 E_y(x,t)}{\partial t^2} = 0 \quad . \tag{3.116}$$

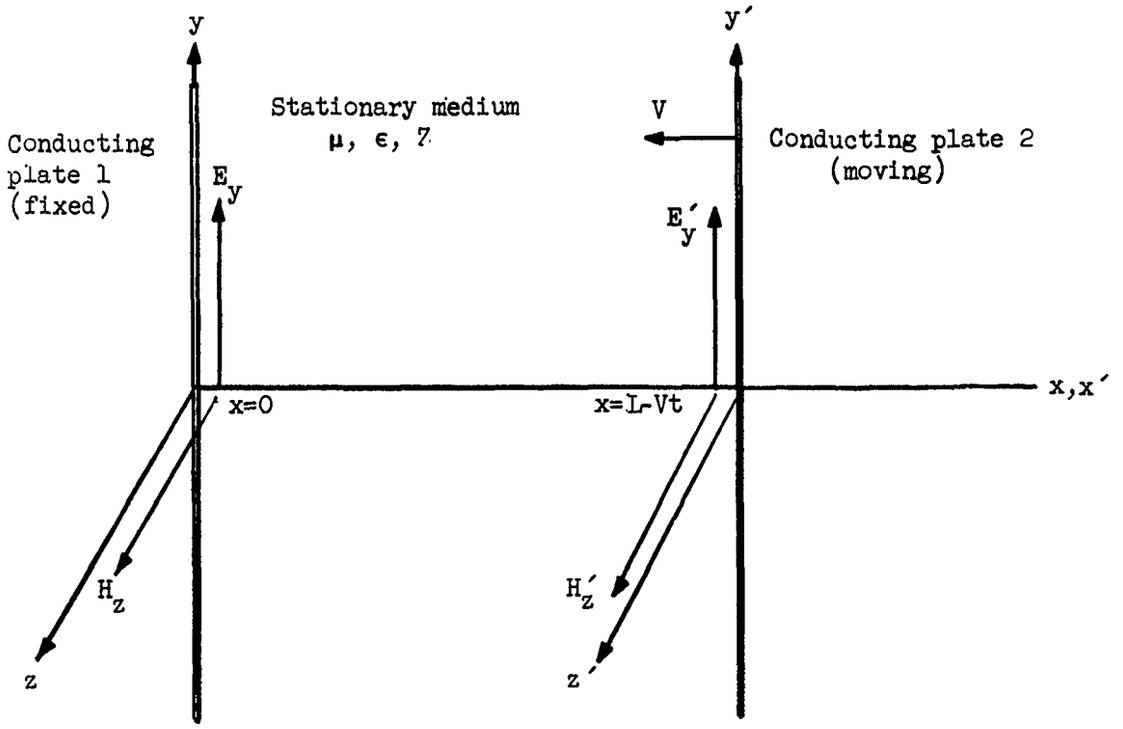

FIG. 3.16--The configuration showing the compression of a uniform TEM wave between two conducting plates (one fixed, one moving).

Since the frequency ω and the amplitude A are functions of time, the field will have the following time dependence:

$$E_y(x,t) = A(t) \left(\sin \int \omega(t)\, dt \right) g(x) \quad , \qquad (3.117)$$

where $\omega(t)$ and $A(t)$ are slowly-varying functions of time compared with the term $\sin \int \omega(t)dt$, and

$$\frac{d\omega(t)}{dt} \ll \omega(t) \quad , \quad \frac{dA(t)}{dt} \ll A(t) \quad .$$

Thus, we have

$$\frac{\partial E_y(x,t)}{\partial t} = A(t)\, \omega(t) \left(\cos \int \omega(t)\, dt \right) g(x) + \dot{A}(t) \left(\sin \int \omega(t)\, dt \right) g(x)$$

or

$$\frac{\partial E_y(x,t)}{\partial t} \simeq A(t)\, \omega(t) \left(\cos \int \omega(t)\, dt \right) g(x) \qquad (3.118)$$

and

$$\frac{\partial^2 E_y(x,t)}{\partial t^2} = - A(t)\, \omega^2(t) \left(\sin \int \omega(t)\, dt \right) g(x) + A(t)\, \dot{\omega}(t) \left(\cos \int \omega(t)\, dt \right) g(x) + \dot{A}(t)\, \omega(t) \left(\cos \int \omega(t)\, dt \right) g(x)$$

or

$$\frac{\partial^2 E_y(x,t)}{\partial t^2} \simeq - A(t)\,\omega^2(t)\left(\sin\int \omega(t)\,dt\right) g(x) \quad ; \quad (3.119)$$

furthermore,

$$\frac{\partial^2 E_y(x,t)}{\partial x^2} = A(t)\left(\sin\int \omega(t)\,dt\right) \ddot{g}(x) \quad . \quad (3.120)$$

Substituting Eqs. (3.119) and (3.120) into Eq. (3.116), we have

$$\left\{\ddot{g}(x) + \mu\epsilon\,\omega^2(t)\,g(x)\right\} A(t)\,\sin\int \omega(t)\,dt = 0 \quad . \quad (3.121)$$

Thus, the solutions of $g(x)$ can be obtained from the differential equation

$$\ddot{g}(x) + \frac{\omega^2(t)}{v_p^2}\,g(x) = 0 \quad . \quad (3.122)$$

The solutions of $g(x)$ are $\sin[\omega(t)/v_p]x$ and $\cos[\omega(t)/v_p]x$, where $v_p = (1/\sqrt{\mu\epsilon})$, is the phase velocity of the wave in the medium.

In order to satisfy the boundary condition on the surface of the fixed reflector 1, i.e., $E_y(0,t) = 0$, $\sin\omega(t)\sqrt{\mu\epsilon}\,x$ must be chosen for $g(x)$. Then we have

$$E_y(x,t) = A(t)\left(\sin\int \omega(t)\right) dt\,\sin\frac{\omega(t)}{v_p}\,x \quad . \quad (3.123)$$

From Eq. (3.115), we have

$$H_z(x,t) = \frac{A(t)}{Z}\left(\cos\int\omega(t)\,dt\right)\cos\frac{\omega(t)}{V_p}\,x \quad , \qquad (3.124)$$

where $Z \equiv \sqrt{\mu/\epsilon}$ is the wave impedance of the medium.

(a) Frequency Variation $\omega(t)$:

Using the Lorentz transformation, the electric field measured in a frame attached to the moving conducting plate 2, $E_y'(x',t')$, is

$$E_y'(x',t') = \frac{1}{\sqrt{1-(V^2/c^2)}}\,(E_y + VB_z)$$

$$= \frac{A(t)}{\sqrt{1-(V^2/c^2)}}\left[\left(\sin\int\omega(t)\,dt\right)\sin\frac{\omega(t)}{V_p}\,x\right.$$

$$\left. + \frac{V\mu}{Z}\left(\cos\int\omega(t)\,dt\right)\cos\frac{\omega(t)}{V_p}\,x\right] \quad ,$$

or

$$E_y'(x',t') = \frac{A(t)}{\sqrt{1-(V^2/c^2)}}\left[\left(\sin\int\omega(t)\,dt\right)\sin\frac{\omega(t)}{V_p}\,x\right.$$

$$\left. + \frac{V}{V_p}\left(\cos\int\omega(t)\,dt\right)\cos\frac{\omega(t)}{V_p}\,x\right] \quad . \qquad (3.125)$$

Now since $E_y'(x',t') = 0$ at $x' = 0$ (i.e., at $x = L - Vt$) we have, from Eq. (3.125),

$$\left(\sin \int \omega(t)\, dt\right) \sin \frac{\omega(t)}{V_p} (L - Vt) + V/V_p \left(\cos \int \omega(t)\, dt\right) \cos \frac{\omega(t)}{V_p} (L - Vt) = 0 \tag{3.126}$$

Notice that the second term is a small perturbation for the nonrelativistic case, in which $V/V_p \ll 1$. Thus the frequency variation in the zero-order approximation, $\omega^0(t)$, for the nonrelativistic case will be determined by Eq. (3.126),

$$\left(\sin \int \omega^0(t)\, dt\right) \sin \frac{\omega^0(t)}{V_p} (L - Vt) = 0 \quad . \tag{3.127}$$

When $\sin \int \omega^0(t)\, dt = 0$, we have

$$\int \omega^0(t)\, dt = n\pi \quad , \quad n = 0, 1, 2, \quad . \tag{3.128}$$

This cannot hold for all times and the frequency condition is $\sin [\omega^0(t)/v_p](L - Vt) = 0$, or

$$\frac{\omega^0(t)}{V_p} (L - Vt) = n\pi \quad , \quad n = 0, 1, 2, \quad . \tag{3.129}$$

From Eq. (3.129) we obtain

$$\omega^0(t) = \frac{n\pi v_p}{(L - Vt)} = \frac{(n\pi v_p)/L}{1 - (V/L)t} = \frac{\omega_0}{1 - (V/L)t} \qquad (3.130)$$

where $\omega_0 = n\pi v_p / L$ is the initial frequency of the fields.

The frequency variation in the zero-order approximation as given by Eq. (3.130) can be simply interpreted by considering that the linear motion of the conducting plate 2 causes the wave number of the resonant system and hence the frequency to increase. As $t \to L/V$ (i.e., when the second plate almost touches the first one), the frequency will increase to a very high value (see Fig. 3.17). The increase in frequency is also explainable by the principle of conservation of the number of photons in the resonant system during the course of comparison while the energy of the resonant system increases due to the work done by the moving conducting plate 2.

To take the perturbation term in Eq. (3.126) into account, we could carry out a first-order approximation by letting

$$\omega^1(t) = \omega^0(t) + \Delta(t) \quad . \qquad (3.131)$$

Substituting Eq. (3.131) into Eq. (3.126) we could, in principle, determine $\Delta(t)$. Since we are particularly interested in the non-relativistic case, the perturbation $\Delta(t)$ will be very small and we omit the calculation.

It is worth noting that the frequency variation obtained by the approach used here checks with that obtained by Kurilko,[22] who treated the same problem in a slightly different way.

Kurilko treated the problem as a transient process by tracing the multiple reflections one by one. The frequency variation of the fields

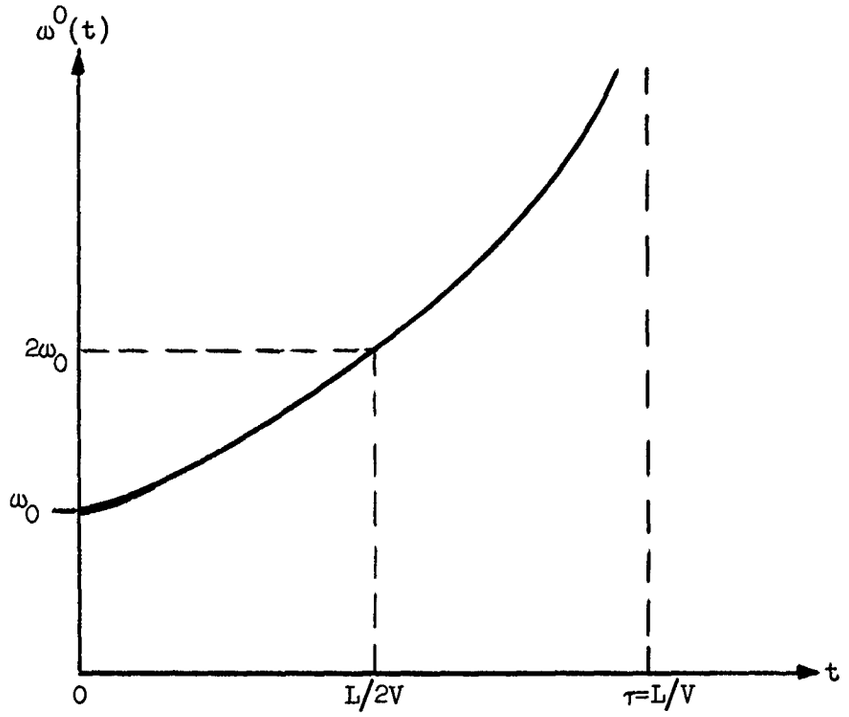

FIG. 3.17--The frequency variation of a uniform TEM wave during the course of compression by two moving conducting plates.

is given as

$$\omega(t) = \omega_0 \, \delta^{-m} \tag{3.132}$$

$$\sum_{m=1}^{\infty} \Delta t_m = \sum_{m=1}^{\infty} \frac{2a}{S + V} \delta^{m-1} \quad , \tag{3.133}$$

where

m = the number of reflections

ω_0 = the frequency of the fields at $t = 0$

δ = $1 - \beta/1 + \beta = S - V/S + V$, $\beta = V/S < 1$

S = the phase velocity of the waves

$\sum_{m=1}^{\infty} \Delta t$ = the sum of the time intervals between two successive reflections.

$2a$ = the separation of the two conducting plates at $t = 0$.

m = the number of reflections .

From Eq. (3.133), we have

$$t = \sum_{m=1}^{\infty} \Delta t_m = \sum_{m=1}^{\infty} \frac{2a}{S + V} \delta^{m-1} = \frac{2a}{S + V} (1 + \delta + \delta^2 + \delta^3 + \ldots)$$

or

$$t = \frac{2a}{S + V} \left(\frac{1 - \delta^m}{1 - \delta} \right) \quad ; \tag{3.134}$$

hence

$$\delta^m = 1 - \frac{2V}{2a} t \quad . \tag{3.135}$$

Substituting Eq. (3.135) into Eq. (3.132), we have the frequency variation,

$$\omega(t) = \omega_0 \frac{1}{1 - (2V/2a)t} \quad . \tag{3.136}$$

By noticing that $2a$ corresponds to L and $2V$ corresponds to V (Kurilko considered the case in which both conducting plates move with velocity V) in our case, we see that the result of Eq. (3.136) checks with that of Eq. (3.131).

(b) Energy Density Variation:

If we adopt the usual definitions of the time average electric energy density $\bar{U}_E$ and the time average magnetic energy density $\bar{U}_M$, we have in zero order

$$\bar{U}_E \equiv \frac{1}{2} \overline{(\vec{D} \cdot \vec{E})} = \frac{\epsilon}{2} \frac{1}{T} \int_0^T A^2(t) \left(\sin \int \omega^0(dt)\, dt \right)^2 \sin^2 \left(\frac{\omega^0(t)}{V_p} x \right) dt \tag{3.137}$$

$$\bar{U}_M \equiv \frac{1}{2} \overline{(\vec{B} \cdot \vec{H})} = \frac{\mu}{2Z^2 T} \int_0^T A^2(t) \left(\cos \int \omega^0(t)\, dt \right)^2 \cos^2 \left(\frac{\omega^0(t)}{V_p} x \right) dt \quad , \tag{3.138}$$

where $T \equiv 2\pi/\omega(t)$ is the period of the fields.

As the period T is much smaller than the total compression time L/V, it is appropriate to assume that during the time period T the frequency $\omega^0(t)$ is a constant. With this assumption, Eqs. (3.137) and (3.138) reduce to the following forms:

$$\overline{U}_E = \frac{1}{4} \epsilon \overline{A^2}(t) \sin^2 \left(\frac{\omega^0(t)}{V_p} x \right) \tag{3.139}$$

and

$$\overline{U}_M = \frac{1}{4} \epsilon \overline{A^2(t)} \cos^2 \left(\frac{\omega^0(t)}{V_p} x \right) \quad . \tag{3.140}$$

Thus, the average total energy density per unit crossectional area, $\overline{U}_T$, is

$$\overline{U}_T = \frac{1}{4} \epsilon \overline{A^2}(t) \int_0^{L-Vt} dx = \frac{1}{4} \epsilon \cdot (L - Vt) \overline{A^2}(t) \quad . \tag{3.141}$$

Now, as the average radiation pressure,[9] $\overline{F}_x$, upon the moving conducting plate 2 is $\partial/\partial x(\overline{U}_T)$, the average external power per unit crossectional area applied to the plate 2 in order to keep it moving at the velocity V will be

$$P_a = V \frac{\partial}{\partial x} (\overline{U}_T) = \frac{1}{4} \epsilon \overline{A^2}(t) \cdot V \quad . \tag{3.142}$$

Finally, the spatial average power loss per unit crossectional area due to the dielectric loss of the medium is

$$P_\sigma = \sigma \overline{E_y^2} = \frac{1}{4} \sigma (L - Vt) \overline{A^2}(t) \quad , \tag{3.143}$$

where σ is the conductivity of the medium.

If we neglect the conduction losses of the plates, we have the following energy balance equation by the law of conservation of energy:

$$\frac{d}{dt}(\bar{U}_T) = P_a - P_\sigma \quad ,$$

or

$$\frac{d}{dt}\left[\frac{1}{4}\epsilon(L - Vt)\,\overline{A^2}(t)\right] = \frac{1}{4}\epsilon V\overline{A^2}(t) - \frac{1}{4}\sigma(L - Vt)\,\overline{A^2}(t) \tag{3.144}$$

i.e.,

$$\frac{d\,\overline{A^2}(t)}{\overline{A^2}(t)} = \left(\frac{2V}{L - Vt} - \frac{\sigma}{\epsilon}\right) dt \quad . \tag{3.145}$$

Thus, we have

$$\overline{A^2}(t) = \overline{A^2}(0)\,\frac{1}{(1 - \frac{V}{L}t)^2}\,e^{-(\sigma/\epsilon)t} \quad , \tag{3.146}$$

and the average total energy density per unit crossectional area is

$$\bar{U}_T = \frac{1}{2}\epsilon L \cdot \frac{1}{(1 - \frac{V}{L}t)}\,e^{-(\sigma/\epsilon)t} \quad . \tag{3.147}$$

Notice that the average of the electric field amplitude squared is strongly dependent upon the dielectric loss of the medium (see Fig. 3.18).

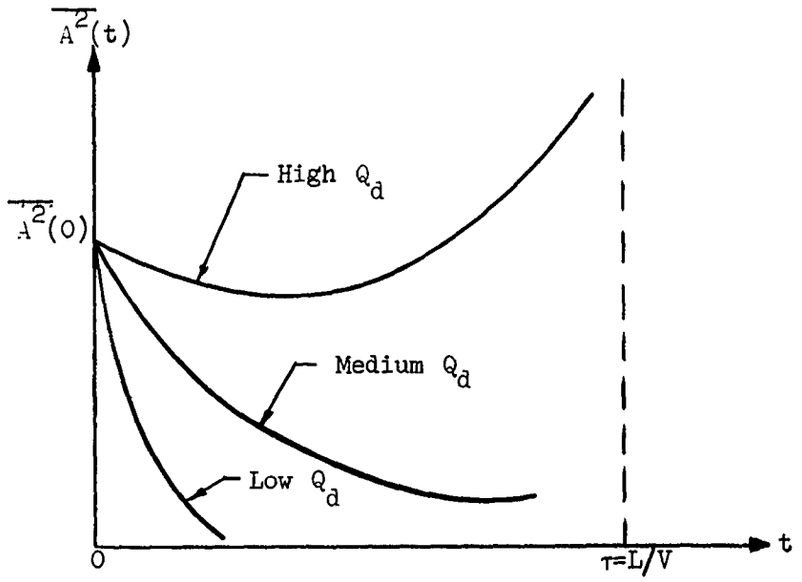

FIG. 3.18--Energy density variation of a uniform TEM wave during the course of compression between two conducting plates (one fixed, one moving).

A metallic transition can be induced by a pressure shock wave in some ionic and molecular cystals.[23] An increase in conductivity by a factor of 10^6 to 10^{20} from the uncompressed to the compressed state has been observed.[23,24] Thus the simulation of a moving reflector by a pressure shock wave in a proper solid is feasible. In view of this possibility, the assumption of a perfect reflector in the analysis of the compression of electromagnetic waves given in this section is a good approximation, although the analysis for the case of a partial reflector requires only the slight modification of taking the transmission loss into account. Finally, we notice that a large mechanical pressure can be obtained by using piezoelectric ceramic[25] PZT - 4 as a transducer. By operating in the thickness mode and with electric field strength 100 kV/cm, a pressure of the order of 30×10^3 Pounds/in.^{2} can be obtained.

CHAPTER IV

THE REALIZATION OF DOPPLER INTERACTIONS IN REAL MATERIALS

In the previous theoretical analysis of wave interactions with a moving interface or a series of moving interfaces in solids, we have assumed that the moving interfaces are induced in a nonlinear material such as ferroelectrics (or ferromagnets) by applying a large amplitude electric (or magnetic) field step function or a series of pulses through the materials.

The general theory developed in Chapter III for the interaction of electromagnetic waves with moving boundaries, specifically that given in Section 3.3, will be applied to the case of ferromagnetic and ferroelectric materials in this chapter. First, wave interaction with a moving interface in a ferromagnetic material is analyzed with the dispersive property taken into account. We omit the corresponding calculation for the dispersive ferroelectrics, however. An illustration is given for the case of a ferromagnet, followed by a survey of the existing potentially useful ferroelectric materials. The conversion between the transverse acoustic wave and the longitudinal acoustic wave in a ferromagnetic material using the Doppler shift principle is then discussed. Several possible arrangements for Doppler shift experiments are briefly described. Finally, two examples of Doppler shift experiments appearing in the literature are given.

4.1 REFLECTION AND TRANSMISSION OF AN ELECTROMAGNETIC WAVE AT A LARGE MAGNETIC FIELD STEP FUNCTION OR PULSE

A moving reflector and hence the compression of electromagnetic waves can be realized, at least in principle, by applying a magnetic field step function or pulse to a ferromagnetic material. This is due to the fact that the permeability tensor elements of a ferromagnetic material are functions of the dc magnetic field, and consequently so is the

impedance of the medium. This scheme appears even more promising when we consider the feasibility of creating an abrupt moving interface or series of moving interfaces, or electromagnetic shock waves in gyromagnetic media (see work by Gaponov and Freidman;[26] Hatfield and Auld;[27] etc.,) and the generation of nigh amplitude, fast rising pulsed magnetic fields (Elliott,[28] Heiter,[29] etc.).

We now analyze the problem of an electromagnetic wave interacting with such a moving interface, taking the dispersive property of the ferromagnetic medium into account. Consider an infinite ferrite medium traversed by a zero rise-time magnetic field step function as shown in Fig. 4.1. A small-signal TEM wave comes in from the left end to interact with the moving interface created by the step function. The difference in the resultant magnetic fields in front of the interface and behind the interface leads to the change in frequency and amplitude for the reflected and transmitted waves. The general results given in Section 3.2 will be applicable here when the dispersion property of the medium is taken into account. The equality of phases for all waves on the

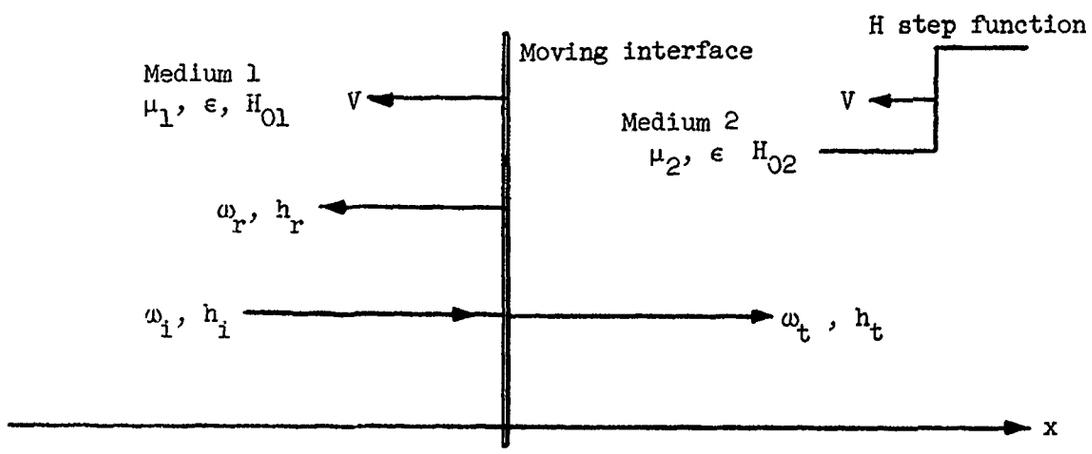

FIG. 4.1--The configuration of a uniform TEM wave interacting with a moving boundary in a ferromagnetic medium.

interface at all time leads to

$$\omega_i + K_i(\omega_i)\, V = \omega_r - K_r(\omega_r)\, V = \omega_t + K_t(\omega_t)\, V \quad . \qquad (4.1)$$

To solve for ω_r and ω_t in Eq. (4.1), the dispersion relation $K = f(\omega)$ must be known. The general form of the dispersion relation[30] in an infinite medium is given in Eq. (4.2) and the dispersion diagram shown in Fig. 4.2:

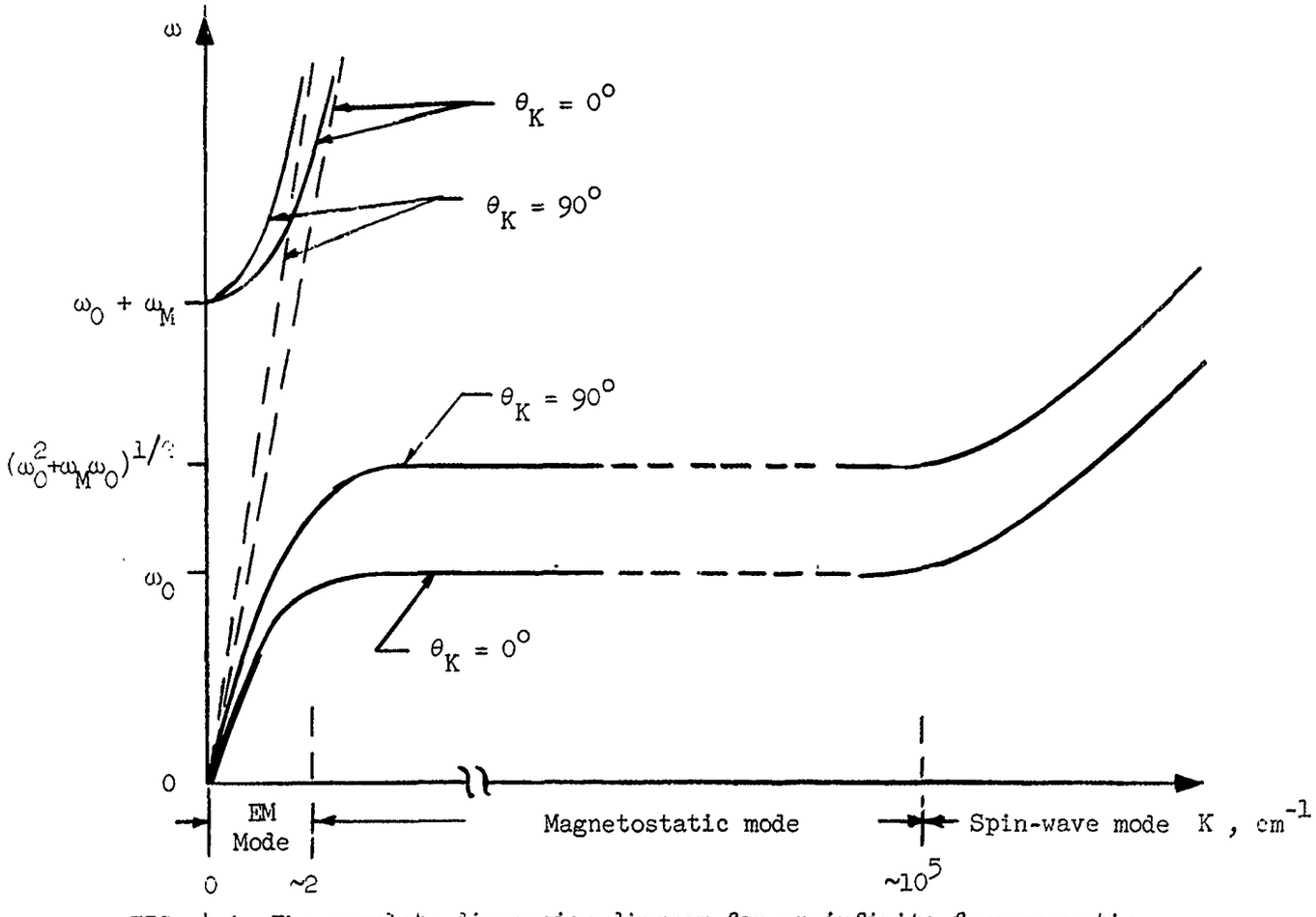

FIG. 4.2--The complete dispersion diagram for an infinite ferromagnetic medium. The dashed lines are for the ordinary waves and the solid curves for the extraordinary waves.

$$\frac{K^2}{K_0^2} = \frac{(\mu^2 - \mu - \kappa^2)\sin^2\theta_K + 2\mu \pm [(\mu^2 - \mu - \kappa^2)\sin^4\theta_K + 4\kappa^2\cos^2\theta_k]^{1/2}}{2[(\mu - 1)\sin^2\theta_K + 1]} \tag{4.2}$$

where

ϵ = the permittivity of the medium
μ_0 = the permeability of free space
γ = the gyromagnetic ratio
H_0 = the dc magnetic field
M_0 = the saturation magnetization
H_{ex} = the exchange field
a = the atomic spacing
θ_K = the angle between the wave vector and the dc magnetic field
ω = the radian frequency
$K_0^2 = \omega^2 \epsilon \mu_0$
$\omega_M = 4\pi\gamma M_0$
$\omega_0 = \gamma H_0$
$\omega_{ex} = \gamma H_{ex}$
$\omega_r = \omega_0 + \omega_{ex} a^2 K^2$
$\mu = 1 + \omega_r\omega_M/\omega_r^2 - \omega^2$
$\kappa = \omega\omega_M/\omega_r^2 - \omega^2$

For the electromagnetic mode, K is very small. By letting $K \to 0$, the following approximate dispersion relations are obtained:

$$\omega^2 \simeq \frac{\omega_0}{\epsilon\mu_0(\omega_0 + \omega_M)} K^2 \qquad \text{lower branch} \tag{4.3}$$

$$\omega^2 \simeq (\omega_0 + \omega_M)^2 + \frac{K^2}{\epsilon\mu_0} \qquad \text{upper branch.} \tag{4.4}$$

Thus, if we are operating along the linear portion of the lower branch of the electromagnetic mode, the frequency shifts in the reflected and transmitted waves will be obtained by combining Eqs. (4.1) and (4.3):

$$\frac{\omega_r}{\omega_i} = \frac{1 + \left(\frac{\epsilon\mu_0(\omega_{01} + \omega_{M1})}{\omega_{01}} \right)^{1/2} V}{1 - \left(\frac{\epsilon\mu_0(\omega_{01} + \omega_{M1})}{\omega_{01}} \right)^{1/2} V} \tag{4.5}$$

$$\frac{\omega_t}{\omega_i} = \frac{1 + \left(\frac{\epsilon\mu_0(\omega_{01} + \omega_{M1})}{\omega_{01}} \right)^{1/2} V}{1 + \left(\frac{\epsilon\mu_0(\omega_{02} + \omega_{M2})}{\omega_{02}} \right)^{1/2} V} \quad , \tag{4.6}$$

where

$$\omega_{01} = \gamma H_{01} \quad , \quad \omega_{02} = \gamma H_{02} \quad .$$

Similarly, if we operate along the upper branch of the electromagnetic mode, we have the following simultaneous equations relating ω_i , ω_r and ω_t :

$$\begin{aligned} \omega_i + \left\{ [\omega_i^2 - (\omega_{01} + \omega_{M1})^2] \, \epsilon\mu_0 \right\}^{1/2} V \\ = \omega_r - \left\{ [\omega_r^2 - (\omega_{01} + \omega_{M1})^2] \, \epsilon\mu_0 \right\}^{1/2} V \\ = \omega_t + \left\{ [\omega_t^2 - (\omega_{02} + \omega_{M2})^2] \, \epsilon\mu_0 \right\}^{1/2} V \\ \equiv \omega' \quad , \end{aligned} \tag{4.7}$$

and ω_r/ω_i and ω_t/ω_i can be solved graphically or numerically. This can be done by plotting the function of Eq. (4.7), denoted by ω', as functions of ω_i, ω_r and ω_t, respectively.[17]

As indicated in Section 3.6, the necessary condition for the existence of a reflected wave (when the interface moves towards the incident wave) is that the group velocity of the reflected wave be larger than the interface velocity. Otherwise, the waves cannot "break away" from the interface, and hence no reflection can occur. Therefore, the maximum frequency shift available in the reflected wave is determined by the condition

$$V = V_g(\omega_{r_{max}}) = \frac{d\omega}{dK}\Big|_{\omega=\omega_{r_{max}}} , \qquad (4.8)$$

where $V_g(\omega_{r_{max}})$ is the group velocity of the reflected wave at the maximum frequency $\omega_{r_{max}}$.

Thus, maximum frequency shifts in the reflected waves, when operating along the lower branch of the dispersion diagram of the electromagnetic mode will occur at

$$\omega_{r_{max}} = \frac{K}{V} \cdot \frac{\omega_{01}}{\epsilon\mu_0(\omega_{01} + \omega_{M1})} .$$

We note that on the lower branch there is an upper limit to the frequency where the group velocity approaches zero. Consequently for reflection to occur at this frequency, the velocity of the interface must approach zero.

On the contrary, when operating along the upper branch there exists no limit for the maximum frequency shifts in the reflected waves as the group velocity increases with increasing frequency on this branch.

4.2 A SURVEY OF POTENTIAL FERROELECTRIC MATERIALS FOR THE DOPPLER SHIFT EXPERIMENT

In the previous section it was shown that there are some limitations to the use of ferromagnetic materials for Doppler shift experiments. The difficulty, due to the high dispersion of the medium, is not present in ferroelectrics. Ferroelectric materials are those which, for some range of temperatures (at and below the Curie temperature Tc), show spontaneous polarization, the direction of which may be reversed by an external electric field.[31,32] Many ferroelectrics have high dielectric constants. The fact that ferroelectrics have high dielectric constants makes them exhibit a high degree of dielectric nonlinearity at electric field strengths which are safely below the breakdown limit and easily obtainable. Consequently, ferroelectrics are by far the most important nonlinear dielectrics. Thus, it is important to give a brief description of the outstanding properties and also the unfavorable properties of the ferroelectrics for the frequency range of interest (microwave range) and in particular for application in the Doppler shift experiment. Relevant parameters of a few most potentially useful ferroelectrics for this experiment will also be given at the end of this section.

The most important property for the Doppler shift experiment of many ferroelectric materials is that there exists a phase transition between the various states, e.g., paraelectric to ferroelectric state, antiferroelectric to ferroelectric state, ... etc, and that this phase transition can be induced in various ways: an electric field, a mechanical pressure, a temperature change, etc. This phase transition will be accompanied by a change in structure of the material and hence in the physical properties.

It is worth noting in passing that an analogous phase transition may also occur in some ferromagnetic materials. A possible transition between ferromagnetic state and antiferromagnetic state for the intermetallic compound $MnSn_2$ at $73^{\circ}K$ has been suggested.[33]

That a phase transition between various states may be induced by electric field or mechanical pressure is well demonstrated by the fact that the Curie temperature for many ferroelectrics can be shifted by applying an electric field or mechanical pressure. For example, the change of the Curie temperature per unit electric field strength,

$\Delta T_c/\Delta E$, for single-crystal $BaTiO_3$ is in the order of $+ 1.3 \times 10^{-3}$ °C/Volt cm^{-1} ,[34,35] and the change of the Curie temperature per unit pressure, $\Delta T_c/\Delta p$, for (Ba, Sr) TiO_3 ceramic is in the order of $+ 4.0 \times 10^{-3}$ °C cm^2/Kg .[26]

In the first-order phase transition[32] the temperature dependence of the permittivity will have a finite jump at the transition temperature while for the second-order phase transition,[32] the permittivity has a sharply defined peak around the Curie temperature.

The second important property of the ferroelectric materials is that in the ferroelectric state the direction of the spontaneous polarization in the form of domain structure can be changed and new domains can be formed by an external electric field, while in the paraelectric state a very large field-dependent polarization can be induced by an external electric field. These properties lead to a large nonlinear relationship between the permittivity of the material and the amplitude of the electric field[37] in both the ferroelectric and paraelectric states.

Other advantages[38] of the ferroelectrics in comparison with the variable-capacitance diode are the high breakdown field strength, the independence of loss on power level at small signal, and that they can be treated both as distributed elements as well as lumped elements. Furthermore, unlike the ferromagnetic materials, the ferroelectrics require relatively simple, inexpensive biasing equipment and small amounts of dc control power. The response time of the rf dielectric properties to changes in dc bias will be short compared to that of ferromagnetic materials.[38]

Although the ferroelectric is one of the most promising materials for the Doppler shift experiment, there exist several unfavorable properties which will limit the extent of application.

First, the high nonlinearity in the dielectric constant at the range of temperatures around the Curie point is often accompanied by high loss at the microwave frequency. For example, single-crystal $BaTiO_3$ has high loss as well as high nonlinearity in the dielectric constant at the range of temperatures around the Curie point of 120°C over the frequency range of 0.5 Gc/s to 24 Gc/s.[39-42] Thus the loss

and the dielectric constant nonlinearity often go together, and the high dielectric constant nonlinearity can hardly be utilized to the utmost extent.

Secondly, many ferroelectric materials have the frequency of dielectric relaxation in the microwave range or lower,[43] and this sets an upper bound on the frequency of operation. For example, TGS crystal has a relaxation frequency of 0.5 Gc at the Curie point.

Lastly, ferroelectric materials have temperature dependent, high dielectric constants which require a temperature control system on one hand, and make the matching problem difficult on the other hand.

Before we give a list of the potential ferroelectrics for the Doppler shift experiment, it is most important to emphasize the difference between the rf dielectric constant and the reversible dielectric constant,[44] and consequently the difference between the rf dielectric constant nonlinearity and the reversible dielectric constant nonlinearity. The rf dielectric constant is by definition the dielectric constant measured by an rf signal alone, while the reversible dielectric constant is the one measured by a small amplitude rf signal with a dc bias. The rf dielectric constant nonlinearity is determined by the nonlinear dependence of the dielectric constant on rf signal amplitude, while the reversible dielectric constant nonlinearity is determined by the nonlinear dependence of the small signal dielectric constant on dc bias amplitude.

The nonlinearity of the rf dielectric constant in the ferroelectric state depends mainly on whether the domain polarizations can follow the rf field variation, while in the paraelectric state it depends on the nonlinear relation between the induced polarization and the amplitude of the rf field. The nonlinearity of the reversible dielectric constant in the ferroelectric state, on the other hand, can persist to a higher frequency as the nonlinearity is mainly due to domain orientation by the dc bias field.

Thus, a significant nonlinearity of the reversible dielectric constant at the microwave frequency does not necessarily mean a significant nonlinearity of the rf dielectric constant at the same frequency.

In view of the favorable and unfavorable properties of the ferroelectrics at microwave frequencies, one must consider the following factors in chosing a given ferroelectric for a Doppler shift experiment:

1. As both the nonlinearity of the dielectric constant and the loss have a peak at the Curie temperature and decrease from there, a compromise in the operating temperature must be made.

2. As there might be a big difference between the reversible dielectric constant nonlinearity and the rf dielectric constant nonlinearity, the reversible dielectric constant nonlinearity data should be used when an electric step function or a series of dc pulses are used to induce a single moving interface or a series of moving interfaces; while the rf dielectric constant nonlinearity data should be used when large amplitude microwaves, sinusoidal or rectangular, are used to induce a series of wave-packet type interfaces or the semi-infinite moving periodic structure (which will be considered in Chapter V).

In the following list of potential ferroelectrics (Table 4.I), the numerical values of the dielectric constant nonlinearity are estimated using the experimental data in the literature.

Although the parameters of some of the ferroelectrics which are currently available, as illustrated in the table, are not as we desire, the ferroelectrics show the greatest promise for Doppler shift experiments in view of the increasing number of new ferroelectric materials and the progress in the technology of controlling the physical properties of a material.

4.3 CONVERSION OF A LONGITUDINAL ACOUSTIC WAVE TO A TRANSVERSE ACOUSTIC WAVE IN A FERROMAGNETIC MATERIAL

So far in this discussion the reflected component of an electromagnetic wave interacting with a moving interface has been emphasized. In this section we discuss a specific application of the general theory of the transmitted component developed in Chapter III. As indicated previously, the frequency shift in the transmitted component of an electromagnetic wave will be in practice more easily observed than

TABLE 4.I

Microwave Experimental Data For Ten Potential Ferroelectrics

(The number in parenthesis refer to the references for this table only)

Materials	Curie temp. or transition temp. (Tc)	Dielectric constant (ϵ)	Loss tangent ($\tan\delta$)	Measured at		Reversible dielectric constant non-linearity ($\Delta\epsilon/\epsilon$)	Measured at	
				Temp.	Frequency		Temp.	Frequency
$KTaO_3$	1 ± 0.5^oK (1)	4400 (2)	$\sim10^{-4}$ (2)	4.2^oK (2)	3 Gc/s (2)	~0.1 at 10 kV/cm (2)	4.2^oK (2)	~3 Gc/s (2)
$KTa_{0.65}Nb_{0.25}O_3$ (KTN)		$\sim10^4$ (3)	~0.007 (3)	295^oK (3)				
$SrTiO_3$ Singe crystal	$\sim37^oK$ (4)	~1600 (4)	$\sim2\times10^{-3}$ (4)	90^oK (4)	6 Gc/s (4)	~0.065 at 10 kV/cm (4)	90^oK (4)	~6 Gc/s (4)
$BaTiO_3$ 0.73 $SrTiO_3$ 0.27 Ceramic	$\sim294^oK$ (6)	3300 (6)	~0.16 (6)	$\sim294^oK$ (6)	8~12Gc/s (6)	~-0.35 at 10 kV/cm (6)	$\sim294^oK$ (6)	8-12Gc/s (6)
TGS	320^oK (7)	~19.7 (8)	~0.043 (8)	$\sim295^oK$ (8)	9.6 Gc/s (8)	~-0.6 at 10 kV/cm (9)	$\sim318^oK$ (9)	2.6 Gc/s (9)
$BaTiO_3$ - $BaHfO_3$ Single crystal	$\sim343^o$ - 353^oK (12)	~500 (12)	~0.03 (12)	$\sim295^oK$ (12)		~-10 at 1.0 kV/cm (12)		1 Gc/s (12)
KD_2PO_4	$\sim213^oK$ (13)	~100 (14)	0.3 (14)	$\sim211^oK$ (14)	1 Gc/s (14)	~-0.4 at 10 kV/cm (14)	211^oK (14)	0.62 Gc/s (14)
KH_2PO_4	$\sim123^oK$ (13)	$\epsilon_c \sim 60$ $\epsilon_a \sim 60$ (15)	$\tan\delta_c \sim 0.016$ $\tan\delta_a \sim 0.004$ (15)	$\sim173^oK$ (15)	9.2 Gc/s (15)			
Rochelle salt	255^oK and 297^oK (16)	~75 (17)	~0.4 (17)	$\sim293^oK$ (17)	3.0 Gc/s (17)	~-0.4 at 10 kV/cm (17)	293^oK (17)	3.0 Gc/s (17)
$PbZrO_3$ Ceramic	$\sim363^oK$ (18)	~1000 (18)	~0.01 (18)	$\sim363^oK$ (18)	1 Kc/s (18)			

TABLE 4.I (Continued)

RF Dielectric constant nonlinearity ($\Delta\epsilon/\epsilon$)	Measured at		Dielectric dispersion frequency (f_d)
	Temp.	Frequency	
			> 200 Gc/s (3)
~0.065 at 10 kV/cm (4)	90°K (4)	~6 Gc/s (4)	> 35 Gc/s (5)
~-0.03 at 10 kV/cm (6)	~325°K (6)	3 Gc (6)	~60 Gc/s (6)
~0 at 10 kV/cm (10)	295°K (10)	0.2 Gc/s (10)	< 0.5 Gc/s (11)
> + 100 at 1.0 kV/cm (12)		0.05 Gc/s (12)	
			~1.0 Gc/s (14)
			> 9.2 Gc/s (15)
~ + 0.3 at 3 kV/cm (17)	293°K (17)	0.2 Gc/s (17)	1.0 - 10.0 Gc/s (17)

REFERENCES FOR TABLE 4.I

(1). S. H. Wemple, Ph.D. Dissertation, M.I.T. (1963).
(2). J. E. Geusic, S. K. Kurtz, T. J. Nelson and S. H. Wemple, Appl. Phys. Letters 2, 185 (1963).
(3). J. E. Geusic, S. K. Kurtz, L. G. Van Uitert, and S. H. Wemple Appl. Phys. Letters 4, 141 (1964).
(4). G. Rupprecht, R. O. Bell, and B. D. Silverman, Phys. Rev. 132, 97 (1961).
(5). G. Rupprecht, B. D. Silverman and R. O. Bell, AFCRC Labs, Bedford, Mass., June 16, 1958, and October 15, 1960.
(6). D. A. Johnson, Ph.D. Dissertation, Stanford University (1961).
(7). F. Jona and G. Shirane, Ferroelectric Crystals, (Pergamon Press, the MacMillan Company, New York, 1962).
(8). A. Nishioka and M. Takeuchi, J. Phys. Soc. (Japan) 14, 971 (1957).
(9). R. M. Hill and S. K. Ichiki, Phys. Rev. 132, 1603 (1963).
(10). V. M. Petrov, Soviet Phys. Crystallography 6, 508 (1962).
(11). A. Lurio and E. Stern, J. Appl. Phys. 31, 1125 (1960).
(12). A. L. Khodakov and M. L. Scholokhovich, Soviet Phys. Doklady 6, 964 (1962).
(13). W. Bantle, Helv. Phys. Acta. 15, 373 (1942).
(14). R. M. Hill and S. K. Ichiki, Phys. Rev. 132, 1603 (1963).
(15). I. P. Kaminov and G. O. Harding, Phys. Rev. 129, 1562 (1963).
(16). Ibid (8).
(17). V. M. Petrov, Soviet Phys. Crystallography 7, 319 (1962).
(18). B. Jaffe, Proc. IRE 49, 1264 (1961).

that of the reflected component, since it does not require an abrupt interface. In fact, the frequency shift is independent of the steepness of the transition. We consider specifically the conversion of a longitudinal acoustic wave to a transverse acoustic wave or vice versa, in a ferromagnetic material. In view of the fact that ferromagnetic materials such as YIG are known to have small microwave acoustic losses, this is a problem of practical interest.

Before entering the main discussion, we describe briefly the problem of a spin-wave interaction with a moving interface in a ferromagnetic material. Consider the configuration shown in Fig. 4.3. A spin-wave interacts with an abrupt moving interface induced by a magnetic step-function in a ferromagnetic material. The direction of the magnetic step-function $\vec{H}_p$ is perpendicular to the dc field $\vec{H}_0$. The spin-wave dispersion curves are shown in Fig. 4.4 for medium 1 and 2, where θ_K designates the angle between the wave vector and the resultant dc field $\vec{H}_0 + \vec{H}_p$. In medium 2, θ_K may also be equal to zero as a special case where the step field is parallel to H_0 .

Since the velocity of the interface V is of the order of electromagnetic wave velocity, it is therefore larger than the spin-wave velocity. Following the same argument for the existence of reflected wave as described previously, we conclude that only the transmitted wave exists. From the general results of Chapter III, we have

$$\frac{\omega_t}{\omega_i} = \frac{1 + V/V_{p_i}}{1 + V/V_{p_t}} \quad , \tag{4.9}$$

where ω_i and ω_t are the frequencies of the incident and transmitted spin-waves, respectively, and V_{p_i} and V_{p_t} are the phase velocities of the spin-waves in medium 1 and 2, respectively.

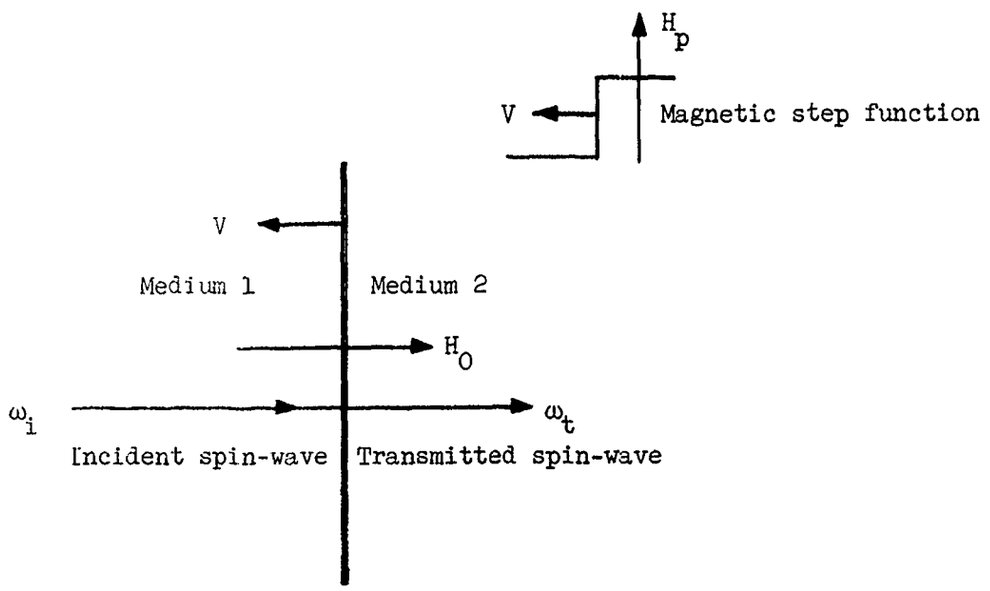

FIG. 4.3--The configuration showing a spin-wave interacting with a moving interface.

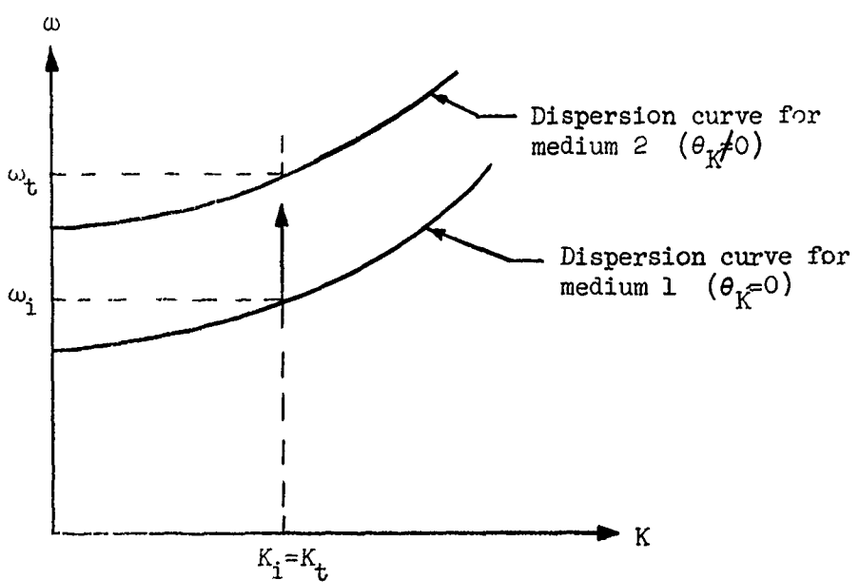

FIG. 4.4--The spin-wave manifold.

Since $V \gg V_{p_i}$, $V \gg V_{p_t}$, Eq. (4.9) reduces to

$$\frac{\omega_t}{\omega_i} \simeq \frac{V_{p_t}}{V_{p_i}} \tag{4.10}$$

$$\text{i.e.,} \quad \frac{\omega_t}{V_{p_t}} \simeq \frac{\omega_i}{V_{p_i}} \quad , \tag{4.11}$$

or

$$K_t \simeq K_i \quad , \tag{4.12}$$

where, K_i and K_t are the wave numbers of the spin-wave in medium 1 and 2, respectively. Thus, it is seen that the wave number of the spin-wave is approximately conserved, while the frequency of the spin-wave changes in the interaction process. In other words, the momentum of the spin-wave is approximately conserved, while the energy is not during the interaction process.

Now we proceed the main topic of this section [46,47] Consider the configuration shown in Fig. 4.5. The ω - K diagrams for the acoustic waves and spin-wave alone are shown in Fig. 4.6 and Fig. 4.4. respectively. The combined ω - K diagram[48] showing the coupling between the spin-wave and the acoustic waves is given in Fig. 4.7. Transverse acoustic waves are excited at the left end of the YIG rod using conventional techniques. The transverse acoustic wave traveling into the rod has frequency ω_i and wave number K_i , as shown in Fig. 4.7. After the rod is essentially filled with the acoustic energy, a nonabrupt magnetic step is sent through the rod from the right end. The direction of the magnetic step $\vec{H}_p$ is orthogonal to the original dc field $\vec{H}_0$. As the magnetic-step function propagates through the rod, the angle of the resultant dc magnetic field $\vec{H}_0 + \vec{H}_p$ rotates with respect to the acoustic wave vector, θ_K . From Fig. 4.4 we know that a new dispersion diagram

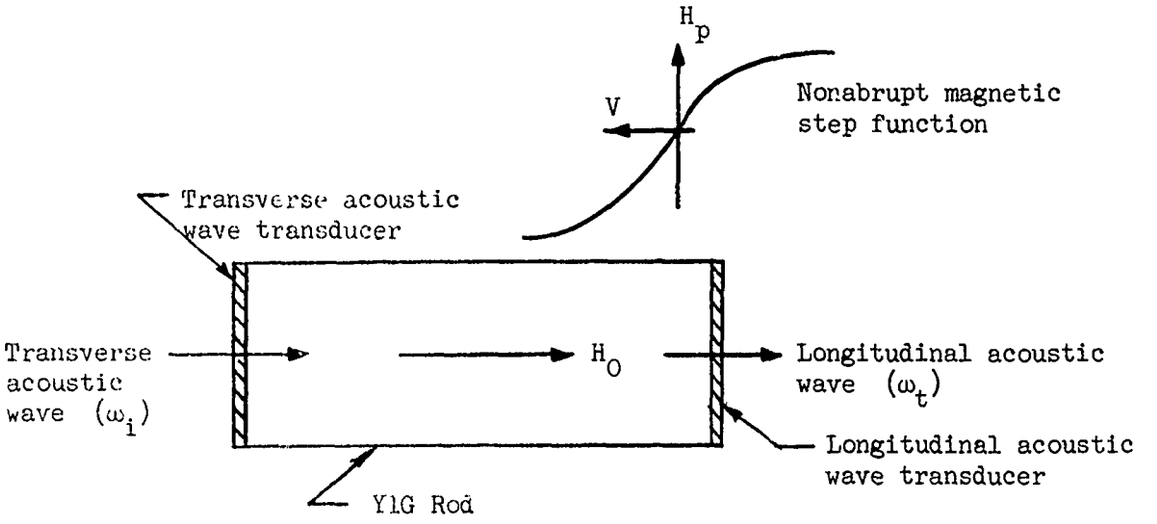

FIG. 4.5--The configuration showing the conversion of a transverse acoustic wave to a longitudinal acoustic wave using a nonabrupt magnetic step function.

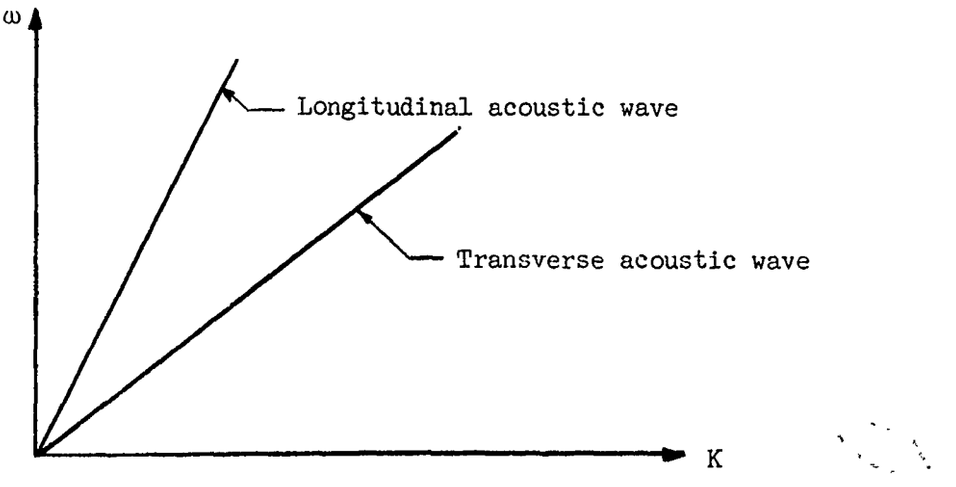

FIG. 4.6--The ω - K diagram of the longitudinal and transverse acoustic waves.

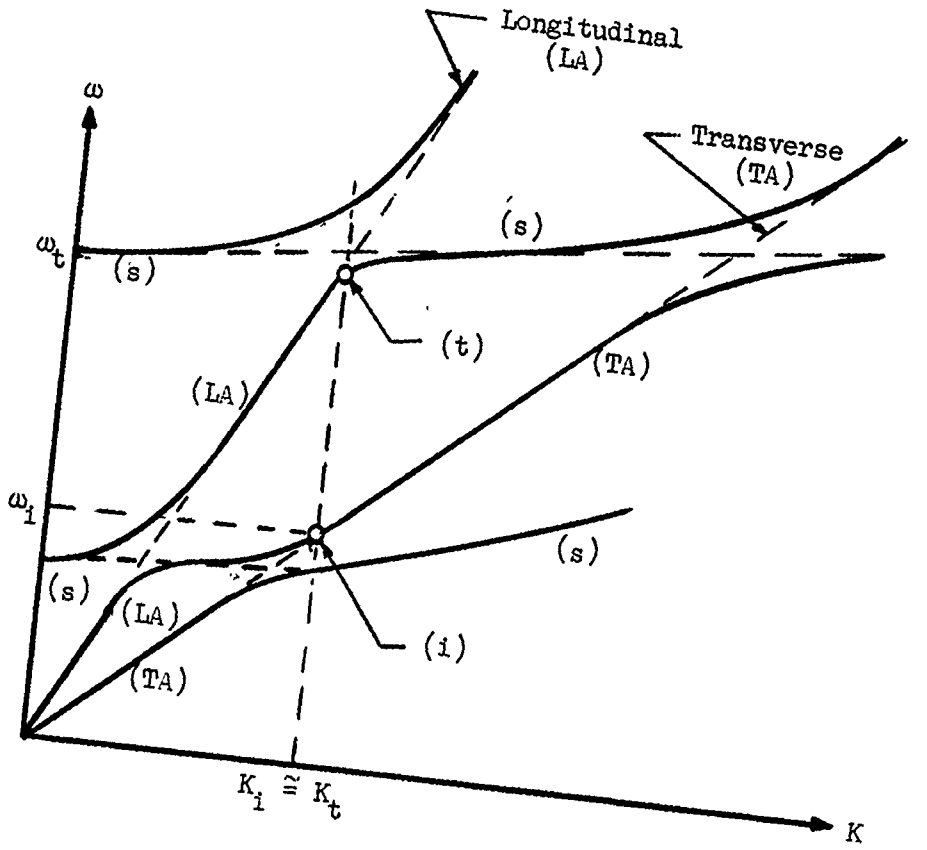

FIG. 4.7--The combined ω - K diagram showing the spin-phonon coupling region (indicated by the dashed lines) and the shift in operating point.

(S) ≡ Spin-wave

(LA) ≡ Longitudinal acoustic wave.

(TA) ≡ Transverse acoustic wave

(i) ≡ Operating point of the incident wave

(t) ≡ Operating point of the transmitted wave.

corresponding to a new θ_K results, as shown in the broader curves in Fig. 4.7, and the transverse acoustic wave is transformed into a longitudinal acoustic wave with a higher frequency ω_t and wave number $K_t \simeq K_i$.

The fact that the wave number is approximately conserved in the conversion process can be derived in the same way as done in the first part of this section, i.e . from

$$\frac{\omega_t}{\omega_i} = \frac{1 + V/V_{p_i}}{1 + V/V_{p_t}} \quad . \tag{4.9}$$

Since $V \gg V_{p_i}$, $V \gg V_{p_t}$, Eq. (4.9) reduces to

$$\frac{\omega_t}{V_{p_t}} \simeq \frac{\omega_i}{V_{p_i}} \tag{4.13}$$

or

$$K_t \simeq K_i \quad . \tag{4.14}$$

In most acoustic materials, the longitudinal acoustic wave velocity is approximately twice that of transverse acoustic wave, and therefore the frequency of the longitudinal acoustic wave is approximately twice that of the incident transverse wave. Since the velocity of the interface is much larger than that of the acoustic or spin-waves, no reflected wave can exist. To avoid spin-wave losses, the conversion should be made in a time short compared with the spin-wave relaxation time. When the losses are ignored the conversion gain can be obtained from the result given in Section 3.3.2,

$$\frac{P_t}{P_i} = \left(\frac{1 + V/V_{p_i}}{1 + V/V_{p_t}}\right)^2 \simeq \left(\frac{V_{p_t}}{V_{p_i}}\right)^2 = \left(\frac{\omega_t}{\omega_i}\right)^2 \quad . \tag{4.15}$$

Thus, a conversion gain of approximately 6 dB will be produced in this conversion process. The transmitted longitudinal acoustic wave could be easily coupled out from the right end of the rod by a conventional longitudinal wave transducer.

Similarly, a longitudinal acoustic wave can be converted into a transverse acoustic wave using the configuration of Fig. 4.5 with slight modification. In this case, the directions of $\vec{H}_0$ and $\vec{H}_p$ should be interchanged. The transmitted transverse wave is down-shifted in frequency, and attenuated in amplitude.

Notice that the conversion process stops when the magnetic step-function completely fills the YIG rod. In medium 2 there is no coupling of the incident acoustic wave to the spin wave, for now the relevant part of the ω - K diagram is that of the upper (not lower) cross-over region $\theta_K \neq 0$ (see Fig. 4.4). Thus the magnetic field needs to be pulsed. Furthermore we notice that the same conversion process will occur when the magnetic step propagates in the same direction as the incident acoustic wave. In this case the step overtakes the acoustic wave. We also note that it is possible, by applying a magnetic pulse of finite length to achieve a variable rf delay. We can control the timing of the magnetic pulses which mode-convert the acoustic wave by conventional pulse delay circuits. One hardly needs to point out that what the world needs is a $10 variable delay line! (cf. Ford).

4.4 POSSIBLE CONFIGURATIONS FOR DOPPLER SHIFT EXPERIMENTS

It has been indicated previously that an abrupt interface is required to produce a large reflection coefficient in the Doppler shift experiment considered, and consequently a fast rise time high voltage step-function or pulse generator is required. This requirement seems, at least in principle, not diffiuclt to achieve since a subnanosecond risetime multikilovolt pulse generator[45] has been developed.

A few possible experimental configurations for the observation of the frequency shifts and amplitude changes predicted both in Chapter III and this chapter will be briefly described in this section.

To observe the frequency and amplitude changes resulting from a single reflection from a moving interface or a moving slab we may use a strip line filled with a nonlinear ferroelectric material, a strip line loaded with variable-capacitance diodes, or a coaxial line filled with a ferromagnetic material. A possible arrangement is shown in Fig. 4.8, where we specifically consider the case in which a nonlinear ferroelectric material is contained between the two parallel conducting planes. The advantages of this structure operating in the dominant TE_{10} mode have been explored.[49] A voltage step-function (or pulse) applied to the strip line at one end induces a moving interface (or a moving slab) inside the ferroelectric material. A small microwave signal is applied to the strip line at either the same end or the other. That is, to produce a reflected signal up-shifted in frequency, the pump should be applied at the other end; while to produce a reflected signal down-shifted in frequency, both the pump and the small signal should be applied at the same end. For detecting the frequency shifts of the reflected and transmitted signals, a conventional superheterodyne receiver can be used. We note that the metal strip line shown in Fig. 4.8 can also be employed for inducing a moving periodic structure in which a rectangular or more practically a sinusoidal pump is used.

When a ferromagnetic material is used, the strip line in Fig. 4.8 would be replaced by a coaxial line filled with the ferromagnetic material, and the voltage step-function would be replaced by a current step-function.

The advantage of strip line loaded with variable-capacitance diodes over strip line filled with nonlinear ferroelectric is that the former requires a much smaller voltage pulse than the latter. The sharpening of the wavefront, and consequently the formation of an electromagnetic shock wave, has been theoretically predicted and experimentally observed (in a transmission line loaded with variable-capacitance diodes[49-52] and also in ferromagnets).

For the observation of frequency and amplitude changes due to multiple reflection from a moving interface or the compression of electromagnetic waves, a rectangular or cylindrical cavity filled with nonlinear material can be employed. A typical configuration is shown

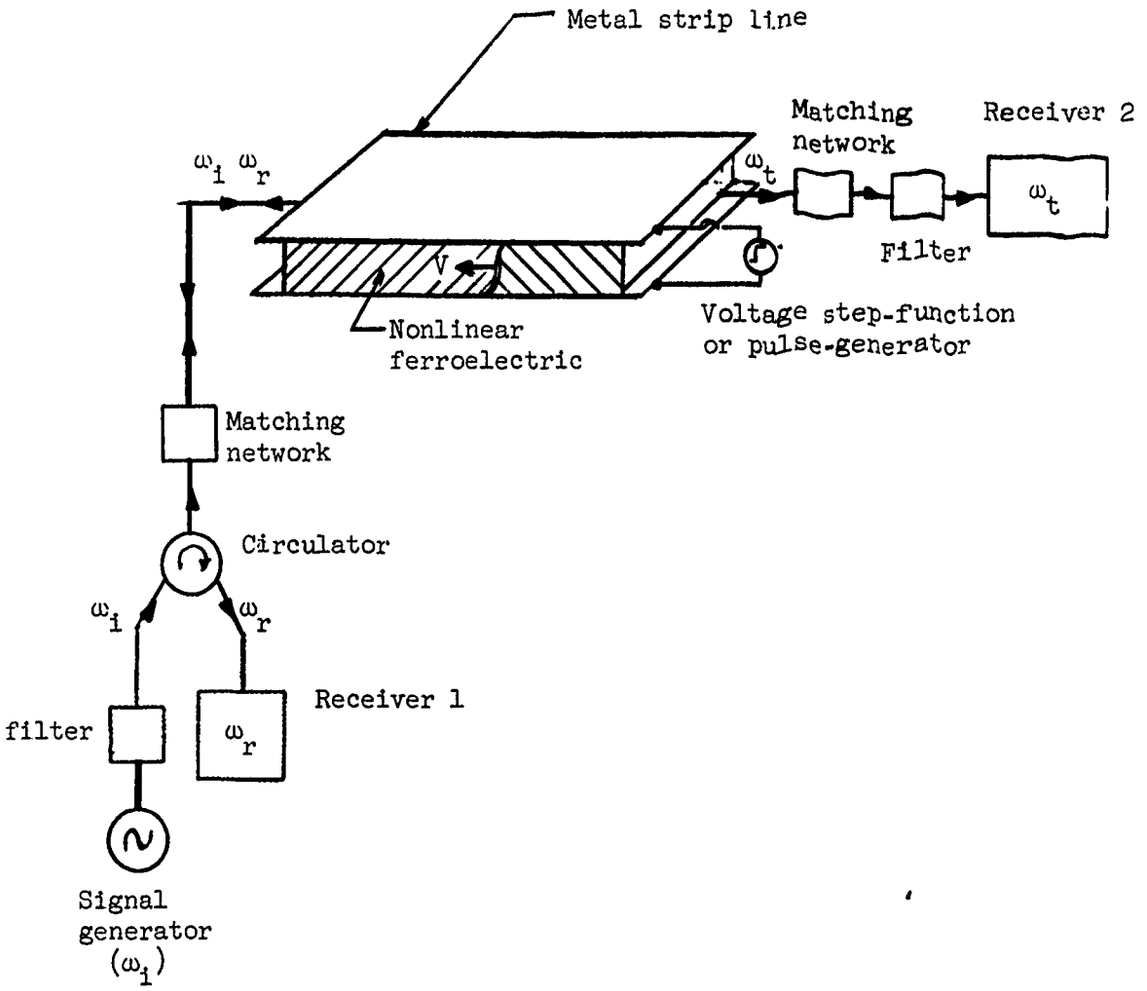

FIG. 4.8--Possible arrangement for the Doppler shift experiment utilizing single reflection.

in Fig. 4.9. Notice that a structure in which a dielectric resonator is inserted inside a waveguide can also be used. A superheterodyne receiver can also be employed in this experiment for the observation of the frequency shift in the compressed waves.

When a pressure step-function or pulse is used to induce the moving interface, it is necessary to install a piezoelectric transducer at the open end of the cavity.

4.5 EXAMPLES OF FREQUENCY CONVERSION AND AMPLIFICATION USING DOPPLER SHIFT METHODS.

To demonstrate the feasibility of the various kinds of Doppler shift experiments described in the last section, we give, in this section, two examples of the Doppler shift experiments which are closely related to the models and theoretical predictions given in the previous chapters.

(a) Frequency Multiplication With A Plasma "Piston"[7]

This is an example of the compression of electromagnetic waves analyzed in Chapter III. A pulsed electromagnetic field (from a magnetron) which has an initial wave length of 10 cm is compressed in a rectangular metal waveguide (in the H_{011} mode). One end surface of the waveguide is a moving plasma piston, while the second end forms a smooth transition into a waveguide with a cutoff wavelength of 4.6 cm. The plasma piston is formed by means of a condenser discharge. The plasma bunch is set to enter the waveguide 2-3 μsec after the rf pulse from the magnetron is turned on. Due to the compression by the plasma bunch, the frequency of the electromagnetic field is increased. Although the plasma bunch moves with a nonrelativistic velocity ($\sim 2.0 \times 10^7$ cm/sec), by virtue of multiple reflection, a signal of much higher frequency ($\lambda = 3$cm) is generated and detected at the output terminal of the second waveguide.

(b) Doppler Effect-Like Phenomenon[53]

This is an example of frequency conversion and amplitude amplification due to moving interface in real materials as most of the examples considered in this study. The theoretical results and the simulated experiment

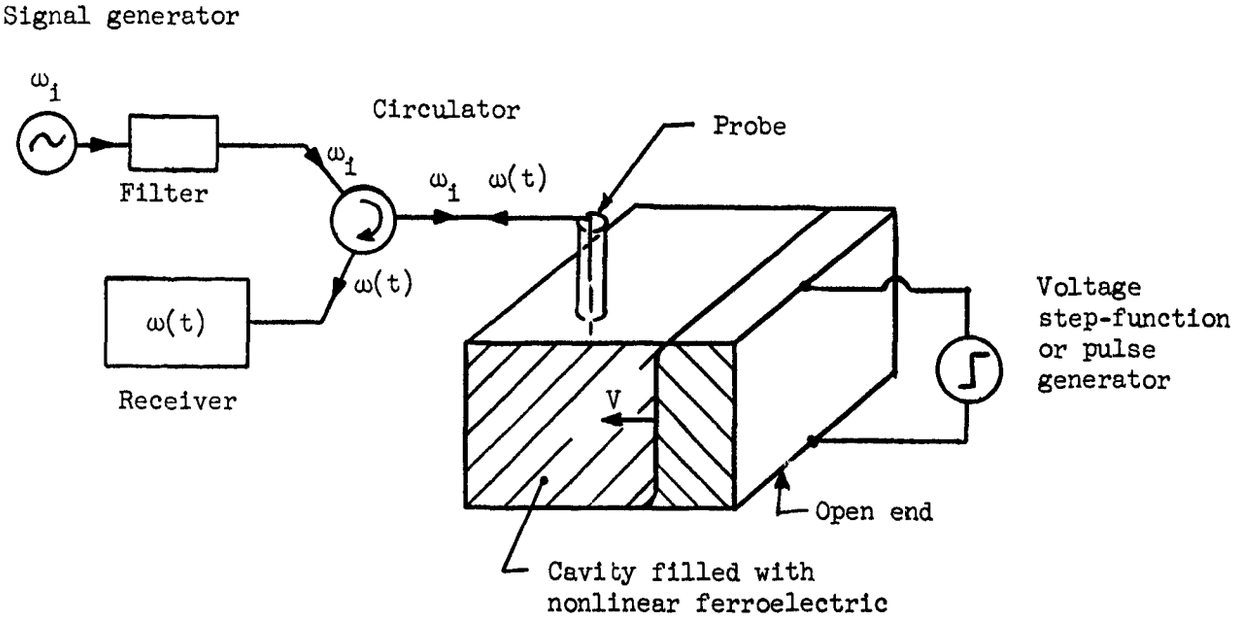

FIG. 4.9--Typical arrangement for the Doppler shift experiment utilizing multiple reflection - the compression of electromagnetic waves.

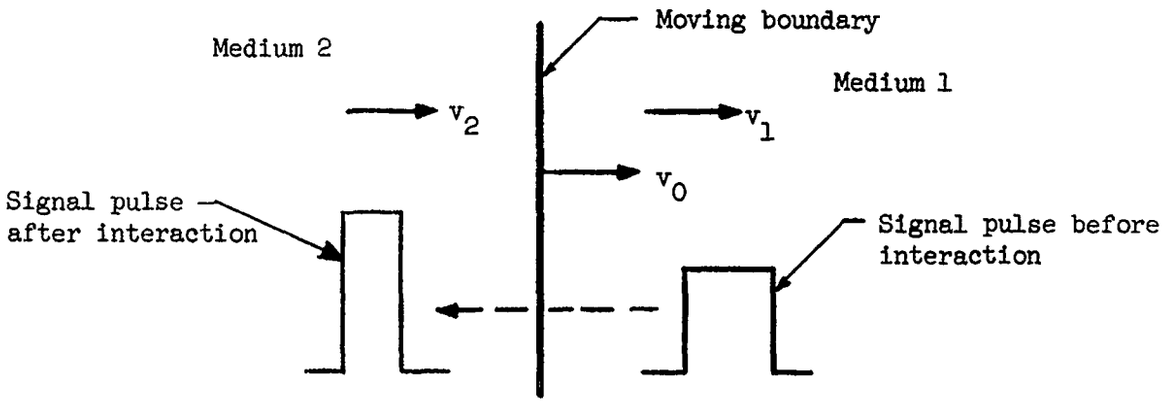

FIG. 4.10--Configuration showing a moving boundary interacting with a video pulse.

reported in reference 53 are very closely related to those considered in Chapter III. A moving boundary (interface) separating two stationary media with different phase velocity and impedance is simulated by sending a control pulse into a parametric distributed amplifier. The distributed lines for the signal pulse and the control pulse are coupled by the variable reactance diodes. The video control pulse is fed into the control line a few microseconds after a video signal pulse is fed into the signal line. The front edge of the control pulse changes the permeability of the parametron from μ_1 to μ_2 . Due to the permeability change, the inductance of the signal line and hence the phase velocity of the wave in the signal line changes accordingly from V_1 to V_2 . The length of the control pulse used is long, and the case $\mu_1 > \mu_2$ is considered. Thus the phase velocity V_1 corresponding to μ_1 is smaller than the phase velocity V_2 corresponding to μ_2 . On the other hand, the velocity of the control pulse and hence the velocity of the interface, V_0 , remains almost unchanged and larger than V_2 and V_1 , because the inductance in the control line is much larger than the inductance change in the parametron. Thus a configuration as shown in Fig. 4.10 is simulated. An input pulse of amplitude 1 volt and length ~3 μsec, after being over-run by the moving boundary induced by a control pulse of amplitude 5 volts and long length, results in an output pulse of amplitude 100 volts and length ~1 μsec.

CHAPTER V

WAVE INTERACTIONS WITH A MOVING PERIODIC STRUCTURE

In the first section of this chapter the laws of conservation of energy and momentum are used to give a further proof that the frequency and power of a plane electromagnetic wave, after interacting with a single perfect moving reflector or a single moving "nonreflecting interface," change according to the formulas given in Section 3.3.

In Section 5.2, the model of a nonlinear spring is employed to illustrate the transfer of power between the pumping field and the small signal in a nonlinear dielectric or elastic material.

The general theory developed in Chapter III is extended to moving periodic structures of semi-infinite and infinite lengths in Sections 5.3 and 5.4. The frequency components existing in these kinds of structures are found, and the method of determining the various wave amplitudes is briefly described. Various similarities with and distinctions between the electromagnetic wave interaction with a train of moving reflectors (i.e., using a square-wave pump) and that of conventional parametric amplification using a sinusoidal pump are discussed.

Finally, an electrically or mechanically tunable filter using an electromagnetic or elastic rf pulse is described in Section 5.5.

5.1 DERIVATIONS OF THE POWER RELATIONS FOR THE CASES OF A SINGLE, PERFECT MOVING REFLECTOR AND A SINGLE MOVING "NONREFLECTING INTERFACE" USING THE LAWS OF CONSERVATION OF ENERGY AND MOMENTUM

The power relation for the case of a nonrelativistic perfect nonreflecting interface was found in Section 3.5, using the transmission line analogy and the principle of conservation of energy.

We derive in this section, using the laws of conservation of energy and momentum, the power relations which are valid for both the nonrela-

tivistic and relativistic cases for a perfect moving reflector and a moving "nonreflecting interface." This approach has been employed in deriving the power relation for a plane electromagnetic wave interacting with a moving reflector in free space.[54]

5.1.1 A Perfect Moving Reflector

Consider the configuration shown in Fig. 5.1. A plane electromagnetic wave of frequency ω_i and power P_i traveling in a material medium impinges upon a perfect reflector moving with a velocity V, and as a result a wave of frequency ω_r and power P_r is reflected. As previously demonstrated, a moving reflector separating two stationary media can be simulated by applying a voltage step to a proper nonlinear ferroelectric material. An arbitrary reference plane is chosen as shown. We consider the region bounded by the reference plane and the reflector as a system.

For a plane electromagnetic wave, the momentum per unit length is P/V_p^2 and the momentum transfer per unit time (energy density) is P/V_p, where P and V_p are the power and phase velocity of the wave in the nondispersive medium, respectively. Assuming that the momentum flow in the positive x direction is positive, the rate of momentum flow out of the system is

$$\frac{1}{V_{p_i}} (-P_r - P_i) \quad . \tag{5.1}$$

The total momentum of the system is

$$\frac{x}{V_{p_i}^2} (P_i - P_r) \quad . \tag{5.2}$$

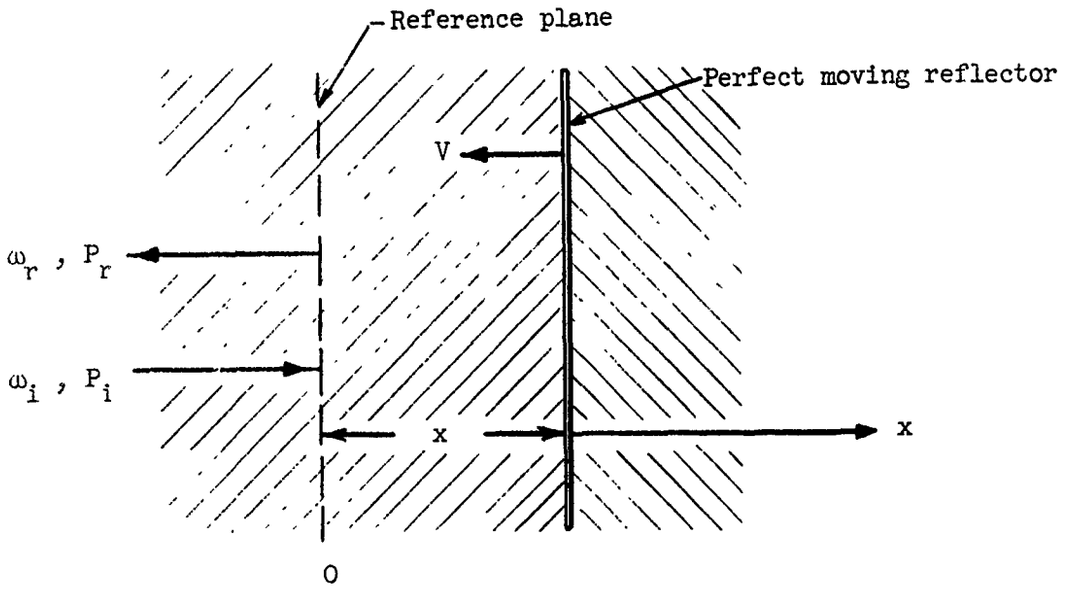

FIG. 5.1--A perfect moving reflector in a material medium. The region bounded by the reflector and the reference plane is considered as a system.

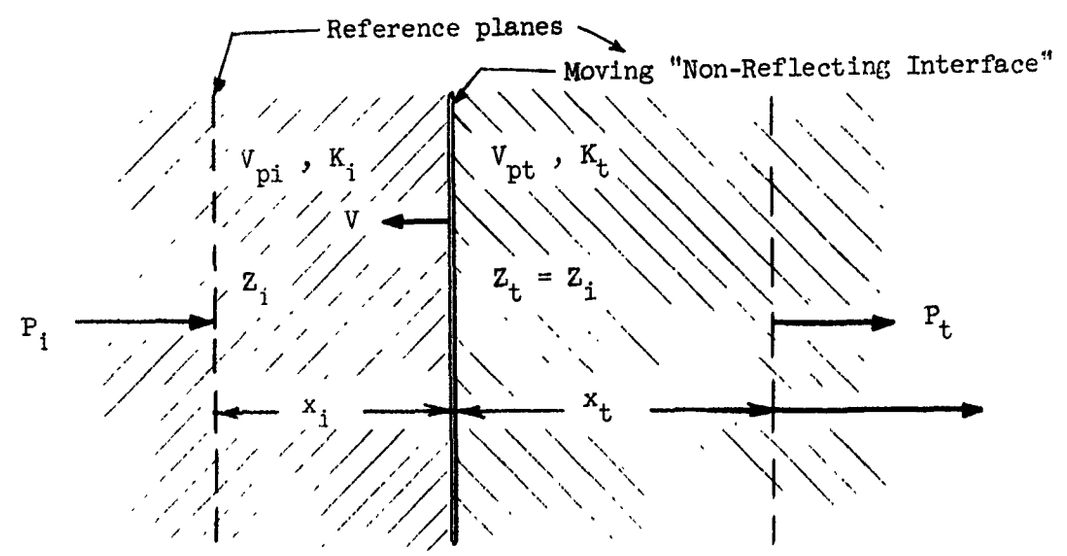

FIG. 5.2--A moving "nonreflecting interface" in a material medium. The region bounded by the two reference planes is considered as a system.

Since $dx/dt = - V$, the rate of increase of the total momentum of the system is

$$\frac{d}{dt}\left[\frac{x}{V_{p_i}^2}(P_i - P_r)\right] = \frac{V}{V_{p_i}^2}(P_r - P_i) \quad . \qquad (5.3)$$

If F is the force the reflector exerts on the waves, then by the law of conservation of momentum the total rate of increase of momentum must be equal to F , yielding

$$F = -\frac{1}{V_{p_i}}(P_i + P_r) + \frac{V}{V_{pi}^2}(P_r - P_i) \quad . \qquad (5.4)$$

Next, we consider the energy of the system. The total rate of energy flow out of the reference plane is

$$P_r - P_i \quad . \qquad (5.5)$$

The total energy stored in the system is

$$\frac{x}{V_{p_i}}(P_i + P_r) \quad , \qquad (5.6)$$

and the rate or change of the total energy stored is

$$-\frac{V}{V_{p_i}}(P_i + P_r) \quad . \qquad (5.7)$$

By the law of conservation of energy, we have

$$\vec{F} \cdot \vec{V} = (P_r - P_i) - \frac{V}{V_{p_i}} (P_i + P_r) \quad . \tag{5.8}$$

Combining Eqs. (5.4) and (5.8), we have the power relation for a perfect reflector:

$$\frac{P_r}{P_i} = \left(\frac{1 + V/V_{p_i}}{1 - V/V_{p_i}} \right)^2 \quad . \tag{5.9}$$

Since from Eq. (3.60)

$$\frac{\omega_r}{\omega_i} = \left(\frac{1 + V/V_{p_i}}{1 - V/V_{p_i}} \right) \quad , \tag{5.10}$$

we have, furthermore,

$$\frac{P_r}{P_i} = \left(\frac{1 + V/V_{p_i}}{1 - V/V_{p_i}} \right)^2 = \left(\frac{\omega_r}{\omega_i} \right)^2 \quad . \tag{5.11}$$

This power relation agrees with that given in Section 3.3 for a perfect moving reflector and is what we set out to prove.

5.1.2 A Perfect Moving "Nonreflecting Interface"

We consider the case of a perfect transmitter as shown in Fig. 5.2. The two media separated by the moving interface have the same impedance $Z_i = Z_t$, hence no reflections will occur; but the wave numbers K_i

and K_t are different so that the transmitted wave has a frequency shift, and hence there is a transfer of energy between the interface and the transmitted wave.

Consider the region bounded by the two reference planes as a system; then, following the same approach as given above, the rate of flow of momentum out of the system is

$$\left(\frac{P_t}{V_{p_t}} - \frac{P_i}{V_{p_i}}\right) \tag{5.12}$$

The total momentum of the system is

$$\left(\frac{x_i}{V^2_{p_i}} P_i + \frac{x_t}{V^2_{p_t}} P_t\right) \quad . \tag{5.13}$$

The rate of increase of the total momentum in the system is

$$\frac{d}{dt}\left(\frac{x_i}{V^2_{p_i}} P_i + \frac{x_t}{V^2_{p_t}} P_t\right) = -\frac{V}{V^2_{p_i}} P_i + \frac{V}{V^2_{p_t}} P_t \quad . \tag{5.14}$$

Combining Eqs. (5.12) and (5.14), we have the total rate of increase of momentum in the system. From the law of conservation of momentum, this must equal to the force the interface exerts on the waves F :

$$F = \left(\frac{P_t}{V_{p_t}} - \frac{P_i}{V_{p_i}}\right) + \left(-\frac{V}{V^2_{p_i}} P_i + \frac{V}{V^2_{p_t}} P_t\right) \quad . \tag{5.15}$$

Next, the total rate of energy flow out of the system is

$$P_t - P_i \quad . \tag{5.16}$$

The total energy stored in the system is

$$x_i \frac{P_i}{V_{p_i}} + x_t \frac{P_t}{V_{p_t}} \quad , \tag{5.17}$$

and the rate of change of the total energy stored in the system is

$$\frac{d}{dt}\left(x_i \frac{P_i}{V_{p_i}} + x_t \frac{P_t}{V_{p_t}}\right) = -\frac{V}{V_{p_i}} P_i + \frac{V}{V_{p_t}} P_t \tag{5.18}$$

By the law of conservation of energy, we have

$$\vec{F} \cdot \vec{V} = (P_t - P_i) + \left(-\frac{V}{V_{p_i}} P_i + \frac{V}{V_{p_t}} P_t\right) \quad . \tag{5.19}$$

Finally, combining Eqs. (5.15) and (5.19), we have the power relation for a perfect "nonreflecting interface:"

$$\frac{P_t}{P_i} = \left(\frac{1 + V/V_{p_i}}{1 + V/V_{p_t}}\right)^2 \tag{5.20}$$

Since, from Eq. (3.59),

$$\frac{\omega_t}{\omega_i} = \left(\frac{1 + V/V_{p_i}}{1 + V/V_{p_t}}\right) \quad , \tag{5.21}$$

we have, furthermore,

$$\frac{P_t}{P_i} = \left(\frac{1 + V/V_{p_i}}{1 + V/V_{p_t}}\right)^2 = \left(\frac{\omega_t}{\omega_i}\right)^2 \quad . \qquad (5.22)$$

Again, this power relation agrees with that given in Section 3.3 for a moving interface with perfect transmission.

5.2 THE POWER TRANSFER BETWEEN THE PUMPING WAVE AND THE SMALL SIGNAL WAVE IN A NONLINEAR MATERIAL

In most of the previous analysis, we have assumed that a moving interface or a series of moving interfaces is induced in a nonlinear material by a (large-amplitude) pumping field. Thus the change in the power of the reflected and transmitted waves after interacting with the moving interface or series of moving interfaces necessarily implies a transfer of power between the pumping field and the small signal waves.

We demonstrate the physical mechanism of this conversion by using the model of a "nonlinear spring" for a nonlinear elastic material and also for a nonlinear dielectric material. This calculation will follow the method used for the transmission line model of Section 3.5.2. Consider a nonlinear spring as shown in Fig. 5.3. Assume the force-displacement law of the nonlinear spring is represented by

$$F = Q_1 x + Q_2 x^2 \quad , \qquad (5.22)$$

where

F = force exerted on the spring

x = displacement of the spring from the quilibrium position

Q_1 = linear spring constant

Q_2 = nonlinear spring constant.

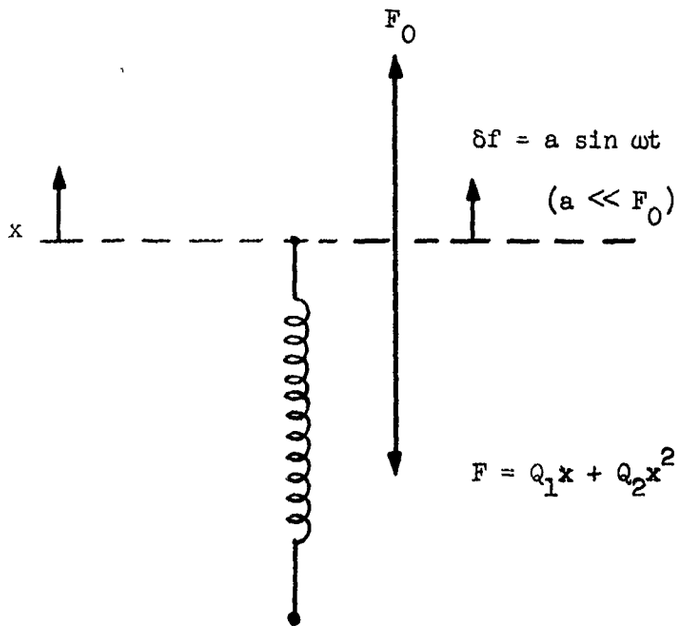

FIG. 5.3--The nonlinear spring used to illustrate the power transfer between the pumping wave and the small signal wave in a nonlinear material.

A static force F_0 and a sinusoidal force $\delta f = a \sin \omega t$, where a is much smaller than F_0, are simultaneously applied to the spring. From Eq. (5.22), we have

$$F_0 + \delta f = F_0 + a \sin \omega t = Q_1 x + Q_2 x^2 \quad . \qquad (5.23)$$

To solve for x in Eq. (5.23), we let

$$x = x_0 + \delta x \quad , \qquad (5.24)$$

and carry out a perturbation calculation; x_0 and δx designate the static and sinusoidal displacements, respectively. Substituting Eq. (5.24) into Eq. (5.23), we have the following equations of harmonic balance:

$$F_0 = Q_1 x_0 + Q_2 x_0^2 + Q_2 \overline{(\delta x)^2} \tag{5.25}$$

$$\delta f = (Q_1 + 2Q_2 x_0)\, \delta x \quad , \tag{5.26}$$

where $\overline{(\delta x)^2}$ denotes the time average of the square of the perturbation displacement, $(\delta x)^2$.

Now, if F_0 is a slowly-varying function of time such that it has no frequency component at ω or higher, Eqs. (5.25) and (5.26) remain valid when the average of $(\delta x)^2$ is taken over only a few cycles of sin ωt . Let us denote this short time average as $\overline{\overline{(\delta x)^2}}$. Then Eqs. (5.25) and (5.26) become

$$\begin{cases} F_0(t) = Q_1 x_0(t) + Q_2 x_0^2(t) + Q_2 \overline{\overline{(\delta x(t))^2}} & (5.27) \\ \delta f = (Q_1 + 2Q_2 x_0(t))\, \delta x(t) \quad . & (5.28) \end{cases}$$

Now, consider the short time average power delivered to the system (the nonlinear spring) by the forces $F_0(t)$ and δf :

$$\overline{\overline{F_0(t)(\dot{x}_0(t) + \delta\dot{x}(t))}} \simeq \overline{\overline{F_0(t)\, \dot{x}_0(t)}} = \overline{\overline{(Q_1 x_0(t) + Q_2 x_0^2(t))\, \dot{x}_0(t)}} + \overline{\overline{Q_2 (\delta x(t))^2\, \dot{x}_0(t)}} \tag{5.29}$$

$$\overline{\overline{\delta f(\dot{x}_0(t) + \delta\dot{x}(t))}} \simeq \overline{\overline{\delta f\, \delta\dot{x}(t)}} = \overline{\overline{(Q_1 + 2Q_2 x_0(t))\, \delta x(t)\, \delta\dot{x}(t)}} \quad . \tag{5.30}$$

From the law of conservation of energy, the sum of Eqs. (5.29) and (5.30) must equal the average rate of increase of the stored energy in the spring. This is given by expression (5.31) if the loss is ignored:

$$(\varrho_1 x_0(t) + \varrho_2 x_0^2(t))\, \dot{x}_0(t) \qquad , \tag{5.31}$$

yielding

$$\overline{\overline{\overline{\varrho_2 (\delta x(t))^2}}}\, \dot{x}_0(t) = - \overline{\overline{\delta f\, \delta x(t)}} \quad . \tag{5.32}$$

The right hand term represents the average power delivered to the force δf by the spring, while the term on the left hand side represents the average power supplied to the spring, over and above the amount required to increase the stored energy as the spring is stretched.

Thus, Eq. (5.32) states that an extra power $\delta P = - \overline{\overline{\delta f\, \delta \dot{x}(t)}}$ is delivered to the oscillating force δf . If δf is the inertial force due to an oscillating mass, then this extra power goes into the oscillation, increasing its amplitude. This transfer of power is what we set out to show.

Similarly, for a nonlinear dielectric, we assume the nonlinear relation between the polarization P and the electric field E as given by

$$E = \eta_1 P + \eta_2 P^2 \qquad , \tag{5.33}$$

where η_1 and η_2 are the linear and nonlinear inverse polarizabilities, respectively.

By using Eqs. (5.34) and (5.35), with $a \ll E_0$, we may proceed in the same way as before and obtain Eq. (5.36) for the power conversion

in the lossless case:

$$\begin{cases} E(t) = E_0(t) + \delta e(t) = E_0(t) + a \sin \omega t & (5.34) \\ P(t) = P_0(t) + \delta p(t) & (5.35) \end{cases}$$

$$\overline{\eta_2 (\delta p(t))^2 \dot{P}_0(t)} = - \overline{\delta e \, \delta \dot{p}(t)} \quad . \qquad (5.36)$$

The right-hand term represents the average power gain of the small-signal wave δe, while the term on the left hand side represents the corresponding average power lost by the pumping field $E_0(t)$. Again, this transfer of power is what we set out to prove.

5.3 WAVE INTERACTION WITH A SEMI-INFINITE MOVING PERIODIC STRUCTURE

Consider that a plane electromagnetic wave is incident upon a semi-infinite moving periodic structure as shown in Fig. 5.4. The moving periodic structure is considered to be induced in a nonlinear material by a rectangular pumping wave. The notation appearing in this figure is the same as used previously.

Applying the principle of "equality of phases" on all moving interfaces, we easily obtain the following four frequency components:

$$\begin{cases} \omega_r = \left(\dfrac{1 + V/V_{p_i}}{1 - V/V_{p_i}} \right) \omega_i \\ \omega_m^+ = \left(\dfrac{1 + V/V_{p_i}}{1 + V/V_{p_t}} \right) \omega_i \\ \omega_m^- = \left(\dfrac{1 + V/V_{p_i}}{1 - V/V_{p_t}} \right) \omega_i \\ \omega_t^+ = \omega_i \\ \omega_t^- = \omega_r \end{cases} \qquad (5.37)$$

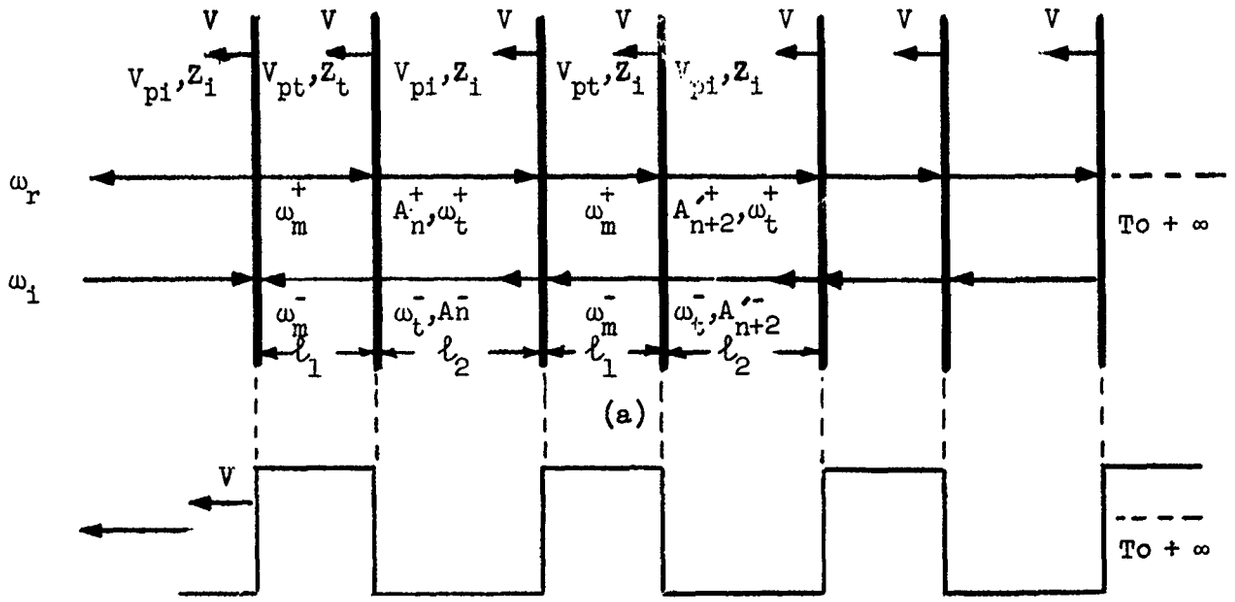

FIG. 5.4--(a) A semi-infinite moving periodic structure.
(b) The rectangular pumping wave used to induce the moving periodic structure (a) in a nonlinear material.

To calculate the reflection and transmission coefficients for the semi-infinite moving periodic structure, we first use the wave matrix technique introduced in Chapter III to determine the equivalent wave matrix for a single period, $[W]$. The wave amplitudes at the input terminal of a period, A_n^+ and A_n^- , are related to the wave amplitudes at the output terminal of the same period, $A_{n+2}'^+$ and $A_{n+2}'^-$ by

$$\begin{bmatrix} A_n^+ \\ A_n^- \end{bmatrix} = [W] \begin{bmatrix} A_{n+2}'^+ \\ A_{n+2}'^- \end{bmatrix} = \begin{bmatrix} W^{++} & W^{+-} \\ W^{-+} & W^{--} \end{bmatrix} \begin{bmatrix} A_{n+2}'^+ \\ A_{n+2}'^- \end{bmatrix}$$

$$n = 1,2,3 \ldots \quad , \qquad (5.38)$$

where W^{++} , W^{+-} , W^{-+} and W^{--} are the components of the wave matrix [W] .

To solve Eq. (5.38), we let

$$\begin{bmatrix} A_n^+ \\ \\ A_n^- \end{bmatrix} = \xi \begin{bmatrix} A'^{+}_{n+2} \\ \\ A'^{+}_{n+2} \end{bmatrix} \quad ; \tag{5.39}$$

then Eq. (5.38) reduces to

$$\xi \begin{bmatrix} A'^{+}_{n+2} \\ \\ A'^{-}_{n+2} \end{bmatrix} = \begin{bmatrix} W^{++} & W^{+-} \\ \\ W^{-+} & W^{--} \end{bmatrix} \begin{bmatrix} A'^{+}_{n+2} \\ \\ A'^{-}_{n+2} \end{bmatrix} . \tag{5.40}$$

Thus, the problem of determining the wave amplitudes reduces to an eigenvalue problem for determining the constants ξ (eigenvalues).[55] From Eq. (5.40), the eigenvalues are found by solving the following equation:

$$\begin{vmatrix} W^{++} - \xi & W^{+-} \\ \\ W^{-+} & W^{--} - \xi \end{vmatrix} = 0 \tag{5.41}$$

i.e.,

$$\xi_1 , \xi_2 = \frac{1}{2}(W^{++} + W^{--}) \pm \frac{1}{2}\sqrt{(W^{++} + W^{--})^2 - 4(W^{++}W^{--} - W^{+-}W^{-+})} . \tag{5.42}$$

After the eigenvalues ξ are found, the wave amplitudes can be easily determined by substituting ξ into Eqs. (5.39) and (5.40). The reflection coefficient R and transmission coefficient T will be given by the following equations:

$$R \equiv \frac{A_n^-}{A_n^+} = \frac{A'^-_{n+2}}{A'^+_{n+2}} = \frac{\xi - W^{++}}{W^{+-}} \tag{5.43}$$

$$T \equiv \frac{A'^+_{n+2}}{A_n^+} = \xi \quad . \tag{5.44}$$

Due to the extremely complicated espressions for W^{++}, W^{+-}, W^{-+} and W^{--}, no analytical method for determining the constants ξ has yet been found. Nevertheless, numerical calculation can be carried out. We omit this numerical calculation and pursue a more interesting topic in the next section.

5.4 APPLICATION OF THE GENERAL THEORY TO THE FREQUENCY CONVERTERS

Consider that a square-wave pumping signal induces changes in the permittivity ϵ of a nondispersive nonlinear material as shown in Fig. 5.5 and Fig. 5.6 for the cases of infinite and semi-infinite structures, respectively. The general theory predicts that there will be four frequency components present in both structures: ω_1, ω_m^+, ω_m^- and ω_2, plus the repetition rate or the fundamental pumping signal frequency $\omega_p = 2\pi V/\ell$. They are as follows:

$$\omega_2 = \left(\frac{1 + V/V_{p_1}}{1 - V/V_{p_1}}\right) \omega_1 \tag{5.45}$$

$$\omega_m^+ = \left(\frac{1 + V/V_{p_1}}{1 + V/V_{p_2}}\right) \omega_1 \tag{5.46}$$

$$\omega_m^- = \left(\frac{1 + V/V_{p_1}}{1 - V/V_{p_2}}\right) \omega_1 \quad , \tag{5.47}$$

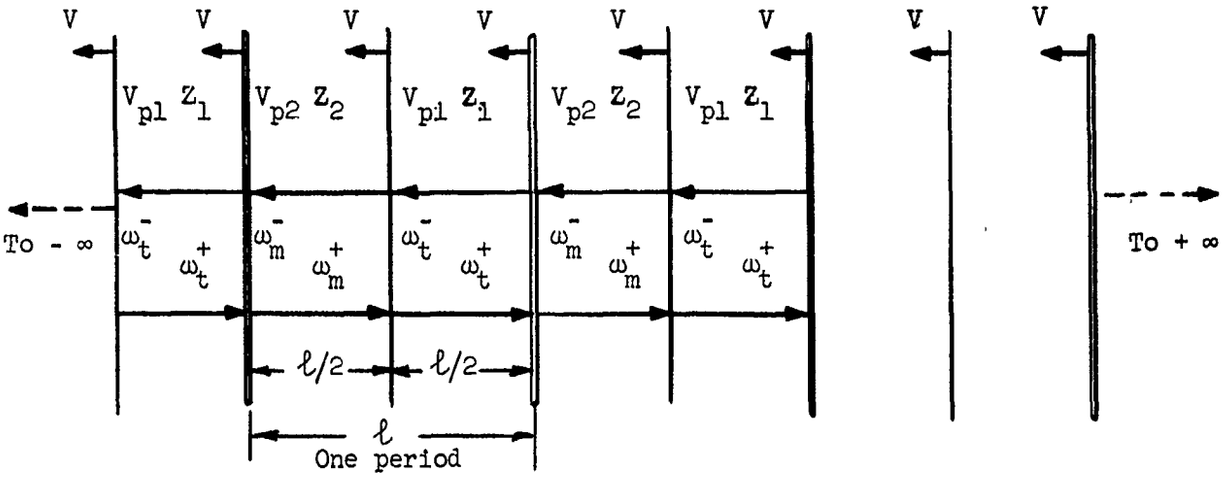

FIG. 5.5--An infinite moving periodic structure induced in a nonlinear material using a square-wave pump.

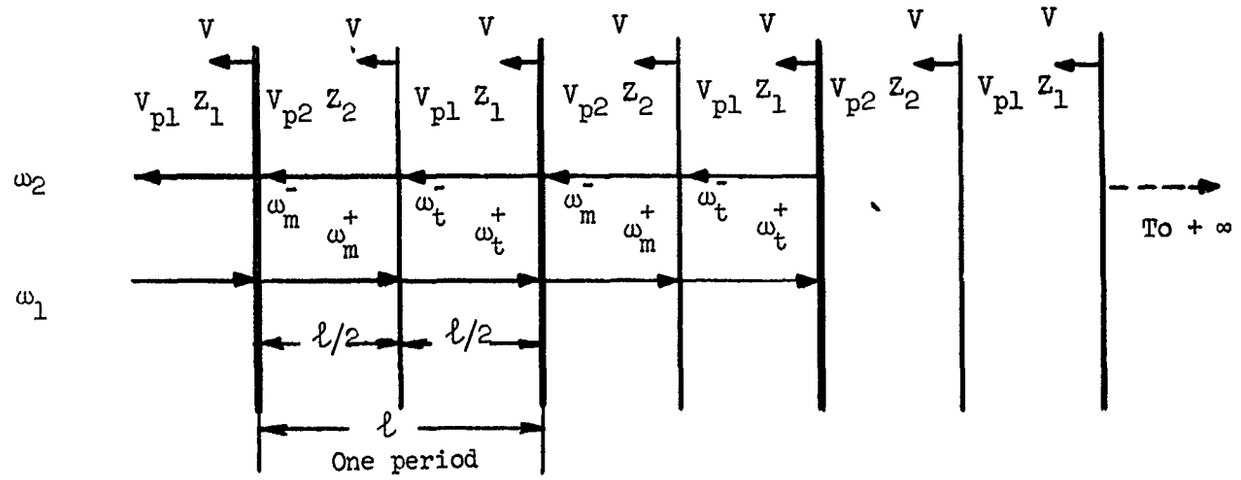

FIG. 5.6--A semi-infinite moving periodic structure induced in a nonlinear material using a square-wave pump.

and

$$\omega_t^+ = \omega_1 \tag{5.48}$$

$$\omega_t^- = \omega_2 \tag{5.49}$$

$$\omega_p = \frac{2\pi V}{\ell} \quad . \tag{5.50}$$

The smaller number of frequency components resulting from a square wave pump is a remarkable result of this analysis. This is in contrast with the sinusoidal pump case, where there is an infinite number of frequency components:[56,57]

Consider more specifically the case of a semi-infinite structure in which the frequency component ω_2 can be utilized (see Fig. 5.6). In order to have a maximum amplitude for the frequency component ω_2, the separation $\ell/2$ and hence the pumping pulse width must be properly adjusted so that reflections from the various periods will add in phase. This can be achieved by imposing the following condition:

$$\frac{\omega_m^+}{V_{p_2}} \cdot \frac{\ell}{2} + \frac{\omega_t^+}{V_{p_1}} \cdot \frac{\ell}{2} + \frac{\omega_t^-}{V_{p_1}} \cdot \frac{\ell}{2} + \frac{\omega_m^-}{V_{p_2}} \cdot \frac{\ell}{2} = 2n\pi$$

$$n = 1,2, \ldots \quad . \tag{5.51}$$

Substituting Eqs. (5.45) - (5.49) into Eq. (5.51), we obtain the length ℓ for optimum reflection:

$$\ell = \frac{2n\pi}{\omega_1 \left\{ \dfrac{1}{V_{p_1}(1 - V/V_{p_1})} + \dfrac{(1 + V/V_{p_1})}{V_{p_2}[1 - (V/V_{p_2})^2]} \right\}}$$

$$n = 1,2,3, \ldots \quad . \tag{5.52}$$

For the case $V_{p_1} \approx V_{p_2} = V_p$, which will be discussed in detail later, Eq. (5.52) reduces to

$$\ell \approx \frac{n\pi V_p(1 - V/V_p)}{\omega_1} \qquad (5.53)$$

$$n = 1,2,3, \ldots \quad .$$

Notice that when $V \to 0$, $\ell \to n\lambda/2$ as it should, and we can interpret the large reflection as due to the stop-band of a moving periodic structure.

When the change of dielectric constant induced by the pumping signal is small, as in the case of conventional frequency converters,[58,59] the following approximation for the phase velocity is valid:

$$V_{p_1} \approx V_{p_2} \equiv V_p \quad . \qquad (5.54)$$

Using Eq. (5.54), Eqs. (5.45), (5.46) and (5.47) reduce to

$$\begin{cases} \omega_m^+ \approx \omega_t^+ \approx \omega_1 & (5.55) \\ \omega_m^- \approx \omega_t^- \approx \omega_2 & (5.56) \\ \omega_p = \dfrac{2\pi V}{\ell} \quad . & (5.50) \end{cases}$$

Thus, the system reduces to one containing only the three frequency components ω_1 , ω_2 and ω_p , when $V_{p_1} \approx V_{p_2}$.

We continue to consider the case $V_{p_1} \approx V_{p_2}$. In order to have a strong interaction and hence a large reflection, we impose the following condition so that all reflections add in phase:

$$\frac{\omega_2}{V_p} \ell + \frac{\omega_1}{V_p} \ell = 2n\pi \quad , \quad n = 1,2, \ \ldots \quad . \tag{5.57}$$

But from Eq. (5.45) (the pumping wave and the incident wave are contra-directional), we have

$$\frac{V}{V_{p_1}} \approx \frac{V}{V_p} = \frac{\omega_2 - \omega_1}{\omega_2 + \omega_1} \quad . \tag{5.58}$$

Combining Eqs. (5.50), (5.56) and (5.58), we have the following frequency relation for large reflection:

$$\omega_2 = \omega_1 + n\omega_p \quad , \quad n = 1,2,3, \ \ldots \quad . \tag{5.59}$$

For $n = 1$, we have

$$\omega_2 = \omega_1 + \omega_p \tag{5.60}$$

If we define the wave number of the pump signal K_p as ω_p/V , then Eqs. (5.59) also leads to

$$K_2 = nK_p - K_1$$

or

$$\vec{K}_2 = n\vec{K}_p + \vec{K}_1 \tag{5.61}$$

and

$$K_2 = K_p - K_1$$

$$\vec{K}_2 = \vec{K}_p + \vec{K}_1 \tag{5.62}$$

for $n = 1$. It is interesting to notice that the frequency relations (5.60) and the wave number relation (5.63) are just that of the conditions for optimum interaction in a conventional frequency converter (up-conversion) using a sinusoidal pump, where ω_1 , ω_2 and ω_p are, respectively, the signal, idler and pump frequencies.[58] Figure 5.7a shows the frequency and wave number relations for up-conversion.

Simon[60] considers this circuit and obtains the same frequency shift in the reflected wave for $n = 1$ for a sinusoidal pumping wave. Simon calls this a case of Bragg interference of the first order and attributes the frequency shift in the reflected wave to the Doppler effect, as we do.

For $n > 1$, Eqs. (5.59) and (5.61) predict the existence of higher order sidebands with higher frequencies. This also has been predicted for the case of the conventional frequency converter using a nondispersive medium.[56,57] Following Simon, we designate these as Bragg interference of higher orders. It is important to remember that we have been considering the case in which the pump signal propagates in the direction against the signal wave.

Similarly, for the case in which both the pump and signal propagate in the same direction, with the same assumption $V_{p_1} \approx V_{p_2} \equiv V_p$, the system also reduces to one containing only three frequencies ω_1 , ω_2 and ω_2 . They are as follows:

$$\begin{cases} \omega_m^+ \approx \omega_t^+ \approx \omega_1 & (5.55) \\ \omega_m^- \approx \omega_t^- \approx \omega_2 = \left(\dfrac{1 - V/V_{p_1}}{1 + V/V_{p_1}} \right) \omega_1 & (5.63) \\ \omega_p = \dfrac{2\pi V}{\ell} & (5.50) \end{cases}$$

From Eq. (5.63), we have

$$\frac{V}{V_{p_1}} \approx \frac{V}{V_p} = \frac{\omega_1 - \omega_2}{\omega_1 + \omega_2} \quad . \qquad (5.64)$$

Combining Eqs. (5.50), (5.56) and (5.64), we have the frequency relation for strong interaction:

$$\omega_2 = \omega_1 - n\omega_p \quad , \qquad n = 1,2,3, \ldots \quad . \tag{5.65}$$

For $n = 1$, Eq. (5.65) becomes

$$\omega_2 = \omega_1 - \omega_p \quad . \tag{5.66}$$

If K_p is defined as previously, i.e., $K_p = \omega_p/V$, then Eq. (5.54) also leads to

$$K_2 = nK_p - K_1$$

or

$$\vec{K}_2 = -n\vec{K}_p + \vec{K}_1 \tag{5.67}$$

and

$$K_2 = K_p - K_1$$

or

$$\vec{K}_2 = -\vec{K}_p + \vec{K}_1 \quad , \tag{5.68}$$

for $n = 1$.

Again, we notice that Eqs. (5.66) and (5.68) are the frequency and wave number relations of a conventional frequency converter (down-conversion) using a sinusoidal pump, where ω_1 , ω_2 and ω_p are the signal, idler, and pump frequencies, respectively. Figure 5.7b shows the frequency and wave number relations for down conversion. When $n > 1$, Eq. (5.67) indicates the possibility of higher-order parametric interaction.

It is important to note that although higher-order interactions for both the square-wave pump assumed in this analysis and the sinusoidal-wave pump used in the conventional frequency converter or parametric amplifier, the higher order interactions will be larger in the case of square-wave pump because of its harmonic content.

Finally, we proceed to discuss another important aspect of this analysis of wave interaction with a series of moving interfaces, namely,

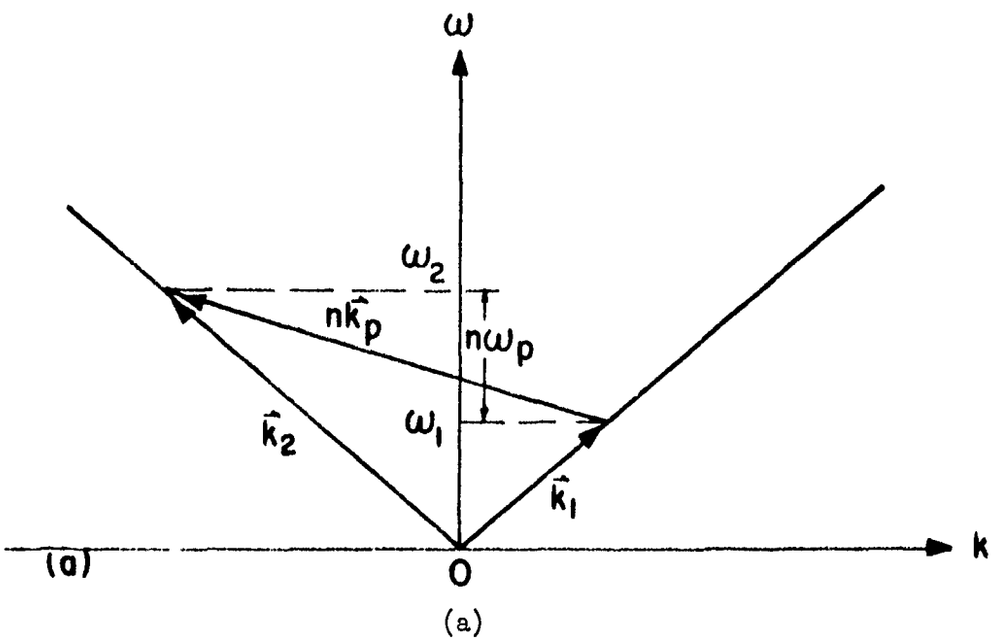

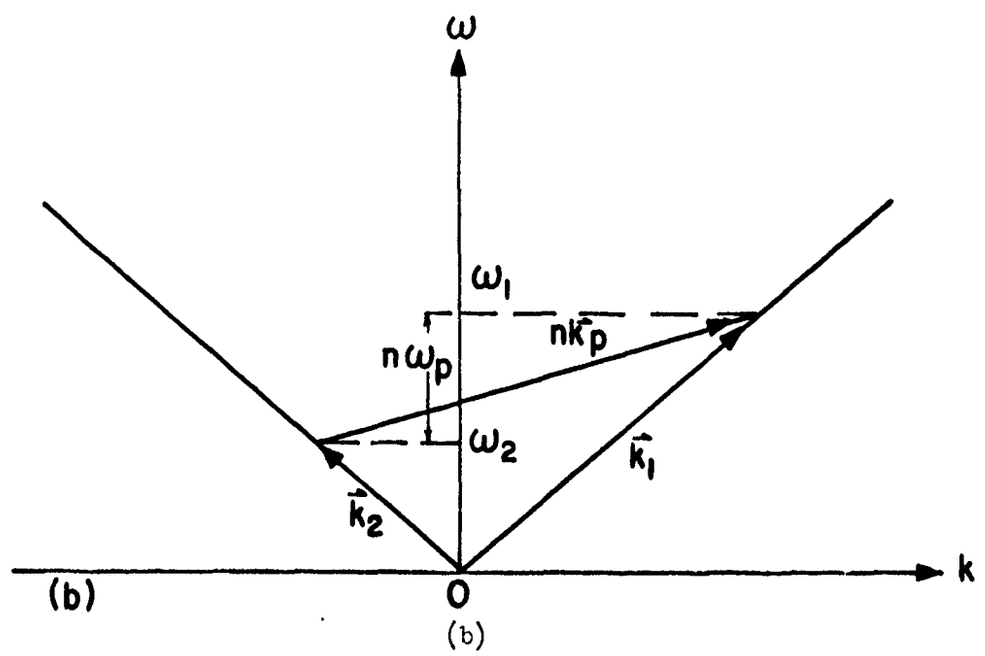

FIG. 5.7--Frequency and wave number relations for frequency converters: (a) up-conversion; (b) down-conversion.

to see if the Manley-Rowe power relations[58,61] are satisfied. The Manley-Rowe power relations involving frequency conversion for a purely reactive system are

$$\frac{P_1}{\omega_1} = \frac{P_2}{\omega_2} = \frac{P_3}{\omega_3} \cdots\cdots = \frac{P_n}{\omega_n} \quad , \tag{5.69}$$

where P_1 , P_2 , P_3 , . . . P_n are the net input or output powers, and ω_1 , ω_2 , ω_3 . . . ω_n are the corresponding frequencies.

From the results of Section 3.3 and Section 5.1, the power relations for a perfect moving reflector, a perfect moving "nonreflecting interface," and a moving interface separating two dielectric media are given by Eqs. (5.70), (5.71) and (5.72), respectively:

$$\frac{P_i}{\omega_i^2} = \frac{P_r}{\omega_r^2} \quad , \tag{5.70}$$

$$\frac{P_i}{\omega_i^2} = \frac{P_t}{\omega_t^2} \quad , \tag{5.71}$$

and

$$\frac{P_i}{\omega_i^2} = \frac{P_r}{\omega_r^2 \left(\frac{Z_2 - Z_1}{Z_1 + Z_2}\right)^2} = \frac{P_t}{\omega_t^2 \left(\frac{2\sqrt{Z_1 Z_2}}{Z_1 + Z_2}\right)^2} \quad . \tag{5.72}$$

Obviously, the simple Manley-Rowe relationships are not satisfied in any of the three cases considered. This conclusion should not be considered surprising, since the stored energy of the system (bounded by the reference plane and the reflector or by the two reference planes as shown in Figs. 5.1 and 5.2 has a steady decrease, while the Manley-Rowe relationship is derived for a stationary process in which the stored

energy does not steadily increase or decrease with time.[55]

In order to see whether the Manley-Rowe power relations are satisfied in the infinite or semi-infinite moving periodic structures induced by the rectangular-pumping wave or more specificially the square-pumping wave, we have to carry out the calculations for the wave amplitudes as indicated in Section 5.3. Here we consider a special case in which a train of short pulses is used to induce a train of moving discontinuities or "moving paddles"[55] (see Fig. 5.8). The spacing of the paddles is such that all reflections from the paddles add in phase.

Since the moving periodic structure considered is infinite, the stored energy and momentum can be assumed to be constant for steady-state operation. Applying the principles of conservation of energy and momentum employed by Pierce[55] and also illustrated in Section 5.1 for plane electromagnetic waves, the rate of momentum (force F) in the system is

$$F = \frac{1}{V_{p_1}} (P_2 + P_1) \quad , \tag{5.73}$$

and the rate of increase of energy $(\vec{F} \cdot \vec{V})$ in the system is

$$FV = (P_2 - P_1) \quad . \tag{5.74}$$

Solving Eqs. (5.73) and (5.74), we have

$$\frac{P_2}{P_1} = \left(\frac{1 + V/V_{p_1}}{1 - V/V_{p_1}} \right) \quad . \tag{5.75}$$

But, from Eq. (5.45), we have

$$\frac{\omega_2}{\omega_1} = \left(\frac{1 + V/V_{p_1}}{1 - V/V_{p_1}} \right) \quad . \tag{5.76}$$

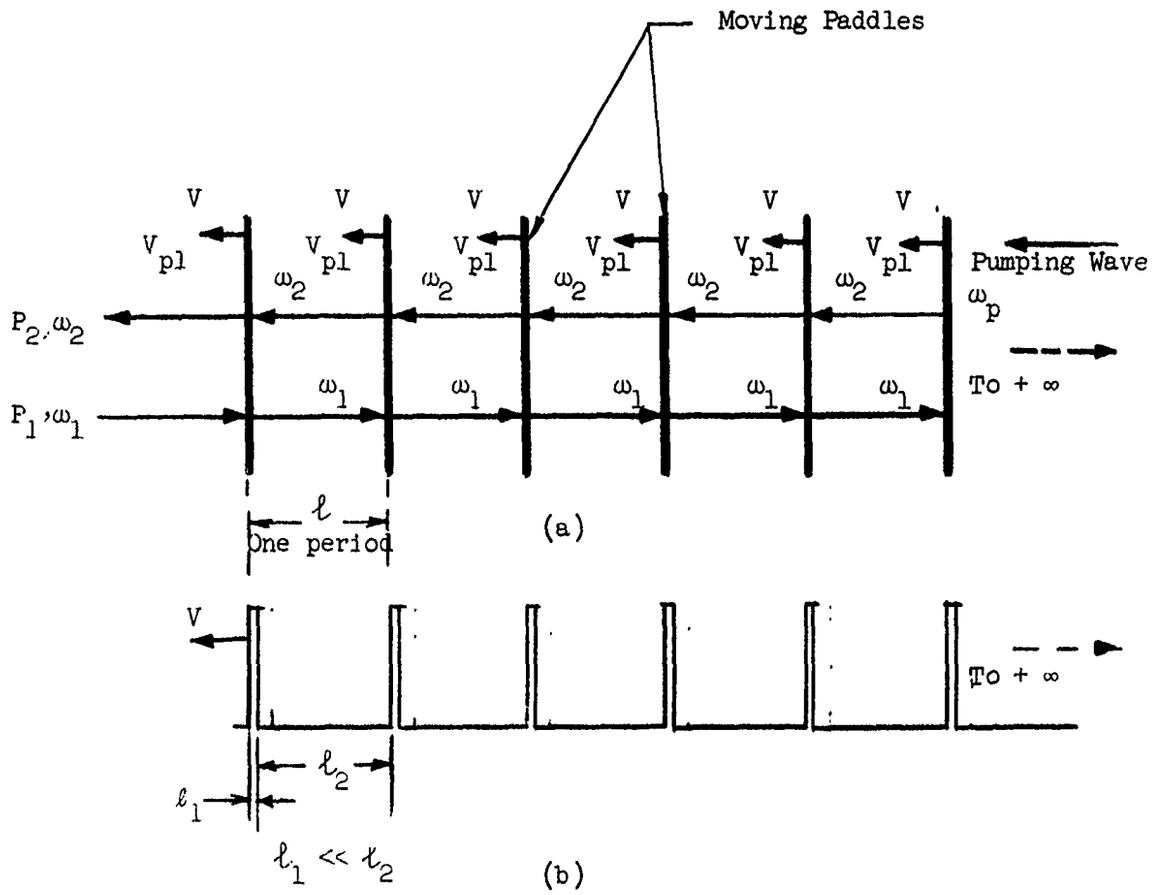

FIG. 5.8(a)--A semi-infinite "moving paddles" structure.
(b)--A semi-infinite train of short pulses used to induce the structure of (a) in nonlinear materials.

Finally, we have the Manley-Rowe relation

$$\frac{P_2}{P_1} = \frac{\omega_2}{\omega_1} \quad . \tag{5.77}$$

It is important to emphasize again that for this to occur, the frequency of the incident, reflected, and pump waves must satisfy a relation of the following form:

$$\omega_2 = \omega_1 + n\omega_p \quad , \qquad n = 1,2, \ldots \tag{5.78}$$

$$\vec{K}_2 = \vec{K}_1 + n\vec{K}_p \qquad n = 1,2, \ldots \quad . \tag{5.79}$$

Furthermore, if we consider the pumping power P_p to be equal to FV, we have the following Manley-Rowe power relations by combining Eqs. (5.74), (5.77) and (5.78):

$$\frac{P_1}{\omega_1} = \frac{P_2}{\omega_2} = \frac{P_p}{n\omega_p} \quad , \quad n = 1, 2, \ldots \quad . \tag{5.80}$$

5.5 DOPPLER SHIFT FREQUENCY CONVERTER AND ELECTRICALLY OR MECHANICALLY TUNABLE FILTER.[62]

From the analysis given in Section 5.4, it is conceivable that a device can be constructed to convert an input frequency and power to a higher output frequency and power by using an electromagnetic or elastic rf pulse. The pulse will induce in a nonlinear material a series of moving periodically-spaced regions of differing impedance (see Fig. 5.9). The advantage of using an rf pulse is that a large reflection, if the periodicity is adjusted according to Eqs. (5.52) or (5.53), can be achieved even if the rf pulse builds up slowly over a large number of wavelengths. Thus this device could be used for frequency conversion of either electromagnetic or elastic waves. By

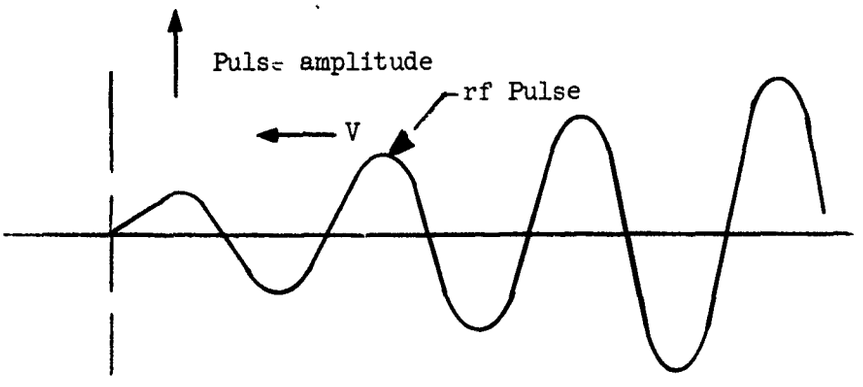

(a)

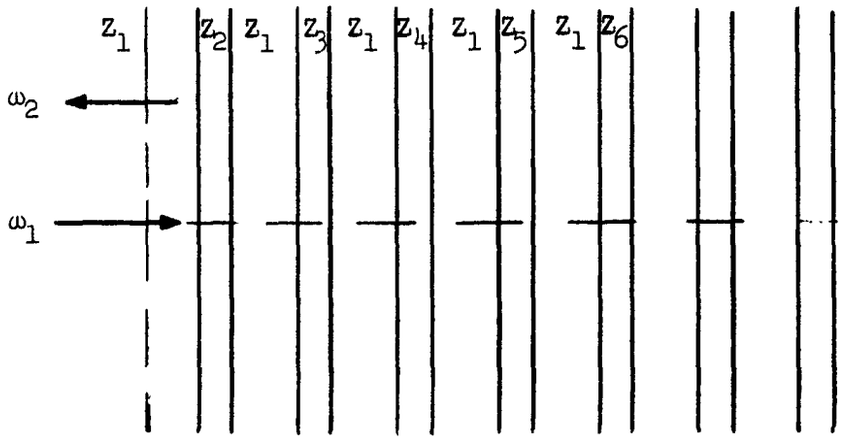

(b)

FIG. 5.9(a)--An rf pulse.
(b)--A moving periodic structure induced by the rf pulse in a nonlinear material.

using a semi-infinite periodic medium, one obtains better than a Manley-Rowe power conversion, according to Eqs. (5.70) - (5.72).

Similarly, by using the same principle a spatial periodicity in dielectric constant can be induced by setting up a standing electromagnetic or elastic wave in a material which has an electric field, pressure-dependent dielectric constant. The medium which has a spatial periodicity in dielectric constant behaves as a filter structure, with stop-band frequencies determined by the periodicity and stop-band widths determined by the degree of dielectric modulation. Thus an electrically or mechanically-tunable filter can be constructed by adjusting the frequency and amplitude of the modulating electromagnetic or elastic wave.[62,63]

CHAPTER VI

A NONRELATIVISTIC CASE: LASER LIGHT INTERACTIONS WITH HIGH FREQUENCY ACOUSTIC WAVES

6.1 INTRODUCTION

In the first part of this study a theoretical analysis of the frequency shifts and amplitudes changes of an electromagnetic wave interacting with a single moving interface or a series of moving interfaces in nonlinear solids was given. The results suggest many Doppler shift experiments provided that appropriate materials are available. Specifically considering the case of a semi-infinite periodic structure such as that discussed in Section 5.3 and 5.4, an example of electromagnetic wave – electromagnetic wave interaction at a microwave frequency is that of a microwave EM wave interacting with a moving periodic structure induced by a second (large amplitude) microwave EM wave. For this case the $KTaO_3$ single crystal at liquid-helium temperature shows the greatest promise.[64] Unfortunately, reasonably large $KTaO_3$ single crystals are not available at present. For the case of a light wave-light wave interaction, i.e., a laser light interacting with a moving periodic structure induced by a giant pulse laser, $LiNbO_3$ and KDP crystals at room temperature are among the potential materials to be used.[65] This experiment, although feasible, seems to require an extremely large amount of laser power. A similar experiment is also possible for acoustic waves at microwave frequency using nonlinear crystals such as MgO and SiO_2.

As a result of the availability of CW laser sources such as helium-neon gas lasers and the development of experimental techniques for generating high-frequency acoustic waves, there has been a renewed and active interest in the topic of light interaction with acoustic waves. It will be shown in this chapter that this subject can be considered as a nonrelativistic case of the general theory developed in the previous

chapters. Various experiments involving laser light interactions with high frequency acoustic waves in solids have been carried out, and some results are considered in the experimental part of this study. That the interaction of laser light with acoustic waves in solids can be treated by analogy with the problem of an electromagnetic wave interacting with a large number of nonrelativistic moving interfaces can be explained by the following intuitive argument. An acoustic wave will excite density modulation which varies periodically in time and in space in solids. Since the refractive index or dielectric constant of a solid is a function of its density, it will vary periodically in time and in space according to the density modulation. That the scattering from a medium with refractive index varying periodically in time and in space can be treated using an equivalent "series of moving interfaces" is shown in Section 6.4. Thus an acoustic wave can be considered to induce a series of moving interfaces. A light wave will encounter diffraction or scattering (or reflection, following the language used previously) when propagating through such a series of moving interfaces. The frequencies present in the diffracted and transmitted light are expected to be shifted from that of the incident light, due to the Doppler effect.

The frequency shifts of the diffracted light (predicted according to the Doppler principle as discussed in the previous chapters) are shown to agree with these obtained by the Raman-Nath theory and the experimental results. Due to the small value of the ratio of the acoustic wave velocity to the light velocity in the crystal, the frequency shifts in the diffracted and transmitted light are very small compared with the frequency of the incident light.

A brief description of the Raman-Nath theory and some extended theories which successfully interpret the experimental results of light diffraction using ultra high frequency acoustic waves in liquids are given in Section 6.2. The frequency shifts in the diffracted and transmitted light and the conditions for strong diffraction are derived in Section 6.3 using the moving reflector theory. Section 6.4 gives the derivation for the diffraction intensity using the "Ray-Tracing and Cascade Network" method. The diffracting power of various crystals is

also predicted in this subsection. An alternative method for calculating the diffraction intensity using the parametric principle and coupled-mode theory is briefly described in Section 6.5. The dependence of the diffraction intensity on the acoustic wave frequency, when the Bragg condition is not satisfied exactly, is given in this subsection. Section 6.6 describes means for diffracting a large portion of laser light. Finally, in Section 6.7 an analysis of the enhancement of diffraction due to acoustic resonance is given.

6.2 THE RAMAN-NATH AND THE RELATED THEORY

We first give a brief survey of the theory of light diffraction using high frequency acoustic waves. The diffraction of light by ultrasonic waves, commonly known as Brillouin scattering, was the subject of extensive experimental and theoretical research in the 1930's and 1940's. Brillouin[66] was first to predict these diffraction phenomena, and Debye, Sears;[67] Lucas, Biquard,[68] etc., experimentally observed this diffraction phenomenon in 1932. R. Bär[69] also carried out various kinds of experiments and theoretical interpretations in the 1930's. During this period the acoustic waves were almost exclusively generated in liquids and at frequencies below 50 Mc/sec.

Probably the most complete theory for the diffraction of light by ultrasonics is the one developed by Raman and Nath[70] in 1935 and 1936. Raman and Nath, in parts 1, 2 and 3 of their theories, considered that the phase of the light is corrugated after traversing through the medium due to the presence of an acoustic wave which induces a sinusoidal change of index of refraction in the medium. The corrugated wave-front then causes the diffraction. Thus the acoustic wave acts as a phase grating. Consider the configuration of Fig. 6.1 in which the change of index of refraction $\eta(x)$ is expressed by Eq. (6.1). The directions for the maximum diffracted light, i.e., the orders of diffraction, θ_n , are determined by Eq. (6.2) and the diffraction intensities I_m , I_n are

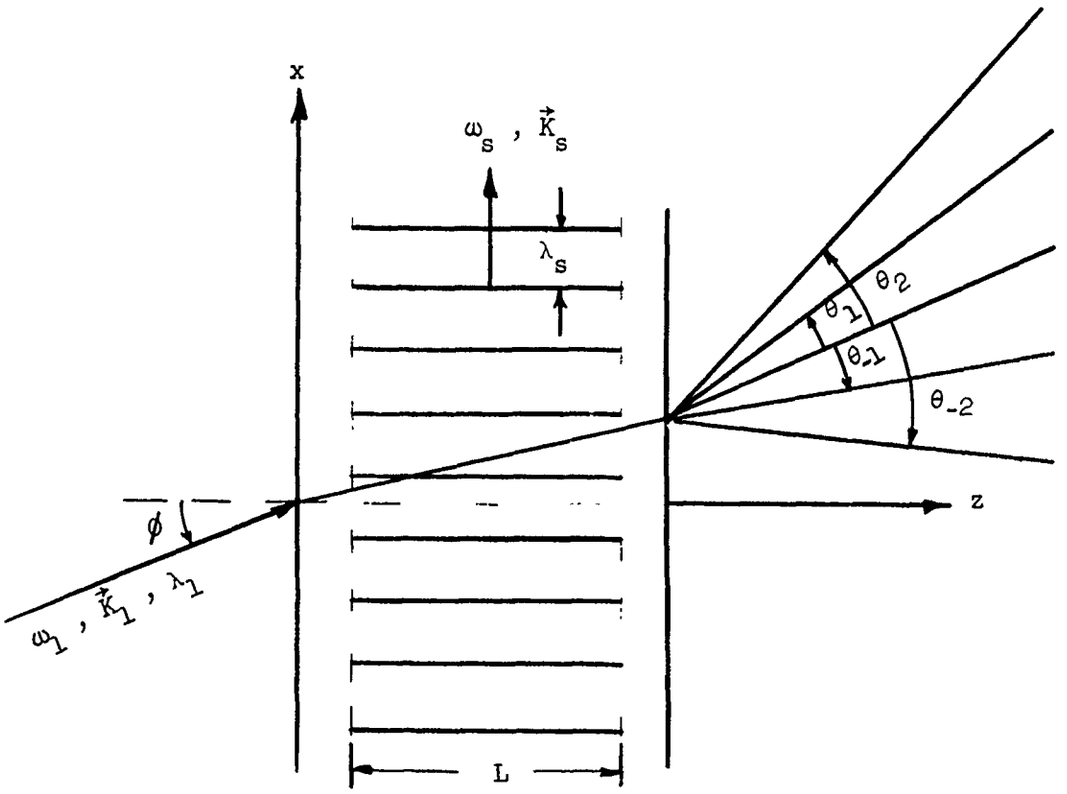

FIG. 6.1--The configuration for the diffraction of light by ultrasonics (oblique incidence).

determined by Eq. (6.3):

$$\eta(x) = \eta_0 - \Delta\eta \sin \frac{2\pi x}{\lambda_s} \tag{6.1}$$

$$\sin(\phi + \theta_n) - \sin \phi = \pm \frac{n\lambda_1}{\lambda_s} \quad , \quad n = 0, 1, 2, \ldots \tag{6.2}$$

and

$$\frac{I_m}{I_n} = \frac{J_m^2(r)}{J_n^2(r)} \quad , \quad m,n = 0, \pm 1, \pm 2, \ldots \tag{6.3}$$

where

$$r \equiv \frac{2\pi\Delta\eta L}{\lambda_1} \sec \phi \cdot \frac{\sin\left(\frac{\pi L \tan \phi}{\lambda_s}\right)}{\left(\frac{\pi L \tan \phi}{\lambda_s}\right)} \tag{6.4}$$

η_0 = the index of refraction of the uperturbed medium

$\Delta\eta$ = the maximum change of index of refraction of the medium due to the acoustic waves

λ_s = the wavelength of the acoustic wave in the medium

λ_1 = the wavelength of the light wave outside of the medium

ϕ = the incident angle of the light wave outside of the medium

θ_n = the angle of the $\pm n^{th}$ -order diffraction outside the medium

L = the acoustic beam width

I_m, I_n = the diffraction intensities of the $\pm m^{th}$- and $\pm n^{th}$ - orders. respectively

J_m, J_n = the Bessel functions of orders m and n , respectively.

For normal incidence (see Fig. 6.2) from Eqs. (6.2), (6.3) and (6.4) with $\phi = 0$, we have

$$\sin \theta_n = \pm \frac{n\lambda_1}{\lambda_s} , \quad n = 0, 1, 2, \ldots \tag{6.5}$$

$$\frac{I_m}{I_n} = \frac{J_m^2(r)}{J_n^2(r)} , \quad m,n = 0, \pm 1, \pm 2, \ldots \tag{6.6}$$

$$r \equiv \frac{2\pi\Delta\eta L}{\lambda_1} . \tag{6.7}$$

We note that for normal incidence, the Raman-Nath theory predicts symmetrical equally-spaced diffracted spots and that the diffraction intensities depend on the incident light wave-length, the interaction length and the ultrasonic intensity. We further notice that for oblique incidence the diffraction intensities among the orders vary and an asymmetry occurs when ϕ varies from 0.

There exist frequency shifts in the diffracted light. The frequency shift in the $\pm n^{th}$ order diffraction is $\pm n\omega_s$ when a traveling acoustic wave is used (see Fig. 6.3). When a standing acoustic wave is used, the frequency shifts in all even orders diffractions are $\pm 2n\omega_s$. In all odd orders, diffractions are $\pm(2n + 1)\,\omega_s$, where n is positive integer (see Fig. 6.4).

In the case of a traveling acoustic wave, the relative intensities of the $\omega_1 \pm n\omega_s$ components are given by Eq. (6.6), while for the case of a standing acoustic wave, the relative intensity of the $\omega_1 \pm 2n\omega_s$ sub-components in the $2N^{th}$ order is given by $J^2_{N-n}(r/2)\, J^2_{N+n}(r/2)$, and the relative intensity of the $\omega_1 \pm (2n + 1)\,\omega_s$ sub-components in the $(2N + 1)^{th}$ order is given by $J^2_{N-n}(r/2)\, J^2_{N+n+1}(r/2)$.

It is important to remember that in the above-quoted results only the phase changes in the light beam due to acoustic waves are considered. In parts 4 and 5 of the series of papers by Raman and Nath both the

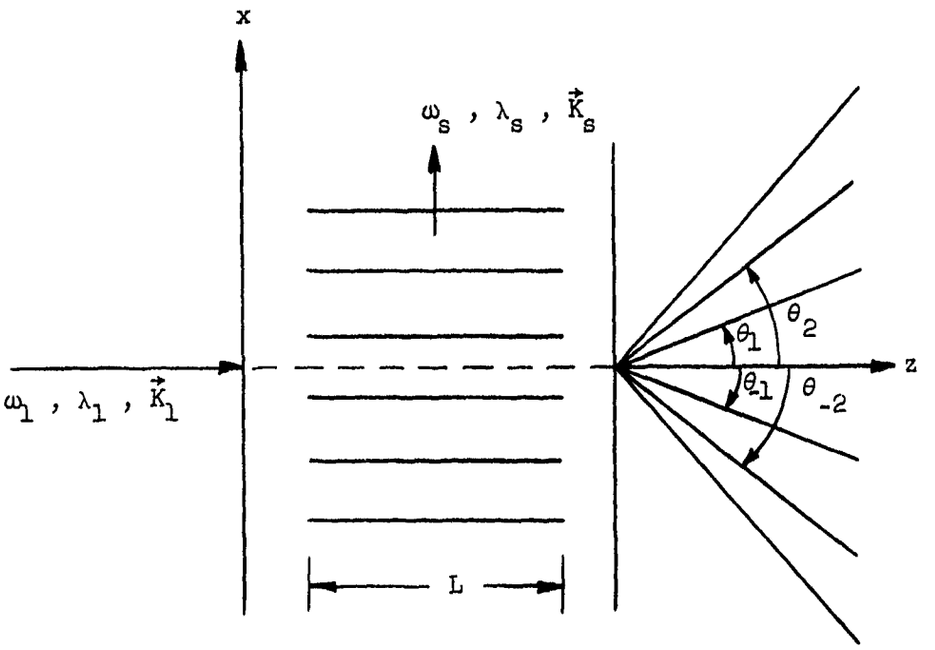

FIG. 6.2--Configuration for the diffraction of light by ultrasonics (normal incidence).

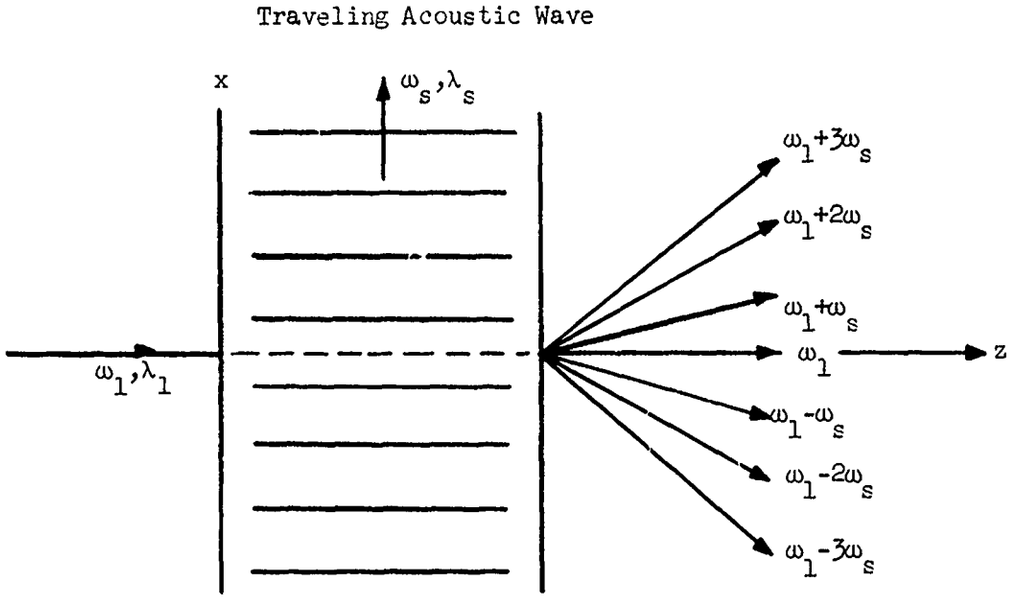

FIG. 6.3--The frequency shifts in the diffracted light using traveling acoustic waves.

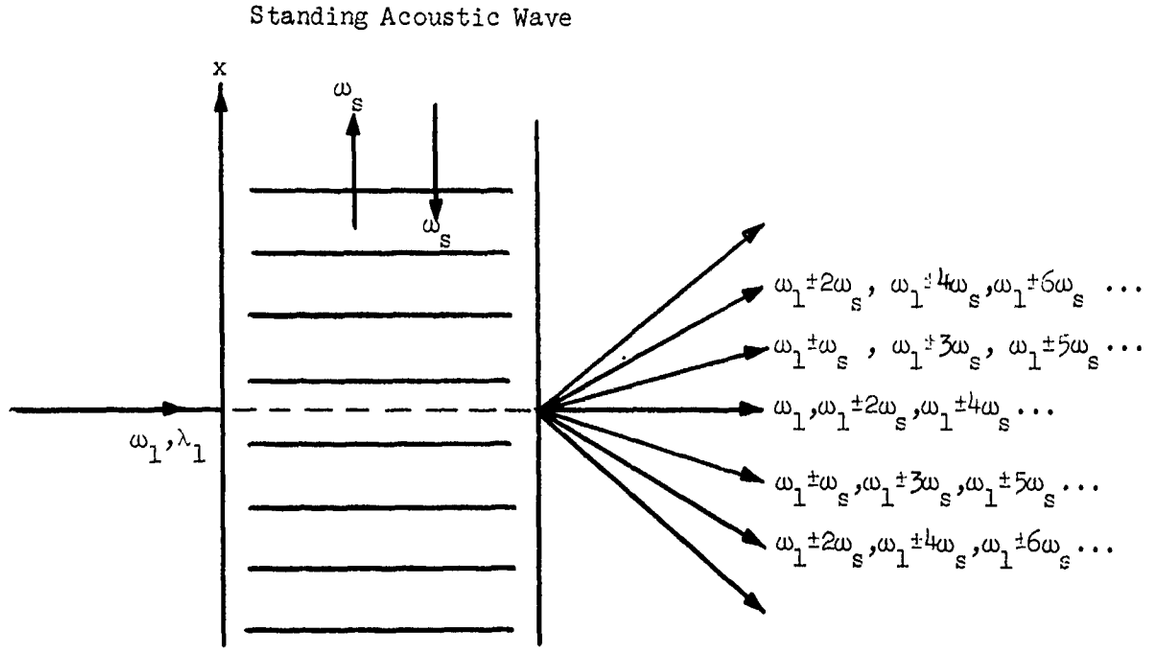

FIG. 6.4--The frequency shifts in the diffracted light using standing acoustic waves.

amplitude changes and the phase changes in the light beam due to acoustic waves are taken into account. This is called the generalized Raman-Nath theory. The conclusions on the angles of diffraction and the frequency sub-components in all orders given previously remain valid, but the relative intensities of various orders $|\Phi_n|^2$ are determined by the differential-difference equations [(6.8), (6.9)] for traveling and standing acoustic waves, respectively:

$$(\Delta\eta)^2 \frac{d^2\Phi_n}{d\xi^2} - 2i\eta_0\Delta\eta \frac{d\Phi_n}{d\xi} - \frac{n^2\lambda_1^2}{\lambda_s^2} \Phi_n$$

$$= - i\eta_0\Delta\eta(\Phi_{n-1} - \Phi_{n+1}) \qquad (6.8)$$

and

$$(\Delta\eta)^2 \frac{\partial^2\Phi_n}{\partial\xi^2} - 2i\eta_0\Delta\eta \frac{\partial\Phi_n}{\partial\xi} - \frac{n^2\lambda_1^2}{\lambda_s^2} \Phi_n$$

$$= - i\eta_0\Delta\eta \sin \omega_s t \, (\Phi_{n-1} - \Phi_{n+1}) , \qquad (6.9)$$

where

$$\xi \equiv 2\pi\Delta\eta \, z/\lambda_1 \quad \text{and} \quad n = 0, \pm 1, \pm 2, \ldots \quad .$$

The validity of the Raman-Nath theory was confirmed for acoustic waves of comparatively lower frequencies by the experimental results of Debye and Sears,[67] Lucas and Biquard,[68] Bar,[69] Sanders,[71] Parthasarathy[72] etc. When the frequency of acoustic wave becomes higher or the acoustic beam width becomes wider, or both, a strong Bragg-type diffraction occurs and the Raman-Nath theory (partsl, 2, 3), which does not include the effect of amplitude change, can only qualitatively explain the experimental results. Nath,[73] Extermann and Wannier,[74] etc., later developed a theory taking into account amplitude changes, but these theories involve

complicated expressions and are valid only for a certain range of parameters. Various theories ignoring orders higher than the second were developed by Rytov,[75] David[76] etc., which give the expressions for the intensities of the various lowest orders, especially for the incident angle close to the Bragg angle.

Related to the generalized theory of Raman and Nath (Parts 4 and 5 of reference 70) is a separate theory developed by Brillouin.[77] He starts from the partial differential equation governing the propagation of light in a quasi-homogeneous medium, as did Raman and Nath. The emerging wave-front is then considered to be equivalent to a set of plane waves traveling in the same direction as the incident light, but with an amplitude grating on each one of them given by a multiple of a Mathieu Function. The diffraction in any particular direction is determined by the plane wave traveling in that direction. This approach, though exact, leads to complicated calculations.

Finally, as pointed out by Aggarwal,[78] the results of Brillouin, Rytov and David are all special cases of the generalized theory of Raman-Nath.[70]

6.3 MOVING REFLECTOR THEORY

An acoustic wave will excite density modulation and hence induce alternating layers of higher and lower refractive index than the unperturbed value. An acoustic wavelength contains one dense and one rare layer. Since these layers are induced by the propagation of the acoustic wave, they act as a series of moving reflectors or moving paddles. This fact indicates, at least in terms of frequency, the validity of using the general theory developed in the previous chapters. For convenience, the medium will be considered to be isotropic and lossless for the light waves. Anisotropy in the photo-elastic effect will be discussed later.

Let η_0 be the index of refraction of an unperturbed medium. Then $(\eta_0 - 1)$ is proportional to the density of the medium ρ_0.[79] If $\Delta\eta$

and $\Delta\rho$ are respectively the small increment of the index of refraction and density due to acoustic waves, we have

$$\frac{\Delta\eta}{\eta_0} = \frac{\eta_0 - 1}{\eta_0} \cdot \frac{\Delta\rho}{\rho_0} \quad . \tag{6.7}$$

The maximum values of $\Delta\rho/\rho_0$ in solids are of the order of 10^{-4} or lower for acoustic waves of moderate amplitude. Thus we are considering a very small variation in refractive index, and have a moving periodic structure as shown in Fig. 6.5. Since $\eta_1 \approx \eta_2$ and $V_s/V_p \ll 1$, following the argument given in Section 5.4, we have, for the co-linear case,

$$\begin{cases} \omega_2 \cong \left(\dfrac{1 + V_s/V_p}{1 - V_s/V_p}\right) \omega_1 \approx (1 + 2\, V_s/V_p)\, \omega_1 \\ \omega_m^+ \cong \left(\dfrac{1 + V_s/V_p}{1 + V_s/V_p}\right) \omega_1 \approx \omega_1 \\ \omega_m^- \cong \left(\dfrac{1 + V_s/V_p}{1 - V_s/V_p}\right) \omega_1 \approx (1 + 2V_s/V_p)\, \omega_1 \\ \omega_t^+ = \omega_1 \\ \omega_t^- = \omega_2 \end{cases} \quad . \tag{6.8}$$

Thus we have two frequency components for the light wave: ω_1 and ω_2. The frequency component ω_2 is the scattered or diffracted wave. Depending on whether the incident light wave and the acoustic wave are

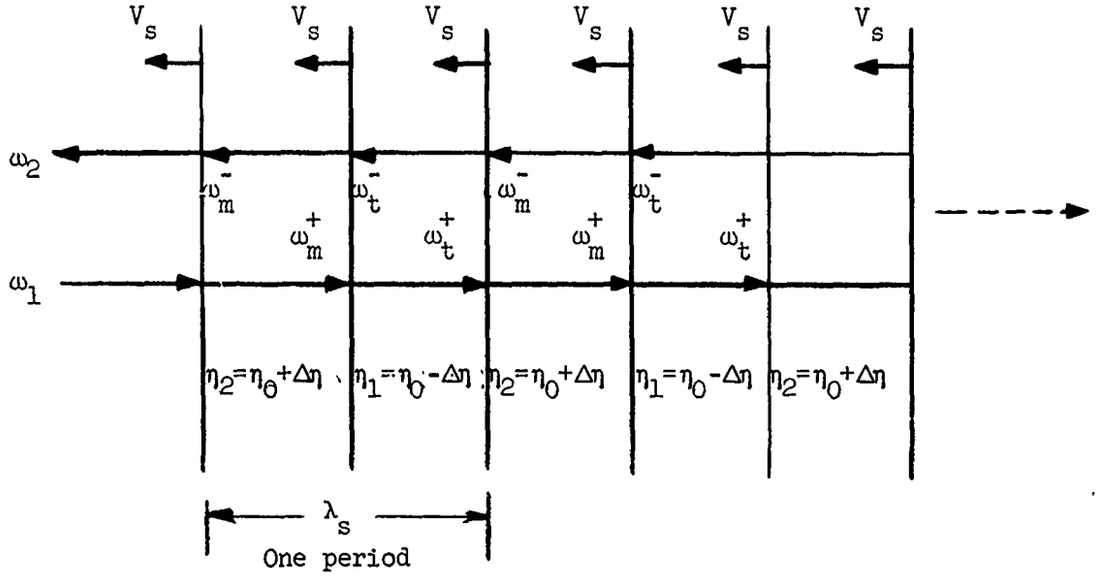

FIG. 6.5--The moving periodic structure induced by a traveling acoustic wave.

codirectional or contradirectional the frequency of the diffracted wave is down-shifted or up-shifted by the amount $2(V_s/V_p)\,\omega_1$. The number of frequency components and the amount of frequency shift, of course, agree with the conventional parametric theory as shown in Section 5.4, and this agreement will be explored in more detail in the following analysis. From Eq. (5.53) the period or the acoustic wavelength λ_s for maximum first-order diffraction is

$$\lambda_s = \frac{\lambda_1^*}{2}(1 - V_s/V_p) \approx \frac{\lambda_1^*}{2} \quad , \tag{6.9}$$

where λ_1^* is the light wavelength in the medium. This corresponds to the Bragg condition.

Now, we consider the case of most interest, in which an oblique light wave is incident at an angle with respect to the acoustic wave front such that all scatterings or reflections from the acoustic wave front (or moving interfaces) add in phase (i.e., Bragg diffraction). This coherent effect is illustrated in Fig. 6.6. According to the Doppler principle, the frequencies for the reflected and transmitted waves ω_2 and ω_3 are obtained as follows from the general expressions (3.9) and (3.11) by letting $\beta_2 = 0$, $\beta = V_s/c$, $\mu_1\epsilon_1 \approx \mu_2\epsilon_2$ and ignoring the second-order terms β^2 , $\mu_1\epsilon_1\beta^2$, ..., etc.

$$\omega_2 \simeq \omega_1 (1 + 2V_s/V_p \cdot \sin\ \theta_1) \quad , \tag{6.10}$$

and

$$\begin{aligned}
\omega_3 &\simeq -(I_2 - \beta\sqrt{I_2^2(1 + \chi_2) - c^2 I_1^2} \\
&\simeq -(I_2 - \beta\omega_1\sqrt{\mu_1\epsilon_1}\sqrt{1 + 2\beta\sqrt{\mu_1\epsilon_1}\sin\theta_1 - \cos^2\theta_1}) \\
&\simeq \omega_1[1 + \beta\sqrt{\mu_1\epsilon_1}\sin\theta_1 - \beta\sqrt{\mu_1\epsilon_1}(\sin\theta_1 + \beta\sqrt{\mu_1\epsilon_1}\sin\theta_1)]
\end{aligned}$$

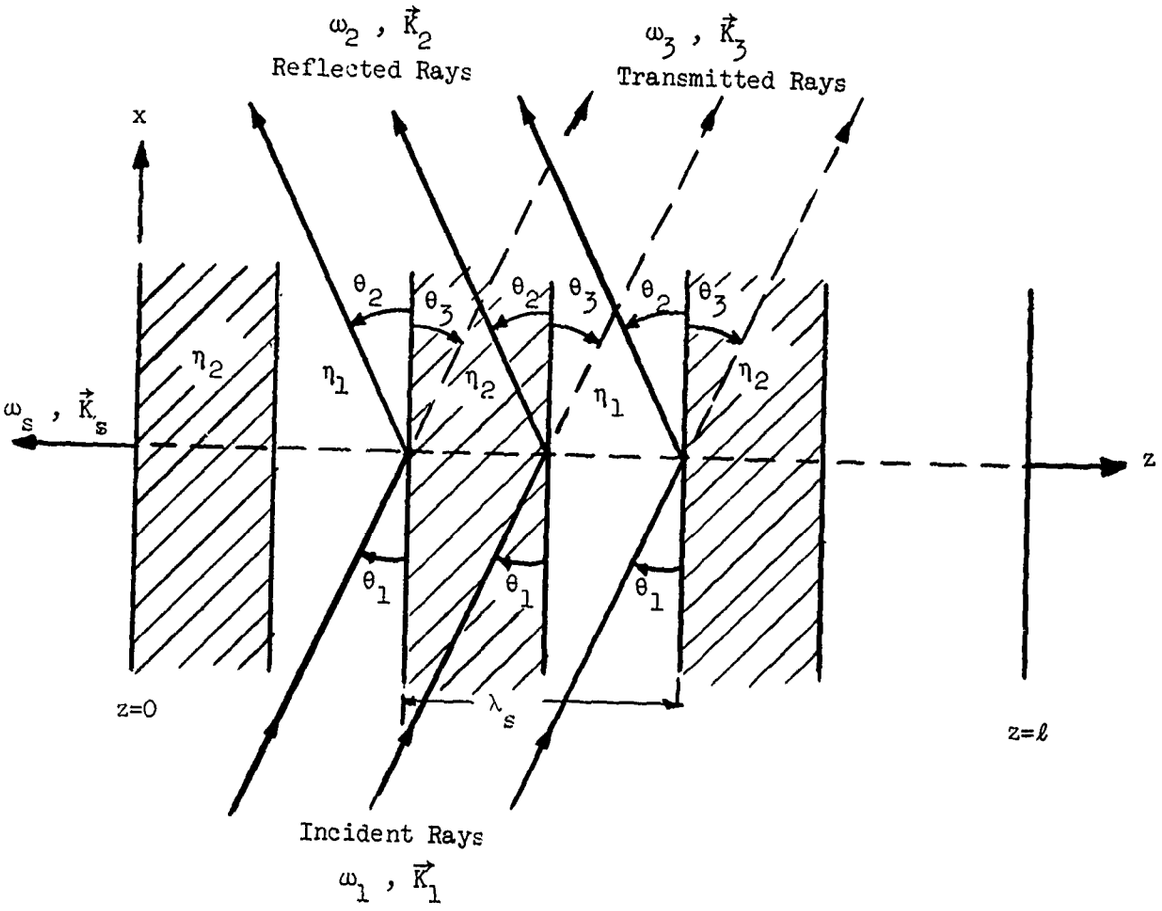

FIG. 6.6--The configuration showing the reflection and transmission from a series of moving interfaces.

i.e.,

$$\omega_3 \cong \omega_1 [1 - \beta^2 \mu_1 \epsilon_1 \sin \theta_1] \approx \omega_1 \quad . \tag{6.11}$$

Furthermore, the angles of reflection and refraction θ_2 and θ_3, respectively, can be obtained from Eq. (3.1):

$$\cos \theta_2 = \frac{K_1}{K_2} \cos \theta_1 = \frac{\omega_1}{\omega_2} \cos \theta_1$$

i.e.,

$$\cos \theta_2 \simeq \frac{1}{(1 + 2V_s/V_p \cdot \sin \theta_1)} \cos \theta_1 \tag{6.12}$$

and

$$\cos \theta_3 = \frac{K_1}{K_3} \cos \theta_1 = \frac{\omega_1}{\omega_3} \cos \theta_1$$

i.e.,

$$\cos \theta_3 \simeq \cos \theta_1 \quad . \tag{6.13}$$

Since V_s/V_p is in the order of 10^{-4} or lower, we have

$$\theta_2 \simeq \theta_1 \simeq \theta_3 \quad . \tag{6.14}$$

To have all scattering from the acoustic wave fronts add in phase, the well-known Bragg condition of Eq. (6.15) is required from a simple geometrical consideration:

$$\lambda_1 = 2\lambda_s \sin \theta_1 = 2\lambda_s \sin \theta_B \quad . \tag{6.15}$$

Notice that this is analogous to the Bragg condition of first-order X-ray diffraction from crystal planes.

Substituting Eq. (6.15) into Eq. (6.10), we have the following frequency relation:

$$\omega_2 \approx \omega_1 + 2\frac{\omega_1}{V_p} \cdot V_s \cdot \sin\theta_B$$

$$= \omega_1 + 2 \cdot \frac{2\pi}{\lambda_1} \cdot V_s \cdot \sin\theta_B$$

$$= \omega_1 + 2\pi \cdot \frac{V_s}{\lambda_s}$$

i.e.,

$$\omega_2 \cong \omega_1 + \omega_s \quad . \tag{6.16}$$

In accordance with the frequency relation (6.16), the wave-vector relation (6.17) is satisfied. This is illustrated in Fig. 6.7 using the fact that $\omega_s \ll \omega_1$ or $\vec{K}_1 \approx \vec{K}_2$:

$$\vec{K}_2 = \vec{K}_1 + \vec{K}_s \tag{6.17}$$

or

$$K_s = K_1 \sin\theta_B + K_2 \sin\theta_B \quad . \tag{6.18}$$

Equations (6.16) and (6.17) are just the frequency and phase constant relations for strong interaction in the conventional frequency converter.[80] Thus the frequency and phase constant relations using the Doppler principle agree with those of the parametric coupling principle when the Bragg condition is satisfied.

If we consider $\hbar\omega_1$, $\hbar\omega_2$ and $\hbar\omega_s$ as the energy of the incident, scattered photons and the scattering phonons $\hbar K_1$, $\hbar K_2$ and $\hbar K_s$ as the momentum of the incident, scattered photons and the scattering phonons, we have Eqs. (6.16) and (6.17) as the conditions of conservation of energy and momentum.

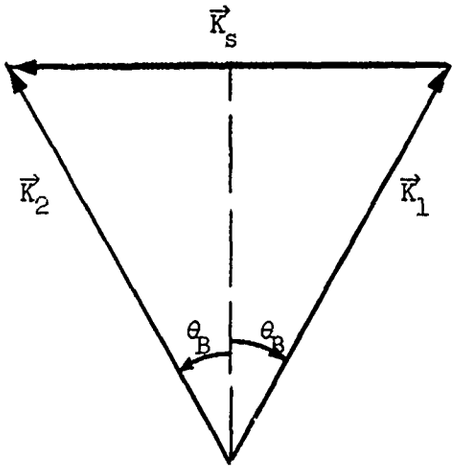

FIG. 6.7--The wave-vector relation for Bragg diffraction.

6.4 THE CALCULATION OF DIFFRACTION INTENSITY USING THE RAY-TRACING METHOD

In order to compute the intensity of light diffraction from an acoustic wave, or in the language of our analysis the reflections from a series of moving interfaces, we compute the reflection coefficient for oblique incidence from a single nonrelativistic moving interface first. Then we use Tien's Ray-Tracing Method[81] to calculate the resultant intensity of diffraction. Consider Fig. 6.8. A light wave which is polarized in the direction normal to the plane of incidence impinges on a moving interface. The reflection coefficient ζ can be obtained by solving Eqs. (3.13) and (3.14) with $\beta_2 = 0$ and ignoring the second-order terms β^2, $\mu_1\epsilon_1\beta^2$ and $\mu_2\epsilon_2\beta^2$. The reflection coefficient calculated by this approach will take the motion of the interface into account to the first-order in β. Since β is in the order of 10^{-4} or smaller, the effect of motion on the reflection coefficient will be very small. Thus it is proper to use the reflection coefficient of a stationary interface for our purpose. From the well-known Fresnel's law

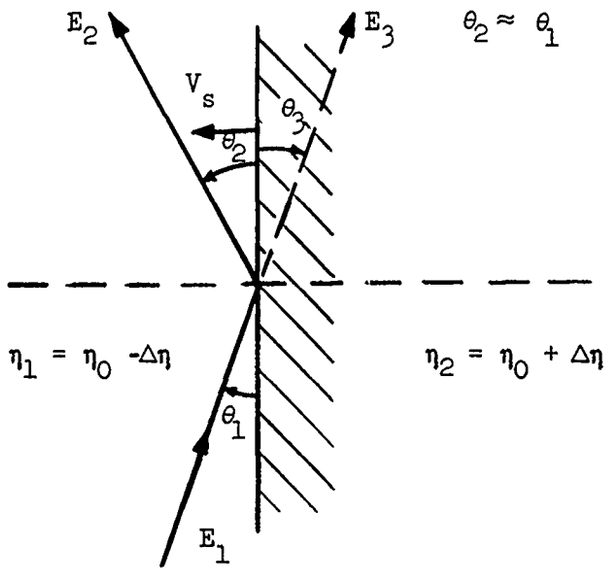

FIG. 6.8--The reflection and refraction of a light wave from a single nonrelativistic moving interface.

of reflection, the reflection coefficient is

$$\zeta \equiv \frac{E_2}{E_1} = -\frac{\sin(\theta_1 - \theta_3)}{\sin(\theta_1 + \theta_3)} \quad . \tag{6.19}$$

Since $\Delta\theta \equiv \theta_1 - \theta_3$ is a very small quantity, the following approximations are valid:

$$\begin{aligned} \sin(\theta_1 - \theta_3) &= \sin \Delta\theta \cong \Delta\theta \\ \cos\theta_1 &= \cos(\theta_3 + \Delta\theta) \cong \cos\theta_3 - \Delta\theta \sin\theta_3 \quad , \end{aligned} \tag{6.20}$$

or

$$\Delta\theta \cong -\frac{\cos\theta_1 - \cos\theta_3}{\sin\theta_3} \cong -\frac{\cos\theta_1 - \cos\theta_3}{\sin\theta_1} \quad . \tag{6.21}$$

Using the approximation of Eq. (6.21) and the Snell's Law given in

$$\frac{\cos \theta_1}{\cos \theta_3} = \frac{\eta_2}{\eta_1} \quad , \tag{6.22}$$

Eq. (6.19) reduces to the useful expression

$$\zeta \cong - \frac{\Delta\theta}{2 \sin \theta_1 \cos \theta_1} \cong + \frac{\cos \theta_1 - \cos \theta_3}{2 \sin^2 \theta_1 \cos \theta_1}$$

$$\cong + \frac{1}{2 \sin^2 \theta_1} \cdot \frac{\eta_2 - \eta_1}{\eta_2}$$

i.e.,

$$\zeta \cong + \frac{1}{\sin^2 \theta_1} \cdot \frac{\Delta\eta}{\eta} \quad , \tag{6.23}$$

where $\Delta\eta \equiv \eta_2 - \eta_1$ and $\eta \cong \eta_1 \cong \eta_2$. It is important to note that the reflection coefficient for a single interface is inversely proportional to the square of the sine of the incident angle.

From the continuity relation the transmission coefficient τ is obtained:

$$\tau \equiv \frac{E_3}{E_1} = 1 + \frac{E_2}{E_1} = 1 + \zeta \quad . \tag{6.24}$$

We now follow very closely Tien's ray-tracing and cascade networks method to calculate the resultant reflection for the case when the Bragg condition is satisfied. We return to Fig. 6.6. Consider that there is a total of $2N$ layers, or N acoustic wavelengths. The first layer starts at $z = 0$ and the last layer ends at $z = \ell$. The layers are considered to be infinite in the x and y directions.

Consider a typical section which contains two layers or one acoustic wavelength as shown in Figs. 6.9a,b. A unit amplitude incident light

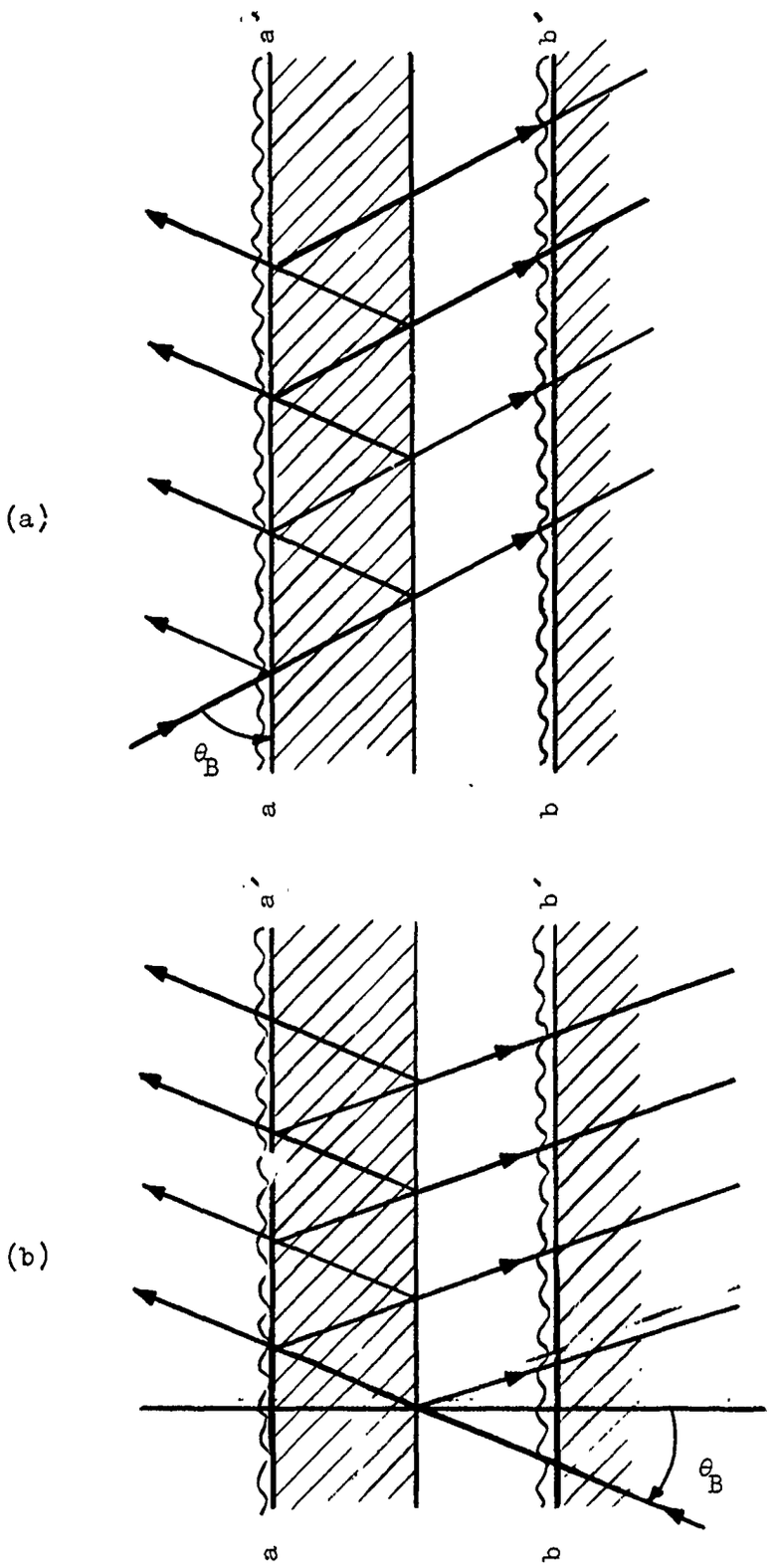

FIG. 6.9--a. Configuration showing the multiple reflection of light between the interfaces of two layers (light incident from left)
b. Configuration showing the multiple reflection of light between the interfaces of two layers (light incident from right)

ray is reflected back and forth between the interfaces of the two layers. In Fig. 6.9a with the Bragg condition satisfied, the resultant amplitude of the reflected rays at the plane a - a' is

$$r = \zeta + \zeta(1 - \zeta^2)(1 - \zeta^2 + \zeta^4 - \ldots) = \frac{2\zeta}{1 + \zeta^2} , \qquad (6.25)$$

and the resultant amplitude of the transmitted rays at the plane b - b' is

$$t = -(1 - \zeta^2)(1 - \zeta^2 + \zeta^4 - \ldots) = -\frac{1 - \zeta^2}{1 + \zeta^2} . \qquad (6.26)$$

Similarly, in Fig. 6.9b with the Bragg condition satisfied, a unit amplitude incident light ray will have a resultant reflection at the plane b - b' ,

$$r' = -\frac{2\zeta}{1 + \zeta^2} , \qquad (6.27)$$

and the resultant amplitude of the transmitted rays at the plane a - a' :

$$t' = -\frac{1 - \zeta^2}{1 + \zeta^2} . \qquad (6.28)$$

Knowing the reflection and transmission coefficients of one section, we now consider the system of N sections as shown in Fig. 6.10. As shown, let T_r and S_r ; T_{r+1} and S_{r+1} be respectively the reflection and transmission coefficients at the two reference planes a - a' and b - b' of the r^{th} section. By superimposing Eqs. (6.25) - (6.28) we have the following set of equations:

$$\begin{cases} S_r = \dfrac{2\zeta}{1 + \zeta^2} T_r - \dfrac{1 - \zeta^2}{1 + \zeta^2} S_{r+1} & (6.29) \\ T_{r+1} = -\dfrac{1 - \zeta^2}{1 + \zeta^2} T_r - \dfrac{2\zeta}{1 + \zeta^2} S_{r+1} . & (6.30) \end{cases}$$

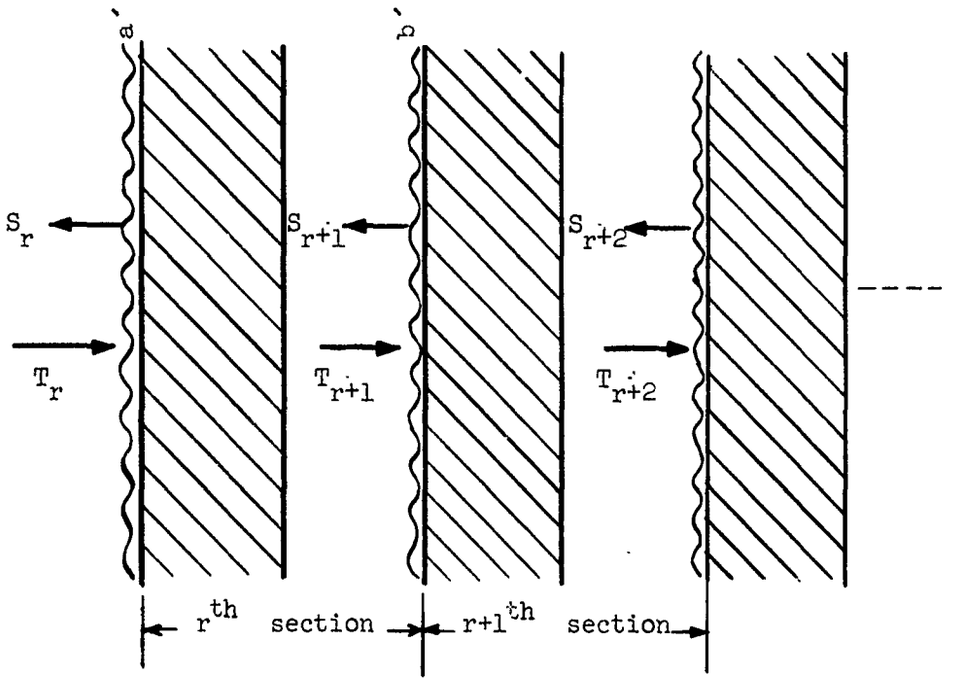

FIG. 6.10--Configuration showing the cascade network for a series of moving interfaces.

After rearangement, this becomes

$$\begin{cases} S_r + T_r = -e^{2\zeta}(S_{r+1} + T_{r+1}) & (6.31) \\ S_r - T_r = -e^{2\zeta}(S_{r+1} - T_{r+1}) \quad . & (6.32) \end{cases}$$

Let T_0 and S_0 be the incident and reflected amplitudes at $z = 0$; correspondingly T_N and S_N at $z = \ell$. By induction and using Eqs. (6.31) and (6.32), we have

$$\begin{cases} S_0 + T_0 = (-1)^N e^{2N\zeta}(S_N + T_N) & (6.33) \\ S_0 - T_0 = (-1)^N e^{-2N\zeta}(S_N - T_N) \quad . & (6.34) \end{cases}$$

Since $S_N = 0$, we have, from Eqs. (6.33) and (6.34),

$$\begin{cases} S_0 = (-1)^N T_N \sinh(2N\zeta) & (6.35) \\ T_0 = (-1)^N T_N \cosh(2N\zeta) \quad , & (6.36) \end{cases}$$

giving

$$S_0 = T_0 \tanh(2N\zeta) \quad . \qquad (6.37)$$

Equation (6.37) gives the resultant amplitude of reflection in terms of the incident amplitude T_0 , the number of sections N , and the reflection coefficient of a single interface ζ .

It is important to remember that we have been considering a square acoustic wave of wavelength (or more correctly, period) λ_s . In practice, a sinusoidal acoustic wave is used. For a sinusoidal acoustic wave, the amplitude of the equivalent square wave will be taken $\pi/4$ times that of the sinusoidal wave. This is justified from the fact that when the factor $\pi/4$ is chosen, the solution obtained by using the cascade-network method agrees with the exact solution obtained by using Mathieu's

equation.[81] The reason we employ the "Ray-Tracing and Cascade Network" method instead of the Mathieu's method is that the former is much more closely related to the model we employ for a moving periodic structure in Chapter V. Consequently, for the case of sinusoidal acoustic wave we have the following expression for ζ :

$$\zeta \cong -\frac{\pi}{4} \cdot \frac{1}{\sin^2 \theta_1} \cdot \frac{\Delta\eta}{\eta} \quad . \tag{6.38}$$

We now go back to Eq. (6.37). Since an unit amplitude incident light wave is considered, $T_0 = 1$, and the resultant intensity of the reflected or diffracted light is

$$S_0^2 = \tanh^2(2N\zeta) \quad , \tag{6.39}$$

where ζ is given by Eq. (6.38). For the region $2N\zeta \leq 0.5$, Eq. (6.39) reduces to

$$S_0^2 \approx (2N\zeta)^2 \quad . \tag{6.40}$$

When $2N\zeta >> 1$, S_0^2 approaches to unity and a total diffraction will occur. The saturation of the diffraction intensity inherent in the function of hyperbolic tangent is depicted by the plots shown in Fig. 6.11.

In order to compare the diffracting efficiencies of various crystals, we extend this calculation and express the intensity of diffracted light S_0^2 in terms of the index of refraction of the crystal η , the strain induced in the crystal S , the acoustic beam width d and the wavelength of the light in vacuum λ_1 (see Fig. 6.12). Using the Lorentz-Lorentz formula[82] connecting the strain and the change of index of refraction and the Bragg condition, we have

$$\frac{\Delta\eta}{\eta} = \frac{1}{6} \cdot \frac{(\eta^2 - 1)(\eta^2 + 2)}{\eta^2} \, S \tag{6.41}$$

$$\frac{\lambda_1}{\eta} = 2\lambda_s \sin\theta_{B_i} \quad , \tag{6.42}$$

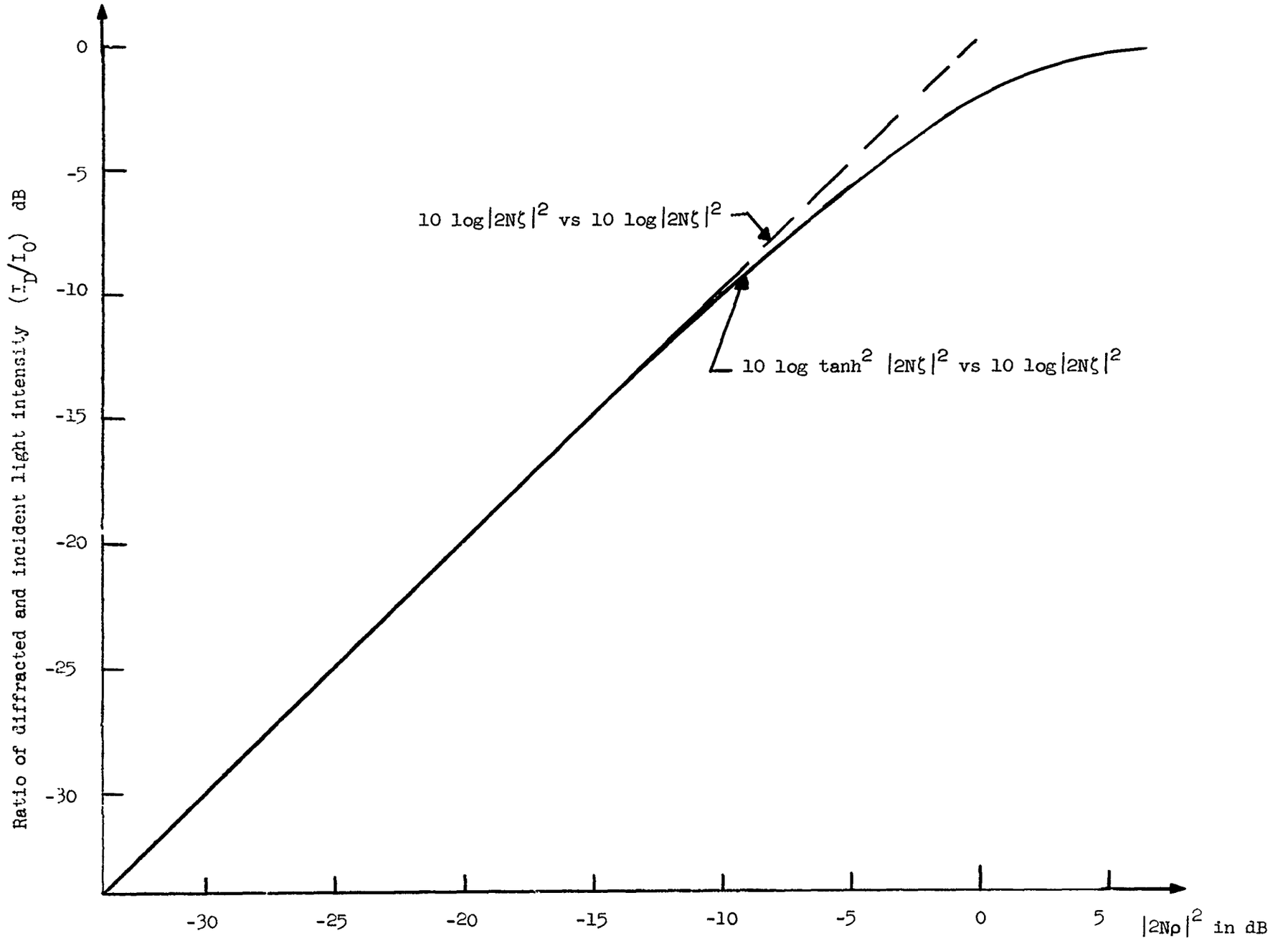

FIG. 6.11--Saturation of the diffraction intensity.

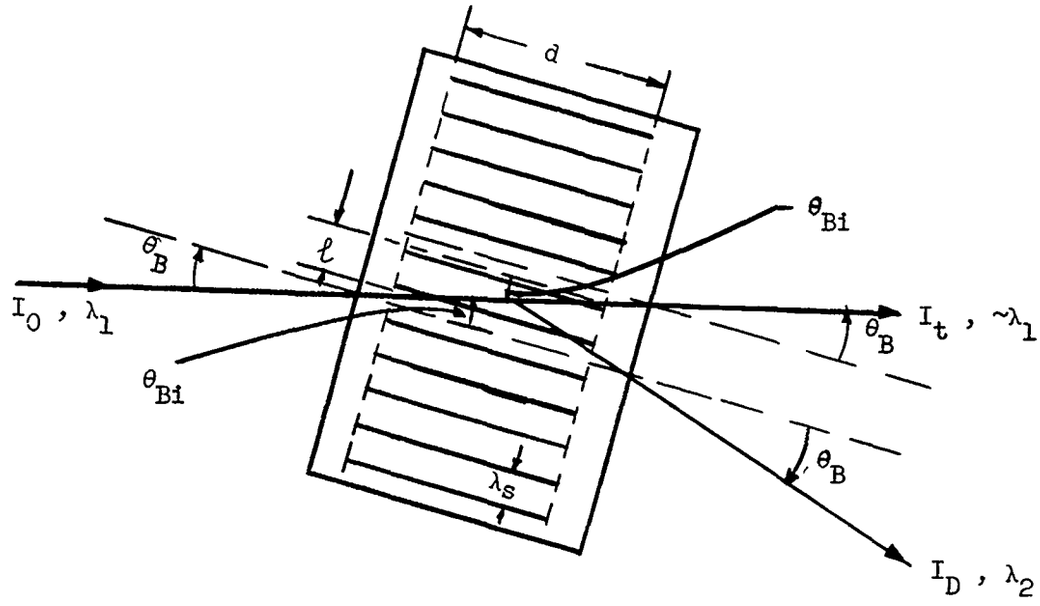

FIG. 6.12--Configuration showing the diffraction of light from an acoustic column.

where θ_{B_i} denotes the Bragg angle inside the crystal. Furthermore, for reasonably small θ_{B_i} , we have

$$N = \frac{\ell}{\lambda_s} \simeq \frac{d \sin \theta_{B_i}}{\lambda_s} , \tag{6.43}$$

giving

$$\frac{I_D}{I_0} \equiv S_0^2 = \tanh^2(2N\zeta)$$

$$= \tanh^2 \left(-2 \cdot \frac{d \sin \theta_{B_i}}{\lambda_s} \cdot \frac{\pi}{4} \cdot \frac{1}{\sin^2 \theta_{B_i}} \cdot \frac{(\eta^2 - 1)(\eta^2 + 2)}{6\eta^2} s \right), \tag{6.44}$$

i.e.,

$$\frac{I_D}{I_0} = \tanh^2\left(\frac{\pi d(\eta^2 - 1)(\eta^2 + 2)}{6\lambda_1 \eta} S\right) \quad . \tag{6.45}$$

The saturation of the diffraction intensity, well illustrated by the hyperbolic tangent variation appears, in the expression of diffraction intensity. For the region $2N\zeta \leq 0.5$, Eq. (6.45) reduces to

$$\frac{I_D}{I_0} \approx \left(\frac{\pi d(\eta^2 - 1)(\eta^2 + 2)}{6\lambda_1 \eta} S\right)^2 \quad . \tag{6.46}$$

For convenience, we express the strain S in terms of the acoustic power density P_s ,

$$P_s = \frac{T^2}{2Z_0} = \frac{C^2 S^2}{2Z_0} \quad , \tag{6.47}$$

or

$$S = \frac{\sqrt{2Z_0}}{C} P_s^{1/2} \quad , \tag{6.48}$$

where

T = the stress
Z_0 = the mechanical impedance
C = the related elastic modulus,

and Eq. (6.44) becomes

$$\frac{I_D}{I_0} = \tanh^2\left(\frac{\pi d(\eta^2 - 1)(\eta^2 + 2)}{6\lambda_1 \eta} \cdot \frac{\sqrt{2Z_0}}{C} P_s^{1/2}\right) . \tag{6.49}$$

For the region $2N\zeta \leq 0.5$, it reduces to

$$\frac{I_D}{I_0} \approx \left(\frac{\pi d(\eta^2 - 1)(\eta^2 + 2)\sqrt{2Z_0}}{6\lambda_1 \eta C} \right)^2 P_s \quad . \tag{6.50}$$

As an alternative to the Lorentz-Lorentz formula, the photoelastic constants[83] can be used in connecting the change of index of refraction (or dielectric const.) and the strain. For cubic crystals, the relations between the change of dielectric constant and the stress due to the propagation of a longitudinal acoustic wave along the axis 1 are

$$\frac{\Delta\epsilon}{\epsilon} = - \frac{\epsilon}{\epsilon_0} \pi_{11} T_1 \quad , \tag{6.51}$$

for light polarized in the plane of incidence along the axis 1 and

$$\frac{\Delta\epsilon}{\epsilon} = - \frac{\epsilon}{\epsilon_0} \pi_{12} T_1 \quad , \tag{6.52}$$

for light polarized normal to the axis and parallel to the acoustic wave fronts. Here π_{11} and π_{12} are the photo-elastic constants for the corresponding light polarization; ϵ and ϵ_0 are the dielectric constants of the crystal and the free space, respectively.

Since

$$\frac{\Delta\eta}{\eta} = \frac{1}{2} \frac{\Delta\epsilon}{\epsilon} \quad \text{and} \quad T = (2P_s Z_0)^{1/2} \quad ,$$

we have

$$(2N\zeta)_{11} = \frac{\pi d}{\lambda_1} \cdot \frac{\Delta\eta}{\eta_{11}} = - \frac{\pi d}{\lambda_1} \cdot \frac{\epsilon}{2\epsilon_0} \pi_{11} (2P_s Z_0)^{1/2} \tag{6.53}$$

$$(2N\zeta)_1 = \frac{\pi d}{\lambda_1} \cdot \frac{\Delta\eta}{\eta_1} = - \frac{\pi d}{\lambda_1} \cdot \frac{\epsilon}{2\epsilon_0} \pi_{12} (2P_s Z_0)^{1/2} \quad , \tag{6.54}$$

and

$$\frac{I_D}{I_{0_{11}}} = \tanh^2(2N\zeta)_{11} = \tanh^2 \left| \frac{\pi d}{\lambda_1} \cdot \frac{\epsilon}{2\epsilon_0} \pi_{11}(2P_s Z_0)^{1/2} \right| \quad (6.55)$$

$$\frac{I_D}{I_{0_1}} = \tanh^2(2N\zeta)_1 = \tanh^2 \left| \frac{\pi d}{\lambda_1} \cdot \frac{\epsilon}{2\epsilon_0} \pi_{12}(2P_s Z_0)^{1/2} \right| \quad . \quad (6.56)$$

For the region $2N\zeta \leq 0.5$, these reduce to

$$\frac{I_D}{I_{0_{11}}} \approx \frac{Z_0}{2}\left(\frac{\pi}{\lambda_1}\right)^2 \left(\frac{\epsilon}{\epsilon_0} \pi_{11}\right)^2 d^2 P_s \quad (6.57)$$

$$\frac{I_D}{I_{0_1}} \approx \frac{Z_0}{2}\left(\frac{\pi}{\lambda_1}\right)^2 \left(\frac{\epsilon}{\epsilon_0} \pi_{12}\right)^2 d^2 P_s \quad . \quad (6.58)$$

The difference in diffraction intensity due to the anistropy of the photoelastic constants is seen to be $(\pi_{11}/\pi_{12})^2$.

If we keep λ_1 and d constant and assume that $\Delta\eta/\eta$ is independent of the acoustic wave frequency, then Eqs. (6.55) or (6.56) show that the diffraction intensity is independent of the acoustic wave frequency. Equations (6.55) and (6.56) also indicate that the diffraction intensity can be increased by increasing the acoustic beam width, the acoustic power density or using a light source of shorter wavelength. For the region $2N\zeta \leq 0.5$, the diffraction intensity is a linear function of the acoustic power density and a square function of the acoustic beam width. Finally, it is important to point out that in order to obtain the maximum diffraction for a constant input acoustic power, a nonsymmetrical acoustic beam cross-section such as a ribbon-shape should be used.

Related data for various potential diffracting crystals are given in Table 6.I, and the relations between the strain and the acoustic power density for various crystals are plotted in Fig. 6.13. Using the data

TABLE 6.I

Crystal	$\epsilon=n^2$	V_ℓ (m/sec)	C_{11} or C_{33} (newton/m^2)	$Z_{o\ell}$ (Kg/m^2sec)	π_{11} (m^2/newton)	π_{12}	π_{13}	I_D/I_O in dB for d=1mm, P_s=1 mw/mm^2 (square beam)			
								Using Lorentz-Lorentz Relation	Using π_{11}	Using π_{12}	Using π_{13}
ADP	$(1.50)^2$ = 2.25	6.1×10^3	C_{33} 3.42×10^{11} C_{11} 0.67×10^{11}	11.1×10^6			37.3×10^{-12}	-43.7			-30.3
$SrTiO_3$	$(2.38)^2$ = 5.65	8.4×10^3	C_{11} 3.48×10^{11}	40.4×10^6	0.80×10^{-12}			-40	-50		
SiO_2	$(1.54)^2$ = 2.37	5.6×10^3	C_{33} 1.10×10^{11}	15.2×10^6		2.36×10^{-12}		-46		-52.4	
TiO_2	$(2.68)^2$ = 7.18	10.3×10^3	C_{33} 4.84×10^{11}	44×10^6				-40			
Al_2O_3	$(1.76)^2$ = 3.10	11.2×10^3	C_{33} 5.60×10^{11}	44.5×10^6				-51.4			
LiF	$(1.39)^2$ = 1.93	6.5×10^3	C_{11} 1.11×10^{11}	17.0×10^6		1.01×10^{-12}		-48.8	-61.2		

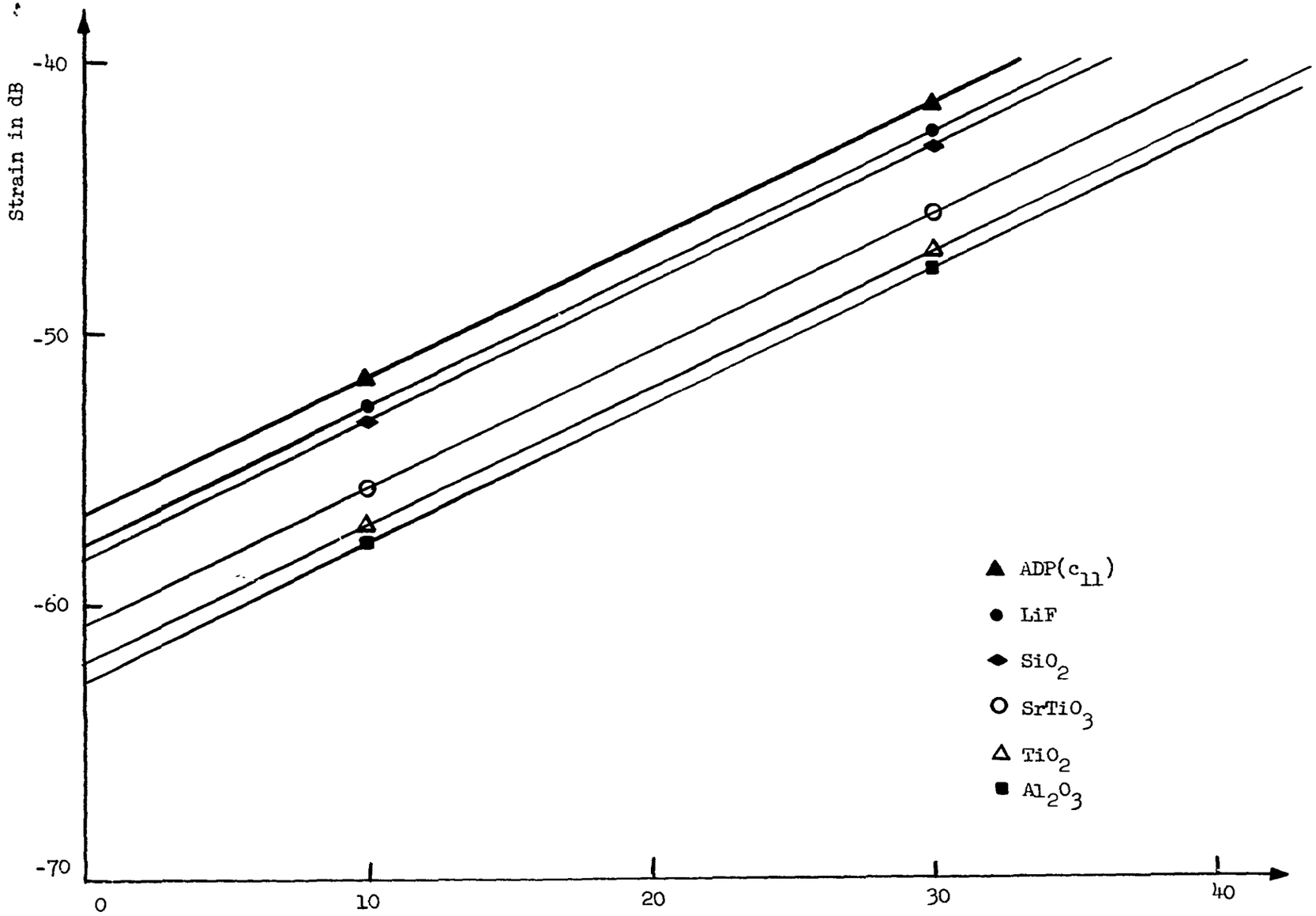

FIG. 6.13--Plots of strain vs acoustic power density for various crystals.

Acoustic power density

as given in Table 6.I and the plots of Fig. 6.13, the diffraction intensity for a He-Ne laser light I_D/I_0 in dB for an acoustic beam width of 1.0 mm and 1 mW/mm^2 acoustic power density is calculated as shown in Table 6.I, using both the Lorentz-Lorentz formula and the known photo-elastic constants. It will be shown in next chapter that the experimental value agrees with the calculated value using the Lorentz-Lorentz formula in some cases and the calculated value using the photo-elastic constants in other cases.

The diffraction intensity I_D/I_0 in dB for an acoustic beam width of 1.0 mm and 1 mW/mm^2 acoustic power density is a very useful figure of merit for the diffracting power of a crystal. It can be used to estimate the input rf power required in order to diffract a certain amount of light when the acoustic beam cross-section and the transducer conversion efficiency are known.

6.5 PARAMETRIC THEORY

In parallel with the method of ray-tracing and cascade-network which was treated in detail in the last section, there are two other methods which give the same results for the Bragg diffraction intensity. The first one[81] is to solve exactly the Mathieu equation which arises from the modulation of the dielectric constant due to the acoustic waves. The second one[81,84] is to solve the Maxwell equations with a dielectric constant which varies in the form of Eq. (6.60) due to the acoustic waves, using conventional parametric principles and coupled mode theory. The incident light wave is considered as the signal wave, the diffracted light wave as the idler wave and the acoustic wave as the pump wave:

$$\frac{\partial^2 \vec{E}}{\partial z^2} + \frac{1}{c^2} \frac{\partial^2 \epsilon(z,t)\vec{E}}{\partial t^2} = 0 \qquad (6.59)$$

$$\epsilon(z,t) \simeq \epsilon_0[1 + 2\frac{\Delta\eta}{\eta} \cos(\omega_s t + K_s z)] \quad . \qquad (6.60)$$

The incident and diffracted light waves are coupled to each other through the time- and space-variable dielectric constant $\epsilon(z,t)$. In reference 82, the photo-elastic constant is specifically used to relate the change of dielectric constant and the amplitude of acoustic waves.

In order to show the variation of the diffracted light intensity with respect to the acoustic wave frequency when the Bragg condition is not satisfied exactly, we describe briefly the parametric mode coupling involved. By imposing the parametric conditions for frequency and wave vector, we have

$$\begin{cases} \omega_2 = \omega_1 + \omega_s \\ \vec{K}_2 = \vec{K}_1 + \vec{K}_s + \Delta\vec{K}_s \end{cases} \tag{6.61}$$

i.e.,

$$\begin{cases} \omega_s = \omega_2 - \omega_1 \\ K_s + \Delta K_s = (K_1 + K_2) \cos\theta_B \end{cases}, \tag{6.62}$$

Combining Eqs. (6.59), (6.60), (6.61) and (6.62), a set of coupled-mode equations relating the amplitudes of the incident light A_1 and that of the diffracted light A_2 will be obtained. The higher-order terms $\partial^2 A_1(z)/\partial z^2$ and $\partial^2 A_2(z)/\partial z^2$ are neglected. After solving the coupled-mode equations with the boundary condition taken into account, the diffracted light intensity is obtained as follows:[81]

$$\frac{I_D}{I_0} = \frac{A_2(0)\, A_2^*(0)}{A_1(0)\, A_1^*(0)} = \frac{K_2}{K_1} \cdot \frac{\sinh^2\left(\frac{1}{2}\zeta\ell\sqrt{1 - \left(\frac{\Delta K_s}{\zeta}\right)^2}\right)}{1 - \frac{\Delta K_s^2}{\zeta^2} + \sinh^2\left(\frac{1}{2}\zeta\ell\sqrt{1 - \frac{\Delta K_s^2}{\zeta^2}}\right)} \tag{6.63}$$

for $\Delta K_s \leq \zeta^2$, and

$$\frac{I_D}{I_0} = \frac{A_2(0)\, A_2^*(0)}{A_1(0)\, A_1^*(0)}$$

$$= \frac{K_2}{K_1} \cdot \frac{\sin^2\left(\frac{1}{2}\zeta\ell\sqrt{\frac{\Delta K_s^2}{\zeta^2} - 1}\right)}{\frac{\Delta K_s^2}{\zeta^2} - 1 + \sin^2\left(\frac{1}{2}\zeta\ell\sqrt{\frac{\Delta K_s^2}{\zeta^2} - 1}\right)} \qquad (6.64)$$

for $\Delta K_s \geq \zeta^2$, where

$$\zeta^2 = \frac{\left(\frac{\Delta n}{n}\right)^2 K_1 K_2}{\sin^2\theta_B} \quad . \qquad (6.65)$$

For small values of $1/2\ \zeta\ell$ (which is the case in practice), Eq. (6.64) can be approximated as follow:

$$\frac{I_D}{I_0} \simeq \frac{1}{4}(\zeta\ \ell)^2 \frac{\sin^2\left(\frac{1}{2}\Delta K_s \ell\right)}{\left(\frac{1}{2}\Delta K_s \ell\right)^2} \qquad (6.66)$$

$$= \frac{1}{4}(\zeta\ \ell)^2 \frac{\sin^2\left(\pi N \frac{\Delta K_s}{K_s}\right)}{\left(\pi N \frac{\Delta K_s}{K_s}\right)^2} \quad . \qquad (6.67)$$

Thus for small values of $(1/2\ \zeta\ \ell)$, the bandwidth of the diffraction intensity in ΔK_s is independent of ζ or the acoustic wave amplitude. But as $(1/2\ \zeta\ \ell)$ approaches to a few tenths, the bandwidth of the diffraction intensity in ΔK_s becomes broader and eventually increases linearly with ζ . Using the relation $\Delta K_s/K_s = \Delta\omega_s/\omega_s$ and Eq. (6.67) the bandwidth of the acoustic wave frequency, $\Delta\omega_s$, defined by a 3 dB decrease in the diffraction intensity from the maximum point is

$$\frac{\Delta K_s}{K_s} = \frac{\Delta\omega_s}{\omega_s} = \frac{1.39}{\pi N}$$

or

$$\Delta\omega_s = \omega_s \cdot \frac{1.39}{\pi N} \quad . \tag{6.68}$$

For the experiment which will be described in Chapter VII, $\Delta\omega_s$ is much larger than the bandwidth of the coaxial cavity and also that of the transducer.

6.6 LARGE DIFFRACTION OF LIGHT

Many applications are inherent in the field of laser light diffraction using high frequency acoustic waves in solids. Frequency and amplitude modulation of the laser in optical communications, display devices, and the generation of laser light with frequency shifted by an integer multiple of the acoustic wave frequency are only some of the examples. But these applications are practical only if a large portion of the laser light can be diffracted with a moderate amount of rf power. Thus it is important to diffract as much light as possible by using a proper crystal and optimizing the various factors affecting the amount of diffraction, and to find out the practical limitations involved. For the various kinds of experiments which will be discussed in detail in the next chapter, a He-Ne gas laser ($\lambda_1 = 6238$ Å) is used for the light source. In order to diffract a large portion of light using a moderate amount of rf power, the following important factors should be considered.

6.6.1 Choice of a Proper Crystal for Diffraction

From Table 6.I, in principle, the crystals with large photo-elastic constants such as ADP is more efficient diffracting crystal than the others. But, due to the high acoustic loss and comparatively inferior mechanical quality, ADP is not as desirable as the other crystals. For the various kinds of experiments discussed in the next chapter, TiO_2 and $SrTiO_3$ are most frequently used. These two crystals have reasonably large photo-elastic constants (diffracting power) as well as excellent mechanical properties. The crystal TiO_2 has low acoustic loss at microwave frequencies and is one of the best for acoustic wave frequencies above 1 GC/s .

6.6.2 The Requirement of a High Efficiency Transducer

In order to reduce the amount of rf power required for large diffraction and hence avoid many difficulties resulting from high input power (such as cavity voltage break-down), a reasonably high transducer efficiency is essential. For the various kinds of experiments described here ZnO wafer transducers are used. This newly discovered transducer has reasonably high efficiency (-11 dB to -17 dB at L-band) and can sustain high power. The CdS film transducer can have conversion efficiency higher than -10 dB but lacks high power capability.

6.6.3 Generation of a Ribbon-Shaped Acoustic Beam

To utilize the acoustic power more economically, and hence reduce the rf power requirement, a ribbon-shaped acoustic beam is essential. This is obvious from the expressions for diffraction intensity Eqs. (6.57) and (6.58) for the region $2N\zeta \leq 0.5$, as the diffraction intensity is approximately proportional to the square of the acoustic beam width. In the next chapter, the advantage of a ribbon-shaped beam over a circular beam will be analyzed quantitatively and the technique of generating a ribbon-shaped beam is described.

6.6.4 Acoustic Resonance

So far, we have been considering the case of a traveling acoustic wave. If the crystal is resonated acoustically by making the end faces of the rod flat, parallel and unterminated, a larger diffraction will be obtained with the same amount of rf power. The detailed analysis and numerical values are given in next subsection. Here we simply point out that the enhancement in diffraction intensity due to acoustic resonance is small when the acoustic loss is high and the length of the crystal rod is long.

To conclude this subsection, we estimate the rf power required for diffracting 50% of the light from a He-Ne gas laser (beam diameter ~ 0.6 mm at the crystal surface) using a TiO_2 crystal. From Table 6.I, I_D/I_0 for $d = 1$ mm, and $p_s = 1$ mW/mm^2 is -40 dB. For an acoustic

beam cross-section of 1 mm × 6 mm with d = 6 mm and assuming the transducer conversion efficiency to be -10 dB , the total input rf power required can be estimated as follows:

$$10^{-4} \cdot d^2 P_s = 0.5$$

and

$$P_s = \frac{0.5}{10^{-4} \cdot (6)^2} = 139 \text{ mW/mm}^2 \quad ,$$

Then the total rf input power is

$$P_{rf} = \frac{\text{Acoustic Beam Cross-sectional Area} \cdot P_s}{\text{Transducer Conversion Efficiency}}$$

$$= \frac{139 \cdot 6}{0.1} \simeq 8.4 \text{ Watts} \quad .$$

6.7 ENHANCEMENT OF DIFFRACTION DUE TO ACOUSTIC RESONANCE

By letting the end of the crystal be acoustically unterminated, the amount of diffraction will be increased from that obtained when it is terminated, for the same amount of input rf power. This is because, for same amount of rf power, the resultant strain, S_r , due to acoustic resonance and hence standing waves is larger than that due to traveling waves.

Consider a crystal rod of length L and unit cross-sectional area (Fig. 6.14). Using the common definition of quality factor Q ,

$$Q \equiv \frac{\omega U}{P} \quad , \tag{6.69}$$

where ω is the radian frequency, U the stored energy density, P the rate of power loss in the acoustic standing wave, then we have

$$U = \frac{1}{2} C_{33} (Sr)^2 \cdot L = \frac{PQ}{\omega} \tag{6.70}$$

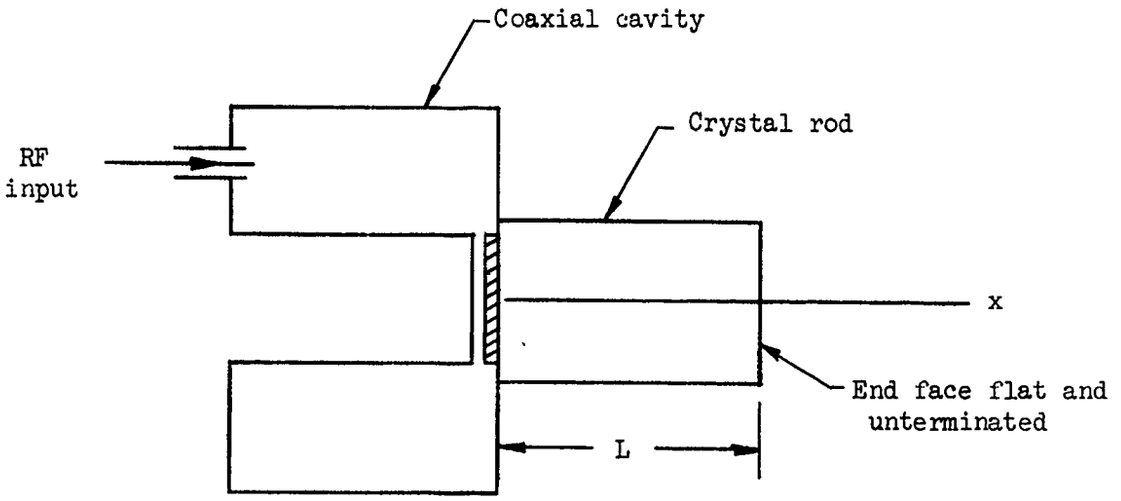

FIG. 5.14--Configuration showing the system of acoustic resonance.

TABLE 6.II

Crystal	Measured Acoustic Attenuation α at 800 Mc/S (neper / cm)	$\left(\frac{S_r}{S}\right)^2$ in dB		$\left(\frac{S_{r+}}{S}\right)^2 = \left(\frac{S_{r-}}{S}\right)^2$ in dB	
		L = 0.4 cm	L = 1.0 cm	L = 0.4 cm	L = 1.0 cm
$SrTiO_3$	0.228	7.4	3.4	1.4	
SiO_2 (z-cut)	0.284	6.4	2.4	0.4	
TiO_2	0.225	7.4	3.4	1.4	
Al_2O_3	0.113	10.4	6.4	4.4	0.4
LiF	0.900	1.4			
ADP	1.125	0.4			

or

$$(Sr)^2 = \frac{2PQ}{C_{33}L\omega} \quad . \tag{6.71}$$

For a traveling acoustic wave with power density P, the associated strain S is determined by the following relation,

$$P = \frac{1}{2} \cdot \frac{T^2}{Z_0} = \frac{1}{2} C_{33} v_\ell S^2 \tag{6.72}$$

or

$$S^2 = \frac{2P}{C_{33}v_\ell} \quad . \tag{6.73}$$

Here C_{33} is the elastic modulus and v_ℓ the velocity of longitudinal acoustic wave propagation.

For α, the attentuation per unit distance, we have[85]

$$\alpha = \frac{\omega}{2Qv_\ell} \quad . \tag{6.74}$$

To compare the resultant strain Sr due to a standing acoustic wave with the strain S due to a traveling acoustic wave with the same input power, we combine Eqs. (6.71), (6.73) and (6.74). Thus we have

$$\left(\frac{Sr}{S}\right)^2 = \frac{1}{2\alpha L} \quad . \tag{6.75}$$

Finally, the resultant strains, S_{r+} and S_{r-}, for the forward-wave or backward-wave components are

$$\left(\frac{S_{r+}}{S}\right)^2 = \left(\frac{S_{r-}}{S}\right)^2 = \left(\frac{\frac{Sr}{2}}{S}\right)^2 = \frac{1}{8\alpha L} \quad . \tag{6.76}$$

Table 6.II gives the numerical values of the enhancement of strain and hence of diffraction intensity due to acoustic resonance in various crystals for an acoustic wave frequency of 800 Mc/sec. The experimental value (which agrees with the theoretical value) will be given in next chapter.

CHAPTER VII

LIGHT DIFFRACTION USING KILOMEGACYCLES ACOUSTIC WAVES IN SOLIDS

7.1 EXPERIMENTAL TECHNIQUE AND PRELIMINARY EXPERIMENTAL RESULTS OF BRAGG-DIFFRACTION

The experimental arrangement[84] for the measurement of Bragg diffraction is as shown in Fig. 7.1. It permits measurement of the following: (1) Intensity of diffraction as a function of rf power level, (2) Intensity of diffraction as a function of incident angle, i.e., diffraction pattern; (3) Enhancement of diffraction intensity due to acoustic resonance; (4) Acoustic beam cross-section; (5) Frequency shift in the diffracted beam using a Fabry-Perot etalon. The light beam from a He-Ne gas laser (λ = 6328 Å) passes through a focusing lens and has a beam diameter of about 25 mils at the front face of the interacting crystal rod. The faces of the crystal are polished. To generate the high frequency acoustic waves propagating through the rod, a piezoelectric transducer is bonded on one end face and inserted into the high-field gap of a re-entrant coaxial cavity. On the end opposite the transducer a mercury pool is attached for terminating the acoustic waves. For convenience, the variation of the laser incident angle is accomplished by rotating the crystal, which is mounted on a rotary table. The intensity of the diffracted beam is measured by a photo-multiplier located at an angle of $2\theta_B$ from the main beam (transmitted beam). The diffracted light beam is modulated because of the 1kc/s acoustic modulation. For calibration purposes the same modulation is induced in the main beam by means of a mechanical chopper. The diffraction pattern (Section 7.4) is plotted by an X-Y recorder. The output of the photo-multiplier is, after passing through a log converter, connected to the Y-axis of the recorder while a calibrated potentiometer, attached to the rotary table, is connected to the X-axis of the recorder.

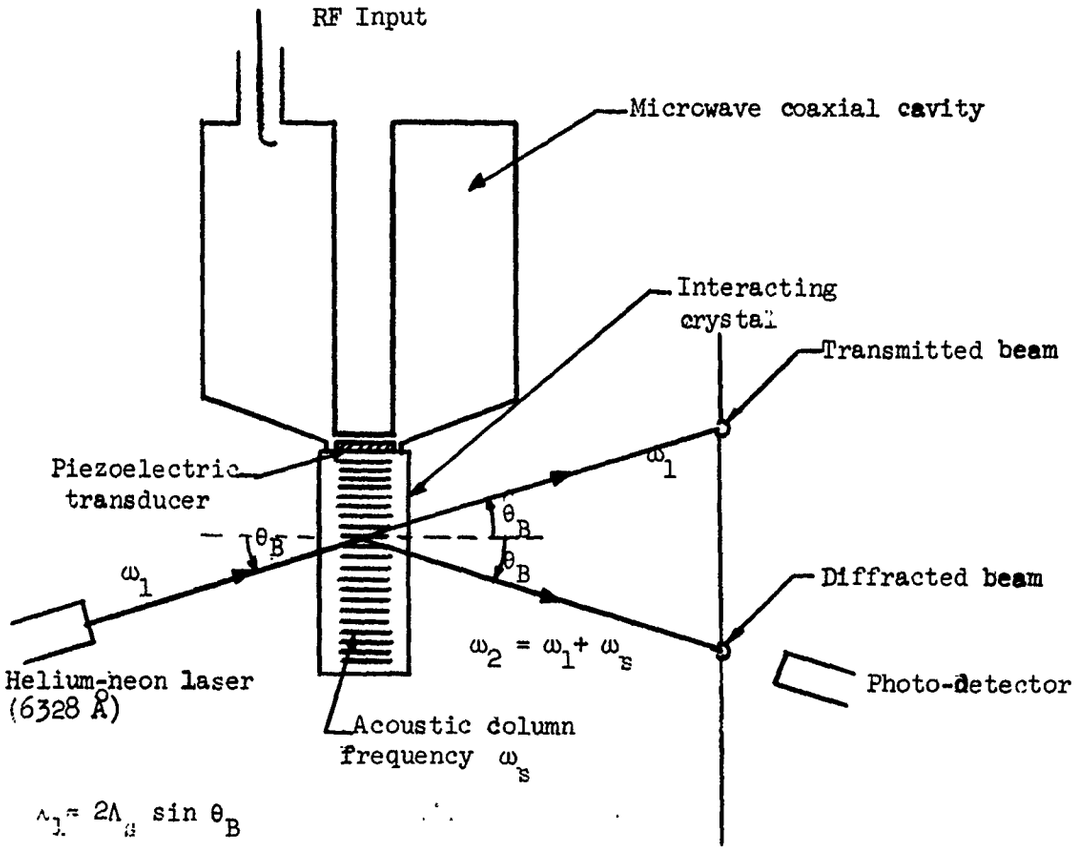

FIG. 7.1--The experiment arrangement for the measurement of Bragg diffraction.

We now give some experimental results[84] which are preliminary to one of the main experiments described in this report, large diffraction of laser light. An X-cut disk (0.005 in. thickness and 0.100 in. diameter) was used as a piezoelectric transducer. The transducer was bonded with an indium film to various kinds of diffracting crystals. The best conversion efficiency (acoustic power/rf power) of the quartz transducer used was -20 dB. The dimensions of the crystals are nominally 6 mm x 6 mm x 20 mm. A circular cross-section acoustic beam (2 mm diameter) was generated in the crystals using a circular center post of this dimension in the coaxial cavity. The frequency used varied from 400 Mc/sec to 3000 Mc/sec; ADP was found to be the most efficient diffracting crystal, and then in the order of decreasing efficiency they are $SrTiO_3$, SiO_2, TiO_2, Al_2O_3, LiF. Both the calculated and measured diffracting powers for 1 mw acoustic power for various crystals are listed in Table 7.I. Note that the converted values of I_D/I_0 for a square cross-section acoustic beam of width d = 1 mm (listed in the second column of the table) are obtained by multiplying the measured values of I_D/I_0 for 1 mW acoustic power and 2 mm diameter circular acoustic beam by the factor $\pi/4$ which results from the difference in cross-sectional area involved.

TABLE 7.I

Crystal	I_D/I_0 in dB for 1 mW acoustic power with 2 mm diameter acoustic beam (measured)	I_D/I_0 in dB for square beam d = 1 mm Ps=1 mW/mm (converted from column 1)	I_D/I_0 in dB for square beam d = 1 mm, Ps = 1 mW/mm^2 (calculated)	
			Using photo-elastic constant	Using Lorentz-Lorentz formula
ADP	-30	-31	-30	-44
$SrTiO_3$	-41	-42	-50	-40
SiO_2	-42	-43	-52	-46
TiO_2	-49	-50		-40
Al_2O_3	-51	-52		-51
LiF	-51	-52	-61	-49

7.2 LARGE DIFFRACTION OF LASER LIGHT USING RUTILE CRYSTAL

For the purpose of diffracting a large portion of laser light, a rutile crystal is used. This is due to the excellent optical and mechanical properties of the rutile crystal (such as the optical transparency, the hardness and especially a low acoustic loss at L-band). Although ADP, among the crystals considered, has the highest measured diffracting power, this advantage is cancelled by the high acoustic loss at L-band frequency. (The measured acoustic loss for longitudinal waves at 800 Mc/sec along the z-axis is 10 dB/cm for ADP. Thus the extrapolated loss using the f^2 law will be 20 dB/cm at 1.1 Gc/s.)

(a) Generation of Ribbon-Shaped Acoustic Beam

As indicated previously, a ribbon-shaped acoustic beam will utilize the acoustic power more economically than a circular acoustic beam. By using a ribbon-shaped center post with cross-section 1.0 mm × 6.5 mm in a coaxial cavity, we were able to generate a 1.1 Gc/s acoustic column of ribbon-shaped cross-section (~ 1.0 mm × 3.5 mm as determined by scanning the acoustic beam with the light beam). The dimensions of the crystal are 12 mm × 10 mm × 6 mm, in which the last number is the length along the optical axis. A lithium-doped ZnO wafer of 7 mils thickness and 3 mm × 6.5 mm cross-section is used as a longitudinal acoustic wave transducer. The gap between the surface of transducer and that of the center post is 1 mil (see Fig. 7.2). The loaded Q of the cavity is 500. The peak conversion efficiency of the transducer is -13 dB and the frequency separation between two consecutive conversion peaks is 40 Mc/sec. Figures 7.3 and 7.4 show the acoustic echoes obtained with the conventional super-heterodyne technique. The acoustic loss is 4 dB/cm.

(b) The Probing of Acoustic Beam

The acoustic beam cross-section is determined by scanning the acoustic beam with the light beam and measuring the diffraction intensity at an incident angle of θ_B. The diffraction intensity as a function of the location of the incident light beam on the crystal face is shown in Fig. 7.5 and 7.6 when the light beam traverses the wider and narrower cross section of the acoustic column respectively. From these plots, the

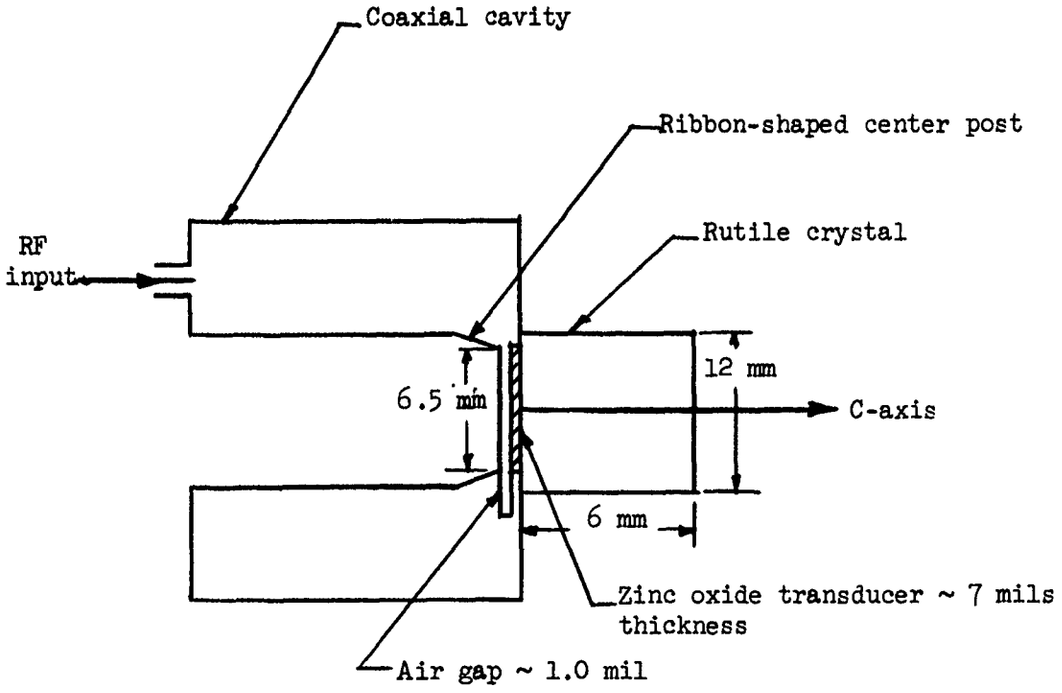

FIG. 7.2--Configuration showing the dimensions of cavity center post, rutile crystal, ZnO transducer and air gap.

acoustic beam cross-section defined by the 10 dB points is about 1.0 mm × 3.5 mm. We thus see that the acoustic beam width is not as long as the design value and that the two ends of the ZnO wafer do not perform satisfactorily. Nevertheless, an approximately ribbon-shaped acoustic beam is generated.

(c) Diffraction Pattern Versus Crystal Rotation

The diffraction patterns for the first, second and third order, obtained by rotating the rutile crystal with the photomultiplier and laser axes fixed at intersection angles of $2\theta_B$, $4\theta_B$ and $6\theta_B$, respectively, are shown in Figs. 7.6a,b,c. The maximum diffraction intensity wanders among the orders as the incident angle varied from $-4\ \theta_B$ to $+4\ \theta_B$. We note that the peaks of the diffraction intensity for the first-, second-, and third-order are at the incident angle of θ_B , $2\theta_B$ and $3\theta_B$, respectively. Thus, one may be led to believe that the second- and third-order beam diffractions originate from the first-order beam diffraction. Figure 7.7 shows the photographs of the diffraction spots for various angles of incidence.

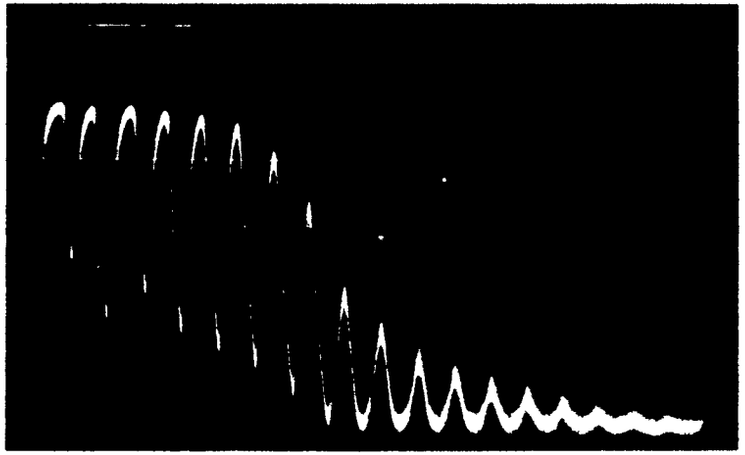

FIG. 7.3--Acoustic echoes at 1.1 Gc/s with no mercury termination.

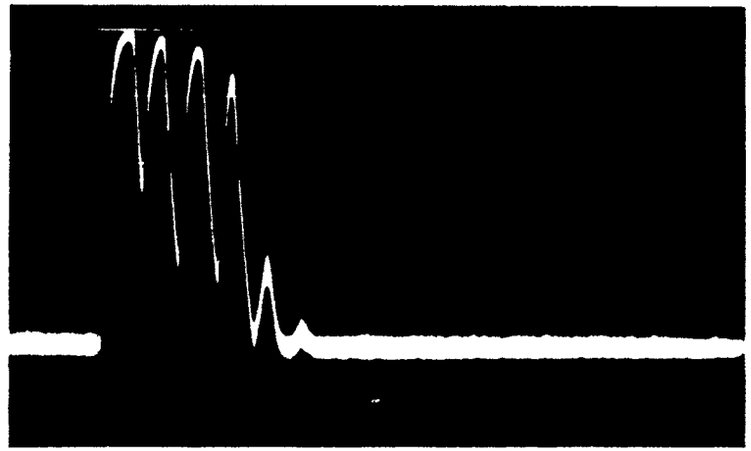

FIG. 7.4--Acoustic echoes at 1.1 Gc/s with mercury termination.

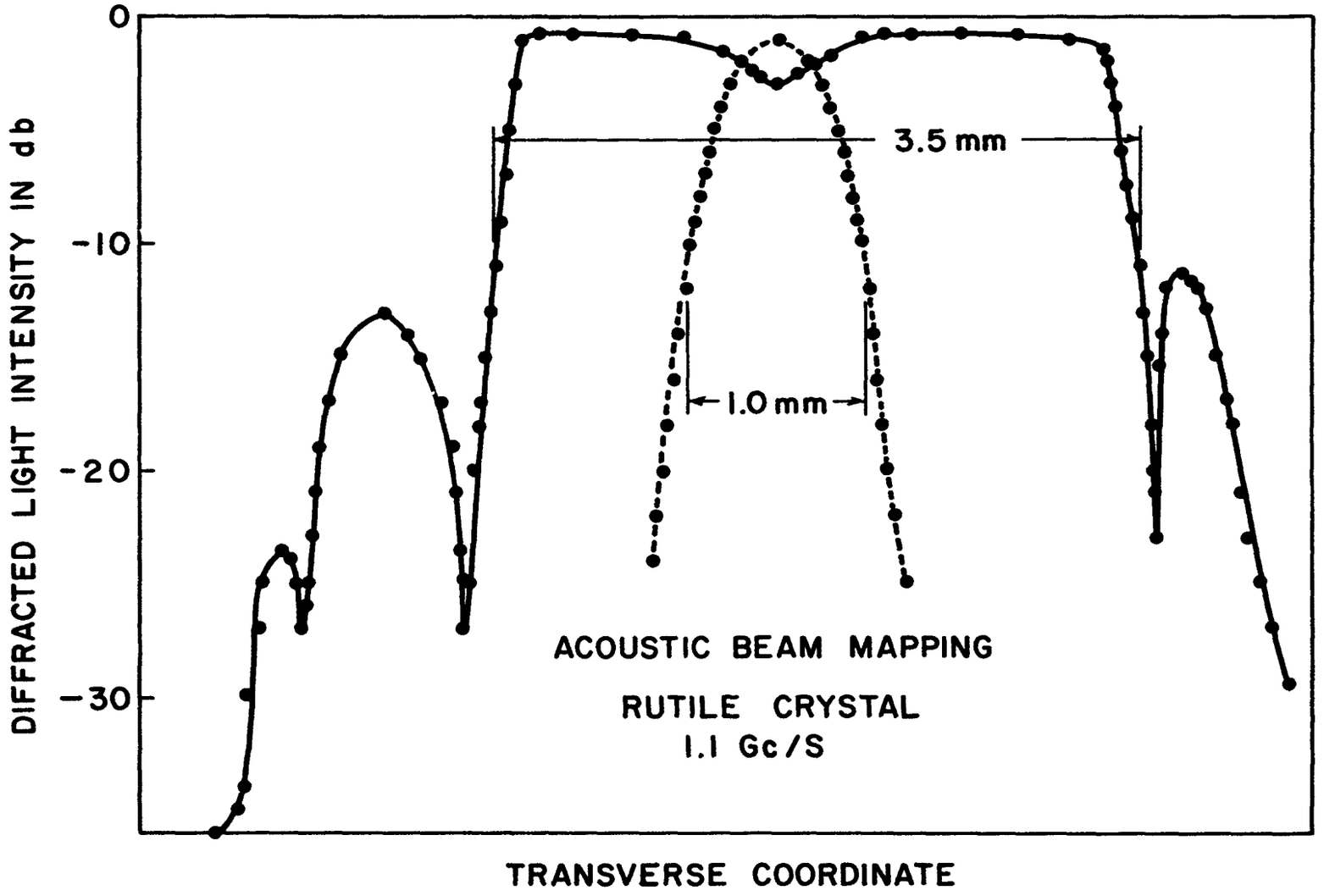

FIG. 7.5--Acoustic beam mapping (along the wide dimension) (along the narrow dimension).

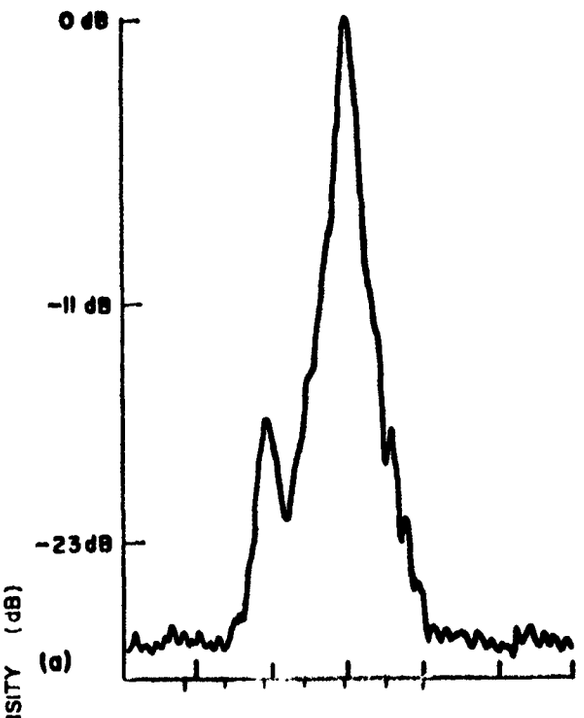

FIG. 7.5a--First-order diffraction pattern.

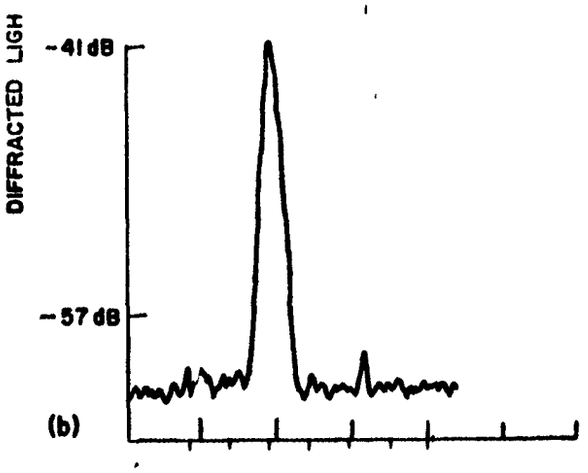

FIG. 7.5b--Second-order diffraction pattern.

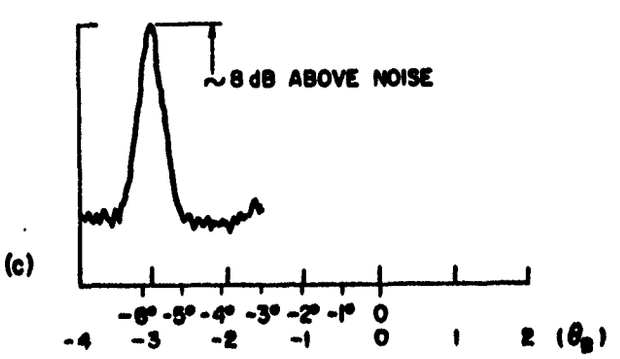

FIG. 7.5c--Third-order diffraction pattern.

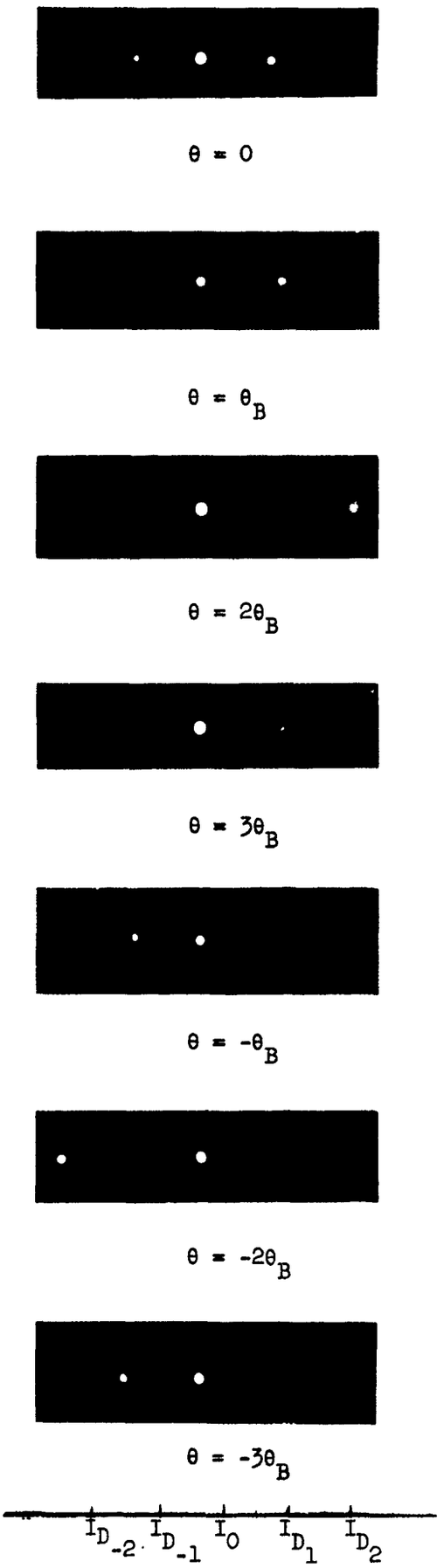

FIG. 7.7--Photographs of the diffraction spots for various angles of incidence.

(d) RF Power Dependence of the First-Order Diffraction Intensity at $\theta = \theta_B$

When the laser light was sent through the wider dimension of the acoustic beam the diffraction intensity was found to be 10 dB greater than for transmission through the narrow dimension of the beam. To determine the intensities of the zero - first- and second- order diffraction, the incident light, after passing through the crystal, was calibrated using a 1 kc/sec mechanical chopper. The rf power dependence of the first-order diffraction intensity is shown in Fig. 7.8, giving both measured and calculated values. The calculated values are obtained by the extended theory of Tien using the Lorentz-Lorentz formula as shown in the last chapter. Assuming that the effective beam width is defined by the 10 dB points in Fig. 7.5 ($d \approx 3.5$ mm), the acoustic power density dependence of the first-order diffraction intensity is as follows:

$$\frac{I_D}{I_0} \cong \tanh^2 \left| 3.72 \times 10^{-2} \, P_s^{1/2} \right| . \qquad (7.1)$$

As the conversion efficiency of the transducer is known (~ -14 dB), the rf power dependence of the first-order diffraction intensity is determined immediately from Eq. (7.1). From Fig. 7.8 the difference between the measured and the calculated values is about 4 dB. In Fig. 7.8, the experimental curve for the first-order diffraction intensity (marked with terminated) is obtained using a square-wave modulated rf signal generator at 1.1 Gc/s with modulation frequency of 1 kc/sec and with a mercury termination. The experimental curve for the first-order diffraction intensity (marked with unterminated) is obtained using a pulse-modulated rf signal generator at 1.1 Gc/s and without mercury termination. We have achieved a 10% first-order diffraction using a square-wave modulated rf input signal at 1.1 Gc/s with modulation frequency of 1 kc/s and peak power of about 15 watts, and about 60% first-order diffraction using pulsed modulated rf input signal with about 60 watts peak power. In the former case the crystal is terminated with mercury and in the latter there is no termination. The difference

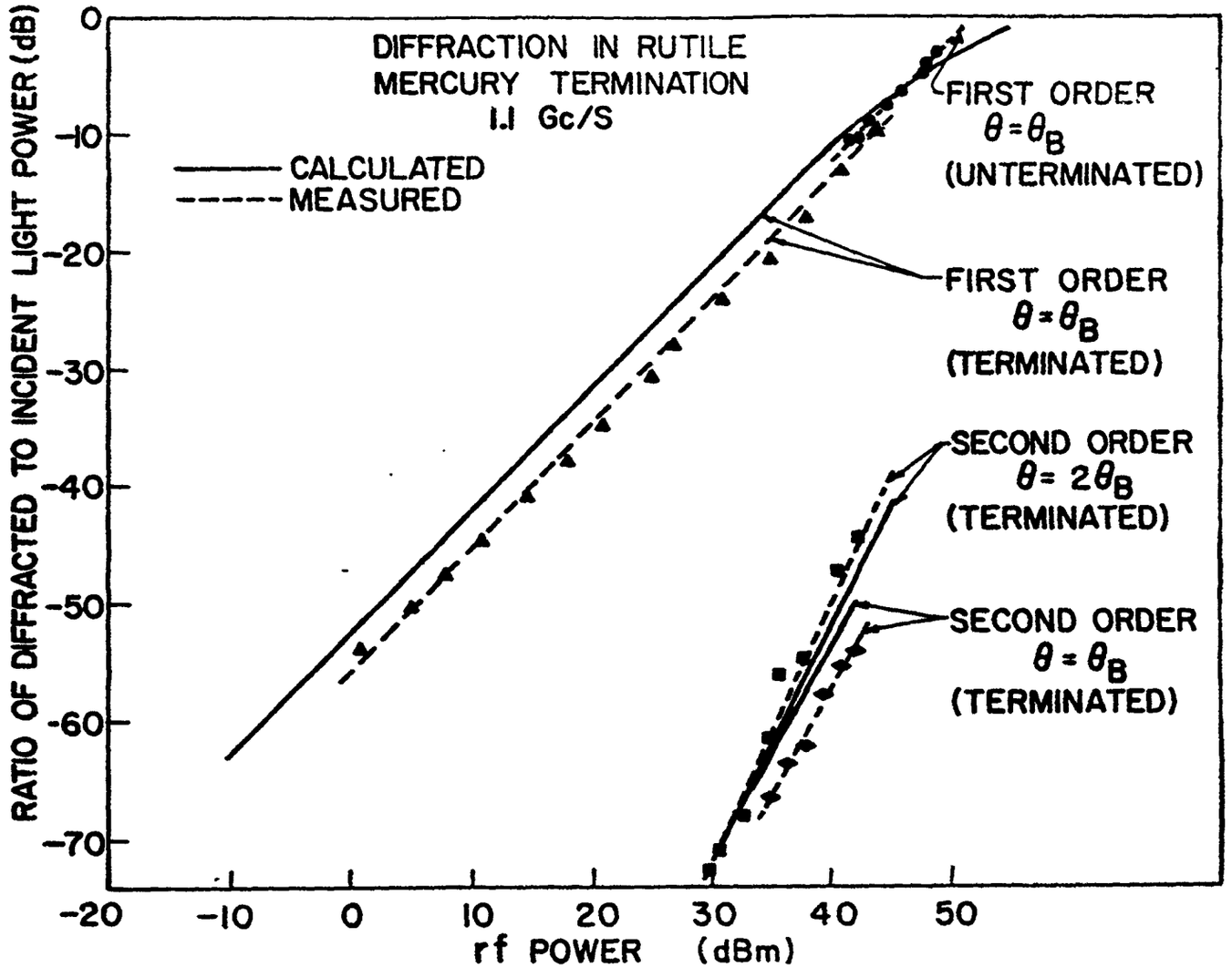

FIG. 7.8--The rf power dependence of the first- and second-order diffraction intensities.

in the diffraction intensity between the terminated and unterminated cases was measured as about 2 dB (see Fig. 7.8). From Eq. (6.75) the calculated value is 2dB.

The difference in the diffraction intensity for a perfect traveling wave and the non-perfect traveling wave (as we actually had, see Fig. 7.4) was estimated to be less than $\pm$ 1 dB. This number was obtained by determining the amplitude of the first echo, at the position of laser light incidence, by comparing the acoustic echoes for the terminated and unterminated cases (see Figs. 7.3 and 7.4). If we take the fourth echo in the terminated case (Fig. 7.4) as a reference, we see that there are approximately 5.5 more echoes in the unterminated case (Fig. 7.3) than in the terminated case. The acoustic loss is 5 dB for a round-trip. The laser light is incident at the middle of the crystal rod (see Fig. 7.9). Assume the incident acoustic power at the point of laser incidence, the incident acoustic power at the mercury pool, the reflected acoustic power at the crystal-mercury interface and the reflected acoustic power at the point of laser incidence are P_i P_t , P_r m and P_{r_1} respectively, then,

$$4 \times (10 \log \frac{P_r}{P_t}) = - 5.5 \times 5 \text{ dB}$$

i.e.,

$$10 \log \frac{P_r}{P_t} \simeq - 7 \text{ dB} \quad .$$

Thus we have

$$10 \log \frac{P_{r_1}}{P_i} = 10 \log \frac{P_{r_1}}{P_r} \cdot \frac{P_r}{P_t} \cdot \frac{P_t}{P_i}$$

$$= - \frac{5}{4} \text{ dB} - 7 \text{ dB} - \frac{5}{4} \text{ dB}$$

$$= - 9.5 \text{ dB} \quad ,$$

or

$$\frac{P_{r_1}}{P_i} \simeq 0.11 \quad ,$$

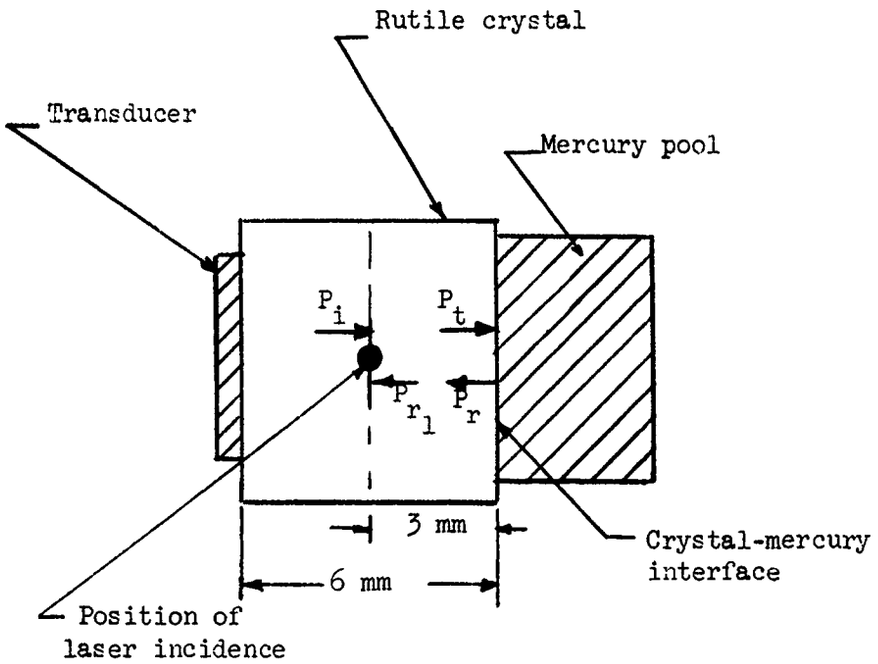

FIG. 7.9--Configuration for estimating the difference in the diffraction intensity between a perfect traveling wave and a non-perfect traveling wave.

giving, finally,

$$10 \log \frac{I_D(P_i \pm P_{r_1})}{I_D(P_i)} = 10 \log \frac{(1 \pm 0.11)}{1} < \pm 1 \text{ dB} \quad .$$

(e) RF Power Dependence of the Second-Order Diffraction Intensity at $\theta = \theta_B$ and $\theta = 2\theta_B$

Included in Fig. 7.8 are the measured and calculated values of the second-order diffraction intensity (both for $\theta = \theta_B$ and $\theta = 2\theta_B$) as a function of the rf power level. The difference between the measured and the calculated values is about 3 dB ($\theta = \theta_B$) and 2 dB ($\theta = 2\theta_B$). The calculated values are obtained by extending the theory of Phariseau.[87] We give the calculation here. Using the same notation as in reference 87, the expressions for the second-order diffraction intensity when the incident angle is the Bragg angle and twice the Bragg angle (or $\phi = \phi_B$ and $\phi = 2\phi_B$ in Phariseau's notation) are given by Eqs. (7.2) and (7.3), respectively:

$$I_{-2} \simeq \frac{1}{4\xi^2} \sin^2 \frac{\xi}{2} \qquad (7.2)$$

$$I_{-2} \simeq \frac{1}{16K_2^2} \cdot \xi^2 \quad , \qquad (7.3)$$

where

$$\xi = \frac{2\pi\mu_1 z}{\lambda}$$

$$K_2 = \sigma - \sqrt{\sigma^2 + \frac{1}{4}}$$

$$4\sigma = \zeta - 2a \sin \phi$$

$$\zeta = \frac{\lambda^2}{\mu_1 \mu_0 \lambda^{*2}}$$

and

$$a = \frac{\lambda}{\mu_1 \lambda^*}$$

λ = wavelength of the incident light wave in free space.
λ^* = wavelength of the acoustic wave in the medium.
μ_o = refractive index of the undisturbed medium.
μ_1 = maximum variation of the refractive index.
z = distance traveled by the light beam through the ultrasonic field.
ξ = incident angle of the light inside the medium.

The square-law dependence of the second-order diffraction intensity with rf peak power at $\phi = \phi_B$ is obvious from Eq. (7.2) for small ξ. Similarly at $\phi = 2\phi_B$ the square-law dependence of the second-order diffraction intensity on rf peak power as shown in the measured curve, is also predicted from Eq. (7.3).

Since $\sigma \gg 1$ (as will be seen later in this subsection) we have

$$K_2 \simeq 2\sigma = \frac{1}{2}(\zeta - 2a \sin 2\phi_B) = \frac{1}{2}\frac{\lambda}{\mu_1 \lambda^*}\left(\frac{\lambda}{\mu_o \lambda^*} - 2 \sin 2\phi_B\right) \tag{7.4}$$

but

$$\phi_B \simeq \frac{\lambda}{2\lambda^* \mu_o} ,$$

so Eq. (7.4) becomes

$$K_2 \simeq \frac{1}{2} \cdot \frac{\lambda}{\mu_1 \lambda^*}\left(\frac{\lambda}{\mu_o \lambda^*} - 2\frac{\lambda}{\mu_o \lambda^*}\right) = -\frac{1}{2\mu_o}\left(\frac{\lambda}{\lambda^*}\right)^2\left(\frac{2\pi z}{\lambda \xi}\right) . \tag{7.5}$$

Substituting Eq. (7.5) into (7.3), we have

$$I_{-2} \simeq \left(\frac{\mu_o \lambda^*}{4\pi \lambda z}\right)^2 \xi^4 . \tag{7.6}$$

As ξ^2 depends linearly on peak acoustic power density and hence peak rf power, so ξ^4 depends on (peak rf power)^2.

The numerical data for the experiment follows:

$$\mu_0 = 2.68 \quad , \quad \lambda = 0.6328 \times 10^{-4} \text{ cm} \quad , \quad \lambda^* = 9.45 \times 10^{-4} \text{cm} \quad ,$$

$$\phi_B = 0.0125 \text{ radian} \quad . \quad 2\phi_B = 0.0250 \text{ radian} \quad , \quad z \simeq 0.35 \text{ cm} \quad .$$

At 41 dBm of rf peak power, the acoustic power density P_s is about 18 dBm/mm^2 . From Fig. 6.13 and using the Lorentz-Lorentz formula [Eq. (6.40)], the strain corresponding to this power density is about 0.5×10^{-5} , and $\mu_1 \sim 1.75 \times 10^{-5}$. Thus we have

$$\xi = 0.61 \quad , \quad a = 3.8 \times 10^3 \quad , \quad \zeta = 95$$

and at $\phi = 2\phi_B$,

$$\sigma = -23.7 \quad , \quad K_2 = -47.5 \quad .$$

Then, at $\phi = \phi_B$, we have

$$I_{-2} \simeq \frac{1}{4 \times (95)^2} \sin^2 \frac{0.61}{2} = 7 \times 10^{-6}$$

or

$$10 \log \frac{I_{-2}}{I_0} = -51.6 \text{ dB} \quad ;$$

also, at $\phi = 2\phi_B$,

$$I_{-2} \simeq \frac{1}{16 \times (47.5)^2} \cdot (0.61)^2 = 10^{-5}$$

or

$$10 \log \frac{I_{-2}}{I_0} = -50 \text{ dB} \quad .$$

These two calculated values are used for plotting the calculated curves in Fig. 7.8.

(f) RF Power Dependence of the First-Order Diffraction Intensity at Normal Incidence ($\theta = 0$)

The rf power dependence of the first-order diffraction intensity (both right and left orders) at normal incidence is shown in Fig. 7.10 for both measured and calculated values. Both the right and left hand side first-order diffractions appeared with equal intensity, but about 30 dB lower than the calculated value using the normal Raman-Nath theory, i.e., Eq. (6.6). A disagreement between the measured values and the calculated values is of course expected following the argument described in Section 6.2, but such a big difference is not expected.

7.3 MEASURED ENHANCEMENT OF THE DIFFRACTION INTENSITY DUE TO ACOUSTIC RE ONANCE

In measuring the effect of acoustic resonance on the diffraction intensity, a rutile crystal with dimensions 4 mm × 4 mm × 12 mm was used. The length of the rod along the C-axis was 12 mm. A ZnO transducer was bonded on one end face (4 mm × 4 mm) and the other end face polished flat. The acoustic frequency was 810 Mc/sec and the one-way acoustic loss at this frequency is 1.5 dB/cm . The conversion efficiency of the transducer at this frequency is -11 dB . A typical acoustic echo is shown in Fig. 7.11. The Q-curves of the cavity with the crystal are shown in Figs. 7.12 and 7.13. The frequency between two consecutive frequency markers in Fig. 7.13 is 1 Mc/sec . We note that the acoustic resonance of the crystal shows up on the Q-curve due to the high conversion efficiency of the transducer. At the incident angle of θ_B , the diffraction spectrum was obtained by sweeping the acoustic wave frequency, as shown in Figs. 7.14 and 7.15 for the terminated and unterminated cases, respectively. The sharp peaks in the diffraction spectrum are due to the acoustic resonance (when the acoustic wave frequency is such that the length of the rod is an integer number of half-acoustic wave-length). The frequency separation between two consecutive peaks is about 0.40 Mc/sec as measured by a frequency marker. The calculated value $V_\ell/2L$ is 0.42 Mc/sec . The envelope along the sharp peaks depicts the Q-curve of the cavity. The band-width is about

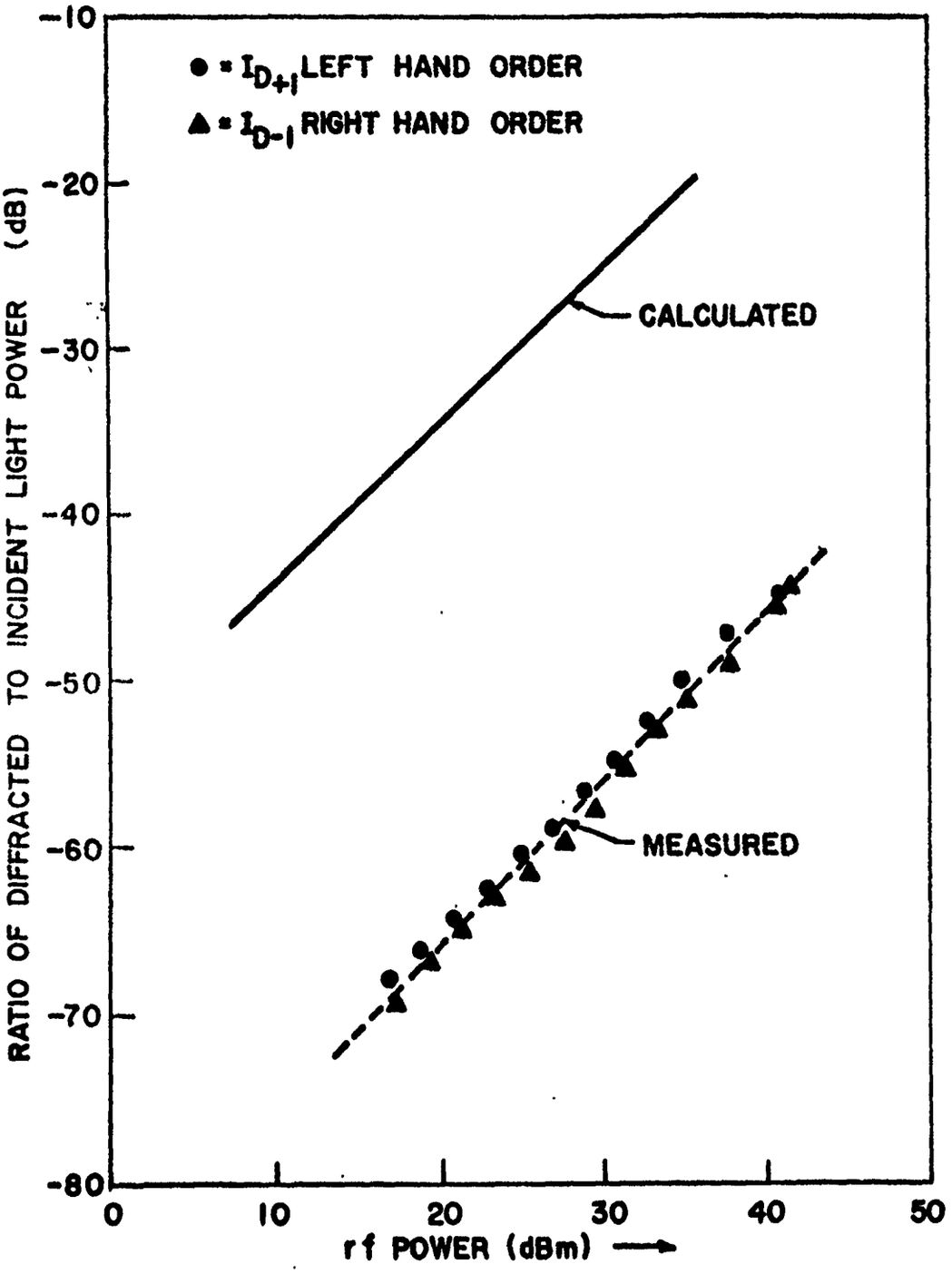

FIG. 7.10--The rf power dependence of the right-and left-hand side first-order diffraction intensities at normal incidence.

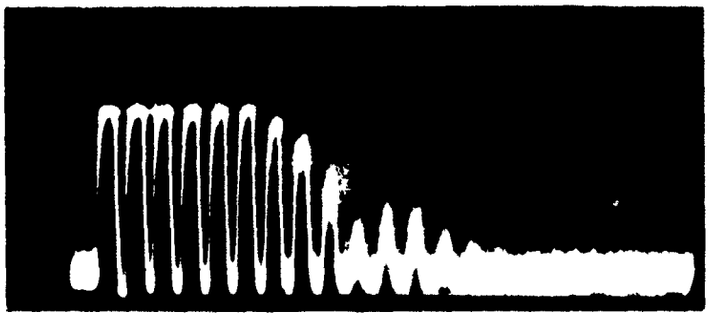

FIG. 7.11--The acoustic echoes at 810 Mc/s with no mercury termination.

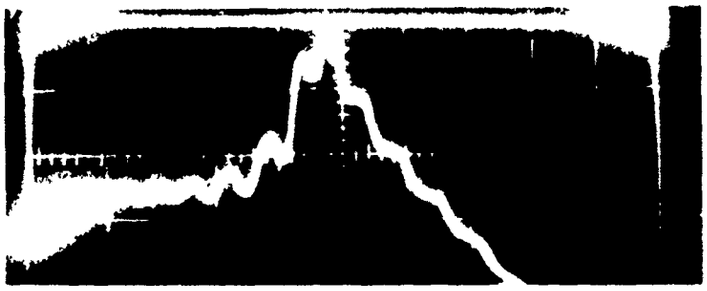

FIG. 7.12--The Q-curve of the cavity with the acoustic delay line (no frequency marker).

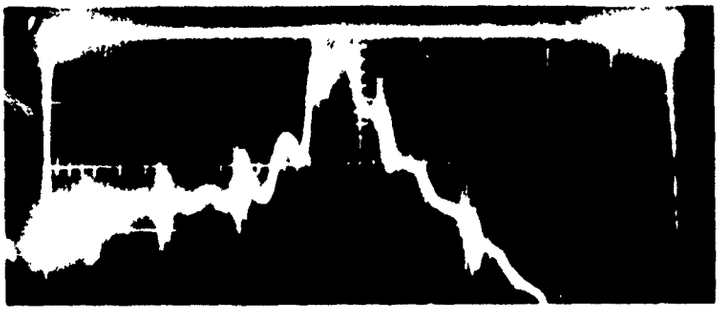

FIG. 7.13--The Q-curve of the cavity with the acoustic delay line. (The frequency between two consecutive frequency markers is 1 Mc/s.

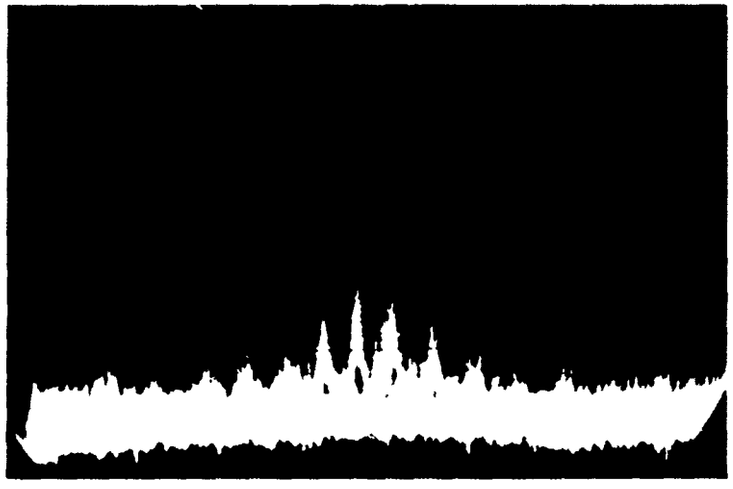

FIG. 7.14--The diffraction spectrum with mercury termination.

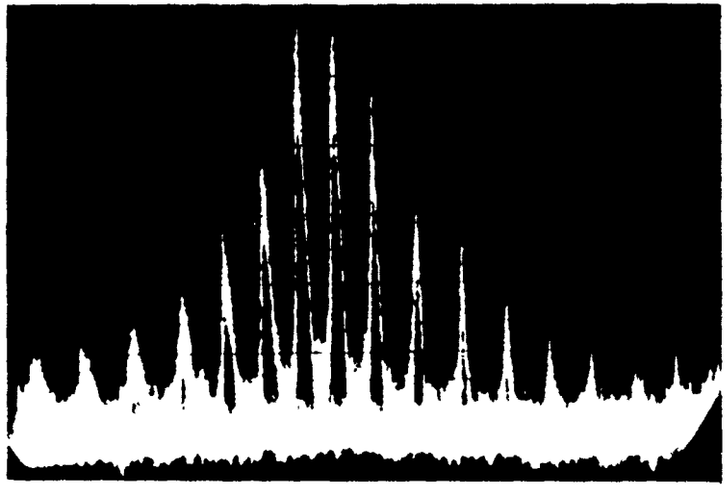

FIG. 7.15--The diffraction spectrum with no mercury termination.

is about 1.5 Mc/sec. We note that due to a nonperfect termination, weak peaks appear in the diffraction spectrum for the terminated case. Using neutral density filters for calibration, the difference between the diffraction intensity with mercury termination and that without is measured at 5 dB . From Eq. (6.75) the calculated value $10 \log 1/2\alpha L = 10 \log 8.9/2 \times 1.5 \times 1.2$ is about 4 dB .

7.4 DIFFRACTION PATTERN

It is of interest to see how the diffraction intensity varies when the incident angle of the laser light deviates from the Bragg angle by rotating the crystal, with the photomultiplier fixed in position. The diffraction pattern is found to be the Fourier transform of the amplitude distribution of the traveling acoustic waves in the plane of the wave front. This fact has been demonstrated by Cohen and Gordon.[88] We simply quote the results here.

Figure 7.16 depicts the configuration involved. The acoustic wave with frequency ω_s and wave number K_s propagates along the X-axis, while the incident light with frequency ω_1 and wave number K_1 impinges at an angle θ_0 with respect to the acoustic wave front. The acoustic wave amplitude varies along the Y-axis, with no variation in the Z direction. The amplitude of the first-order diffracted beam $V_1(\theta_0)$ with an acoustic beam distribution function $\xi(y)$ is

$$V_1(\theta_0) \simeq \left[-\frac{1}{2} iV_0 \exp^{+ iK_s(\theta_0 - \theta_B)y} \right] \times \left[\int_{-\infty}^{\infty} dy' \; \xi(y')^* \exp^{-iK_s(\theta_0 - \theta_B)y'} \right] \tag{7.7}$$

$$\xi(y) = \frac{1}{2} (K_1/\cos \theta_0) \left(\left[\frac{\Delta\epsilon(y)}{\epsilon} \right]_c + 1 \left[\frac{\Delta\epsilon(y)}{\epsilon} \right]_s \right) , \tag{7.8}$$

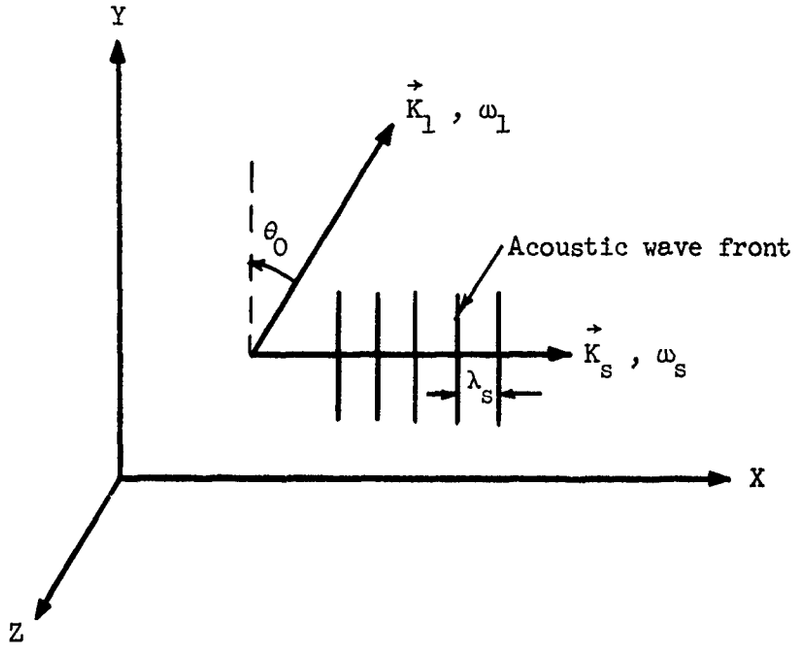

FIG. 7.16--Configuration showing the directions of propagation of the laser light and the acoustic wave.

where

V_0 = amplitude of the incident light before interaction,

θ_B = Bragg angle,

$\xi(y)$ = a function proportional to the change of the dielectric constant $[\Delta\epsilon(y)/\epsilon]$ due to the traveling acoustic waves and is, hence, proportional to the distribution of the acoustic waves,

y' = integration variable,

and * denotes complex conjugation.

Thus $|V_1(\theta_0)|^2$ determines the diffraction pattern versus the angle of crystal rotation and $|V_1(\theta_0)/V_0|^2$ determines the relative intensity of the diffraction pattern.

For a single acoustic beam of rectangular cross-section such that $\xi(y) = \xi =$ constant in the region $-(1/2)d \leq y \leq (1/2)d$ and zero elsewhere, the diffraction pattern reduces to

$$|V_1(\theta_0)|^2 \cong \frac{1}{4} \xi^2 d^2 V_0^2 \frac{\sin^2[\frac{K_s}{2}(\theta_0 - \theta_B)d]}{[\frac{K_s}{2}(\theta_0 - \theta_B)d]^2} \quad . \quad (7.9$$

The diffraction pattern is the same as that for a single-slit Fraunhofer diffraction.[79] The maximum intensity occurs at $\theta_0 = \theta_B$ and the angular dependence of the diffraction intensity is symmetric with respct to θ_B . The zeros on either side of θ_B occur at

$$\frac{1}{2} K_s(\theta_0 - \theta_B) d = n\pi \quad , \quad n = 1, 2, 3, \ldots \quad ,$$

or at incident angles

$$\theta_0 = \left(\frac{2n\pi + dK_s\theta_B}{dK_s} \right) \quad , \quad n = 1, 2, 3, \ldots \quad , \quad (7.10)$$

and the angle between the first zeros on either side of θ_B , $\Delta\theta_0$, is

$$\Delta\theta_0 = \frac{4\pi}{K_s d} = \frac{2\lambda_s}{d} \quad . \quad (7.11)$$

The auxiliary peaks of the diffraction intensity on either side of θ_B occur at

$$\frac{1}{2} K_s (\theta_0 - \theta_B) d = \frac{(n + 2)\pi}{2} \quad , \quad n = 1, 3, 5, \ldots ,$$

or at incident angles

$$\theta_0 = \frac{(n+2)\pi + dK_s\theta_B}{dK_s} \quad , \quad n = 1, 3, 5, \ldots \quad . \tag{7.12}$$

The intensities of the auxiliary peaks are -13.4 dB , -17.9 dB , and -20.8 dB , respectively, below that at $\theta_0 = \theta_B$.

7.5 LIGHT DIFFRACTION USING MULTIPLE ACOUSTIC BEAMS IN $SrTiO_3$ CRYSTAL

For this experiment a $SrTiO_3$ crystal with dimensions 8 x mm x 11 mm x 4 mm was used. The length of the crystal along the C-axis was 8 mm. A ribbon-shaped ZnO wafer transducer with dimensions ~ 2.5 mm x 5.5 mm x 0.175 mm was bonded on one end face (11 mm x 4 mm) of the crystal and inserted in the high field gap of the previously used coaxial cavity. The cross-section of the center post of the cavity was 1 mm x 6.0 mm . The experimental arrangement is the same as the one employed before.

a. Generation of Multiple Acoustic Beams

In this experiment the ZnO wafer was wedge shaped as shown in Fig. 7.17a, and multiple acoustic beams generated. The generation of multiple acoustic beams using a wedge-shaped transducer is obvious from the fact that when the thickness of the transducer is an odd integer multiple of half acoustic wavelength the amplitude of the acoustic wave is a maximum; and when the thickness of the transducer is an even integer multiple of half acoustic wavelength the amplitude of the acoustic wave is a minimum. The profile of the acoustic column across its wide dimension was scanned by observing the diffracted light intensity as the laser beam was shifted across the column (Fig. 7.18). The acoustic profile along the narrow dimension is shown in Fig. 7.19. Notice that the maximum difference in diffraction intensity is seen to be about 13 dB. The decrease in the peaks of the diffraction intensity along the direction of the wide dimension is attributed to the variation in

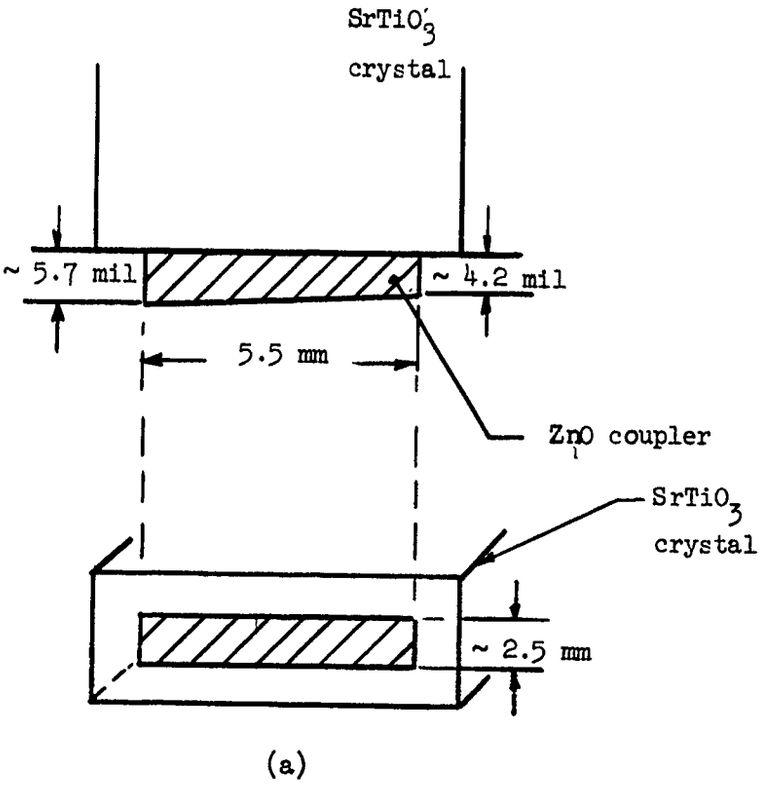

(a)

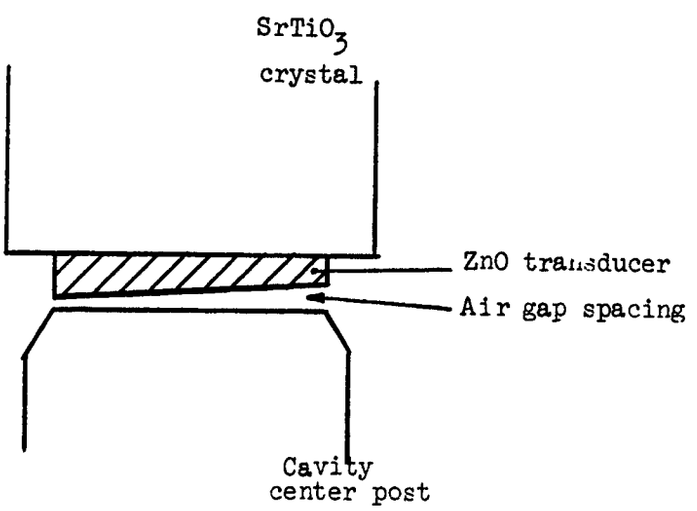

(b)

FIG. 7.17(a)--The dimensions and the orientation of the wedge-shaped transducer,
(b)--The variation of the air gap spacing between the transducer and the center post.

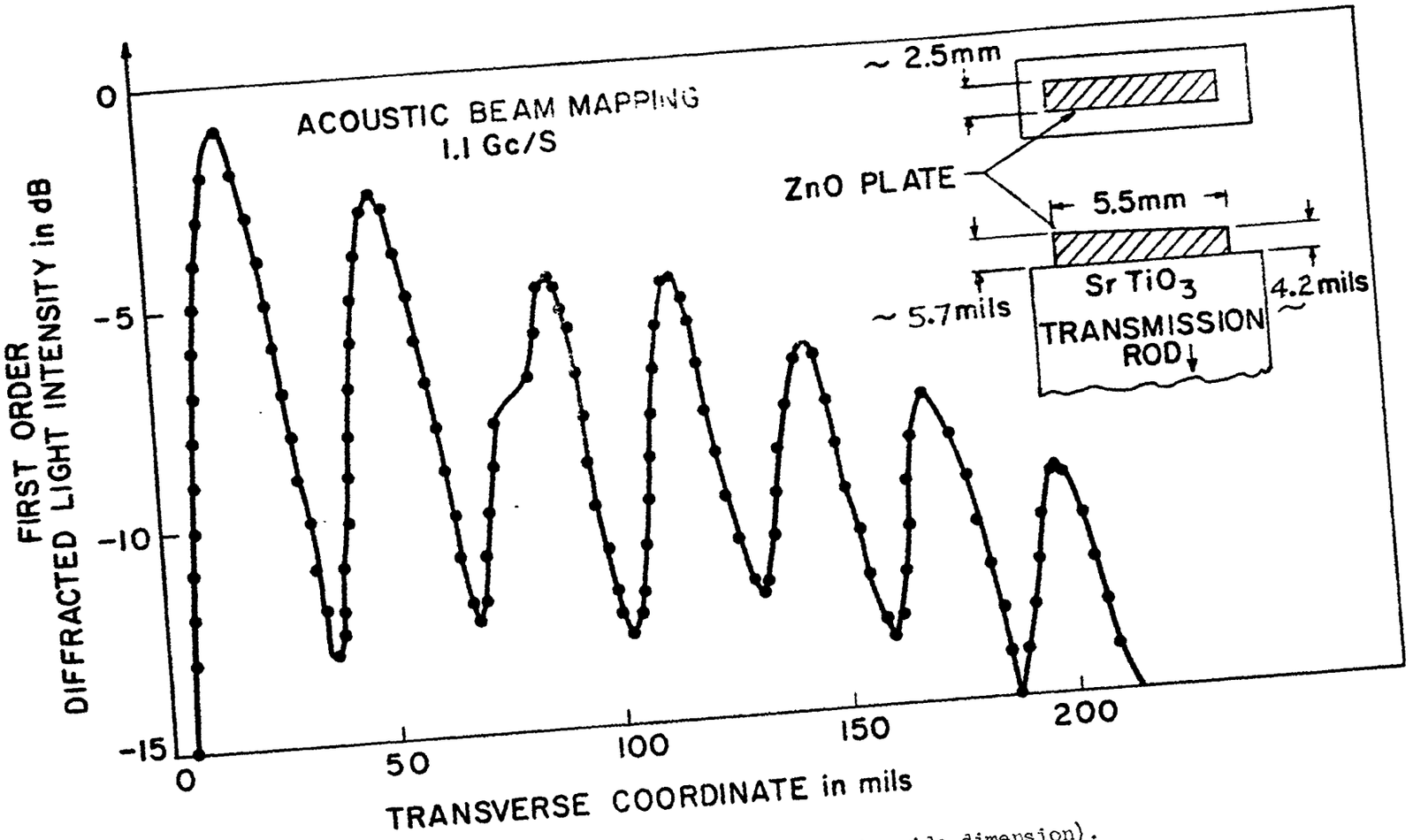

FIG. 7.18--Acoustic beam mapping (along the wide dimension).

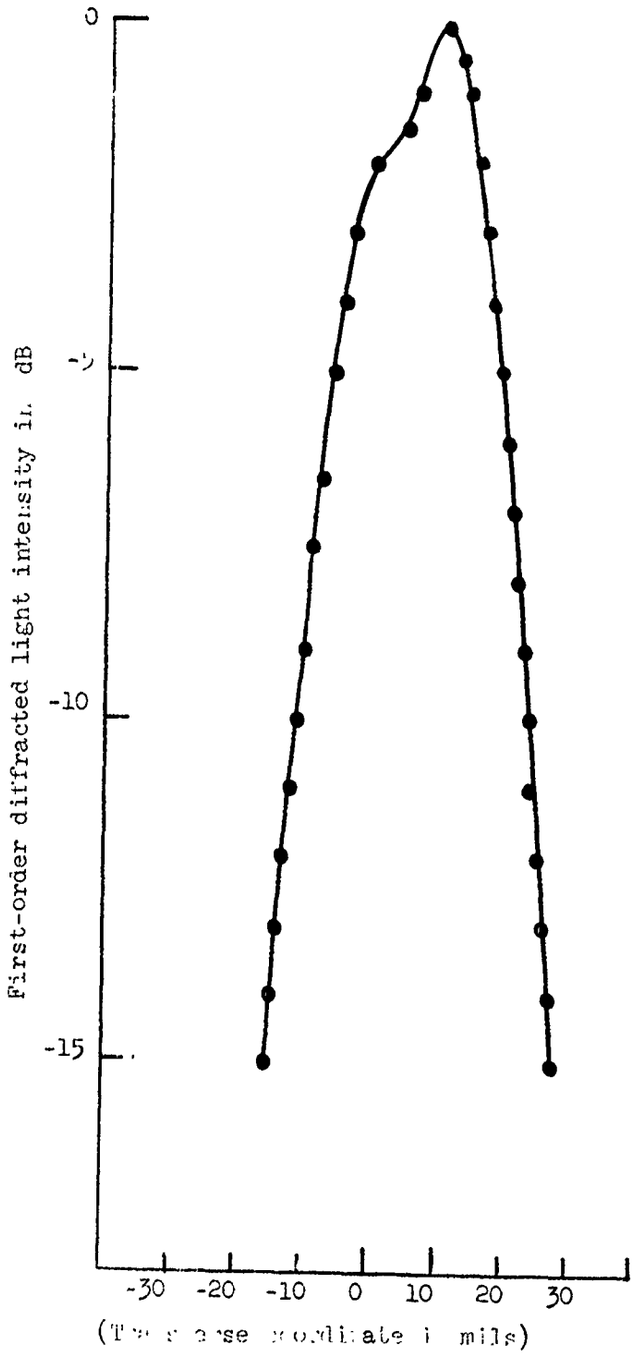

FIG. 7.19--Acoustic beam mapping (along the narrow dimension).

the air gap spacing between the wedge-shaped transducer and cavity center post. The diffracted intensity was measured to be less at the edge of the beam when the air gap was largest.

That we actually had a wedge-shaped transducer, and consequently the generation of multiple acoustic beams, is verified by two means: First, the thickness of the wafer transducer was measured by a microscope; the dimensions are shown in Fig. 7.17(a). Second, the positions of the peaks of the diffraction intensity moved as the rf frequency was swept (Fig. 7.20). The difference in thickness as determined by the method of sweeping the rf frequency agress with that measured by the microscope (Fig. 7.21) within 8%.

From the acoustic beam mappings shown in Fig. 7.20a,b,c, we see that as the rf frequency increases the peaks of the diffraction intensity move in the direction towards the end of narrow thickness. If we compare the first peak (point 1) in Fig. 7.20a with the first peak (point 2) in Fig. 7.20c, we see that the peak moved by about 0.25 mm (see Fig. 7.21) while the rf frequency was swept by 14.5 Mc. From the dimensions shown in Fig. 7.21, we have.

$$\left(\frac{d_1 - d_2}{d_1}\right) \times 100 = \frac{\left(4.2 + \frac{1.5 \times 5.25}{5.5}\right) - \left(4.2 + \frac{1.5 \times 5.0}{5.5}\right)}{\left(4.2 + \frac{1.5 \times 5.25}{5.5}\right)} = 1.2\% \quad .$$

Furthermore, when we utilize the fact that the acoustic transmission is a maximum when the transducer thickness is an odd integer of half acoustic wavelength, we have, for the n^{th} mode,

$$\begin{cases} d_1 = n \dfrac{\lambda_{s_1}}{2} \\ d_2 = n \dfrac{\lambda_{s_2}}{2} \end{cases}$$

(= Odd integer corresponding to 2f in this experiment.)

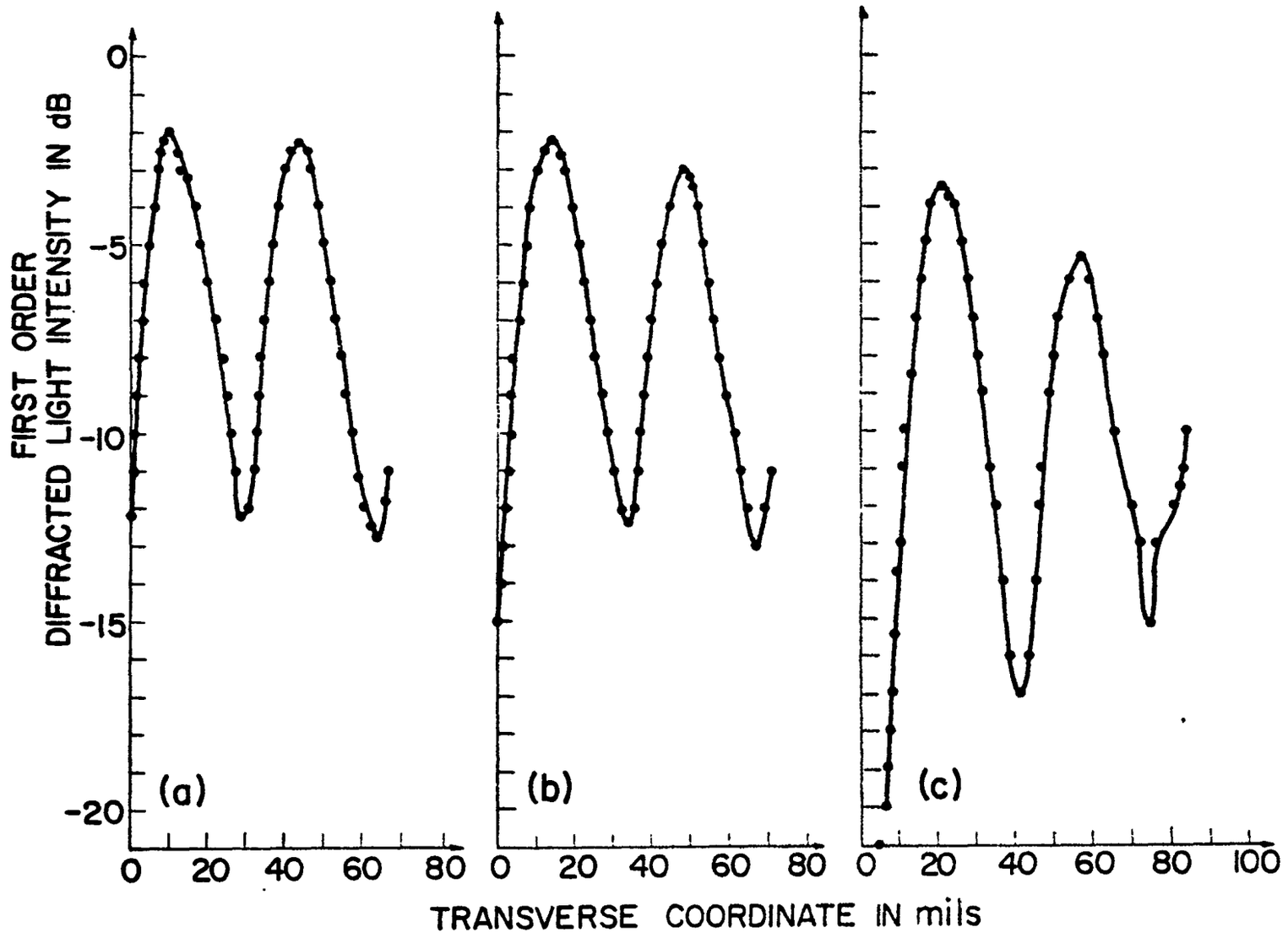

FIG. 7.20---Acoustic beam mapping (along the wide dimension).
(a) f = 1100.5 Mc/sec . (b) f = 1106.5 Mc/sec . (c) f = 1115.0 Mc/sec .

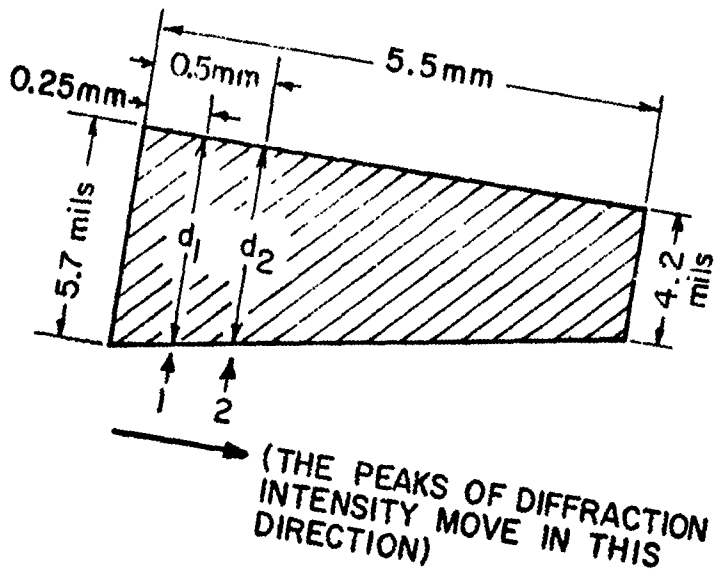

FIG. 7.21--Dimensions of the wedge-shaped transducer.

Since $f_1 = 1100.5$ Mc/sec, $f_2 = 1115.0$ Mc/sec, we have

$$\left(\frac{d_1 - d_2}{d_1}\right) \times 100 = 1.3\% \quad .$$

The excellent agreement in the value of $(d_1 - d_2)/d_1 \times 100$ using these two means supports the statement made above.

b. Diffraction Pattern Due to Multiple Acoustic Beams

The diffraction pattern for the first-order as obtained by rotating the crystal and with the photomultiplier fixed at a deflection angle of $2\theta_B$ is shown in Fig. 7.22a. The acoustic wave was terminated with a mercury pool for this measurement. Notice that there are many peaks in the diffraction pattern and that the angular spread of the envelope of the peaks is very broad. This is analogous to the diffraction pattern of multiple slits in optics and agrees with the concepts of Fourier transformation of the acoustic wave distribution described in the previous section.

Using Eqs. (7.7) and (7.8) in which the distribution of $\xi(Y)$ is given by Fig. 7.13 and $K_s \simeq 20$ per mil , θ_B (outside the crystal) $= 0.04^{rad} = 2.28^{\circ}$, the diffraction pattern obtained by computer calculation is as shown in Fig. 7.22b. The existence of many intensity peaks and broad angular spread in the envelope of the peaks agrees qualitatively with that obtained by an X-Y recorder (see Fig. 7.22a).

The diffraction pattern for the second-order as obtained by rotating the crystal and with the photomultiplier fixed at a deflection angle of $4\theta_B$ is shown in Fig. 23. We note that the peak intensity of the second-order diffraction at $\theta \simeq 2\theta_B$ is about 8 dB below that of the first-order diffraction at $\theta = \theta_B$ and that one satellite peak appears at both sides of the main peak. Figure 7.24 shows the photographs of the diffraction spots for various angles of incidence.

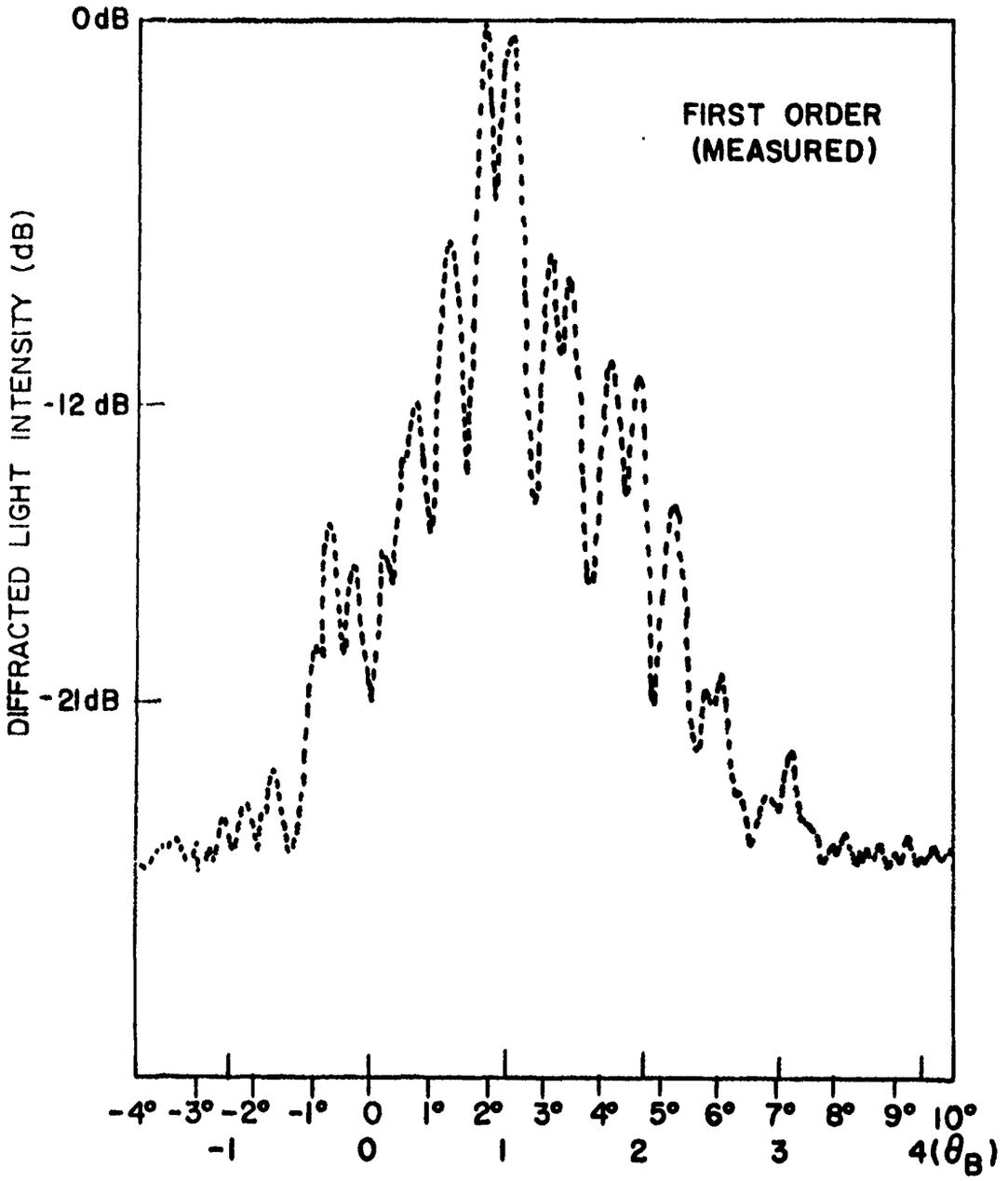

FIG. 7.22a--First-order diffraction pattern (measured).

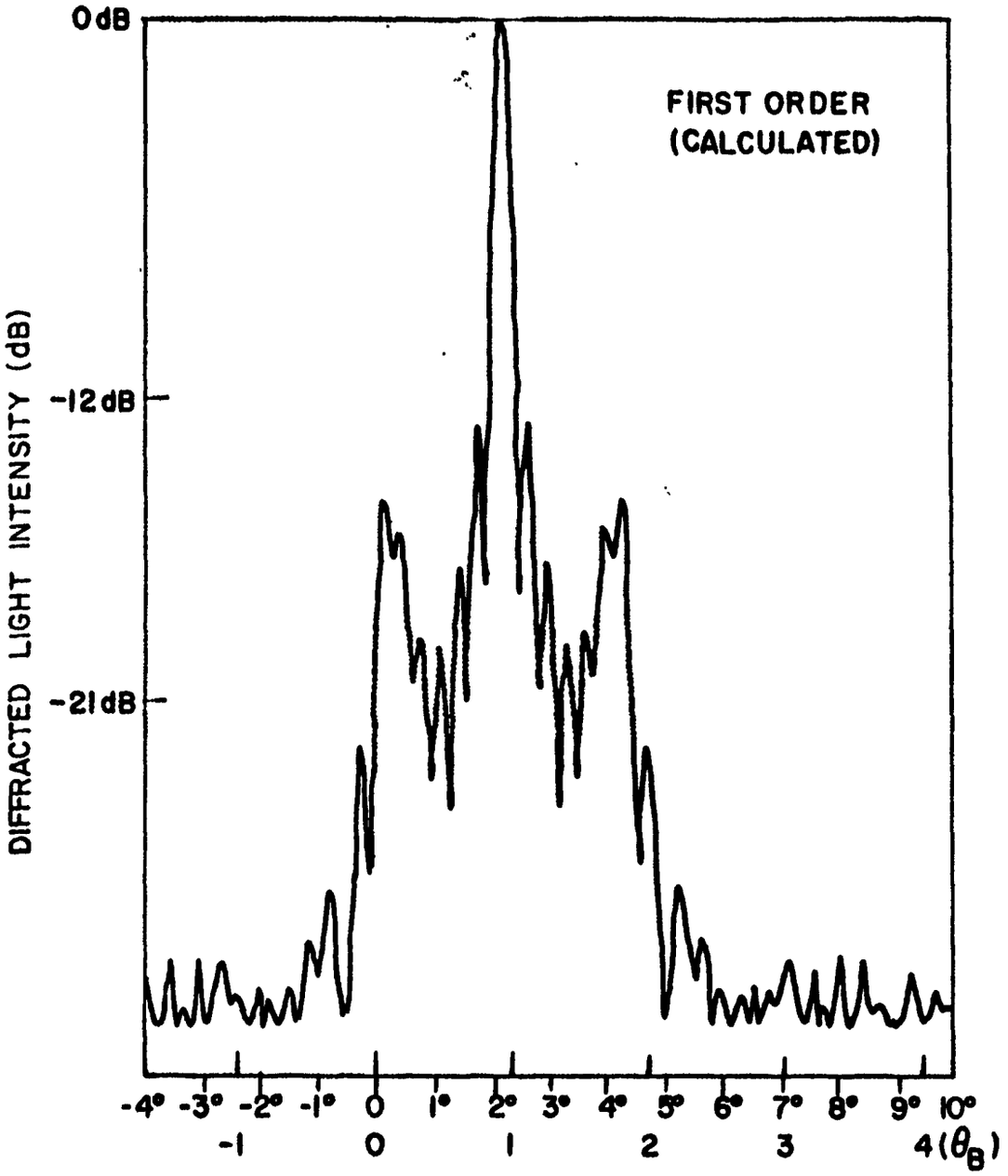

FIG. 7.22b--First-order diffraction pattern (calculated).

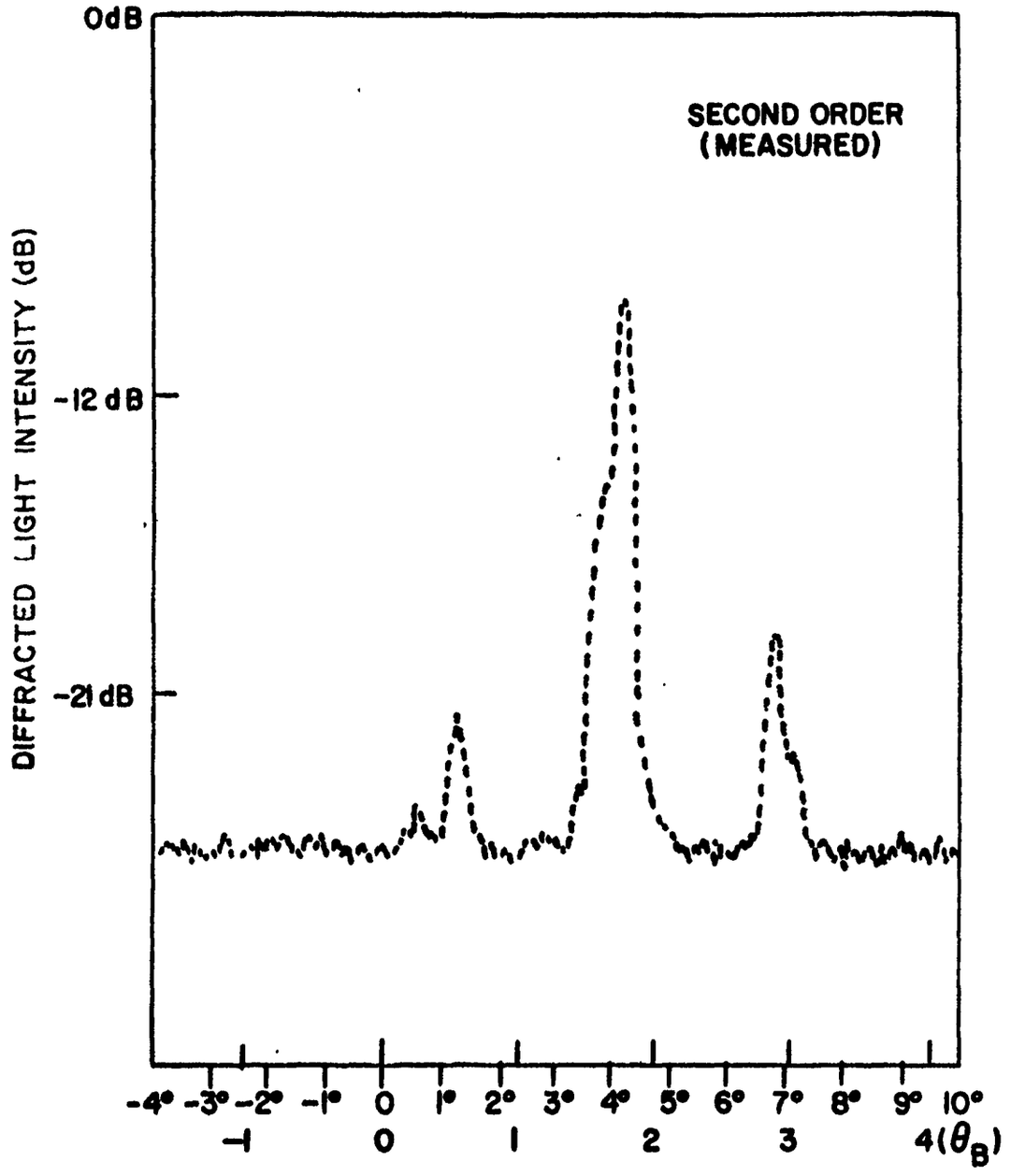

FIG. 7.23--Second order diffraction pattern (measured).

θ = 0

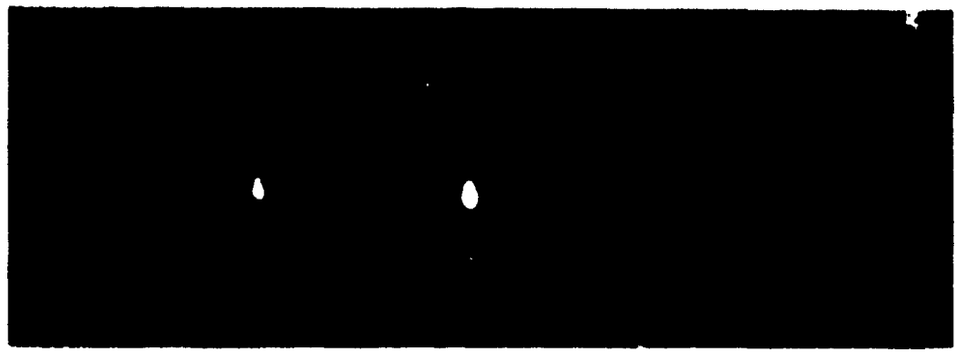

$\theta = -\theta_B$

$\theta = -2\,\theta_B$

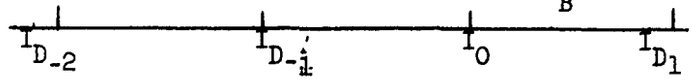

FIG. 7.24--Photographs of the diffraction spots for various angles of incidence.

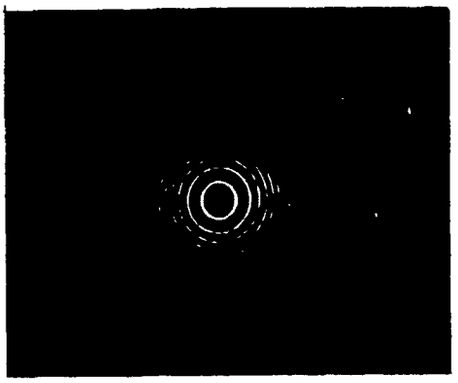

(a)

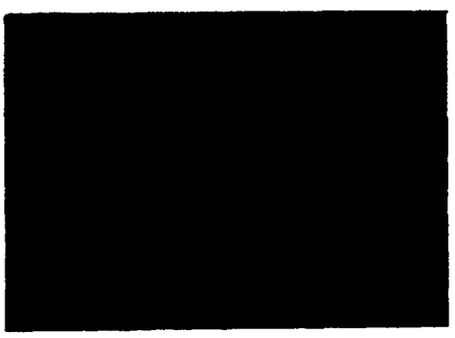

(b)

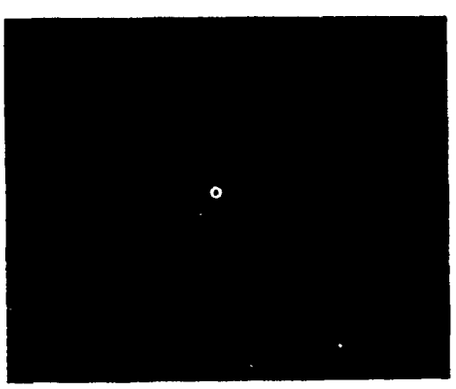

(c)

FIG. 7.25--Fabry-Perot patterns of (a) the undiffracted beam; (b) the diffracted beam with up-shifted frequency; and (c) the diffracted beam with down-shifted frequency.

7.6 THE MEASUREMENT OF FREQUENCY SHIFT IN THE DIFFRACTED BEAM USING FABRY-PEROT ETALON

Figure 7.25 shows the fringes obtained from a 5 cm etalon for the (a) undiffracted, (b) right-hand side first order and,(c) left-hand side first order diffracted beams, respectively. The acoustic wave is at the frequency of 1.07 Gc/s and terminated with a mercury pool. The frequency spacing between two consecutive fringes in the 5 cm etalon is 3 Gc/s. The fringes in Fig. 7.25b are obtained when the acoustic wavefronts are approaching the incident laser beam. By measuring the increase in the diameter of the innermost fringe, the frequency of the diffracted beam is found to be shifted up by ~ 1.05 Gc/s . This result agrees with both the Doppler shift principle and the parametric condition involved. Similarly, the fringes in Fig. 7.25c are obtained when the acoustic wavefronts are receding from the incident laser beam. By measuring the decrease in the diameter of the innermost fringe, the frequency of the diffracted beam is found to be shifted down by ~ 1.1 Gc/s . Again, this result agrees with both the Doppler shift principle and the parametric condition involved.

CHAPTER VIII

MULTIPLE DIFFRACTION TECHNIQUES

With the success of diffracting and Doppler-shifting a large portion of laser light with a moderate amount of rf power, frequency shifting of laser sources using acoustic waves at microwave frequencies in crystals such as TiO_2, $SrTiO_3$, SiO_2, ... etc., becomes feasible.

We analyze in this chapter two schemes of using multiple diffraction to shift the laser frequency by integer multiples of the acoustic wave frequency. One scheme uses a pair of Porro prisms in order to pass the laser beam repeatedly through the acoustic column. The other scheme uses a pair of overlapping optical cavities with their axes tilted by twice the first-order Bragg angle. Laser light is scattered alternately from one cavity to another, the mode spacing of the cavity being set equal to the acoustic wave frequency in order to provide reinforcement.

8.1 SIMULTANEOUS GENERATION OF THE UPPER AND LOWER SIDEBANDS USING A PAIR OF PORRO PRISMS

Consider the configuration shown in Fig. 8.1. Two Porro prisms, 1 and 2, are arranged in a position such that the diffracted light passes successively through them. Two photo-detectors 1 and 2 can be employed to monitor the various upper sidebands in the diffracted light. It is obvious that the sidebands with frequencies shifted by even multiple of acoustic wave frequency come out from one side and the sidebands with frequencies shifted by odd multiple of the acoustic wave frequency come out from the other side. To generate the various lower sidebands, we simply reverse the direction of propagation of the acoustic wave.

If we ignore the acoustic loss and the optical loss due to the crystal and the prisms, the light intensities for the sidebands are

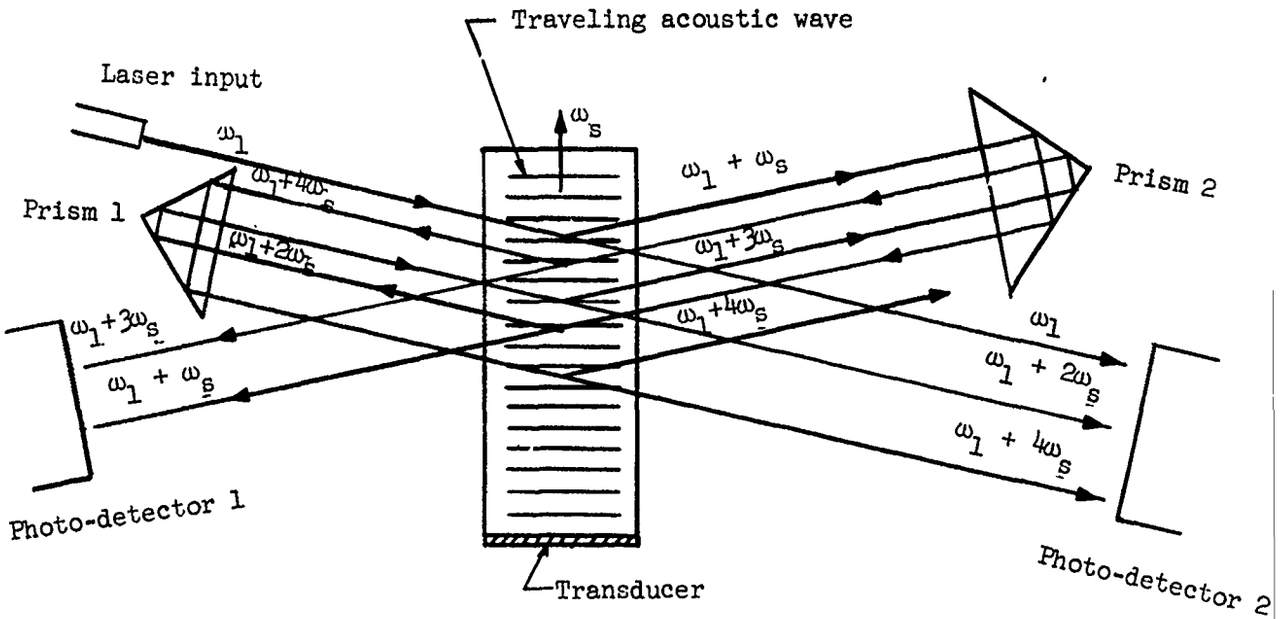

FIG. 8.1--Configuration for simultaneous generation of the upper and lower sidebands using a pair of Porro prisms.

given by

$$\frac{I_D(\omega_1 + n\omega_s)}{I_0(\omega_1)} = \left(\frac{I_{D_1}}{I_0}\right)^n \left(\frac{I_0 - I_{D_1}}{I_0}\right) \qquad (8.1)$$

where

n = order of the sidebands,

$I_D(\omega_1 + n\omega_s)$ = intensity of the n^{th} order sideband,

$I_0(\omega_1)$ = intensity of the incident light,

I_{D_1}/I_0 = the ratio of the diffracted light intensity and the incident light intensity for a single interaction.

As an example, consider $(I_{D_1}/I_0) \simeq 0.5$, as was described in Chapter VII; we have then

$$\frac{I_D(\omega_1 + n\omega_s)}{I_0(\omega_1)} = (0.5)^{+(n+1)} \quad ,$$

the light intensity for the fifth-order sideband is of the order of 1.5%.

8.2 SIMULTANEOUS GENERATION OF THE UPPER AND LOWER SIDEBANDS USING A PAIR OF OPTICAL CAVITIES

8.2.1 Introduction

Consider the configuration shown in Fig. 8.2. A suitable crystal containing an acoustic column for Bragg diffraction is inserted in a pair of optical cavities (i.e., Fabry-Perot etalon). The axes of the overlapping optical cavities are tilted by twice the first order Bragg angle. The separation of the etalon is adjusted so that the axial mode spacing of the etalon, $C/2L$, is equal to the acoustic wave frequency f_s . We assume that the cavities consist of four identical, partially reflecting mirrors with sufficiently large area. The laser light couples into the system from one end of the cavity 1.

The propagation of an acoustic wave in an elasto-optic crystal produces a spatial and time-varying perturbation in the dielectric constant (or the index of refraction). The relations between the change in dielectric constant and acoustic power density, and the resonance effect for various kind of crystals have been treated in Chapter VI. The sidebands or the diffracted components are generated by the perturbed part of the dielectric constant induced by the acoustic waves. Since the frequency shifts of the sidebands are equal to the mode spacings of the optical cavities, reinforcement in the intensities of the sidebands due to multiple diffraction will occur. For example, from Fig. 8.2, the incident light in cavity 1 first mixes with the acoustic waves to excite the first-order sideband (the first-order diffraction) in cavity 2, while the transmitted light, after reflecting back from the mirror, mixes with

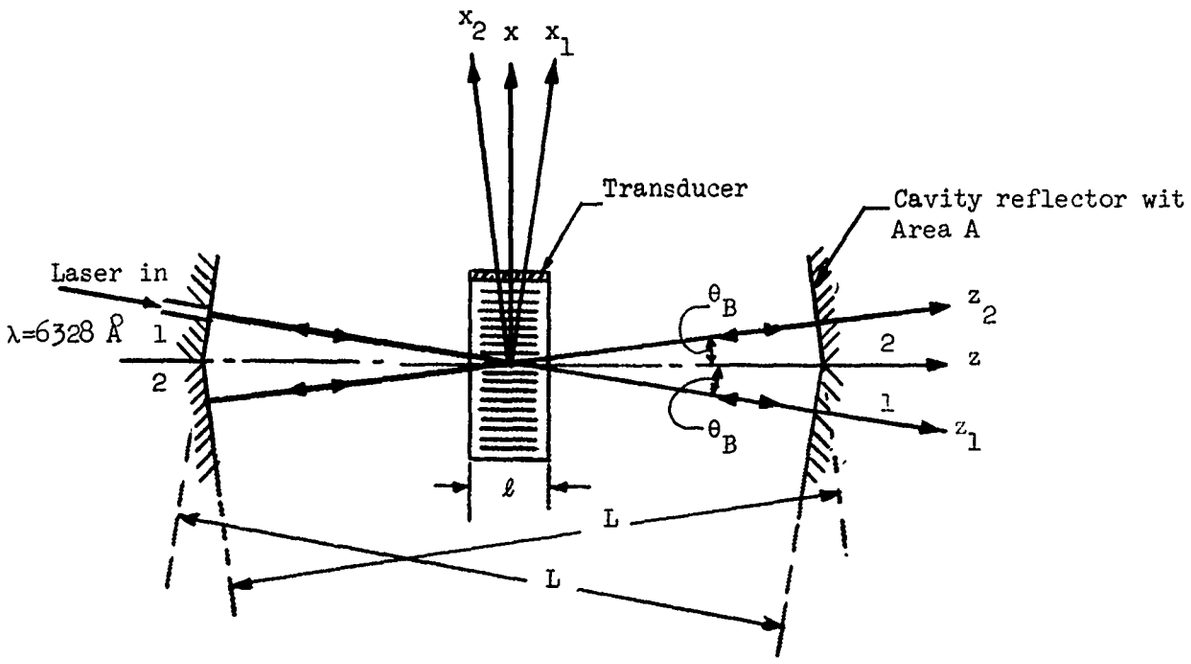

FIG. 8.2--Configuration for the simultaneous generation of the upper and lower sidebands using a pair of optical cavities.

the acoustic waves again to excite the first-order sideband in cavity 2. The first-order sideband is strongly excited in cavity 2 because of resonance, and by mixing with the acoustic waves again, the second-order sideband is excited in cavity 1. The second-order sideband excited in cavity 1 is also resonated. This mixing process continues to develop so that we have a system with many modes or sidebands (both upper and lower sidebands) coupled together.

The formulation of the "harmonic-oscillator-like" linear differential equations for the mode amplitudes is given in Section 8.2.2, and Section 8.2.3 gives their solutions and numerical results.

8.2.2 Derivation of the "Harmonic-Oscillator-like" Linear Differential Equation for the Expansion Coefficients of the Optical Fields

The technique of normal mode expansion given by Slater[85] is used in the following analysis. The expansion coefficients of the optical fields within the cavities are time dependent and satisfy "harmonic-oscillator-like" linear differential equations. They are coupled by the perturbed part of the dielectric constant which is induced by the acoustic waves. Figure 8.2 shows the configuration involved. For the case in which the volume of the crystal is only a small portion of the cavity volume, we ignore the effect of the crystal upon the normal modes of cavity 1 and 2, i.e., we use the normal modes corresponding to those without any crystal present in the cavity; while for the case in which the volume of the crystal is a large portion of the cavity volumn, we use the normal modes corresponding to those with crystal completely filling the cavity. In the filled cavity the waves will travel with velocity $c/\sqrt{\epsilon}$ and in the empty one with velocity c ; otherwise the normal mode expansions are the same. We consider the first case here. This is approximately the case when an L-band acoustic wave is employed as can be seen from the example given in Section 8.2.3. Thus we assume $\epsilon' = \epsilon_0 + \delta\epsilon$, where ϵ_0 is the permittivity in vacuum and $\delta\epsilon$ the change of permittivity due to the acoustic waves.

The acoustic waves induce perturbed displacment currents

$$\frac{\partial(\delta\epsilon\vec{E}_1)}{\partial t} \quad \text{and} \quad \frac{\partial(\delta\epsilon\vec{E}_2)}{\partial t}$$

in cavities 2 and 1, respectively. Thus ignoring both optical and acoustic losses in the crystal, we have the following two sets of Maxwell equations for cavity 1 and 2, respectively:

$$\begin{cases} \nabla \times \vec{E}_1 = -\mu_0 \dfrac{\partial \vec{H}_1}{\partial t} & (8.2) \\ \nabla \times \vec{H}_1 = \epsilon_0 \dfrac{\partial \vec{E}_1}{\partial t} + \dfrac{\partial(\delta\epsilon\vec{E}_2)}{\partial t} & (8.3) \end{cases}$$

$$\begin{cases} \nabla \times \vec{E}_2 = -\mu_0 \dfrac{\partial \vec{H}_2}{\partial t} & (8.4) \\ \nabla \times \vec{H}_2 = \epsilon_0 \dfrac{\partial \vec{E}_2}{\partial t} + \dfrac{\partial(\delta\epsilon \vec{E}_1)}{\partial t} \quad . & (8.5) \end{cases}$$

The terms $\partial/\partial t(\delta\epsilon E_1)$ and $\partial/\partial t(\delta\epsilon E_2)$ have been neglected in Eq. (8.2) and Eq. (8.5), respectively, because, as will be seen, the frequencies of these terms are nonresonant.

Following Slater's cavity perturbation theory, the fields are expanded as follows:[1]

$$\begin{cases} \vec{E}_1(z_1,t) = \sum\limits_{b_1} e_{b_1}(t)\, E_{b_1}(z_1) \\ \vec{E}_2(z_2,t) = \sum\limits_{b_2} e_{b_2}(t)\, E_{b_2}(z_2) \\ \vec{H}_1(z_1,t) = \sum\limits_{b_1} h_{b_1}(t)\, H_{b_1}(z_1) \\ \vec{H}_2(z_2,t) = \sum\limits_{b_2} h_{b_2}(t)\, H_{b_2}(z_2) \end{cases} \qquad (8.6)$$

[1] Idealized one-dimensional cavities are assumed.

and

$$
\begin{cases}
\nabla \times \vec{E}_2 = \sum_{b_2} H_{b_2} \left[k_{b_2} e_{b_2} + \int_{S_{s2}} (\vec{n} \times \vec{E}_2) \cdot \vec{H}_{b_2} \, ds \right] \\
\nabla \times \vec{H}_2 = \sum_{b_2} E_{b_2} \left[k_{b_2} h_{b_2} + \int_{S_{02}} (\vec{n} \times \vec{H}_2) \cdot \vec{E}_{b_2} \, ds \right] \\
\nabla \times \vec{E}_1 = \sum_{b_1} H_{b_1} \left[k_{b_1} e_{b_1} + \int_{S_{s1}} (\vec{n} \times \vec{E}_1) \cdot \vec{H}_{b_1} \, ds \right] \\
\nabla \times \vec{H}_1 = \sum_{b_1} E_{b_1} \left[k_{b_1} h_{b_1} + \int_{S_{01}} (\vec{n} \times \vec{H}_1) \cdot \vec{E}_{b_1} \, ds \right] .
\end{cases}
\tag{8.7}
$$

The orthogonality relations are

$$
\int_{V_1} \vec{E}_{m_1} \cdot \vec{E}_{n_1} \, dV = \int_{V_1} \vec{H}_{m_1} \cdot \vec{H}_{n_1} \, dV = \delta_{mn}
$$

$$
\int_{V_2} \vec{E}_{m_2} \cdot \vec{E}_{n_2} \, dV = \int_{V_2} \vec{H}_{m_2} \cdot \vec{H}_{n_2} \, dV = \delta_{mn} .
$$

The mode amplitudes $e_{b_1}(t)$, $e_{b_2}(t)$, $h_{b_1}(t)$ and $h_{b_2}(t)$ are given

by the following volume integrations:

$$\begin{cases} e_{b_1}(t) = \int_{V_1} \vec{E}_1(z_1,t) \cdot \vec{E}_{b_1}(z_1)\, dV \\ e_{b_2}(t) = \int_{V_2} \vec{E}_2(z_2,t) \cdot \vec{E}_{b_2}(z_2)\, dV \\ h_{b_1}(t) = \int_{V_1} \vec{H}_1(z_1,t) \cdot \vec{H}_{b_1}(z_1)\, dV \\ h_{b_2}(t) = \int_{V_2} \vec{H}_2(z_2,t) \cdot \vec{H}_{b_2}(z_2)\, dV \quad . \end{cases} \tag{8.8}$$

In the above representation, the subscripts 1 and 2 associated with the fields designate cavity 1 and 2, respectively; k_{b_1} and k_{b_2} are the eigenvalues or the wave numbers of the mode b_1 and b_2, respectively; $\vec{n}$ is a unit vector normal to the outer surface of the cavity volume V; S_s and S_0 are the short-circuit and open-circuit parts of the boundary surface[85] for the eigenvalue problem. Note that in the following analysis the dielectric loss corresponding to the volume conductivity of the crystal σ is neglected. However, this effect can be taken into account easily by modifying the Q of the optical cavity.

The "harmonic-oscillator-like" linear differential equations for the expansion coefficients will be derived in detail for cavity 2, then can be written down easily for cavity 1. Substituting Eqs. (8.6) and (8.7) into Eqs. (8.4) and (8.5), dotting with $\vec{H}_{a_2}$, $\vec{E}_{a_2}$, respectively, and integrating with respect to the volume, we have

$$k_{a_2} e_{a_2} + \mu_0 \frac{\partial h_{a_2}}{\partial t} = -\int_{S_{s2}} (\vec{n} \times \vec{E}_2) \cdot \vec{H}_{a_2}\, dS \tag{8.9}$$

$$\epsilon_0 \frac{\partial e_{a_2}}{\partial t} - k_{a_2} h_{a_2} - \int_{S_{02}} (\vec{n} \times \vec{H}_2) \cdot \vec{E}_{a_2}\, dS + \frac{\partial}{\partial t} \sum_{b_1} \langle \vec{E}_{a_2} | \delta\epsilon | \vec{E}_{b_1} \rangle e_{b_1} = 0 \quad , \tag{8.10}$$

where

$$\langle \vec{E}_{a_2} | \delta\epsilon | \vec{E}_{b_1} \rangle \equiv \int_{V_c} \vec{E}_{a_2} \cdot \delta\epsilon \, \vec{E}_{b_1} \, dV \quad .$$

Here V_c is the volume of the acoustic column.

Now, by taking time derivative of Eq. (8.10) and eliminating h_{a_2} from Eqs. (8.9) and (8.10), we have the following differential equation for the mode amplitude e_{a_2} in mode a_2 :

$$\frac{1}{c^2}\frac{\partial^2 e_{a_2}}{\partial t^2} + k_{a_2}^2 e_{a_2} + \frac{1}{c^2}\frac{\partial^2}{\partial t^2}\sum_{b_1}\left\langle \vec{E}_{a_2}\left|\frac{\delta\epsilon}{\epsilon_0}\right|\vec{E}_{b_1}\right\rangle e_{b_1}$$

$$= \mu_0 \frac{\partial}{\partial t}\left(\int_{S_{02}} (\vec{n}\times\vec{H}_2)\cdot\vec{E}_{a_2}\, dS\right) - k_{a_2}\int_{S_{s2}} (\vec{n}\times\vec{E}_2)\cdot\vec{H}_{a_2}\, dS \ , \tag{8.11}$$

where $c^2 \equiv (\mu_0\epsilon_0)^{-1}$.

A similar type of differential equation for h_{a_2} can be obtained by eliminating e_{a_2} . The surface integrals appearing in Eqs. (8.9) and (8.10) contain two types of terms: (a) those accounting for energy lost by radiation, in particular by the transmitted light, and (b) those accounting for external optical fields incident on the cavity, which serve to excite the cavity modes as they appear on the inside boundary wall of the reflector. It is important to point out that in cavity 2 there is no surface integral term which results from an external optical fields incident on the cavity; but there does exist such a term in cavity 1.

We assume the reflecting surfaces of the cavities to be sufficiently large so that the axial modes are essentially TEM waves without diffraction loss and the reflecting surfaces to be of "short-circuit" type for the normal mode problem. The actual system can be characterized by a reflection

coefficient, Γ , for the field amplitude. Then, the electric and magnetic fields on the inside surface of the reflectors are related as

$$\vec{n} \times \vec{E}_2 = c\mu_0\left(\frac{1 - \Gamma}{1 + \Gamma}\right) \vec{H}_2 \quad . \tag{8.12}$$

Substituting Eq. (8.12) into (8.11), we have

$$- k_{a_2} \int_{S_s} (\vec{n} \times \vec{E}_2) \cdot \vec{H}_{a_2} \, dS = - k_{a_2} \, c\mu_0\left(\frac{1 - \Gamma}{1 + \Gamma}\right) \sum_{b_2} h_{b_2} \int_{S_s} \vec{H}_{b_2} \cdot \vec{H}_{a_2} \, dS \quad . \tag{8.13}$$

This illustrates the coupling of modes a_2 and b_2 through the wall losses. Using Eq. (8.10) for h_{b_2} , Eq. (8.13) becomes

$$- k_{a_2} \int_{S_s} (\vec{n} \times \vec{E}_2) \cdot \vec{H}_{a_2} \, dS$$

$$= - k_{a_2} \, c^{-1}\left(\frac{1 - \Gamma}{1 + \Gamma}\right) \sum_{b_2} k_{b_2}^{-1} \left[\frac{\partial e_{b_2}}{\partial t} + \frac{\partial}{\partial t} \sum_{b_1} \left\langle \vec{E}_{b_2} \left| \frac{\delta\epsilon}{\epsilon_0} \right| \vec{E}_{b_1} \right\rangle e_{b_1}\right] \int_{S_s} \vec{H}_{b_2} \cdot \vec{H}_{a_2} \, dS \quad . \tag{8.14}$$

We note that the normal mode boundary conditions have been assumed to be short-circuit. Thus, the open-circuit surface integrals vanish in Eq. (8.10) and in Eq. (8.11).

Using the coordinate systems as shown in Fig. 8.2, we have the following normalized eigenfunctions (or the normal modes):

$$E_{a_1} = \begin{cases} \left(\frac{2}{AL}\right)^{\frac{1}{2}} \sin k_{a_1} z_1 = \left(\frac{2}{AL}\right)^{\frac{1}{2}} \sin k_{a_1}(- x \sin \theta_B + z \cos \theta_B) \\ \qquad\qquad a_1 = \text{even, } 2,4,6, \ldots . \\ \left(\frac{2}{AL}\right)^{\frac{1}{2}} \cos k_{a_1} z_1 = \left(\frac{2}{AL}\right)^{\frac{1}{2}} \cos k_{a_1}(- x \sin \theta_B + z \cos \theta_B) \\ \qquad\qquad a_1 = \text{odd, } 1,3,5, \ldots . \end{cases} \tag{8.15}$$

$$E_{a_2} = \begin{cases} \left(\frac{2}{AL}\right)^{\frac{1}{2}} \sin k_{a_2} z_2 = \left(\frac{2}{AL}\right)^{\frac{1}{2}} \sin k_{a_2}(x \sin \theta_B + z \cos \theta_B) \\ \qquad\qquad a_2 = \text{even, } 2,4,6, \ldots . \\ \left(\frac{2}{AL}\right)^{\frac{1}{2}} \cos k_{a_2} z_2 = \left(\frac{2}{AL}\right)^{\frac{1}{2}} \cos k_{a_2}(x \sin \theta_B + z \cos \theta_B) \\ \qquad\qquad a_2 = \text{odd, } 1,3,5, \ldots . \end{cases} , \quad (8.16)$$

and

$$H_{a_1} = \begin{cases} \left(\frac{2}{AL}\right)^{\frac{1}{2}} \cos k_{a_1} z_1 , & a_1 = \text{even, } 2, 4, 6, \ldots . \\ \left(\frac{2}{AL}\right)^{\frac{1}{2}} \sin k_{a_1} z_1 , & a_1 = \text{odd, } 1, 3, 5, \ldots . \end{cases} \quad (8.17)$$

$$H_{a_2} = \begin{cases} \left(\frac{2}{AL}\right)^{\frac{1}{2}} \cos k_{a_2} z_2 , & a_2 = \text{even, } 2, 4, 6, \ldots . \\ \left(\frac{2}{AL}\right)^{\frac{1}{2}} \sin k_{a_2} z_2 , & a_2 = \text{odd, } 1, 3, 5, \ldots . \end{cases} \quad (8.18)$$

where

A = cross-sectional area of the cavity,
L = separation of the reflecting surfaces of the cavity,
$k_a = \frac{a\pi}{L}$, i.e., $k_{a_1} = (a_1\pi/L)$, $k_{a_2} = (a_2\pi/L)$, ...etc.
a,b = integers designate the number of half-wavelength in mode a and mode b , respectively.

From the given normalized eigenfunctions, the scalar products between the eigenfunctions over S_s , which represents the loss terms due to transmission in Eq. (8.14), are obtained and tabulated in Table 8.I We note that the loss terms couple only between even modes and even modes or between odd modes and odd modes. The commonly defined[89] mode quality factors Q_a , Q_b in a cavity are

$$Q_{a_2} = \frac{1}{4}\pi a_2\left(\frac{1+\Gamma}{1-\Gamma}\right) \quad , \quad Q_{b_2} = \frac{1}{4}\pi b_2\left(\frac{1+\Gamma}{1-\Gamma}\right) \quad . \qquad (8.19)$$

TABLE 8.I

Modes	$\int_{S_s} \vec{H}_{b_2} \cdot \vec{H}_{a_2}\, dS$
a_2 = odd	$\frac{4}{L}$, for $\lvert a_2 - b_2\rvert = 4n$, $n = 0,1,2,..$
b_2 = odd	$-\frac{4}{L}$, for $\lvert a_2 - b_2\rvert = 4n+2$,
a_2 = odd b_2 = even	0 ,
a_2 = even b_2 = odd	0 ,
a_2 = even	$\frac{4}{L}$, for $\lvert a_2 - b_2\rvert = 4n$, $n = 0,1,2,..$
b_2 = even	$-\frac{4}{L}$, for $\lvert a_2 - b_2\rvert = 4n+2$,

Using Eq. (8.19) and the results of Table 8.I, Eq. (8.14) becomes

$$- k_{a_2} \int_{S_{s2}} (\vec{n} \times \vec{E}_2) \cdot \vec{H}_{a_2} \, dS$$

$$= - k_{a_2} c^{-1} \sum_{b_2}^{1} Q_{b_2}^{-1} \left[\frac{\partial e_{b_2}}{\partial t} + \frac{\partial}{\partial t} \sum_{b_1} \left\langle \vec{E}_{b_2} \left| \frac{\delta \epsilon}{\epsilon_0} \right| \vec{E}_{b_1} \right\rangle e_{b_1} \right] \quad , \qquad (8.20)$$

where the summation $\sum_{b_2}^{1}$ is taken over all values of b_2 such that $a_2 + b_2$ is even. When we substitute Eq. (8.20) into Eq. (8.11), we see that the second term in Eq. (8.20) is much smaller than the third term of the left-hand side in Eq. (8.11) and hence can be neglected. Furthermore, in the high-Q approximation, we might assume that any driving trems at frequencies outside the passband of a given mode have negligible effect on that mode, hence, for any of the modes a_2, we have

$$\sum_{b_2}^{1} Q_{b_2}^{-1} \frac{\partial e_{b_2}}{\partial t} \simeq Q_{a_2}^{-1} \frac{\partial e_{a_2}}{\partial t} \quad .$$

Finally, Eq. (8.20) becomes

$$- k_{a_2} \int_{S_s} (\vec{n} \times \vec{E}_2) \cdot \vec{H}_{a_2} \, dS = - k_{a_2} c^{-1} Q_{a_2}^{-1} \frac{\partial e_{a_2}}{\partial t} \quad . \qquad (8.21)$$

Finally, from Eq. (8.11), we have the following "harmonic-oscillator-like" linear differential equation for the mode amplitude e_{a_2} in cavity 2:

$$\frac{\partial^2 e_{a_2}}{\partial t^2} + \omega_{a_2}^2 e_{a_2} + \omega_{a_2} Q_{a_2}^{-1} \frac{\partial e_{a_2}}{\partial t} + \frac{\partial^2}{\partial t^2} \sum_{b_1} \left\langle \vec{E}_{a_2} \left| \frac{\delta \epsilon}{\epsilon_0} \right| \vec{E}_{b_1} \right\rangle e_{b_1} = 0 \quad ,$$

(8.22)

where $\omega_{a_2} = k_{a_2} c$. Note that in Eq. (8.22) the last term is due to the coupling between mode a_2 in cavity 2 and modes b_1 in cavity 1. In the later analysis, we show that only two modes in cavity 1 are coupled strongly to any mode a_2 in cavity 2.

Following a similar approach, the "harmonic-oscillator-like" linear differential equation for the mode amplitude e_{b_1} in cavity 1 is obtained as follows:

$$\frac{\partial^2 e_{b_1}}{\partial t^2} + \omega_{b_1}^2 e_{b_1} + \omega_{b_1} Q_{b_1}^{-1} \frac{\partial e_{b_1}}{\partial t} + \frac{\partial^2}{\partial t^2} \sum_{a_2} \left\langle \vec{E}_{b_1} \left| \frac{\delta\epsilon}{\epsilon_0} \right| \vec{E}_{a_2} \right\rangle e_{a_2}$$

$$= -\frac{1}{2} \omega_{b_1} Q_{b_1}^{-1} \frac{\partial e(\omega t)}{\partial t} \quad , \qquad (8.23)$$

where $\omega_{b_1} = k_{b_1} c$. The term in the right-hand side of Eq. (8.23) is due to the incident external field transformed to the inside surface of the reflector. Here $e(\omega t)$ the electric field of the incident external field appears on the surface of the reflector; and the factor $1/2$ appears due to the fact that only one surface of the cavity 1 is subjected to external excitation.

Now, we come to evaluate the coupling terms $\langle \vec{E}_{a_2} | \frac{\delta\epsilon}{\epsilon_0} | \vec{E}_{b_1} \rangle$. It is assumed that the acoustic wave is resonant and

$$\frac{\delta\epsilon}{\epsilon_0} = \Delta\epsilon \sin K_s x \cos \omega_s t = \sin K_s x \left(\frac{\Delta\epsilon}{2} e^{j\omega_s t} + \text{c.c.} \right) \quad , \qquad (8.24)$$

where

ω_s = frequency of the acoustic wave,
K_s = ω_s / v_ℓ = wave number of the acoustic wave,
v_ℓ = velocity of the longitudinal acoustic wave,
$\Delta\epsilon$ = amplitude of the permittivity perturbation due to acoustic waves.

We furthermore designate the spatial part of $\delta\epsilon/\epsilon_0$ as

$$\left.\frac{\delta\epsilon}{\epsilon_0}\right|_{s.p} ,$$

and we have

$$\left.\frac{\delta\epsilon}{\epsilon_0}\right|_{s.p} = \sin K_s x \quad .$$

Using the eigenfunctions given in Eqs. (8.15) and (8.16), we have for the case b_1 = even , a_2 = odd ,

$$\left\langle \vec{E}_{a_2} \left| \left.\frac{\delta\epsilon}{\epsilon_0}\right|_{s.p} \vec{E}_{b_1} \right\rangle \right.$$

$$= \int_V \left(\frac{2}{AL}\right) \left[\cos k_{a_2}(x \sin\theta_B + z\cos\theta_B)\right] \cdot \left[\sin K_s x\right] \cdot \left[\sin k_{b_1}(-x\sin\theta_B + z\cos\theta_B)\right] dV$$

$$= -\frac{1}{2L}\int_{-\ell/2}^{\ell/2} \Bigg[\cos\Big\{(K_s + k_{a_2}\sin\theta_B - k_{b_1}\sin\theta_B)x + (k_{a_2}\cos\theta_B + k_{b_1}\cos\theta_B)z\Big\}$$

$$+ \cos\Big\{(-K_s + k_{b_1}\sin\theta_B + k_{a_2}\sin\theta_B)x + (k_{a_2}\cos\theta_B - k_{b_1}\cos\theta_B)z\Big\}$$

$$- \cos\Big\{(K_s + k_{a_2}\sin\theta_B + k_{b_1}\sin\theta_B)x + (-k_{b_1}\cos\theta_B + k_{a_2}\cos\theta_B)z\Big\}$$

$$- \cos\Big\{(-K_s - k_{b_1}\sin\theta_B + k_{a_2}\sin\theta_B)x + (k_{b_1}\cos\theta_B + k_{a_2}\cos\theta_B)z\Big\}\Bigg] dz \quad , \quad (8.25)$$

where the relation $dV = Adz$ is used. To have strong interaction, the Bragg condition must be satisfied:

$$\begin{cases} k_{b_1} \sin \theta_B + k_{a_2} \sin \theta_B = K_s \\ k_{b_1} \cos \theta_B = k_{a_2} \cos \theta_B \end{cases} . \tag{8.26}$$

Thus only the second term in Eq. (8.25) is independent of x and z, and hence will contribute dominantly; others can be neglected. We have

$$\left\langle \vec{E}_{a_2} \left| \frac{\delta\epsilon}{\epsilon_0} \right|_{s.p} \vec{E}_{b_1} \right\rangle \simeq - \frac{1}{2L} \int_{-\ell/2}^{\ell/2} dz = - \frac{\ell}{2L} . \tag{8.27}$$

The integration can be carried out similarly for other cases. The results are given in Table 8.II.

TABLE 8.II

Mode	$\left\langle \vec{E}_{a_2} \left\| \frac{\delta\epsilon}{\epsilon_0} \right\| \vec{E}_{b_1} \right\rangle$
b_1 = even a_2 = odd	$\simeq - \frac{\ell}{2L}$
b_1 = even a_2 = even	$\simeq 0$
b_1 = odd a_2 = even	$\simeq \frac{\ell}{2L}$
b_1 = odd a_2 = odd	$\simeq 0$

With $\langle \vec{E}_{a_2} | \delta\epsilon/\epsilon_0 |_{s.p} \vec{E}_{b_1} \rangle$ evaluated for various cases, they can be put into Eqs. (8.22) and (8.23), and the summation performed with respect to b_1 and a_2, respectively. Since the coupled frequencies are specified by

$$\omega_{a_2} = \omega_{b_1} \pm \omega_s \quad \text{for cavity 2} \tag{8.28}$$

$$\omega_{b_1} = \omega_{a_2} \pm \omega_s \quad \text{for cavity 1} \quad , \tag{8.29}$$

we see that only two modes of ω_{b_1} couple strongly to each mode of ω_{a_2}, and only two modes of ω_{a_2} couple to each mode of ω_{b_1}, i.e.,

$$b_1 = a_2 \pm 1 \tag{8.30}$$

$$a_2 = b_1 \pm 1 \quad , \tag{8.31}$$

since the spacing of the resonator modes is assumed to be ω_s. Finally, Eq. (8.22) becomes

$$\frac{\partial^2 e_{a,2}}{\partial t^2} + \omega_a^2 e_{a,2} + \omega_a Q_a^{-1} \frac{\partial e_{a,2}}{\partial t} + (-1)^a \frac{\ell}{2L} \frac{\partial^2}{\partial t^2} \left\{ \left. \frac{\delta\epsilon}{\epsilon_0} \right|_{t.p} (e_{a+1,1} + e_{a-1,1}) \right\} = 0 \quad , \tag{8.32}$$

where $\delta\epsilon/\epsilon_0|_{t.p}$ designates the time-varying part of $\delta\epsilon/\epsilon_0$ in Eq. (8.24), and for convenience we replace the notation a_2 by $a,2$.

To take the dielectric loss into account, we simply replace Q_a by the loaded Q of the cavity, Q_{aL}, where $Q_{aL}^{-1} = Q_a^{-1} + Q_{ad}^{-1}$; Q_{ad} is the equivalent material Q of the crystal, taking the volume ratio of the crystal and the cavity into account.

To conclude this subsection, we write down the differential equation corresponding to Eq. (8.23) for the mode amplitude e_{b_1} in cavity 1:

$$\frac{\partial^2 e_{b,1}}{\partial t^2} + \omega_b^2 e_{b,1} + \omega_b Q_b^{-1} \frac{\partial e_{b,1}}{\partial t} + (-1)^a \frac{\ell}{2L} \frac{\partial^2}{\partial t^2} \left\{ \frac{\delta\epsilon}{\epsilon_0}\bigg|_{t.p} (e_{b+1,2} + e_{b-1,2}) \right\}$$

$$= -\frac{1}{2} \omega_b Q_b^{-1} \frac{\partial e(\omega t)}{\partial t} \quad . \tag{8.33}$$

8.2.3 Recursion Formula for The Pertinent Mode Amplitudes and Their Solutions

In order to simplify the manipulation, we modify the notation for the cavity modes in the following analysis. We assume that the frequency of the exciting laser (drive frequency), ω_d , corresponds to that of the mode $b = d$ in cavity 1, i.e., $\omega_{d,1}$, and designate the order of sidebands from ω_d by the letter n . Using this modified notation, the pertinent mode amplitudes in cavities 1 and 2 are defined as follows:

$$\begin{cases} e_{b,1} = E_{b,1} \exp^{j(\omega_d + n\omega_s)t} + \text{c.c.} & (8.34) \\ \qquad\qquad (n \text{ even}) \\ e_{a,2} = E_{a,2} \exp^{j(\omega_d + n\omega_s)t} + \text{c.c.} & (8.35) \\ \qquad\qquad (n \text{ odd}) \\ e_d = E_d \exp^{j\omega_d t} + \text{c.c.} & (8.36) \\ \frac{\delta\epsilon}{\epsilon_0}\Big|_{t.p} = \frac{\Delta\epsilon}{2} \exp^{j\omega_s t} + \text{c.c.} \quad . & (8.37) \end{cases}$$

The conditions on n in Eqs. (8.34) and (8.35) are clear from the coupling selection rules in Eqs. (8.32) and (8.33) or from the physical considerations of Section 8.2.1. Upper sidebands are denoted by positive values

of n and lower sidebands by negative values; E_d designates the amplitude of the driving field; $E_{b,1}$ and $E_{a,2}$ designate the mode amplitudes in cavity 1 and 2, respectively. As a matter of convenience the mode amplitudes will be labeled only with the sideband subscript, i.e., E_n . There is no ambiguity; n even indicates cavity 1, n odd indicates cavity 2.

Substituting Eqs. (8.35) and (8.37) into Eq. (8.34), we have the following recursion formula:

$$\chi E_{n-1} + \chi^* E_{n+1} + jE_n = 0 \quad . \qquad (8.38)$$

(n odd)

For the cases of interest, $n\omega_s \ll \omega_d$, and the following approximations have been used:

$$Q_n \simeq Q_{n'} \qquad (8.39)$$

and

$$\chi \equiv \frac{\Delta\ell}{4L} Q_n \simeq \frac{\Delta\ell}{4L} Q_{n'} \qquad (8.40)$$

for all n and n' . Equation (8.38) applies when ω_d corresponds to an odd mode in cavity 1, i.e., d = even ; when the drive is applied to an even mode we have to replace χ and χ^* by $-\chi$ and $-\chi^*$ [Eq. (8.32)].

Similarly, substituting Eqs. (8.34) – (8.36) into Eq. (8.33) and using the approximations given in Eqs. (8.40), we have the following recursion formula for the pertinent mode amplitudes in cavity 1:

$$\chi E_{n-1} + \chi^* E_{n+1} + jE_n = -\frac{1}{2} jE\delta_{n0} \quad . \qquad (8.41)$$

(n even)

Again we have to replace χ and χ^* by $-\chi$ and $-\chi^*$ when the drive frequency ω_d corresponds to an even mode in cavity 1.

To obtain recursion relations between the mode amplitudes of cavity 1 only, we substitute Eq. (8.38) into Eq. (8.41). The substitution results in the following recursion relations:

$$\chi^2 E_{-n-2} + \chi^{*2} E_{-n+2} + (1 + 2|\chi|^2) E_{-n} = -\frac{1}{2} E_d \delta_{n0} \quad . \qquad (8.42)$$

(n even)

To solve Eq. (8.42) for the mode amplitudes, we define the normalized mode amplitudes[89,90] as

$$g_n = \left(\frac{1}{\chi^*}\right)^n \left(\frac{E_{-n}}{\frac{1}{2} E_d}\right) \quad ,$$

or

$$E_{-n} = \frac{1}{2} E_d (\chi^*)^n g_n \quad . \qquad (8.43)$$

Substituting Eq. (8.43) into Eq. (8.42), and utilizing the fact that $E_n = (-1)^n E^*_{-n}$ [from Eqs. (8.40) and (8.41)], we have

$$\begin{cases} 2|\chi|^4 \, \mathrm{Re}\, g_2 + (1 + 2|\chi|^2) g_0 = -1 & (8.44) \\ |\chi|^4 g_{n+2} + (1 + 2|\chi|^2) g_n + g_{n-2} = 0 \quad , & (8.45) \end{cases}$$

where Re designates the real part. Let $g_n = q^n$, then Eq. (8.45) leads to

$$|\chi|^4 q^4 + (1 + 2|\chi|^2) q^2 + 1 = 0 \quad . \qquad (8.46)$$

The roots for Eq. (8.46) are

$$q_1^2 = -\left\{ \frac{(1 + 2|\chi|^2) - \sqrt{1 + 4|\chi|^2}}{2|\chi|^4} \right\} \qquad (8.47)$$

and

$$q_2^2 = -\left\{\frac{(1 + 2|X|^2) + \sqrt{1 + 4|X|^2}}{2|X|^4}\right\} \quad . \tag{8.48}$$

Since

$$\frac{E_{-n}}{\frac{1}{2} E_d} = g_n (X^*)^n = q^n (X^*)^n$$

must approach to zero as X^* approaches to zero, only the root q_1^2 is valid. Furthermore, there are two roots for q_1 in Eq. (8.47) and in general we shall have $g_n = A_1 q_1^n + A_1' q_1'^n$. Since n is even, we have $q_1^n = q_1'^n$, and g_n can be written as $A q_1^n$, i.e.,

$$g_n = A q_1^n = A(j)^n \left\{\frac{(1 + 2|X|^2) - \sqrt{1 + 4|X|^2}}{2|X|^4}\right\}^{n/2} \quad . \tag{8.49}$$

The constant A is determined by Eqs. (8.44) and (8.49) with $n = 0$ and $n = 2$:

$$A = -(\sqrt{1 + 4|X|^2})^{-1} \quad . \tag{8.50}$$

Finally, from Eqs. (8.43) and (8.49), the mode amplitudes in cavity 1 are obtained:

$(n = 0,2,4,\ldots)$

$$\frac{E_{-n}}{\frac{1}{2} E_d} = g_n (X^*)^n = -(j)^n \frac{\left\{(1 + 2|X|^2) - \sqrt{1 + 4|X|^2}\right\}^{n/2}}{(\sqrt{1 + 4|X|^2})(\sqrt{2}X)^n} \tag{8.51}$$

and for $n = 0$,

$$\frac{E_0}{\frac{1}{2} E_d} = - \left(\sqrt{1 + 4|X|^2}\right)^{-1} \quad . \tag{8.52}$$

Equation (8.52) shows that as the coupling parameter $|X|$ increases, the exciting mode or carrier mode E_0 decreases:

For large $|X|$,

$$\frac{E_{-n}}{\frac{1}{2} E_d} \rightarrow - (j)^n \frac{1}{2|X|} \cdot \left(\frac{|X|}{X}\right)^n \tag{8.53}$$

or

$$\frac{E_{-n}}{E_0} \rightarrow (j)^n \left(\frac{|X|}{X}\right)^n \quad ; \tag{8.54}$$

for small $|X|$,

$$\frac{E_{-n}}{\frac{1}{2} E_d} \rightarrow - (j)^n \cdot (X^*)^n \tag{8.55}$$

or

$$\frac{E_{-n}}{E_0} \rightarrow (j)^n \cdot (X^*)^n \quad . \tag{8.56}$$

From Eqs. (8.53) and (8.54), we see that as $|X|$ becomes large, all of the sideband amplitudes are inversely proportional to $|X|$, and have the same amplitude. Furthermore, from Eqs. (8.55) and (8.56) we see that as $|X|$ becomes small, the amplitude of the n^{th} sideband is smaller than that of the carrier mode by a factor $(X^*)^n$.

Finally, combining Eqs. (8.38) and (8.51), the mode amplitudes in cavity 2 can be obtained:

$$\frac{E_{-n}}{\frac{1}{2}E_d} = (j)^n \frac{(1 - \sqrt{1 + 4|X|^2})\{(1 + 2|X|^2) - \sqrt{1 + 4|X|^2}\}^{(n-1)/2}}{(\sqrt{1 + 4|X|^2})(\sqrt{2}\ X)^{n-1}\ 2X} \qquad (8.57)$$

$$n = \text{odd},\ 1,3,5,\ldots \quad .$$

For large $|X|$,

$$\frac{E_{-n}}{\frac{1}{2}E_d} \rightarrow - (j)^n \frac{1}{2X} \left(\frac{|X|}{X}\right)^{n-1} \qquad (8.58)$$

or

$$\frac{E_{-n}}{E_0} \rightarrow (j)^n \left(\frac{|X|}{X}\right)^n \quad . \qquad (8.59)$$

For small $|X|$,

$$\frac{E_{-n}}{\frac{1}{2}E_d} \rightarrow - (j)^n (X^*)^n \qquad (8.60)$$

or

$$\frac{E_{-n}}{E_0} \rightarrow (j)^n (X^*)^n \quad . \qquad (8.61)$$

The description given by Eqs. (8.58) – (8.61) is similar to that given by Eqs. (8.53) – (8.56). They indicate that there exists some value of X for maximum intensity in a particular sideband. The optimum values of X are obtained by maximizing $E_{-n}/\frac{1}{2}E_d$ in Eq. (8.51) if we are interested in the modes of cavity 1; and maximizing $E_{-n}/\frac{1}{2}E_d$ in Eq. (8.57) if we are interested in the modes of cavity 2.

Taking the derivative of $E_{-n}/\frac{1}{2}E_d$ with respect to $|X|$, we have the following values of $|X|$ for maximum sidebands intensity in cavity 2:

$$16\,|X|^4 - 4(n)^2\,|X|^2 - (n)^2 = 0 \qquad (8.62)$$

$$n = \text{odd},\ 1,3,5\ \ldots\ ,$$

or

$$|X| = \frac{1}{2}\sqrt{\frac{(n)[(n) + \sqrt{4 + (n)^2}\,]}{2}}\quad . \qquad (8.63)$$

The first sideband corresponds to $n = 1$; the first sideband has maximum intensity when

$$|X| = \frac{1}{2}\sqrt{\frac{1 + 5}{2}} \simeq 0.636\ ,$$

and from Eq. (8.57) the intensity is

$$\left|(j)\ \frac{1 - 1.62}{(1.62)(2 \times 0.636)}\right|^2 \simeq 0.09\quad .$$

Thus the first sideband in cavity 2 has a maximum intensity of 9%. For $n = 3,5,\ldots$, the sidebands intensity are $9 \times 2^{-2(n-1)}\%$ in cavity 2. The corresponding $n-1$ sidebands intensity of the even modes in cavity 1 are determined from Eq. (8.51) as $38 \times 4.5^{-(n-1)}\%$ for $n = 3,5,\ldots$.

Similarly, taking the derivative of $E_{-n}/\frac{1}{2}E_d$ with respect to $|X|$, we have the following values of $|X|$ for maximum sideband intensity in cavity 1:

$$16\,|X|^4 - 4n^2|X|^2 - n^2 = 0 \qquad (8.64)$$

$$(n = 2,4,6,\ldots)\quad .$$

The problems of inducing $|X|$ by means of acoustic waves are treated in Chapters VI and VII; here we simply point out the possibility of inducing $|X|$ of the order of 0.636 or larger. Using a He-Ne laser

($\lambda = 6328$ Å, $\omega_d \simeq \pi \times 10^{15}$ rad/sec), $SrTiO_3$ crystal, acoustic waves of 800 Mc/sec and reflectors with reflection coefficient $\Gamma \simeq 0.95$, we have

$$k_b \simeq \frac{2\pi}{\lambda} = 10^5 \text{ cm}^{-1}$$

$$L = \frac{c}{2f_s} = 18.8 \text{ cm} \quad ,$$

$$Q_{b,1} \simeq Q_{-b,1} \simeq Q_{a,2} \simeq Q_{-a,2} \simeq \frac{1}{4}\pi k_b \frac{+\Gamma}{1-\Gamma} \simeq 2.8 \times 10^6 \quad .$$

For $SrTiO_3$ crystal, we have $\Delta\epsilon \simeq 2.3$ S (S is strain). With strain in the order of 5×10^{-5}, which requires only 10 watts of rf power (assuming an acoustic beam with $\ell = 0.2$ cm and a ZnO transducer with -11 dB conversion efficiency, see Section 7.3), $\Delta\epsilon$ is in the order of 11.5×10^{-5}. Thus we have

$$X = \frac{\Delta\epsilon\ell}{4L} Q_{b,1} \simeq 0.86 \quad .$$

APPENDIX A

1. Frequency Shifts in The Reflected and Transmitted Wave

$$K_i \sin \alpha_i = K_r \sin \alpha_r = K_t \sin \alpha_t \equiv I_1 \tag{A.1}$$

$$\omega_i + K_i V \cos \alpha_i = \omega_r - K_r V \cos \alpha_r = \omega_t + K_t V \cos \alpha_t \equiv -I_2 \quad . \tag{A.2}$$

From the first set of equations of (A.1), we have

$$\cos \alpha_r = \sqrt{1 - \left(\frac{\omega_i}{\omega_r}\right)^2 \sin^2 \alpha_i} \quad . \tag{A.3}$$

Substituting (A.3) into the first set of equations of (A.2) gives

$$\frac{\omega_i}{\omega_r} = \frac{1 - \beta c \sqrt{\mu_1 \epsilon_1} \sqrt{1 - \left(\frac{\omega_i}{\omega_r}\right)^2 \sin^2 \alpha_i}}{1 + \beta c \sqrt{\mu_1 \epsilon_1} \cos \alpha_i} \quad . \tag{A.4}$$

Solving for ω_r/ω_i , we have

$$\omega_r = \omega_i \frac{(1 + \mu_1 \epsilon_1 c^2 \beta^2) + 2\beta c \sqrt{\mu_1 \epsilon_1} \cos \alpha_i}{1 - \mu_1 \epsilon_1 c^2 \beta^2} \quad , \tag{A.5}$$

and

$$K_{rx} = -K_r \cos \alpha_r = -\sqrt{\mu_1 \epsilon_1}\, \omega_r \cos \alpha_r$$

i.e.,

$$K_{rx} = -\omega_r \cdot \frac{\sqrt{\mu_1 \epsilon_1}(1 + \mu_1 \epsilon_1 c^2 \beta^2) \cos \alpha_i + 2\mu_1 \epsilon_1 c\beta}{1 - \mu_1 \epsilon_1 c^2 \beta^2} \quad . \tag{A.6}$$

Similarly, substituting the second set of equations of (A.1) into the second set of equations of (A.2), we have

$$K_t^2 = I_1^2 + \left(\frac{I_2 + \omega_t}{c\beta}\right)^2 \quad , \tag{A.7}$$

and furthermore,

$$\frac{\omega_t^2}{c^2} - K_t^2 + \chi_2 \frac{(\omega_t + cK_t \beta_2 \cos \alpha_t)^2}{(1 - \beta_2^2)} = 0 \quad . \tag{A.8}$$

Combining Eq. (A.7), (A.8) and the second set of equations of (A.2), we have

$$\begin{aligned} &[(1 - \beta_2^2)(\beta^2 - 1) + \chi_2 c^2 (\beta - \beta_2')^2] \omega_t^2 \\ &- 2I_2 [(1 - \beta_2^2) + \chi_2 c^2 \beta_2 (\beta - \beta_2)] \omega_t \\ &- [(1 - \beta_2^2)(I_1^2 \beta^2 + I_2^2) - \chi_2 c^2 I_2^2 \beta_2^2] = 0 \quad , \end{aligned} \tag{A.9}$$

giving

$$(\omega_t)_{1,2} = -(I_2) \frac{1 + \chi_2 c^2 \beta_2 \cdot \frac{\beta - \beta_2}{1 - \beta_2^2} \mp \beta \sqrt{1 + \chi_2 c^2 + \left(\frac{I_1}{I_2}\right)^2 \left[\frac{c^2 \chi_2 (\beta - \beta_2)^2}{1 - \beta_2^2} - (1 - \beta^2)\right]}}{(1 - \beta^2) - \chi_2 c^2 \cdot \frac{(\beta - \beta_2)^2}{(1 - \beta_2^2)}} \quad . \tag{A.10}$$

The root corresponding to the upper sign will be chosen, as this corresponds to transfer of energy from the interface.

Substituting (A.10) into the second set of equations of (A.2), K_{tx} is obtained:

$$K_{tx} = -I_2 \cdot \frac{-\left[\beta + \chi_2 c^2 \frac{\beta - \beta_2}{1 - \beta_2^2}\right] + \sqrt{1 + \chi_2 c^2 + \left(\frac{I_1}{I_2}\right)^2 \left[\frac{c^2 \chi_2 (\beta - \beta_2)^2}{1 - \beta_2^2} - (1 - \beta^2)\right]}}{(1 - \beta^2) - \chi_2 c^2 \cdot \frac{(\beta - \beta_2)^2}{(1 - \beta_2^2)}} \quad . \tag{A.11}$$

2. Amplitude Changes in The Reflected and Transmitted Waves

In medium 1, the following relations hold:

$$\begin{cases} D_i = \epsilon_1 E_i \\ B_i = \mu_1 H_i \\ H_i = \sqrt{\dfrac{\epsilon_1}{\mu_1}}\, E_i \\ B_i = \sqrt{\mu_1 \epsilon_1}\, E_i \end{cases} \tag{A.12}$$

$$\begin{cases} D_r = \epsilon_1 E_r \\ B_r = \mu_1 H_r \\ H_r = \sqrt{\dfrac{\epsilon_1}{\mu_1}}\, E_r \\ B_r = \sqrt{\mu_1 \epsilon_1}\, E_r \end{cases} \tag{A.13}$$

Recalling that $K_{ix} = K_i \cos \alpha_i$, $K_{rx} = - K_r \cos \alpha_r$ and $K_{tx} = K_t \cos \alpha_t$, we have

$$\begin{cases} B_{iz} = \dfrac{K_{ix}}{\omega_i} E_i \\ B_{ix} = \dfrac{I_1}{\omega_i} E_i \\ H_{iz} = \dfrac{K_{ix}}{\omega_i \mu_1} E_i \\ H_{ix} = \dfrac{I_1}{\omega_i \mu_1} E_i \end{cases} \tag{A.14}$$

and

$$\begin{cases} B_{rz} = \dfrac{K_{rx}}{\omega_r} E_r \\ B_{rx} = \dfrac{I_1}{\omega_r} E_r \\ H_{rz} = \dfrac{K_{rx}}{\omega_r \mu_1} E_r \\ H_{rx} = \dfrac{I_1}{\omega_r \mu_1} E_r \end{cases} . \qquad (A.15)$$

In medium 2, the MinKowski relations reduce to:

$$\begin{cases} D_t + \frac{1}{c} \beta_2 H_t \cos \alpha_t = \epsilon_2 E_t + c\epsilon_2 \beta_2 \beta_t \cos \alpha_t & (A.16) \\ B_t + \frac{1}{c} \beta_2 E_t = \mu_2 H_t + c\mu_2 \beta_2 D_t \quad . & (A.17) \end{cases}$$

The boundary conditions are

$$B_{x \text{ medium } 1} = B_{x \text{ medium } 2} \qquad (A.18)$$

$$D_{x \text{ medium } 1} = D_{x \text{ medium } 2} \qquad (A.19)$$

$$E_{y \text{ medium } 1} - E_{y \text{ medium } 2} = \left\{ \vec{V} \times (\vec{B}_{\text{medium } 2} - \vec{B}_{\text{medium } 1}) \right\}_y \qquad (A.20)$$

$$H_{z \text{ medium } 1} - H_{z \text{ medium } 2} = \left\{ \vec{V} \times (\vec{D}_{\text{medium } 1} - \vec{D}_{\text{medium } 2}) \right\}_z \quad . \qquad (A.21)$$

In this case, we have

$$E_{y \text{ medium } 1} = E_i + E_r \tag{A.22}$$

$$E_{y \text{ medium } 2} = E_t \tag{A.23}$$

$$\left\{ \vec{V} \times \vec{B}_{\text{medium } 2} \right\}_y = c\beta B_t \cos \alpha_t \tag{A.24}$$

$$\left\{ \vec{V} \times \vec{B}_{\text{medium } 1} \right\}_y = c\beta (B_i \cos \alpha_i - B_r \cos \alpha_r) \tag{A.25}$$

$$\left\{ V \times \vec{D}_{\text{medium } 1} \right\}_y = - c\epsilon_1 \beta E_i - c\epsilon_1 \beta E_r \tag{A.26}$$

$$\left\{ V \times \vec{D}_{\text{medium } 2} \right\}_y = - c\beta D_t \tag{A.27}$$

$$H_{z \text{ medium } 1} = H_{iz} + H_{rz} = \frac{K_{ix}}{\omega_i \mu_1} E_i + \frac{K_{rx}}{\omega_r \mu_1} E_r \tag{A.28}$$

$$H_{z \text{ medium } 2} = H_{tz} = H_t \cos \alpha_t \quad . \tag{A.29}$$

From (A.18), we have

$$B_{tz} = B_t \cos \alpha_t = K_{tx} \left(\frac{E_i}{\omega_i} + \frac{E_r}{\omega_r} \right) \quad . \tag{A.30}$$

Substituting (A.30) into (A.16), (A.17) and solving for D_t and H_t in terms of E_i , E_r , and E_t , gives

$$H_{tz} = H_t \cos \alpha_t = \frac{\beta_2 (1 - \mu_2 \epsilon_2 c^2) \cos \alpha_t}{c\mu_2 (1 - \beta_2^2 \cos \alpha_t)} E_t + \frac{K_{tx} \left(\frac{E_i}{\omega_i} + \frac{E_r}{\omega_r} \right) \left(1 - \mu_2 \epsilon_2 c^2 \beta_2^2 \cos \alpha_t \right)}{\mu_2 (1 - \beta_2^2 \cos \alpha_t)} \tag{A.31}$$

$$D_t = \frac{(\mu_2 \epsilon_2 c^2 - \beta_2^2 \cos \alpha_t)}{c^2 \mu_2 (1 - \beta_2^2 \cos \alpha_t)} E_t + \frac{K_{tx} \beta_2 (\mu_2 \epsilon_2 c^2 - 1)}{c\mu_2 (1 - \beta_2^2 \cos \alpha_t)} \left(\frac{E_i}{\omega_i} + \frac{E_r}{\omega_r} \right) \quad . \tag{A.32}$$

Finally, substituting (A.22) – (A.29) and (A.31) – (A.32) into (A.20) and (A.21), two simultaneous equations relating E_i , E_r and E_t are obtained. They are given in the main text as Eqs. (3.19) and (3.20).

REFERENCES

1. W. Pauli, Theory of Relativity (Pergamon Press, New York, 1958).
2. K. Landecker, Phys. Rev. 86, 852 (1952).
3. Ya. B. Fainberg and V. S. Tkalich, Soviet Phys. - Tech. Phys. 4, 438 (1959).
4. O. G. Zagorodnov, Ya. B. Fainberg, and A. M. Egorov, Soviet Phys. JETP 11, 4 (1960).
5. Ya. B. Fainberg, Atomnaya Energiya 6, 431 (1959).
6. E. L. Ginzton, Science 127, 841 (1958).
7. O. G. Zagorodnov, Ya. B. Fainberg, A. M. Egorov, and L. I. Bolotin, Soviet Phys. - Tech. Phys. 31, 212 (1961).
8. L. D. Landau and E. M. Lifshitz, The Classical Theory of Fields (Addison-Wesley, Reading, 1951) p. 17.
9. W.K.H. Panofsky and M. Phillips, Classical Electricity and Magnetism (Addison-Wesley, Reading, 1956).
10. C. Møller, The Theory of Relativity (Oxford at the Clarendon Press, New York, 1955), p. 62.
11. W. Rindler, Special Relativity (Interscience, Wiley, New York, 1960).
12. L. D. Landau and E. M. Lifshitz, Electrodynamics of Continuous Media (Addison-Wesley, Reading, 1960).
13. J. A. Stratton, Electromagnetic Theory (McGraw-Hill Book Company, Inc., New York, 1941).
14. B. M. Bolotovskii and A. A. Rukhadze, Soviet Physics - JETP. 37, 958 (1960).
15. V. M. Kontorovich, Soviet Physics - JETP. 33, 1527 (1957).
16. P. G. Bergmann, Introduction to The Theory of Relativity (Prentice-Hall, Engelwood Cliffs, 1955).
17. V. I. Kurilko, Soviet Physics - Tech. Phys. 6, 655 (1962).
18. M. A. Lampert, Phys. Rev. 102, 299 (1956).
19. R. E. Collins, Field Theory of Guided Waves (McGraw-Hill Book Company, New York, 1960) p. 79.

20. F. A. Albini and R. G. John, J. Appl. Phys. 32, 75 (1961).
21. S. N. Stolyarov, Soviet Physics - Tech. Phys. 8, 418 (1963).
22. V. I. Kurilko, Soviet Physics - Tech. Phys. 5, 473 (1960).
23. B. J. Alder and R. H. Christian, Phys. Rev. 104, 550 (1956).
24. A. A. Brish, M. S. Tarasov, and V. A. Tsukerman, Soviet Physics - JETP 11, 15 (1960).
25. C. S. Tsai and B. A. Auld, Microwave Laboratory Report in preparation.
26. A. V. Gaponov and G. I. Freidman, Soviet Phys. - JETP 36, 957 (1959).
27. W. B. Hatfield and B. A. Auld, J. Appl. Phys. 34, 2941 (1963).
28. B. J. Elliott, Ph.D Dissertation, Stanford University (1963).
29. G. L. Heiter, Ph.D Dissertation, Stanford University (1963).
30. B. Lax and K. J. Button, Microwave Ferrites and Ferrimagnetics (McGraw-Hill Book Company, Inc., New York, 1962).
31. W. Kanzig, Solid State Physics (Academic Press Inc., New York, 1957), vol. 4.
32. F. Jona and G. Shirane, Ferroelectric Crystals (Pergamon Press, The MacMillan Company, New York, 1962).
33. J. S. Kouvel and C. C. Hartelius, Phys. Rev. 123, 124 (1961).
34. W. Kanzig and N. Maikoff, Helv. Phys. Acta. 24, 585 (1949).
35. W. J. Merz, Phys. Rev. 91, 513 (1953).
36. Y. Takagi, E. Sawaguchi, and T. J. Akioki, J. Phys. Soc. (Japan) 3, 270 (1948).
37. S. V. Bogdanov, Soviet Phys. Solid State 5, 591 (1963).
38. M. DiDomenico, Jr., Ph.D Dissertation, Stanford University (1962).
39. T. S. Benedict and J. L. Durand, Phys. Rev. 109, 1091 (1958).
40. A. Lurio and E. Stern, J. Appl. Phys. 31, 1805 (1960).
41. E. Nakamura and J. Furuichi, J. Phys. Soc. (Japan) 15, 1955 (1960).
42. E. Stern and A. Lurio, Phys. Rev. 123, 117 (1961).
43. A. Lurio and E. Stern, J. Appl. Phys. 31, 1125 (1960).
44. S. V. Bogdanov, Soviet Phys. Solid State 5, 588 (1963).
45. D. F. McDonald and C. J. Benning, Rev. Sci. Instr. 36, 504 (1965).
46. C. S. Tsai and B. A. Auld, Record of Invention, Docket No. M-195, Microwave Laboratory, Stanford University (June 14, 1965); also B. A. Auld and C. S. Tsai, Microwave Laboratory Report No. 1391, Stanford University (1965).

47. F. R. Morgenthaler, "Phase-Velocity Modulated Magnetoelastic Waves," MIT Report, (October 1965).
48. J. R. Eshbach, Phys. Rev. Letters 8, 357 (1962).
49. E. S. Cassedy, Jr., Proc. IEEE 47, 1374 (1959).
50. R. Landauer, J. Appl. Phys. 31, 479 (1960).
51. R. Landauer, IBM Journal 4, 391 (1960).
52. R. B. Riley, Stanford Electronics Laboratories Technical Report No. 1707-1, Stanford University (January 1961).
53. Masao Otuka, "Doppler-Effect-Like Phenomenon," Institute of Nuclear Physics, University of Tokyo (1965).
54. J. R. Pierce, J. Appl. Phys. 30, 1342 (1959).
55. L. Brillouin, Wave Propagation in Periodic Structures (Dover Publications, Inc., Second Edition, New York, 1953).
56. G. M. Roe and M. R. Boyd, Proc. IRE 47, 1213 (1959).
57. E. S. Cassedy and A. A. Oliner, Proc. IEEE 51, 1342 (1963).
58. P. K. Tien, J. Appl. Phys. 29, 1347 (1958).
59. A. L. Cullen, Nature 181, 332 (1958).
60. J. C. Simon, IRE Trans. MTT, MTT-8, 18 (1960).
61. J. M. Manley, H. E. Rowe, Proc. IRE 44, 904 (1956).
62. B. A. Auld and C. S. Tsai, Record of Invention, Docket No. M-175, Microwave Laboratory, Stanford University (May 1963).
63. R. A. Kallas, "An Ultrasonically Tunable Microwave Bandpass Filter," presented at the Microwave Acoustics Symposium, Boston (October 1965), to be published in IEEE Trans. of the Professional Group on Sonics and Ultrasonics.
64. J. E. Geusic, S. K. Kurtz, T. J. Nelson, and S. H. Wemple, Appl. Phys. Letters 2, 185 (1963).
65. G. D. Boyd, R. C. Miller, K. Nassau, W. L. Bond, and A. Savage, Appl. Phys. Letters 5, 234 (1964).
66. L. Brillouin, Ann. Phys. 17, 88 (1922).
67. P. Debye and F. W. Sears, Proc. Natl. Acad. Sci. U.S. 18, 409 (1932).
68. R. Lucas and P. Biquard, J. Phys. Rad. 3, 464 (1932).
69. R. Bär, Helv. Phys. Acta. 6, 570 (1933); 8, 591 (1953); and 9, 678 (1936).
70. C. V. Raman and N.S.N. Nath, Proc. Ind. Acad. Sci. Part 1, 2A, 406 (1935); Part 2, 2A, 413 (1935); Part 3, 3A, 75 (1936); Part 4, 3A, 119 (1936); Part 5, 3A, 459 (1936).

71. F. H. Sanders, Can. J. Res. 14, 158 (1936).
72. S. Parthasarathy, Proc. Ind. Acad. Sci. 3, 442, 594 (1936).
73. N.S.N. Nath, Proc. Ind. Acad. Sci. 4, 222 (1936); 8, 499 (1938).
74. R. Extermann and G. Wannier, Helv. Phys. Acta. 9, 520 (1936).
75. S. Rytov, Diffraction de la Lumiére par les Ultra-sons (Paris, Hermann, 1938).
76. E. David, Phys. Zeit. 38, 587 (1937).
77. L. Brillouin, La Diffraction de la Lumiére par des Ultra-sons (Paris, Hermann, 1933).
78. R. R. Aggarwal, Proc. Ind. Acad. Sci. 31A, 417 (1950).
79. F. A. Jenkins and H. E. White, Fundamentals of Optics (McGraw-Hill, New York, 1957).
80. P. K. Tien, J. Appl. Phys. 29, 1347 (1958).
81. P. K. Tien, Bell Telephone Laboratories Report, MM-61-124-8 (Feb., 1961).
82. M. Born and E. Wolf, Principles of Optics (Pergamon Press, New York, 1959).
83. J. F. Nye, Physical Properties of Crystals (Oxford University Press, New York, 1957).
84. C. F. Quate, C.D.W. Wilkinson, and D.K. Winslow, Microwave Laboratory Report No. 1355, Stanford University (August 1965).
85. J. C. Slater, Microwave Electronics (D. Van Nostrand, New York, 1950).
86. H. V. Hance, Lockheed Missiles and Space Company Tech. Report: Physics 6-74-64-35 (July 1964).
87. P. Phariseau, Proc. Ind. Acad. Sci., 31, 417 (1950).
88. M. G. Cohen and E.I. Gordon, BSTJ 44, 693 (1965).
89. E. I. Gordon and J. D. Rigden, Bell System Tech. J. 42, 155 (1963).
90. M. DiDomenico, Jr., J. Appl. Phys. 35, 2870 (1964).